The University of Leeds

Faculty of Medicine and Health

Leeds Institute of Cardiovascular and Metabolic Medicine

LICAMM

The impact of diabetes on Weibel-Palade body formation and function in endothelial cells

Harriet Jane Todd BSc (Hons), (MRes)

Submitted in accordance with the requirements for the degree of

Doctor of Philosophy

October 2025

Funded by the British Heart Foundation

Intellectual Property and Publication Statements

i. I confirm that the work submitted is my own and that appropriate credit has been given where reference has been made to the work of others.

ii. This copy has been supplied on the understanding that it is copyright material and that no quotation from the thesis may be published without proper acknowledgement

iii. "The right of Harriet Jane Todd to be identified as author of this work has been asserted by Harriet Jane Todd in accordance with the Copyright, Designs and Patents Act 1988."

iv. I acknowledge the use of Copilot (Microsoft, https://m365.cloud.microsoft/chat) for support with writing style and proof reading but not for content.

Acknowledgements

I would like to begin by thanking my supervisors for their support throughout my PhD. Firstly, I would like to thank my primary supervisor Dr. Lynn McKeown, for taking me on as a student and for helping me find a project I was passionate about when I needed it most. I will always be grateful for your guidance, support and, most importantly, our meetings over coffee throughout. To Dr. Karen Forbes, thank you for being there whenever I needed support or for serving as occasional therapist during my PhD. Your encouragement, advice and kindness have been invaluable. And to Professor David Beech, thank you for your help, support and encouragement throughout my time in the BHF programme and with my project, your input has been truly appreciated.

The past and present members of the McKeown lab created an environment that was a genuine joy to work in. Ryan, the toast to my butter, I'm so glad we got to go through the PhD process together. You were always there, whether to lend a hand, supply a coffee or to deliver a perfectly timed sarcastic comment. From lab work to adventures around Yorkshire, thank you for everything. Ash, thank you for all your help and endless patience showing me the ropes when I first started, your support made those early days so much easier. Melissa, thank you for navigating the chaos of my final year with good humour and flexibility. It's been great working with you and sharing the quirks of microfluidics. You are going to do great, don't hesitate to reach out whenever you need.

I would like to extend my deepest gratitude to the British Heart Foundation for funding me and my project, without it, none of this research would have been possible. Being part of their four-year programme has been an amazing experience and has provided me with so many brilliant opportunities for which I am incredibly grateful.

To everyone I have worked and collaborated with to make this project possible, thank you. Professor Ramzi Ajjan and Professor Khalid Naseem, thank you for sharing resources that enabled me to expand the scope of my investigation.

Thanks to Dr. Tom McKinnon and Dr. Golly Mobayen for hosting me at Imperial College London to learn your multimer gel method, it was a highlight of my PhD and has proved incredibly valuable to my research.

Outside of the lab. I am grateful to every member of the Ariens group and Leeds thrombosis network for adopting me at conferences, encouraging my presentations an offering support without hesitation. Those moments have been among the most enjoyable and memorable parts of this journey.

To the many PhD students who have been there throughout this experience, thank you for the friendship, the support, the laughs and for sharing in both the highs and lows. Cella, Daisie, Jess, Eva, Hannah, Kasia, Anna, Emily, Tom and Amy I genuinely cannot imagine going through this process without you all, thank you for making the journey not only manageable but memorable.

Amanda, Abbie, Marj, Fiona, Beth and Alex, I don't have a neat category to place you in. Whether as post-docs, as my boss (technically) but always as friends, you've offered unwavering support. From the Western Blotting support system to enforcing breaks, thank you for everything both in and out of the lab. You've kept me sane, caffeinated and smiling.

There is no way I would be writing any of this without my family, to my Mum, Dad, Granny and Jean. For getting me through the many stages of education I have insisted on pursuing, thank you. You've not only learnt what a Weibel-Palade body is (and why it is important) but followed along with each new twist and turn. More than that you've lived every high and low of the project with me. I don't have the words to express what that means to me.

Finally, to Tilly, William, Fred, Herbie, Bertie, Hector, Sylvie, Jeff and Hendricks, your presence has brought joy and comfort throughout this journey your support has meant the world to me.

Abstract

Background

The multimerization of pro-thrombotic glycoprotein von Willebrand Factor (VWF) drives the biosynthesis and determines the size and potential function of endothelial-specific storage organelles, Weibel-Palade bodies (WPBs). VWF is the primary cargo of WPBs as well as other vasoactive agents. The biogenesis of WPBs is dependent on the vascular environment, which itself is modulated by factors such as shear stress and blood glucose levels. Dysregulation of such environmental elements can result in pathological phenotypes including elevated VWF levels particularly observed in diabetic patients. This affects vascular function and endothelial cell (EC) physiology.

Aims

To develop assays for quantifying the effects of the diabetic microenvironment on the formation and function of WPBs and VWF release in cells under physiological shear stress

To establish the underlying molecular mechanisms involved.

Methods

An *in vitro* microfluidics system was used to develop models of diabetes mimicking different aspects of the expected environment experienced in blood vessels including glucose concentration and varying ECs. Cells were cultured under HSS conditions for 48hrs and then stimulated with an agonist to induce VWF exocytosis from WPBs.

Results

Exposure to elevated or oscillating glucose concentrations did not elicit many significant effects on WPB numbers size or function in HUVECs. However, ECs derived from diabetic patients displayed significant changes in the numbers and length of WPBs which may be a consequence of altered VWF structure.

Conclusions

The diabetic microenvironment may result in ECs developing a metabolic memory and subsequently an altered pathogenic phenotype even when removed from a damaging environment.

Table of Contents

List of Figures

List of Tables

Abbreviations

ADAMTS13: A disintegrin and metalloproteinase with thrombospondin-like motif

Angpt-2: Angiopoeiten-2

ANOVA: Analysis of Variance

AP-1: Activator Protein-1

BCA: Bicinchoninic acid (Assay)

Ca2+: Calcium Ion

CGM: Continuous Glucose Monitoring

CHD: Coronary Heart Disease

CVD: Cardiovascular Disease

dhAEC: Diabetic Human Aortic Endothelial Cell

DMSO: Dimethyl sulfoxide

DR: Diabetic Retinopathy

DTT: Dithiothreitol

EC: Endothelial Cell

ED: Endothelial Dysfunction

EGM-2: Endothelial growth medium 2

ELISA: Enzyme-linked immunosorbent assay

EMV-2: Endothelial Cell Growth Medium MV2

eNOS: Endothelial Nitric Oxide Synthase

ER: Endoplasmic Reticulum

ET-1: Endothelin-1

FIJI: Fiji is just Image J

FOV: Field of View

GOI: Gene(s) of interest

hAEC: Human Aortic Endothelial Cells

HG: High Glucose

HMW: High Molecular Weight

HRP: Horseradish Peroxidase

HSS: High Shear Stress

HUVECs: Human Umbilical Vein Endothelial Cells

IHD: Ischemic Heart Disease

IL-: Interleukin

kDa: (kilo) Daltons

LMW: Low Molecular Weight

LOSS: Low Oscillatory Shear Stress

LSS: Low Shear Stress

MMW: Medium Molecular Weight

MTOC: Microtubule Organising Centre

MW: Molecular Weight

MyRIP: Myosin VIIA And Rab Interacting Protein

NO: Nitric Oxide

NPP: Normal Pooled Plasma

NS: Not significant

PBS: Phosphate-buffered saline

PBS-T: Phosphate buffered saline and Tween 20

PFA: Paraformaldehyde

PMA: Phorbol 12-myristate 13-acetate

Px: Passage number

RP: Reference Plasma

RT: Room Temperature

SDS: Sodium dodecyl sulphate

SEM: Standard Error of the Means

SS: Shear Stress

t/pAKT: total/phosphorylated Protein kinase B

t/peNOS: total/phosphorylated Endothelial Nitric Oxide Synthase

T1DM: Type 1 Diabetes Mellitus

T2DM: Type 2 Diabetes Mellitus

TGN: Trans-golgi network

ULMW: Ultra-Large Molecular Weight

ULVWF: Ultra-Long von Willebrand Factor

VWD: von Willebrand Disease

VWF: von Willebrand Factor

WPB(s): Weibel-Palade Body/Bodies

WT: Wild Type

Publications and Communications

Publications

Cheng, C.W., Pedicini, L., Alcala, C.M., Deligianni, F., Smith, J., Murray, R.D., **Todd, H.J**., Forde, N., McKeown, L., 2025. RNA-seq analysis reveals transcriptome changes in livers from Efcab4b knockout mice. Biochemistry and Biophysics Reports 41, 101944.

Money A, **Todd HJ**, Jo H, Beech DJ, McKeown L. Low oscillatory shear stress regulates Weibel-Palade body size and VWF release. 2023:2023.05.26.542527.

Communications

A microfluidics approach to endothelial cell growth demonstrates that shear stress modulates Weibel-Palade body size and von Willebrand factor storage and release.

Harriet J. Todd[1], Ashley Money[1], Daisie M. Yates[1], Ryan D. Murray[1], Hanjoong Jo[2], Khalid M. Naseem[1], David J. Beech[1] and Lynn McKeown[1]

British Society for Haemostasis and Thrombosis conference Newcastle upon Tyne (2025)

Shear stress regulates Weibel-Palade Body size and von Willebrand factor release in endothelial cells

Harriet J. Todd[1], Ashley Money[1], Daisie M. Yates[1], Ryan D. Murray[1], Hanjoong Jo[2], Khalid M. Naseem[1], David J. Beech[1] and Lynn McKeown[1]

British Microcirculation and Vascular Biology Society conference Bristol (2024)

Shear stress regulates Weibel-Palade Body size and von Willebrand factor release

Harriet J. Todd[1], Ashley Money[1], Daisie M. Yates[1], Ryan D. Murray[1], Hanjoong Jo[2], Khalid M. Naseem[1], David J. Beech[1] and Lynn McKeown[1]

International Society of Thrombosis and Haemostasis conference Bangkok (2024)

The impact of diabetes on the form and function Weibel-Palade bodies in endothelial cells under laminar flow

Harriet Todd[1], David Beech[1], Karen Forbes[1], Chew Cheng[1] & Lynn Mckeown[1]

British Microcirculation and Vascular Biology Society conference Edinburgh (2023)

Chapter 1 Introduction

Diabetes prevalence has reached global concern, with the population of diabetes rising from 30 million worldwide in 1985 to 217 million in 2005, it is now considered to be an epidemic (1). By 2045 it is projected that prevalence of diabetes will rise globally to 12.2% with 783.2million adults affected (2). It is estimated that by 2030 diabetes treatment will cost the NHS £14 billion annually (3). The rise in prevalence is universal for both type one diabetes mellitus (T1DM) and type 2 diabetes mellitus (T2DM), however 90% of diagnosed cases are T2DM (1, 4). It carries with it an additional burden to both individuals affected and the wider healthcare systems (1). Moreover, it has been demonstrated by recent studies that vascular complications specifically have been associated to diabetic-related mortality in both T1DM AND T2DM (1). Vascular complications of diabetes can be life altering, ranging from blindness to loss of limb (5, 6). Key characteristics of both T1DM and T2DM include hyperglycaemia and disruption to intracellular metabolic activity (7, 8).

The primary goal of diabetic management is to reduce the burden of disease and reduce or prevent the incidence of complications, ultimately improving quality of life. Traditionally this has centred on the control of blood glucose levels, often through insulin and continuous glucose monitoring (2). However, randomised trials have not consistently demonstrated a clear link in glycaemic control and reduction in diabetes-related complications (2). Findings on intensive patient follow up have been mixed; while some studies reported improved cardiac outcomes, others noted, particularly in patients with co-morbidities, an increase of mortality (2). These inconsistencies underscore the need for more personalised treatment strategies that account for individual variability. Over the past decade, diabetes research has increasingly prioritised prevention of diabetes-associated complications and the underlying causes of metabolic dysfunction (2).

One key area of focus is endothelial dysfunction which is now recognised as a central contributor to many diabetes-associated complications (9). In this context, normal day-to-day functioning of the endothelium is disrupted, impairing its ability to regulate vascular tone, inflammation and coagulation, triggering a cascade of pathological consequences (9). My research focuses on a key component of the endothelium, essential in maintaining vascular health, but when disrupted, may contribute to the pathological changes seen in diabetes, such as hyperglycaemia.

1.1 Endothelial Cell Biology

1.1.1 Function of the endothelium

The endothelium is the innermost lining of all vasculature and organs. It is a monolayer comprised of endothelial cells (ECs) that forms an active barrier between blood and tissue and allows interface between the two. This position confers on to them a vital role in co-ordinating dynamic responses to the environment to maintain homeostasis. The endothelium is primed for a myriad of functions (**figure 1.1**), it is responsible for managing vascular tone, inflammation, thrombosis and haemostasis. It performs tissue specific roles where needed, with identifiable genotypes and expression profiles when isolated from different organs(10) (11). Each of these roles requires regulated release of carefully orchestrated combinations of vasoactive compounds, creating a balance of pro and anti-thrombotic cargo. Under quiescent conditions, ECs remain passive, maintaining an optimal environment for day-to-day function. Upon stimulation, e.g., vascular injury, ECs become activated, triggering a rapid launch of haemostatic pathways and coordinated responses (12, 13).

1.1.1.1 Vascular tone

The endothelium regulates vascular tone by releasing a dynamic mix of vasoconstrictors and vasodilators, maintaining blood flood, fluidity and haemodynamic stability (14). Vasodilatory factors include nitric oxide (NO) and prostacyclin (PGI_2), vasoconstrictive factors include endothelin-1 (ET-1) and thromboxane (TXA_2). Compounds such as ET-1 are released from endothelial cells when stimulated with inflammatory markers such as interleukins or TNF-α. ET-1 will bind to a respective receptor (ET_A and $ET\text{-}_{B2}$) located either on smooth muscle or ECs, triggering an influx of Ca^{2+} into the cell and vasoconstriction of the vessel (15). This can be mitigated by concurrent release of NO and PGI_2 to vasodilate the vessel once again (15). NO is the most potent vasodilator synthesised by the endothelium, responding to humoral, physical and chemical stimuli. When released, NO acts directly on the smooth muscle encapsulating the blood vessels, enforcing relaxation of the muscle to allow blood to flow with less resistance (14). Adding to its functionality, NO also has anti-thrombotic capacity, inhibiting platelets and preventing aggregation and adherence. Finally NO can confer anti-inflammatory protection, preventing adherence of leukocytes, accounting for the many roles NO is implicated in, it of no surprise that it is a common marker to assess the health of the endothelium (14).

1.1.1.2 Inflammation

Inflammation is an example of a complex system that the endothelium co-ordinates. When a stimulus in encountered such as vascular injury or infection, the endothelium acts rapidly to rectify the damage and return the environment to one of neutrality. In the presence of this category of stimuli, acute inflammation is triggered, endothelial activation instigates this. Firstly, there is an increase in blood flow localised to the affected tissue, this is followed with controlled 'leakage' of plasma protein rich fluid into the tissue which causes swelling (as is a typical observation of injury) finally circulating leukocytes are recruited to the affected tissue. This reaction will persist until the stimuli is removed or resolved. At which point the endothelium will 'stand down' and return to the quiescent state needed to maintain healthy blood flow (16).

1.1.1.3 Angiogenesis

The sprouting of new vessels from a pre-existing vessel is termed angiogenesis (17). Once the new vessels sprout they are stabilised by mural cells, marking the expansion of existing vessel networks (17). In a healthy environment, angiogenesis is essential for expanding and maintaining vascular networks, subsequently permitting the continued transport of oxygen and nutrients to be circulated around the body (18). As such, angiogenesis is an essential physiological process required for wound healing, allowing damaged vessels to be replaced (18, 19). It forms an anastomosis to maintain blood supply to the wound as new capillaries grow into the wound site, restoring blood flow and supporting remodelling of the extracellular matrix (18, 19). In healthy wound healing, angiogenesis is mediated by factors such as proangiogenic factors angiopoeiten-2 (angpt-2) and vascular endothelial growth factor (VEGF) (20). However, dysregulated angiogenesis has been associated to multiple pathologies. In diabetes, wound healing is impaired, with a decrease in pro-angiogenic factors (19). Other disease aetiologies are characterised by an overactivity of angiogenesis, for example, cancer and atherosclerosis, whereas other are synonymous with inadequate angiogenesis, for example, hypertension and pre-eclampsia (17).

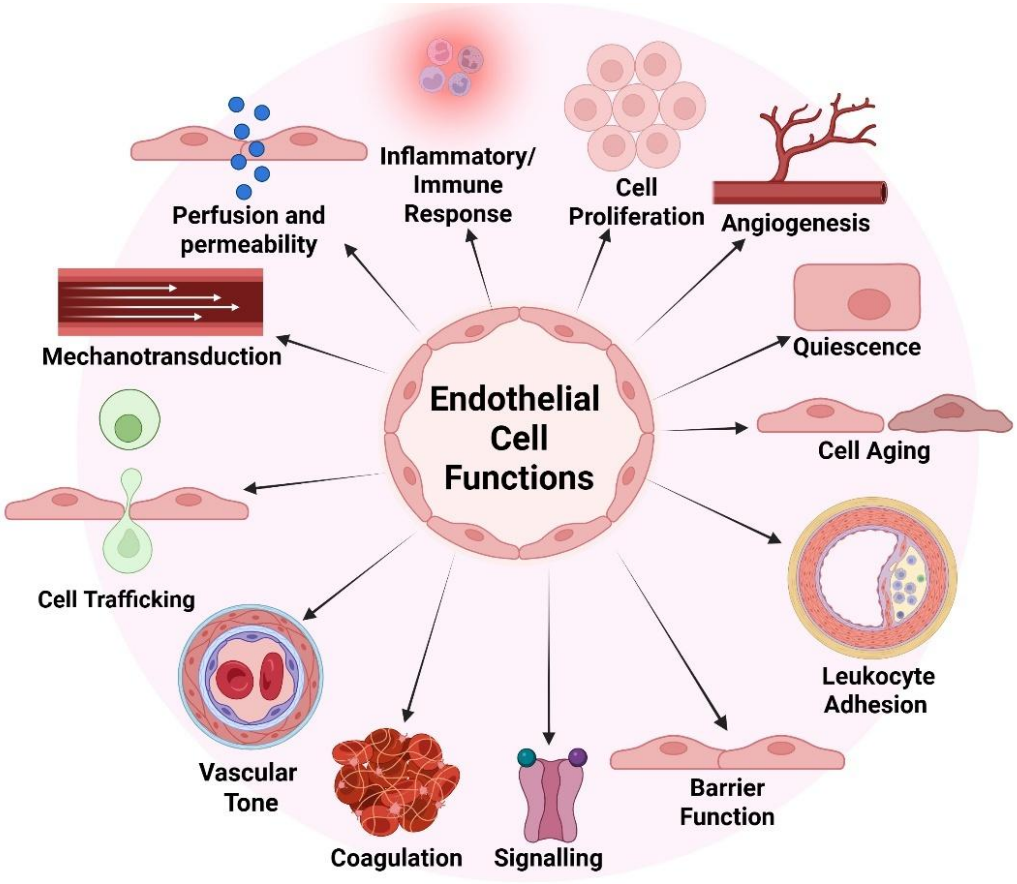

Figure 1.1. A graphical representation of different characteristics of endothelial cells and the different roles they carry out within the endothelium Demonstrating the variety of functions of ECs from angiogenesis to blood pressure regulation. (10) adapted in Biorender.

1.1.2 Primary haemostasis

When a blood vessel experiences injury, the first reaction of the damaged vascular wall and endothelium is to initiate primary haemostasis, this is the process by which a platelet plug is formed to prevent blood loss and initiate immediate wound healing. Upon injury, the fibrous subendothelial matrix (SEM) below the EC layer composed of proteins such as collagen, laminin and fibronectin, is exposed and platelets begin to bind (21, 22). There are three phases applicable to platelets in primary haemostasis, adhesion, activation and aggregation (23). The protein responsible for initiating the binding of platelets to the site of injury is the large adhesive glycoprotein von Willebrand factor (VWF) (further explored in **section 1.2**) (24). Long haemostatically efficient VWF strings are released from ECs, tether to the extracellular matrix collagen and are unravelled by the shear stress (SS) of blood in the direction of flow. This mechanical force exposes the A1 domain of VWF which enables platelets to bind via the GPIb component of their GPIb-IX-V complex (25). It also promotes the recruitments and binding of circulating VWF dimers creating a 'net' with an increased surface area to slow, catch and a tether platelets at the site of injury, thereby facilitating further aggregation (**figure 1.4**) (25). In addition to forming the primary vascular seal during injury repair, this binding event of platelets to VWF activates the platelets, which in turn initiates the steps required to trigger the coagulation cascade (26). Beyond its role in primary haemostasis VWF also serves a critical function in secondary haemostasis as a carrier molecule for factor VIII (FVIII) in plasma (27). VWF contributes to FVIII production, stabilisation and functional activity thereby extending its influence beyond platelet adhesion. By chaperoning FVIII, VWF protects it from premature clearance and proteolytic degradation, effectively doubling it's half-life from approximately 6.6 hours to 11.4 hours (28). The interaction between these proteins, is so essential that there is a subset of patients with VWF deficiency, who present with a phenotype representative of haemophilia (29). Although these individuals can synthesis FVIII, the absence of VWF as a stabilising cofactor prevents FVIII from persisting in circulation, long enough to exert its haemostatic function (29).

The coagulation cascade is a hallmark of secondary haemostasis, that consists of a series of proteolytic events that are localised to the surface of activated platelets (30). This process cumulates in the generation of thrombin and subsequently fibrin, both are needed to finalise stable clot formation and facilitate wound healing (30). Alongside the coagulation cascade, there are several processes such as leukocyte rolling that occur concurrently following primary haemostasis. Regulated recruitment of leukocytes to the site of an injury is an essential aspect of the innate immune response, neutrophils are the

most common subset that is recruited to inflamed tissue (31). Leukocytes bind to expressed P-selectin which is released from Weibel Palade bodies (WPBs, see **section 1.3**) and are 'rolled' along ECs towards the site of injury, once primary haemostasis has been initiated, and platelets are aggregating (**figure 1.4**). Once reaching the site, activated platelets in turn activate the leukocytes (31, 32).

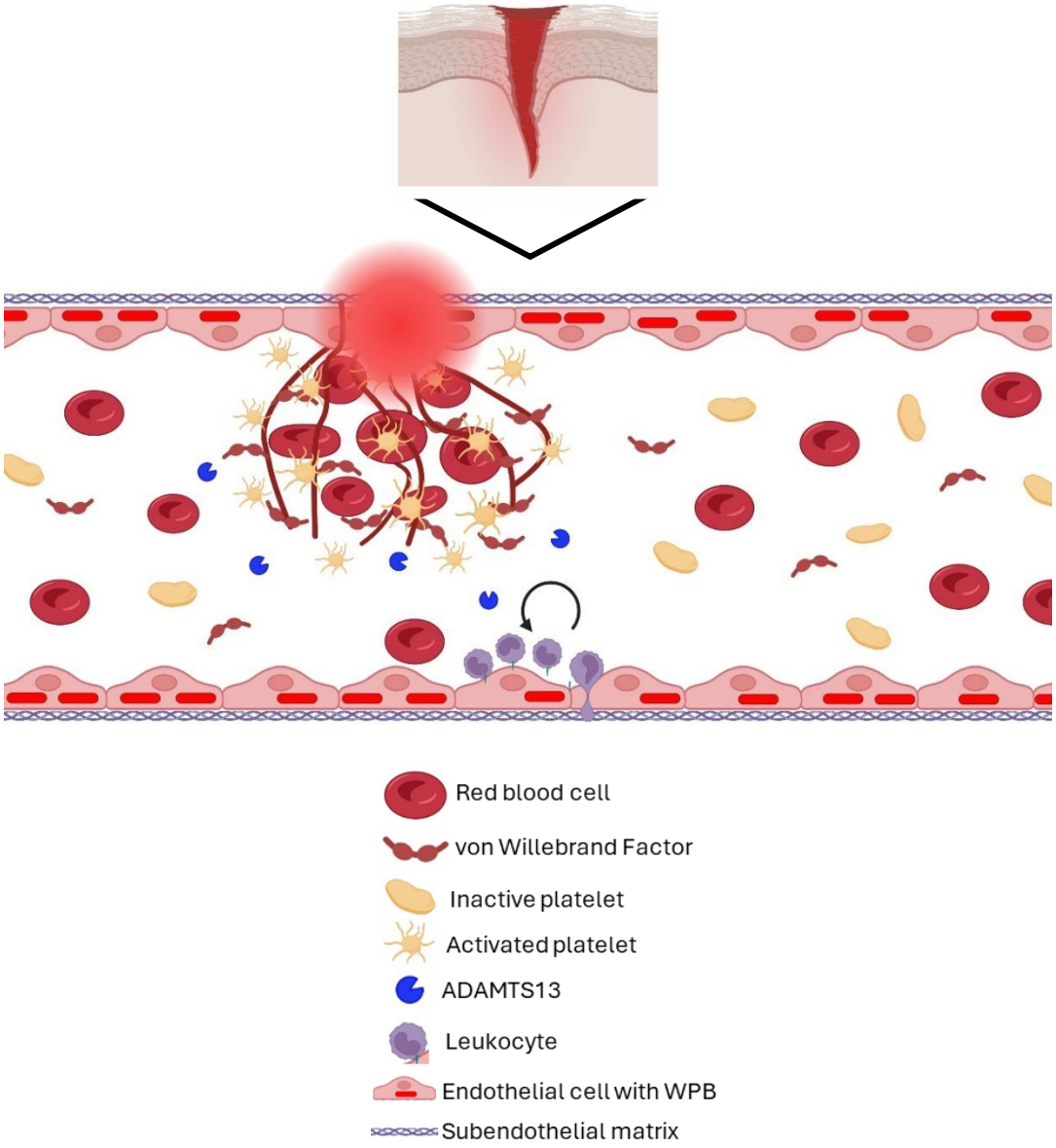

Figure 1.2. Vascular injury triggers a wound healing response from the endothelium initiated by primary haemostasis. This activates ECs to release WPB cargo, including the extrusion of VWF as long strings into the lumen of blood vessels. These strings unravel under shear stress exposing platelet binding sites and facilitating the aggregation of platelets and circulating VWF to form a platelet plug.

1.1.3 Influence of vascular tree on the endothelium

1.1.3.1 Vessel Morphology

Arteries carry oxygenated blood from the left side of the heart under high pressure, while veins return deoxygenated blood to the right side at a lower pressure (33). Although their basic structure is similar, subtle differences in vessel architecture reflect the distinct functional demands of each type (**figure 1.3**). Accordingly, EC specialisation is not unexpected (33). One example is the balance of vasodilators and vasoconstrictors, which is finely tuned for each vessel type based on the blood flow requirements, a process directly mediated by the endothelium and it's resident ECs (11). Human umbilical veins pose an interesting hybrid within the vascular system; although venous in structure, they carry oxygenated blood from the placenta to the foetus (34). Human umbilical vein endothelial cells (HUVECs) derived from these vessels are widely used as *in vitro* models of endothelial function; however, it is important to consider their distinct developmental origin. Unlike adult vessels, which are continuously exposed to long-term physiological and mechanical stressors, umbilical veins are foetal derived and operate within a transient environment (35).

1.1.3.2 Endothelial cell morphology

ECs are present in all vascular beds, each with a different microenvironment and stimuli, resulting in organotypic heterogeneity and identifiable subpopulations of ECs (36). Focusing on aortic and venous ECs as broad categories, fundamental differences between populations arise during development and persist into adulthood, particularly in cell cycle regulation. ECs from aortic and venous origin occupy distinct cell cycle states, driven by divergent signalling pathways. This is reflected in the expression of molecular markers such as EphrinB2, a transmembrane ligand for the Eph receptor tyrosine kinases associated to the promotion of angiogenesis within the endothelium, is expressed by arterial ECs and EphB4 (Ephrin type-B receptor 4) , also a receptor for tyrosine kinases involved in cell migration and proliferation is expressed in venous ECs (37, 38). This highlights the role of upstream signals in specifying EC identity. As a result, ECs from different vascular beds diverge in molecular profile, function and morphology despite being classified under the same cell type (39, 40). Morphologically speaking arterial ECs are typically thicker than venous with a long and narrow, ellipsoidal appearance, comparatively venous are short, wide and flat in profile (33). The intra cell to cell junctions are routinely 'tighter' in the aortic endothelium comparative to the venous (33). This reflects the endothelium's remarkable plasticity, allowing it to adapt to the functional demands of its environment. ECs integrate both intrinsic and extrinsic signals to establish

an identity suited to their vascular context, more so than many other cell types. As a result, their molecular and functional variations closely match the specific roles of the vessel from which they originate (33).

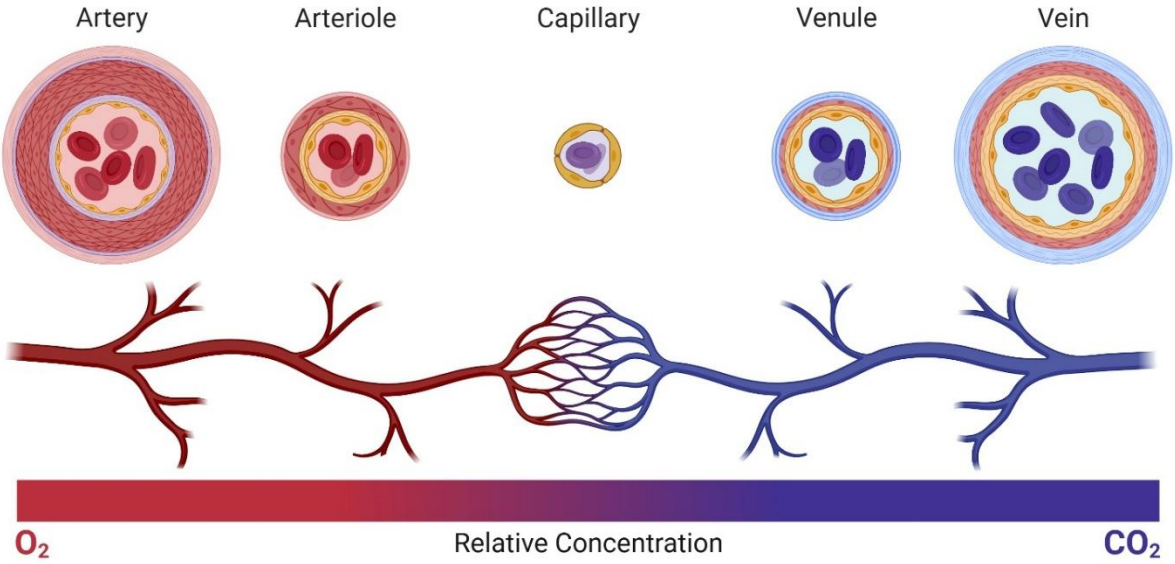

Figure 1.3. Visual comparison of arterial and venous vessel structures adapted from (41) and using a Biorender template. Veins carry deoxygenated blood at lower shear stress through vessels with wider lumen that require valves to prevent back flow of blood. Arterial vessels transport oxygenated blood at higher shear stress permitted by the thicker layer of smooth muscle tissue encapsulating the vessels.

1.1.3.3 Stress

ECs are continuously experiencing stress, circulating compounds, potential pathogenic factors and fluctuations in the blood, all of which increase the risk of damage and functional impairment (42). Given these persistent demands and harsh stimuli, it is unsurprising that endothelial degradation and dysregulation can contribute to the onset and progression of numerous pathologies. Vascular diseases remain among the most life-threatening conditions with endothelial dysfunction at their core (43). Endothelial dysregulation plays a central role in disorders such as cardiovascular disease and diabetes both exacerbated by factors like hyperglycaemia (44). As previously discussed, ECs exhibit exceptional plasticity to maintain function within the endothelium. However, this adaptability also renders them vulnerable to pathological influences, allowing plasticity itself to drive the emergence of disease-associated phenotypes under adverse conditions.

The EC phenotype is shaped by the surrounding environment critically this involves blood dynamics. As the interface between blood and tissue, ECs are constantly exposed to blood flow and the associated shear stress (SS) it generates making mechanical force a key regulator of their behaviour.

1.1.4 Shear Stress

The endothelium dynamically integrates and responds to biological and mechanical stimuli by nature of function; it permanently experiences the mechanical stress created by blood flow. As such, ECs detect flow and transmit signals in response through mechanosensitive receptors (e.g., PIEZO1) and associated pathways (45, 46). Different blood vessels will experience differential shear stress (see **table 1**). Although often overlooked in *in* vitro EC studies, shear stress and mechanical signalling is a key factor in the phenotype and the regulation of the endothelium (47). Both strength of shear and directionality influence the microenvironment of a vessel and can impact responses such as membrane permeability (47). Studies have demonstrated that laminar haemodynamic shear stress as illustrated in **figure 1.4** at arterial pressure (15dyne/cm^2) is atheroprotective and is necessary to maintain proper endothelial function, with a genetic profile expressed to match (48). Conversely, areas of low SS (~4dyne/cm^2) typically expressed an atherogenic phenotype, and are areas with a high prevalence of atherosclerosis (48).

Because of their unique positioning, ECs must react to SS as well as humoral responses (49). There are three primary mechanical forces ECs are sensitive to; pressure,

circumferential stretch/tension and shear stress (49). SS is generated by blood as it is forced through the vasculature by pulsatile pressure generated by the heart, this exerts friction against the ECs forming the inner endothelium of vessels. As vessels are not rigid they will deform under this stress in response, the vessel wall will experience circumferential stretch when blood pressure elevates, this force is perpendicular to the direction of flow (50). In large arteries, ECs will experience a mean shear wall stress ranging from 300-800/s, with a mean wall shear stress of 13.5-36 dyn/cm^2, whereas in veins this will be a mean wall shear rate of 15-200/s and a mean wall shear stress of 0.7-9 dyn.cm^2 (51).

1.1.4.1 Shear Stress in vitro

There is emerging support for use of microfluidics in cell culture to study ECs as both a representative physiological environment but also as a model of disease. It has been demonstrated by the McKeown lab that SS significantly modulates EC behaviour and specifically content within (explored further in **section 1.3.7**). This concept has been supported by a transcriptomic study, that utilised RNAseq to compare the gene expression profiles from umbilical cord tissue, with those of isolated cells (HUVECs) from the same tissue source under different cell culture conditions, including both static and high shear stress (HSS) (52). This highlighted the phenotypic distinctions of an *in vivo* and *in vitro* environment. Under static conditions, ECs adopted a more proliferative and pro-angiogenic phenotype. In contrast, HSS exposure restored the expression of extracellular matrix and flow-responsive genes. HUVECs cultured under HSS for 48hrs showed a 17% gene recovery, the highest of the *in vitro* environments, indicating that this condition most aligned with the native tissue profile (52). Notably, HSS-cultured ECs displayed a distinct transcriptome compared to those in static culture, including recovery of the acute inflammatory response pathway, a hallmark of endothelial function (52). These findings support HSS culture as the closest *in vitro* approximation of physiological endothelial environments currently achievable.

Directionality of SS is critical in whether exposure is atheroprotective or atheroprone, in areas of bifurcations and curvature within a vessel, blood flow is impacted, often resulting in turbulent or oscillatory stress (**figure 1.4**). It is also at these locations that atherosclerotic plaque formation initiates, which can progress into myocardial infarction, stroke or peripheral artery disease (PAD) (53). While Money et al have demonstrated one mechanism by which disturbed flow modulates EC behaviour, an RNAseq study has demonstrated that ECs may undergo reprogramming at a gene expression level in response (54). Using a murine model, the study revealed that under induced disturbed

flow, aortic ECs shifted from a healthy phenotype to one marked by elevated inflammatory markers and metabolic changes associated with atherosclerosis (53).

Table 1.1 Approximate values of shear stress experience in different types of blood vessels, illustrating variations in haemodynamic forces within vasculature. Adapted from Money et al. (55-59)

Blood Vessel	Shear stress (dyn/cm^2)
Arterial	5 - 60
Venous	1 - 10
Ascending aorta	12
Descending aorta	5 - 8
Large vein	5
Small vein	11
Umbilical Vein	4.5 - 6

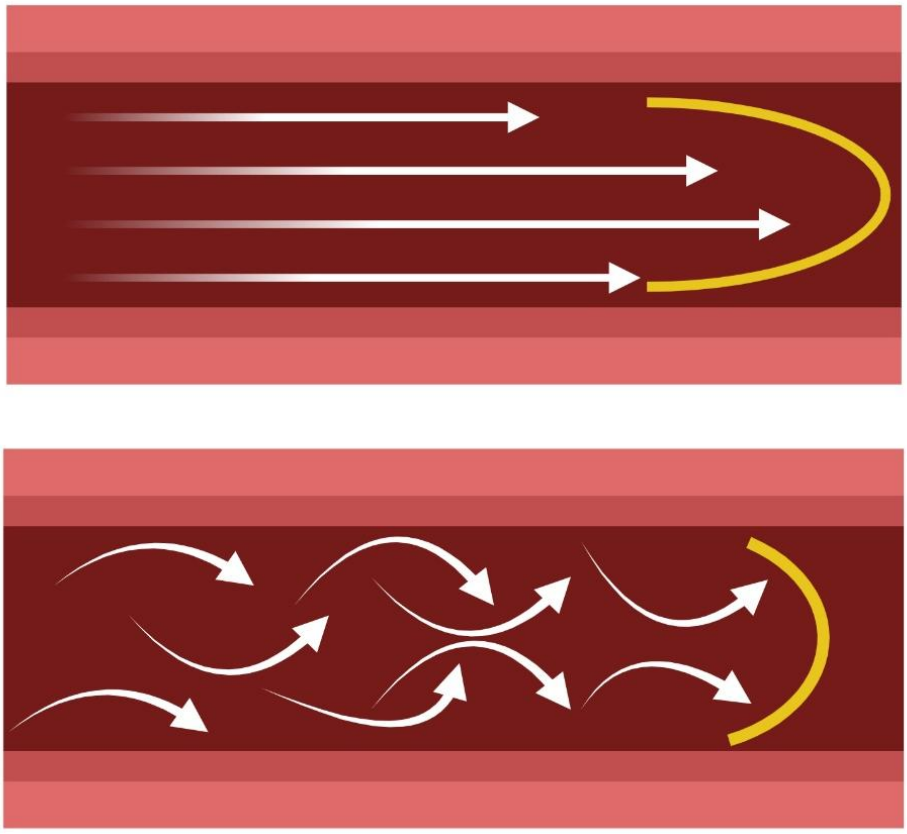

Figure 1.4 Comparison of shear stress profiles within blood vessels. Unidirectional laminar sheer stress generates a stable streamlined flow along the vessel wall, whereas in a vessel turbulent/disturbed shear stress produces irregular, multidirectional flow patterns. Image adapted from IBIDI using Biorender (60).

1.2 von Willebrand Factor (VWF)

In 1926, Erik von Willebrand reported a novel bleeding disorder now known as von Willebrand's disease (VWD), however it wasn't until 1971 that researchers recognised that the condition was caused by a deficiency in a blood factor, this was subsequently referred to as von Willebrand factor (VWF) (61). VWF is a large multimeric haemostatic protein, synthesised by ECs and megakaryocytes (62). It is a protein synonymously associated to ECs and is a routinely used endothelial marker (63, 64). Due to the multimeric nature of VWF, it exists in different molecular weights (MW), within plasma a normal range of VWF exists between 500 and 20,000 kDa, these are broadly categorised into low, medium, high and ultra large MWs (LMW, MMW, HMW and ULMW) (64-66). Multimer formation occurs due to noncovalent bonding between two pro-polypeptides of VWF (64). Functional capacity of VWF is determined by the MW of the multimer, this will be explored further on (65, 67).

1.2.1 Structure

When first transcribed, VWF is a single polypeptide that matures into a 2050 amino acid mature protein (51). This mature protein is comprised of different domains, each with a specific function, global understanding of this organisation is not complete, only the A domains remain well characterised with determined crystal structures (68). VWF is comprised of a series of repeating domains, there are three homologous A domains, A1 which binds to the GPIbα receptor of platelets while under shear stress, A2 (when unfolded by shear stress) is the cleavage site targeted by ADAMTS13 to break apart the protein to regulate the size of circulating protein and finally A3 which primarily binds to collagen and helps tether platelets to the exposed subendothelial matrix following damage (51, 64). There are four distinct D-domains (D-14) and a truncated D' domain (68). A known function of the D1 and D2 domains is assembly of the helical tubules of VWF that are characteristic of WPBs, they are present on the pro-polypeptide form of pro-VWF (68, 69). The D1, D2 and D3 domains permit this assembly through formation of disulphide bonding (70). The D3 and D' domains, present in mature VWF, are essential for the formation of VWF multimers, deletion of these regions prevented assembly of VWF as multimers with expression of only dimer structures of VWF observed (64, 69). Moreover, the D' and D3 domains interact with and bind to FVIII (as discussed in section 1.1.2), ensuring it's presence at the site of injury, aiding in the formation of a platelet plug (70). The C-terminal cystine knot is essential in facilitating the tail-to-tail dimerization of VWF monomers when in the endoplasmic reticulum (71). The D4 domain contains a crucial

docking site for ADAMTS13 that interacts specifically with the c-terminal of the enzyme (**figure 1.5**) (72). The C-domains of VWF remain comparatively less defined than the A and D domains (73). It has been suggested that the cystine rich C-domains of VWF facilitate disulphide bridging to enable multimerization. It has been demonstrated that the C4 domain conveys increased flexibility to VWF under SS, potentially aiding a multimer to withstand blood flow after exocytosis (73). As well as this, the C4 domain contains an Arg-Gly-Asp sequence that aids binding to the GPIIb/IIIa receptor of platelet ((73, 74).

When fully unravelled, VWF is present in long 'strings' which can measure up to 250µm in length, however following cleavage by **A D**isintegrin **A**nd **M**etalloproteinase with a **T**hrombo**s**pondin Type 1 motif, member 13 (ADAMTS13) multimers returning to circulation in plasma range form 3-15µm (70). Interestingly, VWF that has undergone cleavage by ADAMTS13 is activated under hydrodynamic stress, associated to arterial vessels, promoting haemostasis, whereas VWF that has not undergone cleavage is activated under a lower physiological shear stress, this is more likely to promote thrombosis (64). Size and subsequent structure of VWF is proportional to functional capacity. High molecular weight (HMW) and ultra large molecular weight (ULMW) VWF are preferentially utilised in primary haemostasis as thrombotic potential of these structures is greater than low molecular weight (LMW) and medium molecular weight (MMW) VWF (65) . By nature, there are a greater concentration of adhesions sites present on longer strings of VWF.

1.2.2 A Disintegrin And Metalloproteinase with a Thrombospondin Type 1 motif, member 13 (ADAMTS13)

Following the initial phase of primary haemostasis, the immobilised VWF is cleaved into smaller fragments by ADAMTS13 a process essential for regulating the thrombotic capacity of the environment (75). This cleavage of VWF is shear stress dependant as mechanical forces unravel VWF into a formation that exposes previously occluded spacer domain within the A2 domain of VWF allowing the recognition and binding by ADAMTS13 (76, 77). Once engaged, ADAMTS13 cleaves the ultra-large VWF multimers generating smaller, lower molecular weight VWF fragments (500-15,000kDa), which can then circulate in a globular conformation with reduced affinity for platelets and ADAMTS13 (**figure 1.6**) (76, 77). This mechanism serves to control VWF-mediated platelet aggregation and prevent excessive thrombus formation (78). In cases of ADAMTS13 deficiency, ultra large VWF multimers persist in circulation, retaining its high thrombotic capacity which contributes to the aetiology of Thrombotic thrombocytopenic purpura (TTP), a life-threatening pathology, in which spontaneous platelet aggregation can occur

(78, 79). These insights underscore the urgency of understanding VWF biology, not only in the context of haemostasis but also in broader vascular pathology.

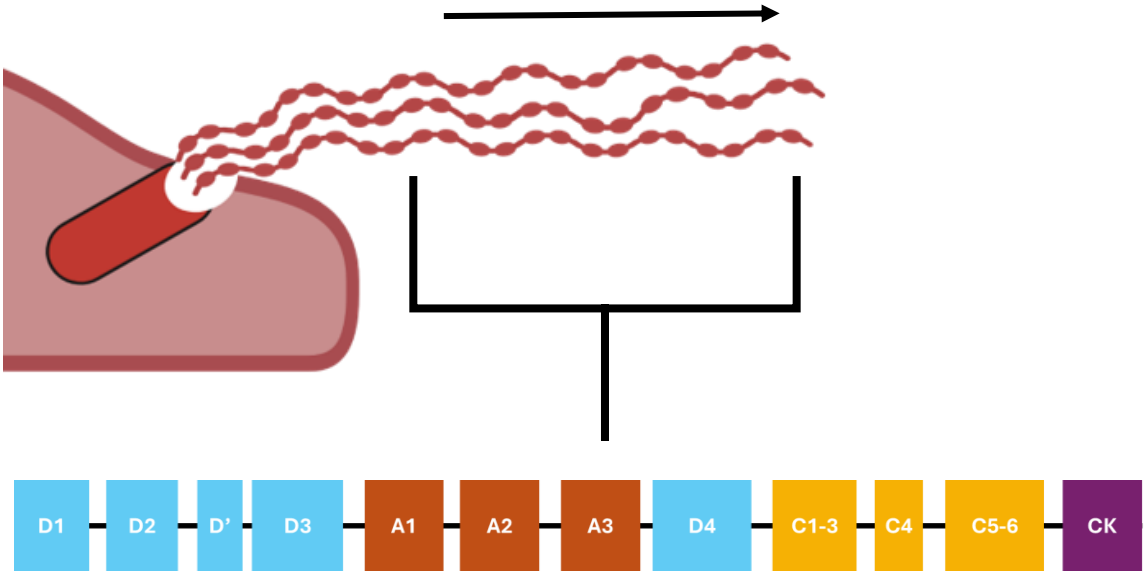

Figure 1.5. von Willebrand Factor is exocytosed from WPBs upon stimulation unravelling in long string structures in the direction of flow. The fundamental protein structure of VWF is highly conserved. Structure adapted from (80) illustrating a single VWF multimer. The diagram highlights the D' domains, A' domains, C' domains and cysteine knot (CK) at the C-terminal which facilitates multimer formation. The A1 domain contains the platelet-binding site, A2 houses the cleavage site for ADMATS13 while the A3 domain mediates collagen binding. These sites become accessible under shear stress which permits the unfolding of VWF.

1.2.3 Synthesis of VWF

The synthesis of VWF is highly ordered, it proceeds in a sequential manner, where each step is dependant of the successful completion of the previous one. For example, without proper dimerization and glycosylation, VWF cannot be secreted, likely due to conformational changes induced by these modifications (81).

Located on chromosome 12 (12p13.3) of the human genome, the VWF gene is 178 kilobases in length composed of 52 exons (82, 83). Once transcribed, an 8.8kDa mRNA is produced which is translated into a pre-pro-VWF polypeptide containing a 22 ammino acid signal peptide (84, 85). There is a 4-fold higher concentration of cystine residues contained within VWF compared to the average human protein, these are essential in permitting the precise folding and secretion of the protein (86). The pre-pro-VWF molecule is then guided to the endoplasmic reticulum (ER) via the secretory pathway by the signal peptide (85). Once translocated to the ER, the signal peptide is cleaved by an ER specific signal peptidase enzyme (87). This creates pro-VWF, at this point post-translational modifications initiate including N-linked glycosylation, dimerization (disulphide bonds are created between C-terminal amino acids in a tail-tail conformation), and pro-peptide cleavage (85, 87). This step is proceeded with transport of the VWF dimers to the Golgi apparatus for further carbohydrate processing and assembly into multimers (69). Biosynthesis of VWF is a pH sensitive process, the Golgi is an acidic environment with a low pH, when this was experimentally raised it inhibited the formation of VWF multimers resulting in poor WPB formation and a presented von Willebrand disease phenotype (see **section 1.2.4**) (81). The resulting protein is a mature VWF molecule which can then be packaged or secreted, which occurs differentially (85). VWF is transported for storage either in alpha granules of megakaryocytes or in endothelial cell specific storage organelles Weibel-Palade bodies (WPBs). Unlike WPBs which require VWF for their formation, megakaryocytes and platelets can function independently of VWF, however the absence of VWF has significant pathological consequences (86).

1.2.4 von Willebrand Disease

von Willebrand disease (VWD) is a genetic blood disorder characterised by a reduction or complete depletion of VWF or VWF activity, it is the most common bleeding disorder worldwide affecting approximately 1/1000 people (88, 89). It follows autosomal inheritance and as such equally affects both males and females (90). VWD is broken down into three classifications, type 1 (with a newly categorised type 1C which is increased clearance of VWF from plasma) is a partial decrease in VWF presenting as a

mild/moderate bleeding phenotype (88). Type 2 (which is further broken into types 2A, 2B, 2M and 2N) is a structural and or functional disruption to VWF and finally type 3, near total depletion of VWF (88). Prevalence varies between type, type 1 occurs most frequently (60-70% of diagnoses), type 2 fall in the middle (20-30% of diagnoses) and type 3 the least (5-10% of diagnoses) (88). Given the severity of the bleeding phenotype of type 3 VWD it is most commonly confused with haemophilia (27).Haemophilia A is characterised by defects in coagulation factors, primarily involving FVIII (91). Genetic background analysis (based on inheritance patterns) can support differential diagnosis, helping to distinguish haemophilia A from VWD (91). In contrast, the diagnosis of VWD focuses on assessing the quantity of VWF and its functional capacity, including its ability to mediate platelet adhesion (90). For example, in type 2A VWD the defect affects multimerization of VWF, therefore evaluation of the multimeric profile of present VWF represents a critical aspect of diagnostic assessment (90).

1.2.5 Exocytosis pathways

There are three distinct pathways through which ECs release VWF, these are basal, constitutive and regulated release (86). Each pathway has a range of different molecular weight (MW) of VWF associated with it. Basal secretion of VWF from ECs is a spontaneous occurrence and does not require any stimulation to trigger release (92). Approximately 80% of VWF released in from ECs occurs through basal secretion (92). A continuous process, basal secretion releases low to medium molecular weight VWF apically into the lumen of blood vessels from WPBs in the absence of stimulus, this is thought to be the predominant source of circulating VWF found in plasma (93) (94). Despite releasing VWF from the same source as the regulated pathway, WPBs, basal secretion occurs at a lower magnitude, producing insufficient VWF to form the extended thrombotic strings required for platelet recruitment (86). Levels of VWF in the plasma are highly variable, ranging from 40%-240% in a population, influenced by both genetic and environmental factors (95).

Constitutive expression involves direct basolateral release of low weight VWF from the TGN to the endothelial surface using anterograde carriers to navigate the secretory pathway (94). From here, VWF is released into the subendothelial matrix (94). Finally there is regulated VWF release, requiring a stimuli (e.g., thrombin or histamine) to trigger exocytosis of stored large and ultra-large molecular weight VWF from WPBs (94). Distribution of VWF multimer weight between each pathway is illustrated in **figure 1.6**. Each pathway plays a distinct but complementary role in maintaining haemostatic balance. Understanding the distinct pathways of VWF release provides important context

for examining the specialised organelles responsible for storage and secretion of VWF from ECs.

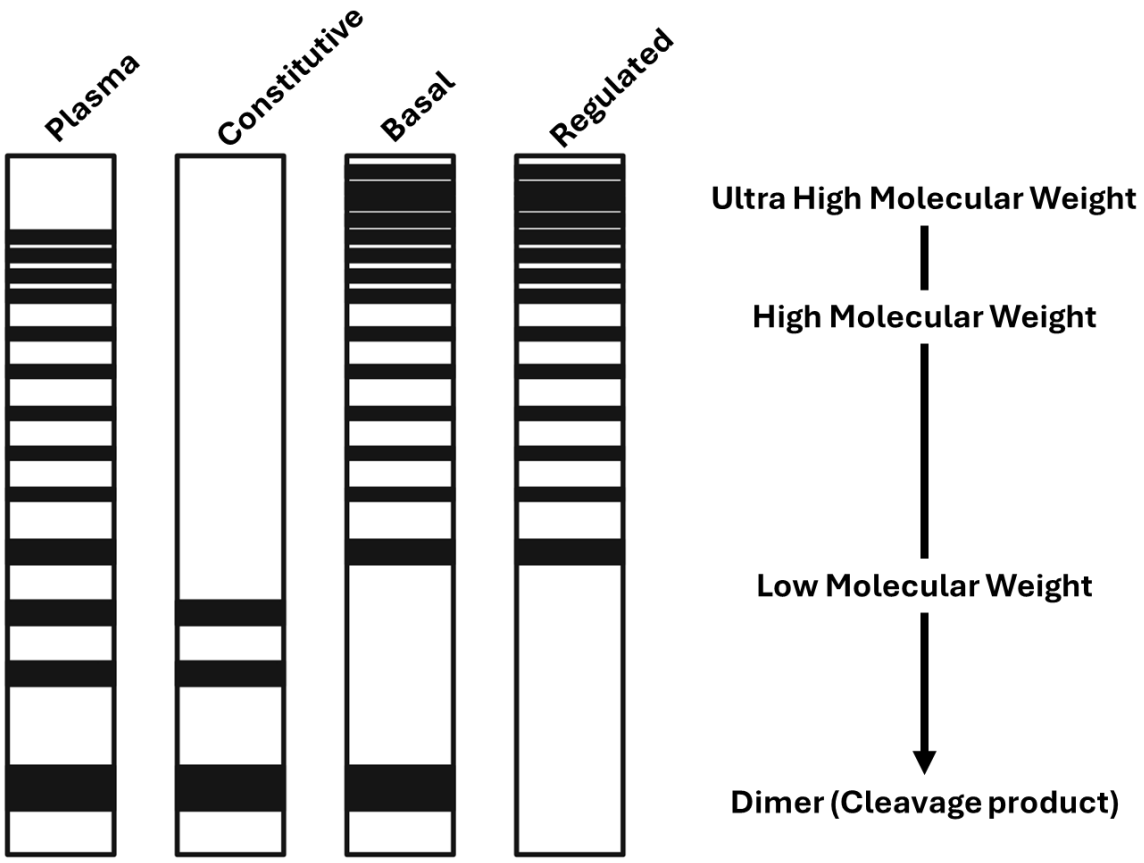

Figure 1.6. Schematic representation of von Willebrand factor (VWF) multimer distribution, illustrating the separation of ultra-large, high and low molecular weight forms. Multimers are differentiated by their source, EC release versus circulating plasma highlighting how secretory pathway and processing influence differences multimer size. Created in Biorender, adapted from (94).

1.3 Weibel Palade Bodies

Weibel-Palade bodes (WPBs) are endothelial cell specific storage organelles discovered in 1964 by Ewald R. Weibel and George Emil Palade (96). They are vascular 'first aid kits' and act as first responders to vascular injury, which triggers exocytosis of their powerful vasoactive cargo. Whilst all vasculature has a population of ECs, there is heterogeneity between vessel types e.g., veins and arteries, allowing optimised responses (97). Much like ECs themselves, WPBs are highly plastic, their composition reflective of their environment (98). VWF is the only ubiquitous protein, found in all WPBs and drives their biosynthesis and cargo recruitment (99). ECs experimentally depleted of VWF do not form WPBs, conversely non-ECs with artificially induced expression of VWF will form de novo pseudo-WPBs (100). Other cargo such as angiopoiten-2 and P-selectin are mutually exclusive and are not found in the same WPB populations as one another (101). VWF is packaged into WPBs at the Golgi apparatus, it is then stored within ECs. When ECs are stimulated, by either vascular injury or induced by a secretagogue such as histamine, VWF is release and unravels while remaining tethered to the EC (102, 103).

1.3.1 Morphology

WPBs are 0.1–0.3 by 1–4μm cigar shaped structures denoted by a striated appearance (104). Wagner et al established that VWF was the essential component in WPB biogenesis (105), they also demonstrated that the synonymous striations of WPBs are created by the longitudinal storage of VWF filaments within the organelle (**figure 1.7**) (100). When dissected in a longitudinal cross section, the observed striae are evident as hollow tubes (98). WPBs are encapsulated by a lipid bilayer which incorporates various membrane proteins during maturation such as Rab27a and Rab3b that endow the organelle with exocytotic capabilities (106).

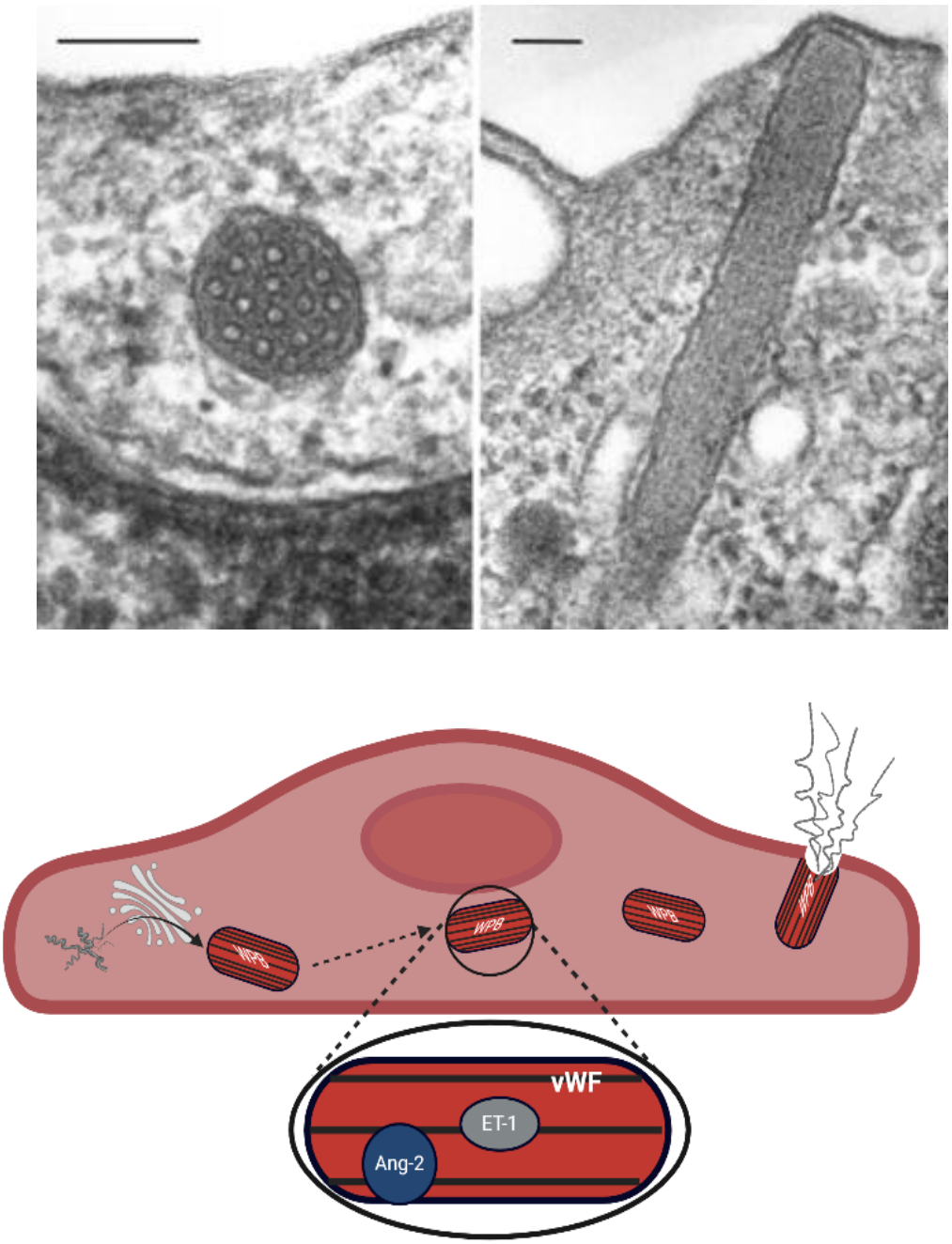

Figure 1.7. Cross sectional and longitudinal scanning electron microscopy (SEM) image of Weibel-Palade bodies illustrating the tubular structures of VWF contained within that gives rise to the characteristic striated appearance. SEM imaging adapted from (107). Accompanying schematic shows an EC with WPB biogenesis at the Golgi apparatus, highlighting three representative WPB cargo proteins and the stimulus-triggered release if VWF into the vessel lumen.

1.3.2 Biosynthesis

WPB biosynthesis is centred on VWF. Once synthesised the immature protein is transported to the ER where it undergoes post translational modifications including multimerization as outlined in **section 1.2.3**.

Following this VWF is transported to the trans Golgi network (TGN) where it undergoes further modification into defined 'quanta' and packaging into WPBs (**figure 1.8**) (108). At this stage, additional WPB-associated cargo is recruited to the site, allowing its incorporation into WPBs upon formation (99). Highly multimerised high molecular weight VWF is preferentially selected to be packaged and stored in WPBs (109). In a pH dependant process, tubulation of the protein is triggered, forming helicoid structures that compresses the VWF strings 100-fold. This compacts the VWF while maintaining the structural integrity, which is essential for its function (99). When tubulation is inhibited, shorter VWF strings are released, tangled together, in place of the long platelet catching fibrils needed for haemostasis. This impairs wound healing. Selective retention of helicoid structured VWF creates aggregation allowing compartmentalisation and promotes granule formation (99). Subsequently this starts protrusions that cumulate in budding off and separation of immature WPBs from the ER (99). From here, the immature WPBs migrate to the Golgi apparatus (110).

The Golgi apparatus is essential for WPB synthesis; the acidic milieu is required for maturation and conformational assembly of VWF for storage. It controls the morphology of WPBs, packaging VWF into the nascent WPBs (108). Populations of WPBs present in a range of sizes, high throughput confocal morphometry identified VWF correlated to the length of WPBs, they appeared in nanoscopic clusters, named as quanta (**figure 1.9**) (108). In vertebrates, the Golgi apparatus is formed of stacks, linked together through homotypic cisternal fusion forming a centralised structure (108). The importance of this structure was demonstrated by forcibly uncoupling of these links using a statin treatment. This resulted in the creation of 'ministacks' that were released individually. The ministack Golgi then synthesised a population of shorter, 'mini', WPBs (108). Heterogeneity of WPBs was retained even in this population, with variation in size observed, the majority of these WPBs contained only 1 quanta (package) of VWF (108).

Prior to WPB maturation, a scaffolding is constructed to support the structure and protect the integrity of the synthesised WPBs (111). This is formed of adaptor protein 1 (AP-1) and clathrin (111). Adaptor proteins are a family with specialised functions to interact with the heavy chain of clathrin and use membrane proteins to form a clathrin coat, binding to

specific cargo proteins, they will then localise to specific regions within the cell (112). AP-1 is specific to the TGN and facilitates movement of cargo and budding off vesicles (112). This coating is essential in creating WPBs with the characteristic rod-shaped structure. The AP-1 clathrin coat is a transient scaffold, aiding the movement of WPBs and forming a 'mould' to allow replicable and reliable formation of WPBs that are in the correct shape for function (113). Knockdown of AP-1 resulted in an increase in overall VWF expression in HUVECs, suggesting that AP-1 may hold an essential role in organisation of VWF into WPBs, without which we see an increase in unregulated release of VWF out of ECs (94).

Once synthesised by the TGN, the size of the WPBs is essentially determined. Immature WPBs are transported into the cytoplasm by microtubules, where they undergo maturation (114). The maturation process is marked by the recruitment of small membrane associated proteins including but not limited to Rab27a and Rab3D (104). There is a reduction in pH in the cytoplasm relative to the TGN, which promotes acidification, leading to further condensing of VWF within WPBs into helicoid structures. This compaction enhances protein stability and reduces the likelihood of spontaneous unregulated release from WPBs (114). WPB cargo are recruited and packaged at the TGN for examples, angiopoteiten-2 (Angpt-2) is tethered to VWF to ensure successful incorporation, alongside other components such as, P-selectin and eotaxin (99, 115).

Mechanisms involved in the maturation of WPBs have not been fully elucidated and are evolving concepts. Through depletion, biogenesis of lysosomal related organelle complex-2 (BLOC-2), a protein complex that is a component of endosomal protein trafficking, has been identified as an essential element of WPB maturation (116, 117). Without BLOC-2 there was a reduction in HMW VWF and ECs demonstrated misdirection of cargo via transport tubules from endosomes. Secretagogue stimulated VWF exocytosis, which occurs exclusively from WPBs within ECs displayed impairment (117). Moreover, CD63, a tetraspanin protein exclusively located in mature WPBs, was not identifiable in any WPB-like structures (118). The incorporation if CD36 into WPBs via endosomal pathways, alongside various other proteins, demonstrates that WPB maturation and cargo uptake are dependant of endosomal involvement.

Recruitment of de novo proteins equips WPBs with the machinery for successful exocytosis. GTPases are essential regulators of exocytosis, their incorporation enables WPBs to interact with the plasma membrane and cytoskeleton (109). Their activity facilitates membrane docking, fusion and then the controlled release of WPB cargo. The now mature WPBs are dependent on actin for dual functions, stability and anchoring and

for facilitating exocytosis. Proteins such as Rab27a and MyRIP mediate tethering of WPBs to the actin cytoskeleton (119). While actin itself also supports membrane docking and exocytosis (109).

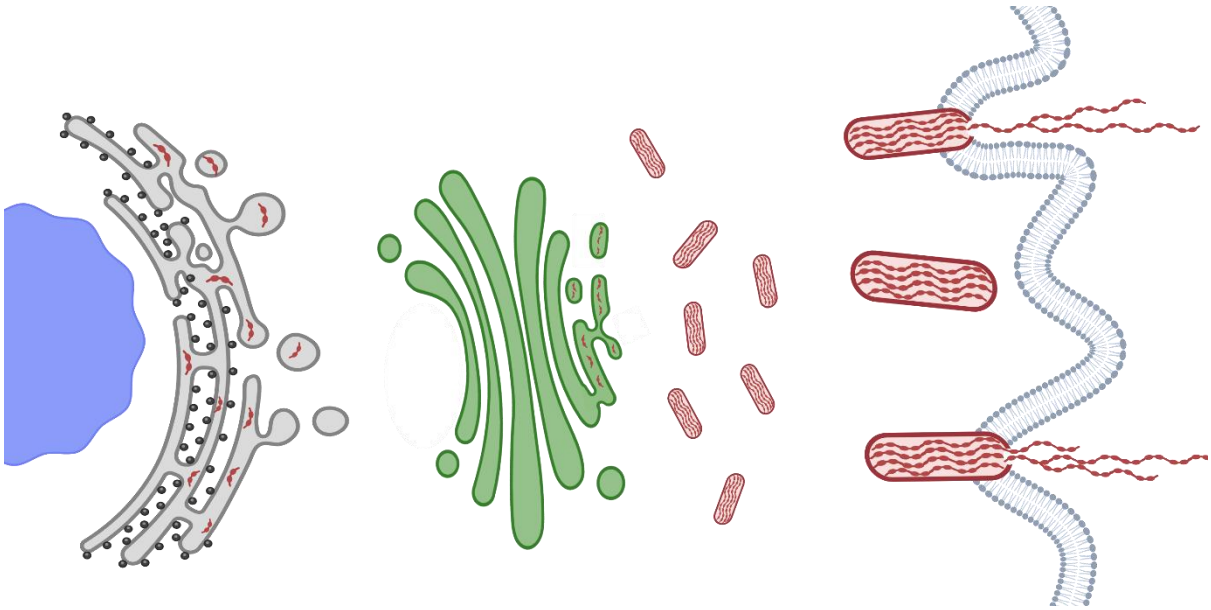

Figure 1.8 Schematic representation of WPB biogenesis within ECs. The process begins with VWF synthesis at the endoplasmic reticulum, followed by further multimerization and packaging in the Golgi apparatus. WPBs bud off from the trans-Golgi network and are trafficked into the cytoplasm where they mature and await stimulus-triggered exocytosis.

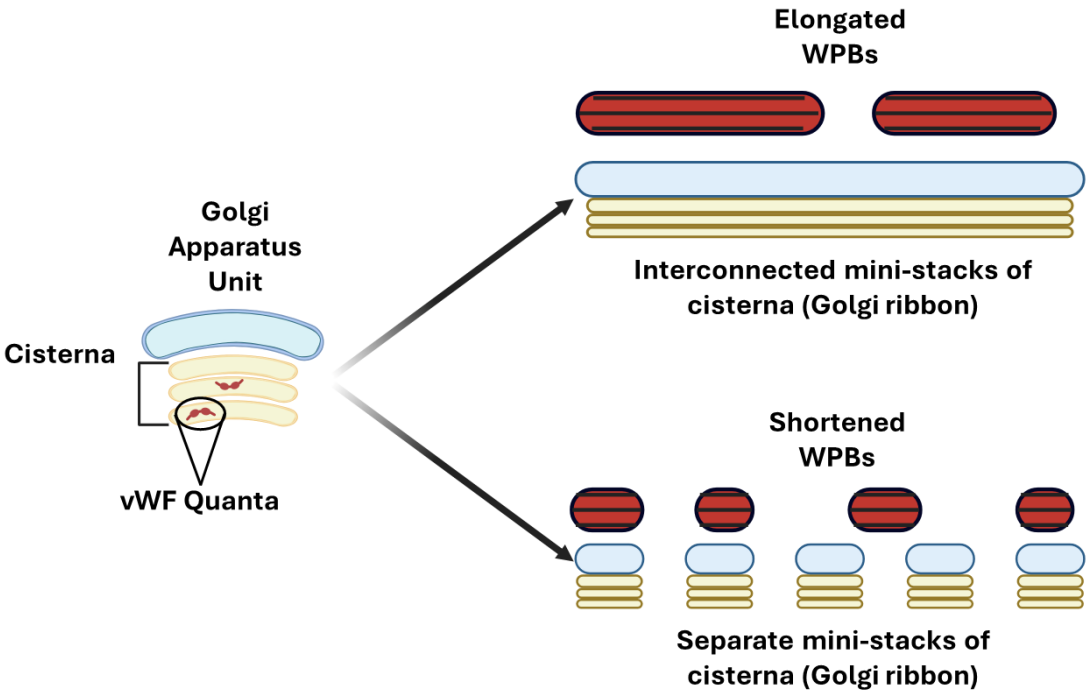

Figure 1.9 The size of WPBs is determined but the architecture of the Golgi apparatus. Long, continuous Golgi stacks support the formation of elongated WPBs, whereas shorter fragmented Golgi stacks give rise to shorter WPBs. Created in Biorender from, adapted from (120).

1.3.4 Cargo

As vascular first aid kits, WPBs contain a large number of cargo necessary to perform this role. This cargo is heterogeneous, WPBs from different vascular beds have specific profiles, asides from VWF, the only ubiquitous protein stored within them due to their necessary role in synthesis. Given this synonymous symbiotic relationship between VWF and WPBs see **section 1.2 for** an in-depth review of this cargo. Key WPB cargo and their associated function is detailed in **table 2**, an exhaustive list of WPB associated protein can be seen in **appendix**. In light of the multitude of WPB cargo and the subsequent vasoactive roles performed, tight regulation is vital in healthy functioning of the endothelium and blood vessels. When this is interrupted or deviates from regular function, it introduces the capacity for pathological downstream responses. I have detailed select WPB cargo emphasizing their physiological roles and the potential pathological outcomes when their activity becomes maladaptive.

As outlined in **section 1.3** angiopoetin-2 (Angpt-2) and P-selectin are mutually exclusive to WPB populations, they cannot be stored in the same vesicle (121). With roles implicated in modulating multiple activities within the vasculature e.g., angiogenesis, permeability and inflammation, Angpt-2 is a proangiogenic growth factor ligand for endothelial tyrosine kinase receptor Tie-2 (122). When Angpt-1 is removed, Angpt-2 will act as an agonist of Tie-2, conversely, in the presence of Angpt-1, Angpt-2 will act as an antagonist in the presence of Tie-2. EC health is reliant on Angpt-2, disruption to synthesis results in decreased phosphorylation of Tie-2 by 60-80% which has a domino effect on downstream pathways including a reduction in PI3K/Akt signalling (123). Moreover, the function of Angpt-2 varies with presence and absence of VEGF, when present together angiogenesis is upregulated, when VEGF is absent then vessel regression is favoured (115). As established, Angpt-2 is not presence in every WPB, to be selectively incorporated, it first binds to VWF which mediates the integration of Angpt-2 into the WPB (115). This occurs in environments that match the required pH and calcium concentration.

P-selectin is a glycoprotein leukocyte receptor, once released from WPBs it is rapidly translocated to the apical membrane of ECs whereby it promotes recruitment of neutrophils at the site of vascular injury (124, 125). P-selectin binds here to P-selectin glycoprotein ligand 1 (PSGL-1), which permits binding of leukocytes (126). It is a principle component of EC-leukocyte interaction termed leukocyte rolling which is required for adhesion of leukocytes at the site of injury (127). Leukocyte rolling occurs early in response to an inflammatory environment (128). P-selectin, primes bound leukocytes,

initiating intracellular signalling and provides contextual information aiding leukocytes to interpret their environment (126). P-selectin and VWF work in tandem to roll leukocytes and platelets along the endothelium, this is closely followed by initiation of expression of other adhesive molecules e.g. vascular-cell adhesion molecule 1 (VCAM-1) which creates a feedback loop by slowing rolling and adhesion of additional leukocytes and platelets from circulation (32). As well as residing within WPBs, P-selectin is present on the surface of activated platelets. In an inflammatory response, EC P-selectin modulates leukocyte rolling in blood vessels as well as their interaction with platelets (129, 130). Dysregulation leading to overexpression of P-selectin has been implicated in the development and progression of atherosclerotic lesions (32).

Table 1.2. Selected examples of WPB cargo and their associated functions in vascular biology. Highlighting the diverse roles WPB-stored proteins play in haemostasis, inflammation and endothelial signalling, while not exhaustive, it illustrated the multifunctional nature of WPBs and their relevance to physiological and pathological processes.

Protein	Function	References
VWF	Primary haemostasis & Thrombosis	(131),(132)
P-selectin	Primary leukocyte adhesion	(133),(134),(135)
Angiopoietin-2	Inflammation & angiogenesis	(121)
Interleukin-8	Granulocytes chemokine	(136)
Endothelin-1	Vasoconstriction	(137),(138)
Endothelin converting enzyme	Vasoconstriction	(139)
CD63/lamp3	Leukocyte adhesion	(140)
IGF binding protein 7	Angiogenesis	(141)

1.3.5 Trafficking

Following maturation, WPBs relocate to a peripheral location within the EC, Rab27a is require for this distribution (142). The actin cytoskeleton and microtubule transport system are essential for the trafficking and exocytosis of WPBs (119). WPBs are tethered to actin filaments by MyRIP and Rab27a to support localisation of the periphery of ECs, they act as anchors and regulate exocytosis (142). If overexpressed, Rab27a and MyRIP reduced WPB exocytosis (142). Use of secretagogues has demonstrated that actin may also regulated WPB exocytosis, if depolymerised, the rate, distance and frequency of WPB movement increases (142). Moreover, in cells treated to diminish actin presence, there was a recorded reduction in VWF release (142). Microtubules are essential in long range movement of WPBs within ECs transporting organelles from the perinuclear region out to the periphery (142).

There is a subset of WPBs that contain Rab46, a member of the Rab GTPase family synonymous with membrane trafficking, it has been demonstrated that Rab46 may regulate Ca^{2+} dependant trafficking of WPBs within ECs (143). When ECs were exposed to a proinflammatory stimuli such as histamine, the Rab46 positive population of WPBs migrated to the microtubule organising centre (MTOC) through dynein-mediated transport along microtubules (143). This retrograde trafficking did not occur if a pro thrombotic stimuli e.g., thrombin was utilised (143). It was uncovered that WPBs located at the MTOC did not contain P-selectin, a cargo required for an inflammatory response but did contain cargo such as Angpt-2, suggesting that histamine stimulation limited the response to vascular injury by restraining WPBs that contained cargo that would be extraneous to an inflammatory immune response (143).

1.3.6 Exocytosis

As established above, there are multiple mechanisms by which WPBs undergo exocytosis, they can fully collapse releasing the entire register of cargo, they can selectively release cargo and can cumulatively release cargo (144). Exocytosis of WPBs in the context of vascular injury is regulated release. It is made feasible due to the acquisition of specific machinery into the organelle that occurs at maturation, such as Rab GTPases, MyRIP and Munc13-4 (109). WPBs are tethered to release sites at the plasma membrane (containing the annexin A2–S100A10 complex) when activated to do so, held in place by the interaction of Rab27A and Rab15 to the Munc13-4 protein (109). Further binding of Rab27a and an isoform of Rab3 occurs with Slp4-a ((synaptotagmin-like protein 4-a)/granuphilin-a) to promote the exocytosis of WPBs (109). This results in a connection between the WPB

and SNARE (Soluble NSF Attachment Protein Receptor) complex which in turn catalyses the fusion of the WPB to the EC plasma membrane to allow exocytosis to occur (109). The attachment of the WPB to the plasma membrane creates a lipidic fusion pore that results in an aqueous channel allowing the movement of contents from the WPB lumen to the extracellular space (109).

Most commonly, WPBs will undergo full fusion and complete exocytosis, however, it has been demonstrated that as well as selectively incorporating cargo WPBs can selectively exocytose cargo via a mechanism called 'lingering-kiss' (145). Rather than observing total loss of cargo, this involves a modified fusion event whereby the characteristic rod morphology shifts to a spherical one and the fundamental WPB proteins including VWF are retained within (145). The retention of VWF within a membrane following fusion to the plasma membrane is thought to be achieved by control of the pore size, limiting it to prevent escape of these large proteins (145). In essence, the lingering-kiss mechanisms acts as a molecular sieve, granting exit to lower molecular weight proteins, ions and membrane components while retaining large core proteins (145). Intensity of stimulation is relational to the proportion of WPBs that undergo the lingering kiss event, under weak stimulation the incidence of events is greater, as such, there is a minimal change to the microenvironment of the vessel (145). Under intense stimulation, the incidence of lingering kiss event decreases, ergo a greater number of WPBs undergo depleting exocytosis (145). This implies that the purpose of the lingering kiss mechanism is to allow a dose-dependent release of cargo, to control the local microenvironment (145).

Selective release from WPBs is continued in the 'kiss and run' principle of exocytosis, allowing moderated release of inflammatory cytokines (146). It applies the same process as a molecular sieve by controlling the size of the fusion pore, in comparison to the lingering kiss mechanism, the kiss and run is a transient process, involving brief connection between the WPB and plasma membrane and formation of a narrow pore (146). Rapidly after fusion, WPBs lose their characteristic rod morphology collapsing into a sphere shape as VWF within becomes disordered, there was accumulation of plasma membrane specific components into the WPB membrane via lateral diffusion, followed by quick release to allow for retention of post-fusion WPBs (146).

Finally, there is the actin ring Ca^{2+} dependant release of cargo from WPBs, occurring in a subset of the population. In a manner of negative regulation of exocytosis, WPBs are anchored to the actin cytoskeleton via binding of proteins including Rab27a and MyRip etc (144). When ECs are stimulated via the inflammatory pathway e.g., with histamine, the

actin cytoskeleton undergoes a dynamic rearrangement, fundamental for effective release of VWF following exocytosis (144). If actin remains in a solid conformation, there is an observed higher incidence of WPBs remaining fused, when ECs were stimulated with histamine approximately 30% formed an actin ring to evoke exocytosis in a RhoA dependant process (144). These structures appeared within 1-7.6 seconds following fusion of WPBs to the membrane, they survived for several seconds, serving the purpose of stabilising the pore in the membrane to allow for prolonged exocytosis facilitating release of larger WPB cargo such as VWF (144).

1.3.7 Shear Stress and WPBs

As outlined in **section 1.1.4**, SS significantly modulates the phenotype of ECs, as WPBs are exclusively located in ECs their formation and function are also subjected to regulation by the same mechanical forces. It has been demonstrated that in ECs exposed to HSS, WPBs are significantly shorter than those cultured under static conditions (54, 59). This translated into alteration in functional ability, assessed by analysis of exocytosed VWF strings when ECs were stimulated. Ultimately it was suggested that this was driven by a fundamental reorganisation of the Golgi architecture which in turn governs the size of synthesised WPBS (54, 59).

The impact of Golgi morphology has been further demonstrated as a key determinant of WPB size. Upon statin treatment the typical ribbon-like structure seen in the Golgi was uncoupled resulting in the formation of ‘mini stacks’. These fragmented structures lacked the capacity to accumulate a sufficient number of VWF ‘quanta’ to synthesise elongated WPBs. As a result, shorter ‘mini’ WPBs were synthesised, mirroring those observed in ECs exposed to HSS (**figure 1.10**) (120). This serves as support that fundamental changes in Golgi architecture occur under SS and result in significant changes to WPB morphology.

WPB cargo composition appears to be influenced by SS exposure, reflecting the dynamic responsiveness of WPBs to their environment. Angpt-2 expression is regulated by SS, the atheroprotective laminar blood flow upregulates transcription factor KLF2, a flow-mediated micro-RNA (miR) that can in turn facilitate modification of gene expression (147). It has been demonstrated under pathological flow conditions, low oscillatory shear stress (LOSS), angpt-2 is upregulated resulting in a significant increase in recruitment into WPBs, compared to that observed under HSS (54). This demonstrates that SS not only induces structural changes in ECs and by extension WPB, it actively modulates the vasoactive constituents available to be incorporated as cargo.

1.3.8 WPBs and disease

WPBs have been identified as potential therapeutic targets in certain disease states, for example TTP (148). As mentioned in **section 1.2.2**, TTP is characterised by a deficiency in ADAMTS13 activity, if untreated it has a >90% mortality rate (148). The reduction in functional ADAMTS13 prevents the proteolysis of VWF released from ECs into the plasma which results in accumulation of UL-VWF multimers, that have the highest affinity to platelets (148). These multimers induce formation of excess platelet thrombi, which has pathological consequences (148). Patella et al sought to exploit WPB modification to assess if artificially 'shrinking' WPBs could reduce the presence of UL-VWF in TTP patients, in turn moderating the thrombotic environment of vessels and reducing platelet aggregation (148). HUVECs were treated with a fluvastatin treatment to induce 'shrinking' of WPBs, through unlinking of the Golgi apparatus ribbons, and were then exposed to TTP patient plasma (148). The fluvastatin treated HUVECs were observed to have a considerable reduction in VWF string length and in platelet adhesion, compared to untreated cells (148). This study suggests that WPBs are a viable target for therapeutic modulation for clinical interventions of vascular related disease.

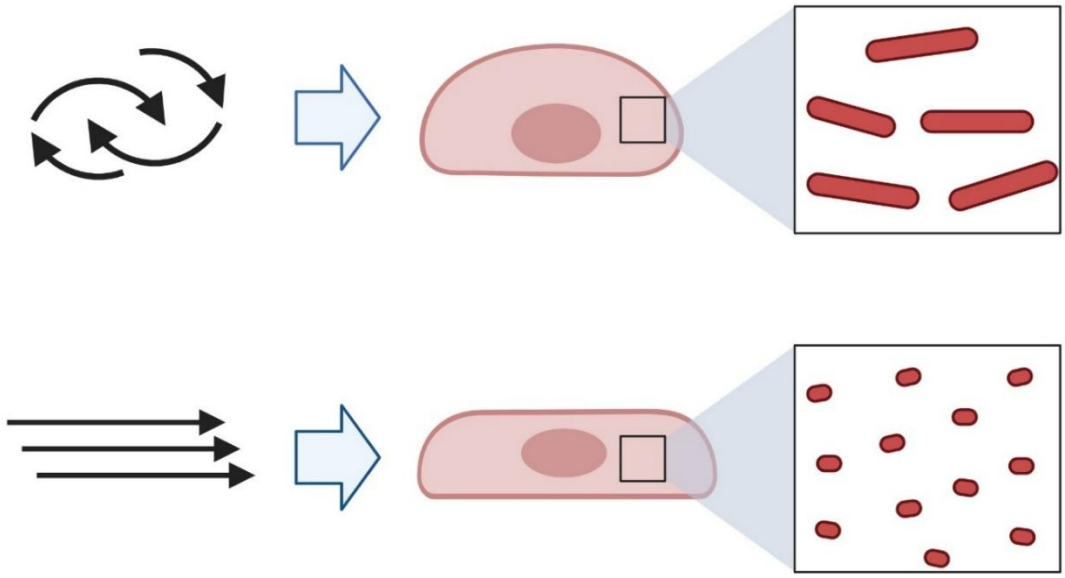

Figure 1.10 The type of shear stress experience by endothelial cells influences the length of WPBs synthesised. Exposed to turbulent or oscillatory flow promotes the formation of longer WPBs, while high shear laminar stress favours the synthesis of shorter WPBs. This mechanosensitive modulation of WPB morphology reflects the dynamic relationship between vascular flow patterns and endothelial secretory architecture.

1.4 Endothelial dysfunction

Endothelial dysfunction causes the normally tightly regulated endothelium to lose co-ordination with the environment, resulting in loss of function preventing successful homeostasis and is a well-established precursor to CVD (149). Endothelial dysfunction (ED) is classically defined by under expression of nitric oxide (NO) by ECs, initiating a breakdown in normal vascular function. A decline in NO bioavailability leads to vasoconstriction and increased oxidative stress. However, ED encompasses a broader spectrum of impairments including disrupted coagulation control and altered vessel permeability (16). Alongside diminished NO, a dysfunctional endothelium will promote generation of reactive oxidative species (ROS), TNF-α and intercellular adhesion molecule 1 (ICAM-1) fostering a pro-inflammatory environment within the vessel (150). In addition, this environment triggers release of adhesion molecules from ECs and leukocytes including, VWF, P-Selectin and E-Selectin which further amplifying dysfunction (151).

ED has been implicated in a variety of disease aetiologies. It can act as an ignition of disease or an accelerant. In atherosclerosis, ED can act as a trigger point, the environment facilitating pro-atherogenic plaque deposition (151). Diabetes increases the likelihood of developing atherosclerosis but is also associated with endothelial dysfunction in of itself.

Several features of diabetes contribute to the onset of vascular pathology, particularly insulin resistance and hyperglycaemia (blood glucose outside of normal range, see **section 1.5.2.2**). Elevated blood glucose levels promote the formation of advanced glycation end products (AGEs), which in turn reduces NO bioavailability and an increase in inflammatory mediators such as ROS and interlukin-6 (Il-6) (152). This is compounded by increased oxidative stress and uncoupling of eNOS, resulting in superoxide generation (151, 153). Together, these factors impair endothelial function and can drive the development of serious vascular complications such as diabetic nephropathy (151, 152).

1.5 Diabetes Mellitus

Diabetes mellitus, a metabolic disorder with varying aetiology, typically it can be classified into type 1 (T1DM) and type 2 (T2DM) (154). Overall, diabetes is characterised by dysfunction between feedback loops in insulin detection in insulin-sensitive tissues such as the liver and secretion of insulin by pancreatic islet β-cells (4). The dysregulation of insulin action and secretion results in inadequacy of the body to utilise glucose and stabilise blood sugar levels, giving rise to hyperglycaemia (4, 155). Hyperglycaemia in turn causes damage to endothelial function, increasing the presence of ROS, impairing NO activity and increasing inflammation (156). This endothelial dysfunction can advance in both T1DM and T2DM and contribute to vascular complications associated with diabetes (156). Glucose criteria are essential diagnostic modalities of both T1DM and T2DM (155).

T1DM presents as an autoimmune condition in which β-cells, located in the pancreas, are damaged or destroyed by the body. These cells mediate production of insulin therefore damage/destruction of them results in disruption or dysregulation of glucose management (157). T1DM varies within a population however the primary defining characteristic is insulin deficiency (157). In contrast, the pathophysiology of T2DM is defined by resistance to insulin that can progress to a compensatory over expression of insulin called hyperinsulinaemia (157).

Other aetiologies of diabetes do exist for example, gestational diabetes (GDM), however this is a transient diagnosis and only exists in pregnant women (158). It affects approximately 9-25% of pregnancies worldwide with increasing prevalence and post pregnancy increases a mother's likelihood of developing T2DM (159). There are multiple different co-morbidities of diabetes, of which, those that are associated with the heart and vasculature are the focus here.

1.5.1 T1DM and T2DM aetiology

Typically, T1DM is diagnosed in childhood or as a young adult. Symptoms prompting T1DM diagnosis include hyperglycaemia (explored further in **section 1.5.2.2**) detected in random blood tests (with plasma glucose exceeding 11.1 mmol/L), polyuria and polydipsia. In severe cases presentation an acute complication of diabetes, diabetic ketoacidosis, which presents with nausea, abdominal pain, dehydration and tachycardia (160). Finally, in some cases diagnosis is aided by assessment of diabetes-related autoantibodies, which is presence of antibodies against glutamic acid decarboxylase (GAD), islet cells and insulin would be expected in T1DM.

Conversely, T2DM aetiology is characterised by impaired insulin signalling and insulin resistance, worsened by risk factors such as age, hyperglycaemia, hypertension and BMI (body mass index) (161). A clinical T2DM diagnostic presentation is established by the presence of risk factors and symptoms such as fatigue, blurred vision and in some cases polyuria and polydipsia (162). However, T2DM may also present asymptomatically, in which case it is typically detected through routine blood screening. A prolonged period of hyperglycaemia is a diagnostic feature of T2DM. Haemoglobin A1c (HbA1c) is a biomarker identifiable through blood testing (163). The baseline for diagnosis is an HbA1c value of 48mmol/mol (6.5%), it reflects the average blood glucose concentration over 2-3 months and is a key diagnostic biomarker and is used for monitoring of diabetes (163). Elevated fasting plasma glucose (≥7.0 mmol/L) and elevated random plasma glucose (≥11.1 mmol/L) are additional tests used to assess this (162).

With evolving populations, previous markers attributed exclusively to one type of diabetes have become blurred. For example, age of T2DM diagnosis is decreasing while BMI of those diagnosed with T1DM increases (164). As such, multiple clinical markers are cross compared for diagnosis of both T1DM and T2DM (164).

1.5.2 Characteristics of Diabetes

Despite the inherent differences in T1DM and T2DM there are characteristics that are experienced in both.

1.5.2.1 Vascular dysfunction leading to complications

Typically, vasculature is tightly regulated to maintain homoeostasis, with the endothelium orchestrating responses to physiological demands. Disruption or dysregulation of this system is a hallmark of complication in both T1DM AND T2DM (165, 166). When the vascular environment becomes imbalanced or impaired, the endothelial profile shifts from one of healthy regulation to a pro-thrombotic and pro-inflammatory state (15). As the central regulator, the endothelium monitors and modulates the release of vasoactive compounds to shape the vessel microenvironment, making it highly responsive to internal and external cues (167). Impairment of this control mechanism has been linked to a range of disease states, weakening vascular resilience and allowing pathologies to take hold (3, 168, 169).

1.5.2.2 Hyperglycaemia

Impairment to glucose regulation is one of the most well-characterised hallmarks of T1DM and T2DM. When glucose levels exceed the normal physiological range, a patient is

considered to be experiencing hyperglycaemia. Clinically, hyperglycaemia is defined as blood glucose levels exceeding 48 mmol/mol in a nonfasted state or over 7 mmol/L fasted (170). If left unmanaged, chronic hyperglycaemia can lead to serious vascular complications associated with diabetes. Consequently, hyperglycaemia has become a highly explored area of diabetes research. In *in vitro* models, hyperglycaemia is typically represented using a 25mM glucose concentration to mimic pathological conditions of the condition (171-173).

1.5.2.3 Metabolic Activity

A key distinction between diabetic and healthy cells lies in their metabolic activity. In healthy cells, glucose uptake, mitochondrial function and redox balance are tightly regulated to maintain homeostasis. In contrast, diabetic cells are exposed to chronic hyperglycaemia, leading to excessive oxidative stress and mitochondrial dysfunction. Within the endothelium, this hyperglycaemic stress imposes a concentrated metabolic burden, altering both the cellular function and phenotype of ECs in diabetes. These shifts contribute to endothelial dysfunction, as outlined in **section 1.4,** resulting in reduced NO bioavailability and elevated oxidative stress. Consequently, the endothelium's ability to regulate vascular homeostasis and maintain essential signalling is impaired, diverging from the behaviour observed in healthy cells (174).

In diabetes, the phosphoinositide-3-kinase–protein kinase B/Akt (PI3K/Akt) signalling pathway undergoes significant dysregulation making it a primary target of metabolic disruption. Under healthy physiological conditions, activation of insulin receptors initiates the PI3K/Akt signalling cascade, leading to Akt phosphorylation. Akt is multifunctional, among other roles, once phosphorylated it regulated cellular metabolism (175). The dysregulation of this pathway has been linked to development of T2DM and associated complications (176). Hyperglycaemia inhibits insulin signalling by reducing the availability of insulin signalling components (IRS proteins), suppressing Akt activation (176). Reduction in Akt phosphorylation results in less pAKT being produced which translates to a reduction in eNOS phosphorylation downstream (177). This impairs the production of NO and subsequently contributes to oxidative stress and endothelial dysfunction by extension. Processes such as oxidative stress and endothelial dysfunction are implicated in pathological processes and have been linked to diabetes associated vascular complications.

1.5.3 Vascular complications of diabetes

Cardiovascular complications are increasingly prevalent with diabetic populations, at both a macro and microvascular scales. Vasculature related complications are core contributors to increased morbidity and mortality within both T1DM and T2DM populations (178). In the macrovascular domain, complications include atherosclerosis (increasing risk of CVD), stroke and myocardial infarction (MI). Whereas the microvascular complications include retinopathy, nephropathy and neuropathy (179). In 2021/22 diabetes-related treatment in the UK was estimated to cost £10.7 billion, of this approximately 40% of this was attributed to diagnosis and direct management, while the remaining 60% reflected the cost of addressing complications (180). An additional £3.3 billion was linked to indirect costs of care (180). Globally, diabetes and its associated complications account for an estimated 12% of total health expenditure (181). Diabetes associated complications are broadly categorised into macrovascular and microvascular, each with further sub-classifications.

1.5.3.1 Macrovascular

Diabetes is a well-established risk factor for CVD, which persists as the leading cause of mortality among diabetic populations, specifically due to MI (182). However, advancement of contemporary interventions has contributed to an overall reduction in mortality rates compared to historic levels (182). Diabetes introduces states of hyperglycaemia an insulin resistance into the vascular environment, this is thought to contribute to the pathophysiology of CVD-related complications (183). In individuals with no prior history of cardiovascular events, the risk of MI is significantly elevated in those with diabetes, estimated at 20% compared to 3.5% in non-diabetic individuals (183). The diagnosis of diabetes markedly increases the likelihood of developing coronary heart disease, a risk further compounded by reduced treatment efficacy in diabetic patients (183). It has been demonstrated by meta-analysis that likelihood of stroke is 2.3x higher in diabetic patients compared to non-diabetics and is associated with worse clinical prognosis post-stroke occurrence (183). Peripheral artery disease (PAD) is another common macrovascular complication of diabetes, characterised by progressive atherosclerosis and associated narrowing of artery walls (183, 184). This condition carries a serious risk of loss of limb due to ischemia resulting from occlusion of arteries (184).

1.5.3.2 Microvascular

As outlined above, the majority of microvascular complications associated with diabetes fall into three broad categories: neuropathy, nephropathy, and retinopathy. Diabetic

neuropathies involve a loss or reduction in sensory function, typically initiating in extremities and progressing with associated pain and increased morbidity (181). Approximately 50% of individuals who received a diagnosis of diabetes will develop some presentation of neuropathy, the most common is distal symmetric polyneuropathy although other presentations may include cardiovascular and gastrointestinal symptoms (181). Diabetic nephropathy refers to progressive renal damage that can lead to end stage renal failure, most frequently affecting the T2DM population, it has a prevalence of approximately 40% (185). Albuminuria, the presence of a blood associated protein (albumin) in urine, is the most utilised biomarker for diabetic nephropathy, indicating glomerular filtration dysfunction and advancing kidney failure (185). Finally, diabetic retinopathy (DR) is generally classed into 2 stages, proliferative (PDR) and non-proliferative retinopathy (186). PDR is considered the end stage of disease often characterised by aggregation of fibrous tissue and hypoxia induced damage to tissue at the back of the retina. Globally, DR prevalence has increased from 14.9% to 18.5% in a 30-year period from 1990 to 2020, making it the 5th leading cause of blindness, but critically it is a preventable one (187).

Disruption or dysregulation within vasculature is the hallmark of these complications for both T1DM and T2DM (165). Established in **section 1.4** endothelial dysfunction plays a central role in the pathogenesis of many diabetic complications and cardiovascular disorders. A healthy endothelium maintains vascular homeostasis by preventing unnecessary pro-thrombotic or inflammatory responses (15). Emerging evidence suggests that endothelial dysfunction, including aberrant unwarranted exocytosis of WPBs cargo may exacerbate the pathological vascular environment in diabetes to accelerate progression of complications.

This underscores the severity of complications associated to diabetes not only in terms of quality of life and mortality of those affected but also in the tangible and systemic costs to the healthcare system. It highlights the critical need to advance our understanding of disease mechanisms to develop more effective interventions.

1.6 Diabetes and WPBs

WPBs act as a molecular reflection of the endothelial cell microenvironment, calibrating contents in response to haemostatic forces. This adaptability is a double-edged sword: in healthy conditions, it enables WPBs to tailor their behaviour to the demands of distinct vascular beds; however, the impact of pathological environments on WPB structure and function remain underexplored. As established, WPBs carry a multitude of powerful cargo, and their tightly regulated release is essential for maintaining vascular homeostasis. There is evidence to suggest that under disease states WPBs regulation become disrupted and may contribute to a pathological intracellular environment. For example, WPBS are altered in size and function under shear stress, with loss of shear stress increasing the thrombotic potential of the phenotype that may contribute to atherosclerosis (59).

Diabetes is disease with well-established links to impaired blood flow and delayed of wound healing, both processes in which WPBs are implicated (188-190). Elevated plasma levels of VWF in diabetic patients with a comorbidity of CVD are not isolated findings; multiple studies have demonstrated associations between diabetes and WPBs dysregulation, both in clinical and basic science contexts (191-196). As established, WPBs play a central role in vascular injury and, by extension, wound healing. Diabetes offers a relevant pathological model in which to investigate their contribution given the disease well-documented impairment of wound healing (188). It has been demonstrated that WPBs are subject to modification in a diabetic disease state in an *in vivo* disease model. Following reports that diabetic patients had elevated plasma levels of VWF compared to those without a diagnosis, Anderson et al in 1994 induced dogs with diabetes for a five-year period, and subsequently harvested the retinal tissue from diabetic and control animals (191). Using streptozotocin and alloxan injections, with glucose sustained between 15-20mM by use of insulin injections, Anderson et al induced a diabetic phenotype young male dog, animals were maintained for five years with glucose sustained between 15-20mM by use of insulin injections (191). Following this, animals underwent enucleation and analysis of the retinas (191). When compared to the control condition, ECs from veins from diabetic retinas presented a significantly higher volume of WPBs (191) i.e. there was a greater number of WPBs synthesised. This provided support for previously identified associations between elevated VWF levels demonstrated in endothelial cells cultured in higher glucose media aimed to mimic hyperglycaemia attributed to a diabetic state may be an attributable factor in the dysregulation of VWF. Potentially by enhancing synthesis of the protein (191). When widening the study to additional vascular beds, e.g. arterial and capillary, there was no significant differences

observed between the diabetic and control conditions (191). As seen in **section 1.3** populations of WPBs from different vascular beds vary to one another, the difference significance observed supports the indication that WPBs are responsive to the specific environments in which they are synthesised creating different effects. Suggesting that diabetes influences EC behaviour and subsequently WPB biogenesis in a manner not yet fully understood.

A similar observation was reported in a diabetic induced mouse model. Popov et al in 1997 used a similar approach, inducing T1DM in mice using streptozocin, without administering treatment to manage the condition allowing unchecked progression of hyperglycaemia (196). Multiple pathological changes were observed across various different organs and tissues but the most relevant in this context were those affecting the aortic endothelium (196). Diabetic mice exhibited an abundance of secretory and degradative components and a 2.8-fold increase in the number of WPBs observed in the endothelium when compared to control animals (196). This was accompanied by both morphological and function changes to characteristics of both the lungs and kidneys in the mice between the diabetic and control conditions (196). Further supporting the association between diabetes and WPB dysregulation (196). This association was not only identified in canines and mice, alterations to WPBs as a result of a diabetic microenvironment was identified in humans. Popov and Simionescu 1997 next induced a diabetic phenotype in hamsters again using streptozocin. Once again it was observed that in animals with induced diabetes there were structural transformations to the internal organs and an 'observed abundance' of WPBs within the venular endothelium of the lungs (197). Based on this, they themselves posited that initiation and or progression of diabetes may be responsible for elevating plasma concentration of VWF as had been previously recorded in diabetic patients. Collectively, the data indicates that diabetes has the capacity to drive vascular dysfunction at both a micro and macrovascular level, with WPBs emerging as a possible mechanistic link.

The link between diabetes and VWF was echoed in a double blinded clinical study comparing individuals with T1DM without retinopathy to those with minimal retinopathy. Although analysis of VWF was not the primary aim of the study, elevated plasma concentrations were observed and prompted further study (194). The study concluded that increased VWF levels correlated with prolonged retinal circulation and reduced blood flow in early-stage retinopathy, creating a hypoxia environment conducive to microvascular damage (194). Critically, Feng et al. emphasised the need for further investigation into the relationship between VWF and diabetes. This association has been

further supported by a transcriptomic analysis comparing human retinas from patients with T1DM and retinopathy to non-diabetic individuals with proliferative vitreoretinopathy (198). Using an RNAseq approach, the study revealed significant differences in the gene expression profiles between the two groups, including marked up and downregulation of genes linked to WPBS (198). Notably, VWF was among the top 30 most significantly affected genes showing clear upregulation in the diabetic retinas (198). These findings reinforce the connection between diabetes and WPB dysregulation, particularly in the context of microvascular complications (198).

Together these finding position VWF as a promising biomarker for endothelial dysfunction specifically in diabetic patients, reflecting both WPB dysregulation and the broader vascular disturbances characteristic of the disease.

1.6.1 VWF as a biomarker in diabetes

Plasma levels of VWF typically rise in response to vascular injury, facilitating formation of a platelet plug (see **section 1.1.2**). As a result, VWF has been garnered considerable interest as a potential biomarker for cardiovascular conditions. CVD is a well-established complication of diabetes. Multiple studies have demonstrated that VWF may serve as a predictive biomarker for CVD risk specifically within diabetic populations but not among individuals without a formal diagnosis of diabetes (192). While no significant associations have been observed between VWF levels and Ischaemic Heart Disease (IHD), cardiovascular events, or cerebrovascular events in the general populations, a significant correlation has been identified in high-risk groups including those with metabolic disorders such as diabetes (p=0.04). This association has been subsequently replicated, in independent cohorts with significantly elevated VWF levels observed in diabetic patients compared to controls (p=0.02) (192, 193, 199, 200).

In its active state, VWF is functionally capable of binding to and aggregating platelets, aberrant timing of VWF activation can contribute to a pathological thrombotic event. A clinical study demonstrated that both inactive and active VWF levels were significantly higher in diabetic populations compared to age matched control groups up to 60 years of age. Moreover, VWF concentrations positively correlated with diabetes duration, reinforcing its potential role as a predictive biomarker for diabetes associated vascular impairment and damage (195). As discussed above, diabetic retinopathy, a major microvascular complication of diabetes, further supports a link between VWF, WPBs and diabetes. Several other studies have reported significantly elevated VWF levels in diabetic populations often accompanied by abnormalities in multimerization particularly in

complex conditions such as retinopathies (201-203). Collectively, these findings suggest that VWF is frequently and significantly associated with diabetes often preceding vascular complications. However, further investigation is needed to fully elucidate the underlying mechanisms and to develop targeted interventions.

Beyond its role as a biomarker, the persistent elevation of VWF in diabetic populations may reflect deeper, long lasting changes in EC behaviour, prompting investigation into the concept of metabolic memory and its implications for vascular dysfunction.

1.7 Metabolic memory

Metabolic memory refers to the phenomena whereby prior exposure to stimuli incurs epigenetic modifications to gene expression that persist even after the stimulus is removed (204). This has been demonstrated within the vasculature, although the underlying molecular mechanisms remain incompletely characterised (204). In the context of diabetes, prolonged exposure to hyperglycaemic conditions is thought to reprogram ECs towards a dysfunctional phenotype, marked by increased inflammation, oxidative stress and cellular senescence (205). One review proposed that the oxidative stress associated with a hyperglycaemic environment may serve as a stimulus contributing to a pathological shift in metabolic memory (206). Supporting this, another study demonstrated that hyperglycaemia induced NF-κB signalling via upregulation of multiple micro RNAs (miRs) that in turn downregulated NO availability and increases ROS generation, ultimately triggering endothelial-to-mesenchymal transition (EndMT) (207). EndMT is a known contributor to cardiovascular complications.

Importantly, the pathological shift in endothelial phenotype persisted even after cells were returned to a normoglycemic condition, suggesting that metabolic memory may have been reprogrammed towards a sustained dysfunctional state (207). The long-term implication of this is that irrespective of treatment, prolonged periods of uncontrolled diabetes may embed maladaptive metabolic drivers within ECs, making disease management increasingly difficult (205). Understanding these mechanisms offers a novel paradigm for diabetes research and presents new opportunities for therapeutic intervention.

Taken together, diabetes presents a complex and costly challenge marked by widespread vascular complications and persistent endothelial dysfunction. Central to this pathology is the disruption of WPBs and the elevation of VWF which may serve not only as a biomarker but as a mechanistic contributor to disease progression. The emerging concept of metabolic memory adds further depth, suggesting that prolonged hyperglycaemic exposure may epigenetically reprogram ECs towards a sustained dysfunctional state. Understanding how WPBs respond to such chronic stresses within a physiological environment offers a compelling avenue for investigation and potential therapeutic insight.

Chapter 2 – Methods and Materials

2.1 Cell Culture

2.1.1 HUVECS

Pooled Human Umbilical Vein Cells (HUVECs) (PromoCell) were cultured in basal endothelial cell growth media with a supplement pack (PromoCell) and Antibiotics-Antimycotic 100x (Gibco) added forming endothelial growth medium (EGM-2). Cells were maintained in a 5% CO2 environment in a 37°C incubator. Cells were utilised between passages 0-5.

2.1.2 hAEC

Primary human aortic endothelial cells (hAECs) from both the ascending and descending aorta (PromoCell) were cultured in Endothelial Cell Growth Medium MV2 (EMV-2) supplemented with Growth Medium MV2 supplement pack (PromoCell) and Antibiotics-Antimycotic 100x (Gibco). Cells were maintained in a 5% CO_2 environment in a 37°C incubator. Cells were utilised between passages 0-5. These patient cells had no formal diagnosis of diabetes.

Table 2.1 Cell line information provided by Promocell for control hAECs and the pair they were assigned to

Lot Number	Sex	Age	Experiment Pair
483z027.6	F	49	A
494z012	M	56	B
479z021.2	F	75	C

2.1.3 dhAEC

Primary human aortic endothelial cells ascending and descending aorta (dhAECs) from 3x patients formally diagnosed with type II diabetes (Promocell) were cultured in EMV-2 supplemented with Growth Medium MV2 SupplementPack (PromoCell) and Antibiotics-Antimycotic 100x (Gibco). Cells were maintained in a 5% CO_2 environment in a 37°C incubator. Cells were utilised between passages 0-5.

Table 2.2 Cell line information provided by Promocell for dhAECs and pairs they were assigned to

Lot Number	Sex	Age	Experiment Pair
4727002.1	M	62	A
482z007.2	M	63	B
431z013.5	F	38	C

2.2 Cell culture conditions for diabetic models

2.2.1 High Glucose Model

EGM-2 was adapted to a high glucose concentration and a mannitol osmolality control. Standard EGM-2 has a glucose concentration of 5.5mM, to raise this to 25mM, 19.5mM of filtered D-(+)-Glucose Solution (100 G/L in H_20 555mM) (Merck) was added, and molarity confirmed using GlucCell® Glucose Monitoring System (Merck). For the mannitol (D-mannitol (M4125, Sigma-Aldrich, UK)) control, a volume equating to 19.5mM was added to EGM-2 to match the level of additional glucose, osmolality was assessed via osmometer (Model 3320, Advanced Instruments, USA). Cells were cultured in a constant glucose concentration for 48 hours.

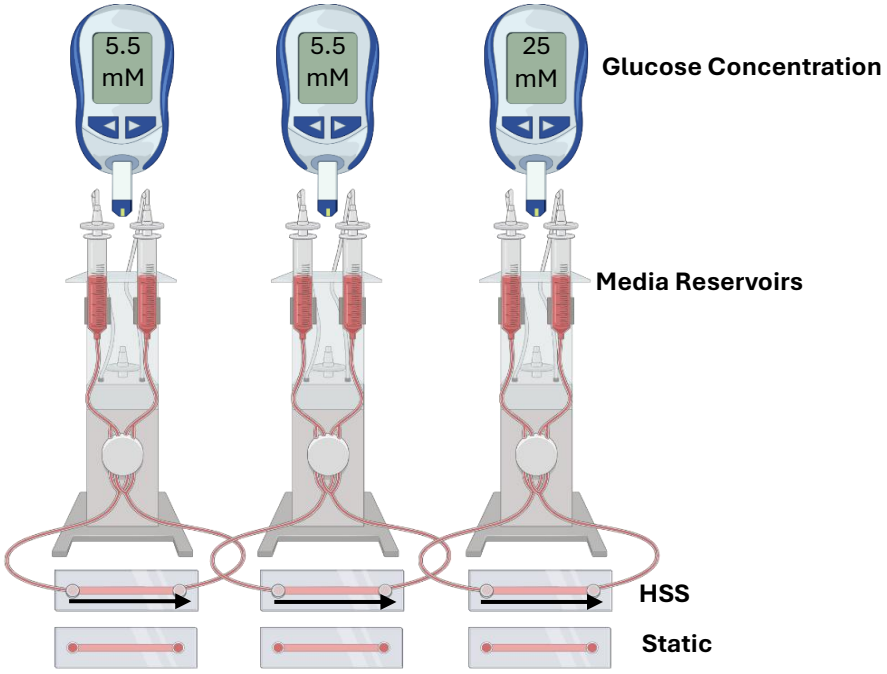

Figure 2.1 High glucose model of diabetes with cells in both static and SS environments. ECs were maintained for 48hrs under normo-glycaemic (5.5mM) EGM2, mannitol supplemented and high glucose supplemented media in both static and HSS environments.

2.2.2 Ambulatory Glucose Model

This model was developed based on continued glucose monitoring data to replicate the extremes in glucose fluctuations throughout an 'average' 8-hour day with 'average' eating habits derived from continuous glucose monitoring data (208) see **figure 2.2**. Custom glucose free EGM-2 media (Promocell) was adapted to reflect extreme clinically relevant hypo and hyperglycaemic environments in either T1DM or control conditions. EMG-2 was supplemented with filtered D-(+)-Glucose Solution (100 G/L in H_20 555mM) (Merck) to create the appropriate conditions. The T1DM model was comprised of low glucose at 2.5mM and high at 20mM conditions and the control of low glucose at 5.5mM and high at 10mM. Cells were placed under the appropriate high glucose condition and 48hrs of HSS was started. After 2hrs cells were moved to the corresponding low glucose condition. This cycle occurred for 10hrs at which cells were left in the low glucose conditions to reflect night, the time in which a person would typically be asleep.

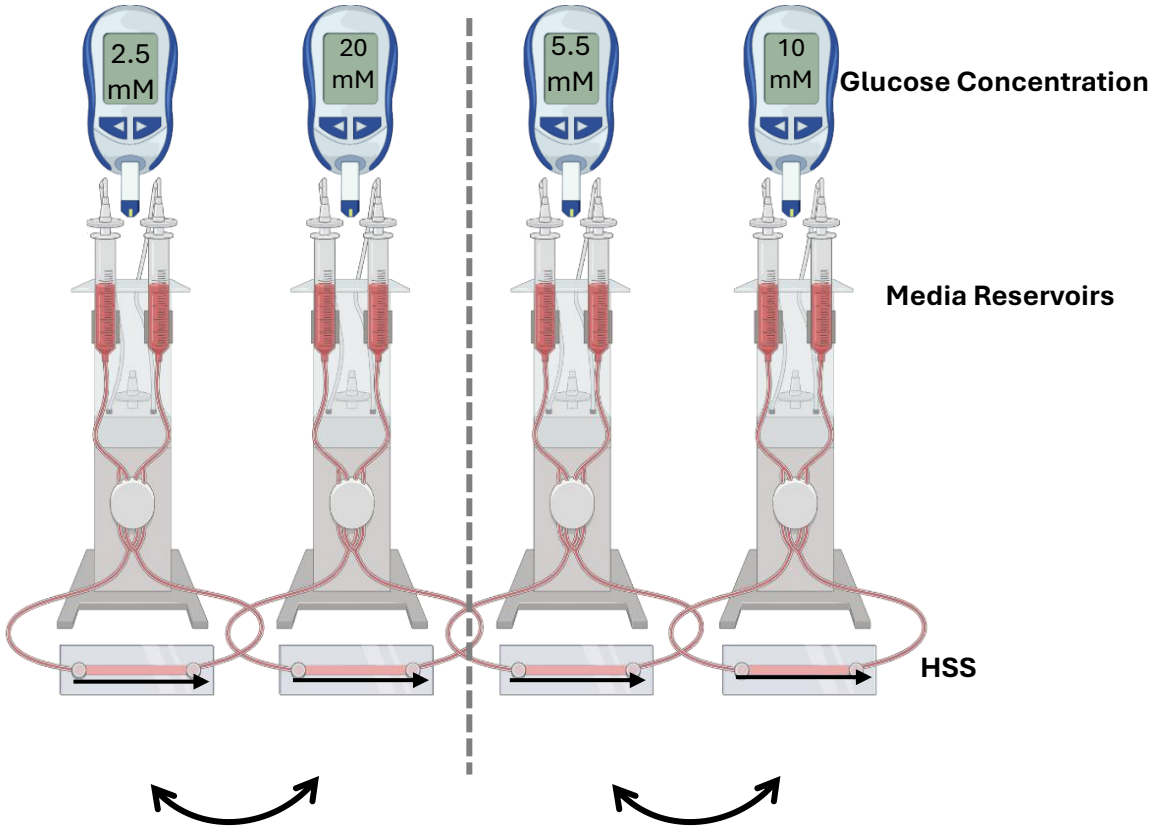

Figure 2.2 Ambulatory glucose model of diabetes with cells in SS environments. ECs were maintained for 48hrs, glucose was cycled between a hypo and hyperglycaemic environment for two twelve-hour periods to mimic an 'average' day of blood glucose fluctuations with eating.

2.2.3 Diabetic Cell Model

hAECs and dhAECs were maintained in EMV-2 as described under culture conditions (both static and HSS) for 48 hours (see above).

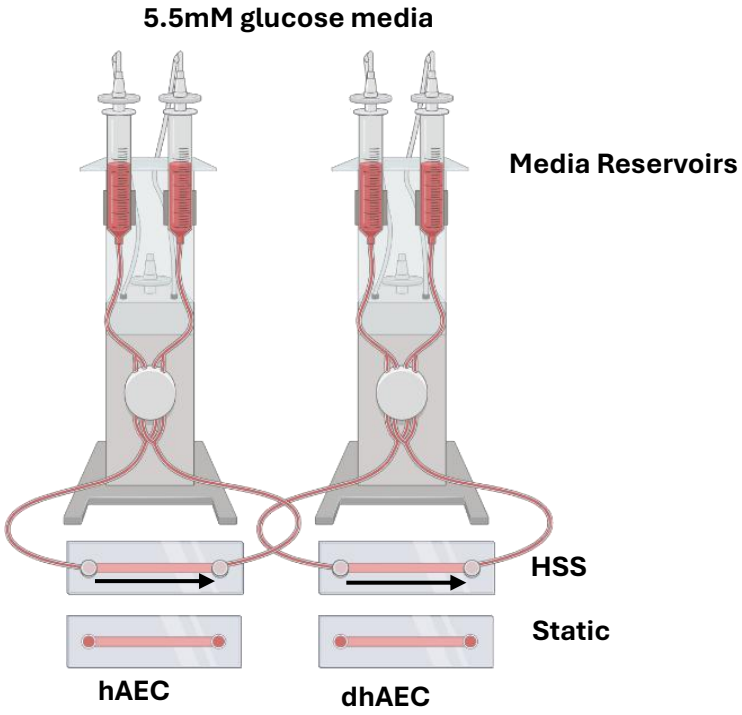

Figure 2.3 Physiological cell model of diabetes with human aortic ECs and diabetic human aortic ECs in SS environment. ECs were maintained for 48hrs under normo-glycaemic (5.5mM) MV2 media in both HSS and static culture.

2.3 Shear Stress

2.3.1 Cells

All experimental cells were subjected to shear stress (SS) for the timeframe of the experiments unless otherwise stated. Cells were detached, spun (100xG 5min) and 100µl plated at $7.5x10^5$ cells/ml on IBIDI µ-Slide I 0.4 Luer (ibiditreat) (IBIDI). Cells were incubated for 30 minutes, had reservoirs filled (60µl of media) then were incubated for 18-24hrs. Prior to flow, the media was changed to the appropriate condition where applicable.

2.3.2 IBIDI Microfluidics System

2.3.2.1 Laminar Shear Stress/High Shear Stress (HSS)

The IBIDI pump system was used to generate shear stress using red perfusion kits (IBIDI). Parameters to determine optimal shear stress rates using this microfluidics system were taken from Money et al (59). Optimisation experiments were conducted to assess the required dyn/cm^2 needed to evoke a repeatable HSS phenotype in endothelial cells. This also included optimisation of perfusion kit, microslide depth and number of seeded cells. Fluidic units were incubated at 37°C 5% CO_2 to acclimate prior to commencing. The IBIDI pump control software parameters were used to set shear stress levels. Unidirectional laminar flow was then reached by flowing media over cells at 5 dyn/cm^2 HSS for the first hour, preventing potential detaching, and increased to 10 dyn/cm^2 for 48hrs. Each condition had a static counterpart incubated for 48hrs at 37°C 5% CO_2 with media changed at 24hrs.

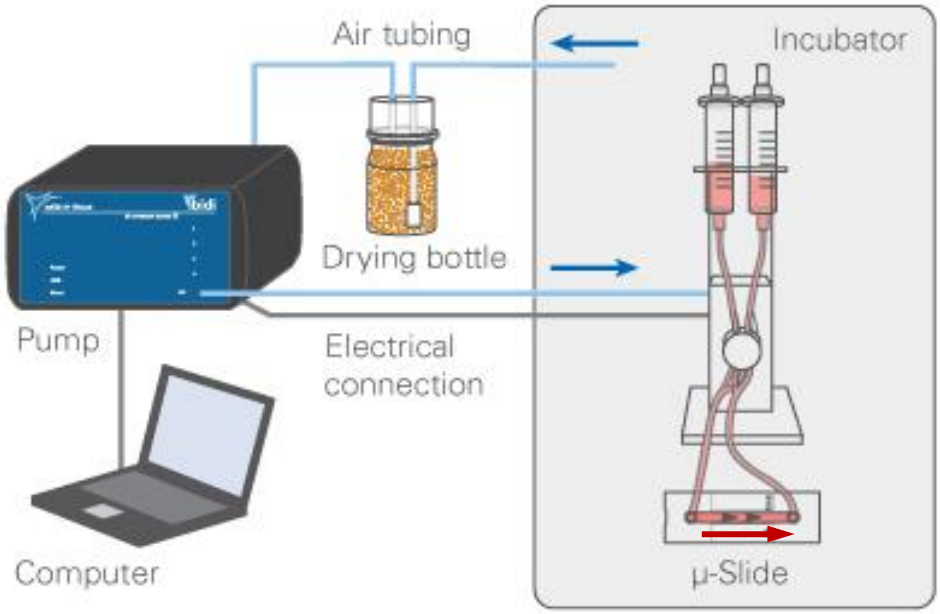

Figure 2.4 IBIDI microfluidics system used for flow experiments. IBIDI software on the computer is used to program pump to control airflow to the fluidic units, determining shear stress delivered across the IBIDI µ-slide I, used to mimic arteries. Cells are seeded and cultured in the channel and flow follows the direction indicated by the red arrow. Adapted from (209).

2.4 Cell Treatments

Table 2.3 Reagent used for each cell treatment. The concentration used in each experiment is detailed alongside the stock concentration. Supplier and solvent used to reconstitute regents is included.

Reagent	Working concentration	Supplier	Stock	Solvent
Histamine	150 µM	Sigma	100mM	dH2O
PMA	1µM	Promega	5mM	DMSO

2.4.1 VWF String Expression

After 48hrs all slides were placed under 2.5 dyn/cm2 LSS laminar flow for 10 minutes and were stimulated with 150µM of histamine (Sigma) or 1 µM PMA (Promega) allowing VWF secretion and string formation. Cells were fixed (4% PFA) before staining.

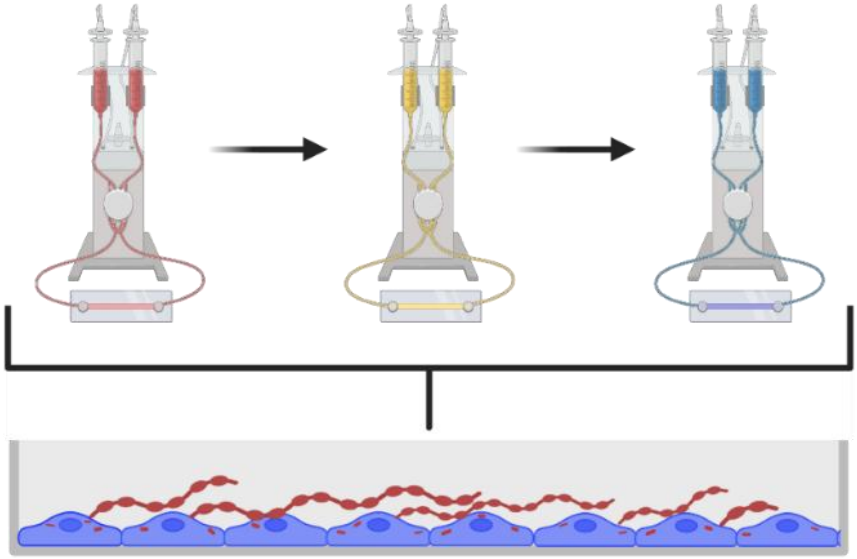

Figure 2.5 IBIDI microfluidic set up for VWF string expression protocol

ECs cultured under HSS, or static conditions were placed in a perfusion set in a 37°C incubator containing media supplemented with 150µM of histamine to stimulate WPB exocytosis. Slides were removed after 10 minutes of exposure and placed immediately under 4% PFA for 10 minutes to fix cells prior to immunofluorescent staining.

2.5 Immunocytochemistry

Table 2.4 All primary antibodies used in immunofluorescence staining

Primary Antibody	Species	Working concentration	Supplier
Anti-VWF Polyclonal	Rabbit	1:100 1:200	Dako
Anti-VWF monoclonal	Mouse	1:200	Dako
Anti-VWF monoclonal	Mouse	1:200	Abcam
Anti-GM100	Mouse	1:200	BD Biosciences
Anti-VWF HRP conjugate	Rabbit	1:5000	Dako

Table 2.5 All secondary antibodies used in immunofluorescence staining

Secondary Antibody	Species	Working concentration	Suplier
Alexa Fluor Anti Rabbit 594	Rabbit	1:300	Jackson ImmunoResearch Labs
Alexa Fluor Anti mouse 594	Mouse	1:300	Jackson ImmunoResearch Labs
Alexa Fluor Anti Rabbit 488	Rabbit	1:300	Jackson ImmunoResearch Labs
Alexa Fluor Anti mouse 488	Mouse	1:300	Jackson ImmunoResearch Labs
Alexa Flour 594 fab fragment	Mouse	1:300	Jackson ImmunoResearch Labs

2.5.1 Intracellular Staining

At 48hrs, media was aspirated, 3x PBS washes, cells were fixed (4% PFA 10 minutes) and permeabilised for 10 minutes (0.1% triton). Monoclonal primary antibody was added for 1 hour room temperature (RT). Following 3x PBS washes secondary antibody was added (30 minutes RT in the dark). Cells were consistently kept under dark conditions. Following a final PBS wash, nuclei were stained with Hoechst 33342 for 7 minutes, then mounted using Prolong gold mounting media (Invitrogen).

2.5.2 Extracellular Staining

For VWF strings permeabilisation was omitted as they are expressed extracellularly. Following fixation of ECs under flow, each sample was washed with PBS. Polyclonal primary antibody was added for 1hr at RT, following which samples were washed 3x with PBS. Corresponding secondary antibody for a further 30 min at RT in the dark, had PBS wash and then nuclei were stained with Hoechst 33342 for 7 minutes. Following a final PBS wash, samples were then mounted using Prolong gold mounting media (Invitrogen). Aspiration at each step was performed in direction of flow, affording increased protection to VWF strands integrity.

2.6 Microscopy

2.6.1 Olympus IX83 widefield fluorescent microscope (inverted)

All slides were imaged in 10x independent randomised fields of view (FOV) with a 60x (oil) objective. Using Olympus cellSens software, an optimum exposure was established for DAPI (blue) and RFP (red) fluorescence filters on the control condition slide for each repeat and was applied to each image on all slides per biological repeat. Z-Stack images were acquired for each FOV composed of 10x 0.2µm steps. Each Z-stack image underwent constrained iterative deconvolution which uses an algorithm to restore out of focus light (deconvolution) from one plane of a z-stack to another and had the maximum intensity projected image produced.

2.6.2 Confocal LSM880 Inverted Zeiss LSM880 microscope

VWF strings were imaged using the inverted confocal microscope. Slides were imaged in 5x independent randomised FOV using a 40x air objective. Using Zeiss ZEN black software, an optimum gain was set for both the DAPI (blue) and RFP (red) lasers and was applied to each image taken on all slides per repeat. Z-Stack images were acquired for each FOV, 5x focal planes taken at 0.2µm steps. Images were tiled (2x2) ensuring longer VWF strings

were captured. Maximum intensity projections were generated and a medium stitch applied ensuring continuity between tiles.

2.7 Image analysis

FIJI (Fiji is just imageJ) was used to analyse all maximum intensity projections. A series of macros were employed for different analyses. Macro 1 (see Appendix II) was used to count the WPB number, providing several measurements including total number of WPBs present in each FOV, feret size (length) of each WPB and feret angle. Number of nuclei were used to calculate the average number of WPB per cell in each FOV (total WPBs divided by number of nuclei). Expression of WPBs per cell across conditions was assessed using macro 4 (see Appendix II). This defines each cell in an FOV and highlights WPBs. Cells with WPBs in their defined area were counted as expressing WPBs, a percentage of cells expressing WPBs was calculated. To analyse the VWF strings macro 3 (see supplementary) was utilised, removing background 'noise' fluorescence and assessing number and length of VWF strings in each FOV.

2.7.1 Cell orientation

Images were rotated to the direction of flow and using macro 2 (see appendix), the orientation of cells was assessed. A Difference of Gaussian plugin defined the edges of cells and automated quantification of cell orientation OrientationJ, created a histogram of the angle of cells in each image. From this a Gaussian distribution curve was fitted and the mean frequency at the distribution mode was determined.

2.7.2 WPB Morphology

Images were split into respective channels with the red (VWF) channel being selected. The scale on images was set in accordance with the microscope. An optimised background subtraction and auto local threshold was performed on the VWF channel. Followed by a particle analysis providing the number of WPBs, the length, the area, angle and other factors. See macro 1 (appendix).

2.7.3 WPB Polarisation

Polarisation of WPB was measured using the Feret angle as recorded from the same ImageJ macro 1 described as above. WPBs are quantified based on the angle between the Feret of each particle and a horizontal 'line' through the image. Angles closer to 0 and 180 degrees indicate WPBs are horizontal and are aligned with the direction of flow.

2.7.4 WPB Expression Distribution

StarDist ImageJ plugin (https://imagej.net/plugins/stardist) was used to create a distance map of the nuclei in each FOV based on the isolated blue channel. From the corresponding red channel, WPBs were identified (using the above macro) and were overlaid onto the distance map. The number of cells that contained WPBs within the mapped area of the nuclei was counted and the percentage of WPB positive cells was calculated. See macro 4 (appendix).

2.7.5 VWF String

An ImageJ macro was used to quantify the VWF strings (see macro 3 (appendix)). Channels were split and the red channel selected, and a local threshold applied. A particle analysis was performed determining the number and length of the VWF strings in each FOV.

2.7.6 Golgi Fragmentation

The number and size of Golgi fragments was assessed for each FOV. Channels were split, the green selected and a local threshold applied. Particle analysis was used to count and measure the area of each Golgi. The number of nuclei was counted and the number of Golgi per FOV was divided by this to give the average number of fragments per cell see macro 5 (appendix).

2.8 Western Blotting

2.8.1 Cell lysis

Static cultures were grown for 48hrs on 6-well plates prior to lysis at a concentration of 250,000 cells/well in complete media.

Cells were washed in ice-cold PBS and lysed with 100µl cold lysis buffer (NP-40 Thermo scientific) containing 1:500µl anti-protease cocktail (Sigma-Aldrich, P8340), and 1:50µl broad-range anti-phosphatase (Sigma-Aldrich, 524629). Each well was manually scraped for 15 seconds, ensuring full coverage of the well. Lysate was collected in individual Eppendorf's left on ice for 30 minutes and then spun in a -4°C centrifuge for 10 minutes (12,000 xg). Supernatant was collected and frozen at -20°C (0-3 months) or -80 °C (>3 months).

2.8.2 Running gel, transfer, and antibodies

Following BCA total protein quantification Rapid Gold BCA Kit (A53225, ThermoFisher Scientific), samples were prepared adding equivalent amounts of protein, lysis buffer (**table 2.8**) and sample buffer to one Eppendorf per condition and heated at 95°C for 5 minutes before use. Precast 4-20% acrylamide gels (Bio Rad mini-PROTEAN TGX) were loaded into a Bio-Rad chamber tank with the required volume of 1x TGS running buffer (diluted from 10X with dH2O, Bio-Rad). Samples were loaded into wells according to individual gel instructions with 4µl of molecular weight protein ladder (Precision Plus Protein Standard Dual colour Bio-Rad, #161-0374). The tank was connected to a powerpack, and gels were run at 160V for ~90 mins or until the terminal band had run out of the gel. The trans-blot turbo system was used to transfer the gels to membranes. Stacks were saturated with transfer buffer (10 ml 100%, (10 ml of 5x transfer buffer (Bio-Rad), 100% ethanol, and 30 ml dH2O) and layered with a pre-cut PVDF membrane (activated with ethanol) and the gel. The turbo blot was then run using the Bio-Rad defined high molecular weight programme to transfer protein. Membranes were blocked in TBS-T with 5% skimmed milk powder (VWR Chemical) (prevent non-specific antibody binding), washed (1xT-BST) and incubated with primary antibodies overnight at 4°C. Following 3x ten-minute washes (1xT-BST), a corresponding secondary antibody was added to incubate (rocker 48hrs RT). Membranes were washed (as above).

2.8.3 Membrane Imaging

The iBright FL1500 (ThermoFisher, Scientific, UK) was used to image membranes. Once covered in a layer of 1:1 SuperSigna West Dura Extended Duration Substrate ECL (ThermoFisher Scientific), membranes were placed into the iBright drawer and the automatic focus employed to determine the exposure time for each. Once determined, the blot was exposed to the imager for the set amount of time.

Table 2.6 All primary antibodies used for Western blot imaging

Primary Antibody	Species	Working concentration	Supplier
pAKT	Rabbit	1:1000	Cell Signalling
pENOS	Mouse	1:500	Cell Signalling
tAKT	Mouse	1:1000	BD Biosciences
tENOS	Mouse	1:1000	Cell Signalling
B-Actin HRP conjugate	Mouse	1:10000	Santa Cruz Biotechnology

Table 2.7 All secondary antibodies used for Western blot imaging

Secondary Antibody	Species	Working concentration	Supplier
Goat anti-rabbit HRP	Rabbit	1:10000	Jackson ImmunoResearch Labs
Goat anti-mouse HRP	Mouse	1:10000	Jackson ImmunoResearch Labs

Table 2.8 Western blotting solutions and reagents

Solution	Composition
Sample loading buffer (4x)	200 mM Tris (pH 6.8), 8% SDS, 40% glycerol, 8% beta-mercaptoethanol, and 0.1% bromophenol blue
Running Buffer	25 mM Tris, 192 mM glycine, and 0.1% SDS, pH 8.3
Transfer Buffer	48 mM Tris, 39 mM glycine, 0.5% SDS, and 20% methanol
Tris Buffered Saline with Tween 20 (TBS-T)	145 mM NaCl, 20 mM Tris-base, 0.5% Tween-20, pH 7.5

2.9 VWF Multimer Gel Assay

2.9.1 Cell Lysis

Cells were cultured in 6 well plates for 48hrs prior to lysis using RIPA buffer (Pierce ThermoScientific) with manual scrapping. Lysates were stored in -80°C conditions until use.

2.9.2 Running gel, transfer and antibodies

Samples were diluted to a 1:5 dilution using sample buffer, the reference plasma (normal pooled plasma, First Link UK (2800850)) was prepped in a similar way, a 1:10 dilution using the same solution. The diluted samples were then heated at 60°C for 30 minutes to denature the protein. Gels (**table 2.8** for composition) were cast a minimum of one day in advance to allow time to settle, using a high gelling temperature agarose (Seakem Lonza, USA) at a 1.2% concentration. The gel tank was set up in a box of ice to maintain a low surrounding temperature for as long as possible. Running buffer was kept at fridge temperature, for a minimum of 12hrs prior to use. A BCA assay as described in (2.8.2) was utilised to quantify protein in cell lysate samples ensuring an equal and uniform quantity of protein was loaded across each gel. Lysates were loaded at 10µl per well then gels were run at 65V for 20 minutes to ensure that protein was forced into the gel. After this, the voltage was lowered to 25V and the gel was left to run until the sample reached the base, this took from 3-5 hours, highly dependent on ambient temperature.

Once complete, the gels were washed and left in DDT (Dithiothreitol) (BioRad, UK) for 20 minutes prior to transfer. Biorad turbo transfer was used, the pre-programmed high molecular weight programme was used but altered to be for 20 minutes. Following this, membranes were placed in PBS-T with 5% milk to block (prevent non-specific antibody binding) for an hour.

2.9.3 Membrane Imaging

Membranes were washed in PBS-T then left overnight on a rocker in 1:5000 VWF anti rabbit conjugated HRP (**table 2.9**) in PBS-T. Following this the iBright FL1500 (ThermoFisher, Scientific, UK) was used to images membranes. Once covered in a layer of SuperSigna West Dura Extended Duration Substrate ECL (ThermoFisher Scientific), auto-exposure determined the optimum time to image membranes. Images were then taken at increasingly higher exposures to a point of overexposure; this ensures even faint bands are captured.

2.9.4 Gel Analysis

Assessment of VWF multimer gels was undertaken in FIJI. Multiple measures were taken to assess the multimeric profile of VWF in samples. The reference plasma was defined as the first lane for analysis; this ensured all banding was captured in each sample. Plots of each sample were generated, from right to left peaks were counted, peaks 1-5 represent bands 1-5 and are LMW VWF, those above 5 are HMW. The area under the HMW peaks was divided by the area under the total peaks, this was then normalised against the control sample. Resulting in the 'multimer index', a ratio of low to high weight VWF multimers.

To create a multimeric fingerprint of each sample, the straight-line tool (set at a line width of 30), drawn from the top of the lane to the bottom, a measurement was recorded into the ROI manager. Using the same line, this was repeated for all lanes within a gel. The image was inverted and then multi plot profile was generated, this provided a figure in which each lane is overlayed with one another and each peak represents a VWF multimer present within the sample.

Densitometry of VWF banding was used to quantify the amount of VWF in each sample. A gel profile plot was created per sample, and the wand tool was utilised to generate relative intensity data.

Table 2.9 Buffers required for multimer gel analysis

Buffer	Composition
Gel	200mM Tris, 100mM Glycine, 0.1% SDS, pH 9.0
Sample	10mM Tris, 10mM EDTA, 2%(w/v) SDS, 0.03%(w/v) bromophenol blue, 15% glycerin pH 8.0
Running	100mM Glycine, 100mM Tris and 0.1% SDS pH 8.4
Transfer	Trans-Blot Turbo 5x Transfer Buffer, ethanol and dH2O 1:1:3

Table 2.10 Antibodies used for multimer gel analysis

Antibody	Species	Working concentration	Supplier
Anti-VWF HRP conjugate	Rabbit	1:5000	Dako

2.10 RNAseq

Using RStudio, published open access RNAseq data (34) was used to identify if WPB related genes, identified by our lab group, were differentially expressed in diabetic retinopathy (DR).

WPB GOI were identified and highlighted in the public data using Excel. A general overview of significantly differentially regulated genes, presented in a volcano plot. The plot was produced using differentially expressed gene data log fold changes against the corresponding P-value, identifying if genes are significantly regulated (up and down) in this condition. Significant changes were denoted in red and gene ID labels applied.

GOI related to WPB were also extracted from this data set for further downstream analysis (see appendix for full list), a volcano plot was also produced using the above protocol.

2.11 Statistical analysis

All data presented are averaged means from three biological repeats (represented by n) ± SEM. Data underwent Shapiro-Wilks testing to establish if normally distributed. Two-way ANOVA was used to establish if there were significant differences between media and cell culture conditions. One-way ANOVA (with post-hoc Bonferroni test) was used to establish significant differences between discrete groups i.e. grouped culture and media (e.g. high glucose and flow) as one condition. T-Tests were used to establish significance between two independent conditions. Statistical significance was regarded as $p < 0.05$, presence marked by an asterisk. GraphPad Prism 9.4.1.681 was used for all statistical analysis.

Chapter 3: Models of Diabetes

3.1 Introduction

3.1.1 ECs under flow

VWF is frequently identified as elevated in diabetic populations, this has been linked to WPBs with multiple animal models demonstrating that WPBs are specifically impacted by diabetes *in vivo* (191, 192, 196, 202, 210). However, further research has somewhat stagnated at the interface between significant findings from *in vivo* models and their translation to human physiology. Recent transcriptomics analysis has identified populations of genes significantly dysregulated in diabetes, particularly in the context of diabetic retinopathy (DR) (198). From this dataset, genes of interest (GOI) associated to WPBs were mined, strengthening the connection between diabetes and disturbance to WPBs and highlighting candidate within an *in-situ* context. However, studies investigating causality remain limited, often relying on static cell culture techniques which may induce physiological changes independent of pathological stimuli.

A microfluidic approach of 48hrs high shear stress (HSS) exposure was implemented to investigate the effects of diabetes on WPBs, as established by Money et al, WPBs are significantly longer cultured under static vs SS environments (59). The 48hr HSS methodology employed in this investigation is further supported by a transcriptomic data from Afshar et al (52). In which, RNA was analysed from umbilical cord tissue and compared to HUVECs isolated from the same source and cultured under varying conditions of cell culture, including static and HSS exposure (52). HUVECs cultured under 48hrs of HSS displayed the closest transcriptomic alignment to the profile of the native tissue, with a 17% higher gene rescue than HUVECs cultured static (52). These findings validate the use of microfluidic HSS culture as a means to enhance the physiological relevance of *in vitro* endothelial models, aligning cellular behaviour more closely with the *in situ* vascular environment. As a static environment is subsequently considered pathogenic, use of shear stress removes this confounding factor allowing for clearer interpretation of disease associated endothelial changes. To investigate the impact of pathological conditions on WPB morphology and behaviour, diabetes was established as a representative model of vascular pathology.

3.1.2 WPB cargo is significantly altered in diabetic populations

WPB related cargo have been shown to be elevated in several conditions including, but not limited to, cardiovascular disease (CVD) (192, 210). In CVD several WPB cargos, including

VWF, contribute to atherosclerotic plaque formation and disease progression (211, 212). This association is particularly pronounced in individuals with a diagnosis of diabetes, where plasma levels of VWF are significantly elevated (192). The extent of this elevation suggests that VWF could serve as a predictive biomarker for developing CVD in diabetic populations (192). For the control group of CVD patient with no formal diagnosis of diabetes, VWF was not significantly elevated (192). Whilst there is clear association of WPB VWF levels with CVD outcomes in diabetes, the underlying mechanisms are unclear. Appropriate models to investigate the impact of a diabetic microenvironment on WPBs are required. While animal models have historically been used to explore the effects of diabetes on WPBs, they present limitations. Although they allow for a holistic view of disease impact across a whole organism, it remains challenging to determine which specific aspects of a complex condition like diabetes drives observed cellular changes. A simplified cell-based approach with tightly controlled variables minimises these confounding factors and enables more precise mechanistic investigation. Moreover, the physiological relevance of animal models to human systems is inherently limited. Alterations in VWF have been consistently documented in human populations with diabetes, reinforcing the importance of studying WPB dynamics in human endothelial models to identify potential therapeutic targets.

Further evidence for a potential role for WPBs comes from analysis of the transcriptomic data set generated by Korhonen et al 202, mentioned above, that assessed gene expression in endothelial cells isolated from the retinas of diabetic and non-diabetic retinopathy patients (198). To explore WPB-related gene expression in diabetes, I preformed independent analysis on this published data set. From this, 45 WPB associated genes, including VWF, P-Selectin and Angiopoeiten-2, were identified as differentially expressed within diabetic retinopathy (DR) (**figure 3.1**; see appendix for extensive gene list). Whilst the original study did not focus on WPBs, this targeted reanalysis strengthens the link between diabetes and WPB disturbance and highlights candidate protein within an *in-situ* context. Although previous studies suggest a clear association between elevated VWF levels and CVD outcome in diabetes, the underlying mechanisms surrounding this remain unclear. Further investigation into the impact of diabetic conditions on WPB dynamics is required using physiologically relevant models to recapitulate the *in-vivo* diabetic microenvironment.

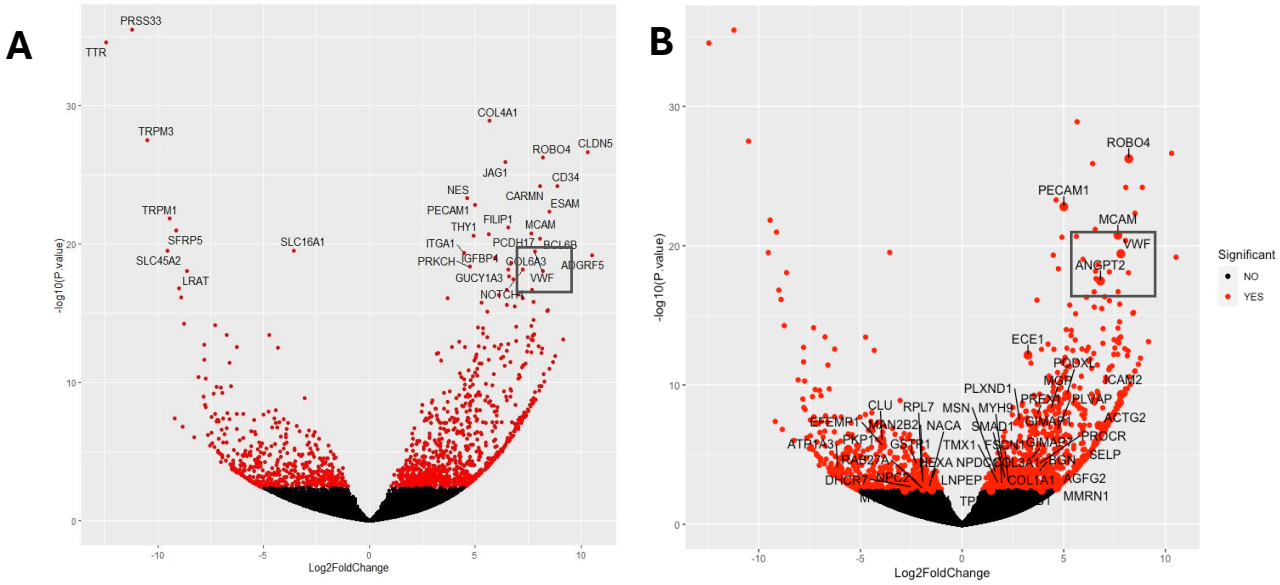

Figure 3.1. Patients with diabetic retinopathy have significantly altered gene pathways compared to control retinopathy patients. Several WPB associated genes are affected in this model.

A. Volcano plot of the top 30 significantly regulated genes from diabetic retinopathy data (ref)

B. WPB associated genes as identified by the McKeown group that are significantly up or down regulated in diabetic retinopathy tissue.

Previous studies of WPBs have been conducted using human cells in static culture. As illustrated, this is a stimulus WPBs will respond to and adapt their physiology to, thus, is not representative of a true *in vivo* environment (59). Subsequently this approach to WPB study may explain why there is little correlation seen between studies traditionally conducted on human cells compared to the animal models discusses above. This has resulted in conclusion that suggest WPBs do not differ in humans in a diabetic environment. As we have seen static culture is inherently pathological as in practice, in a healthy individual no ECs would ever experience an absence of SS, meaning it is a highly artificial environment for investigation (59) Some pathologies such as occlusion within blood vessels, will induce stasis to ECs in vivo, however this could have devastating repercussions to the affected individual (213). The lack of significant observations has contributed to the lack of progression in WPB analysis in disease states. Diabetes is of particular relevance as a disease state given its well-documented impact on vascular health, including disruption to blood flow and damage on both a micro and macrovascular level (9, 190, 214).

As established, one of the potential methods that can be utilised to overcome limitations associated to static cell culture models is microfluidics, which allows contained media to be flowed across cells at a controlled rate thus mimicking the *in vivo* environment. In this study I will utilise a microfluidics approach to test the hypothesis and aims laid out below.

Hypothesis: Diabetes associated glucose dysregulation will impact the form and function of WPBs.

Aim 1: To determine the role of chronic hyperglycaemia on WPB morphology and function

Aim 2: To establish a model to assess the impact of physiologically relevant ambulatory glucose levels to assess the impact of a diabetic hyper- and hypo-glycaemic environment on WPB morphology and function.

3.1.3 Cellular models of diabetes

3.1.3.1 Replicating diabetes in a cellular model

Endothelial cells are at the forefront of the blood microenvironment. They are permanently exposed to any changes hourly, daily, yearly and longer. Diabetes is a multifaceted disease with many factors that could impact the endothelial environment and by extension WPBs. To dissect possible mechanisms and replicate the *in vivo* environment, glucose exposure was manipulated to simulate the dysregulated glucose characteristic synonymous of diabetes.

I created two models to assess the impact of glucose on WPBs in a pathogenic context. Initially with a high glucose (25mM) model, whereby a ECs were maintained in a chronic hyperglycaemic environment. While 25mM is a higher glucose concentration than what is needed for a diagnosis of diabetes (or a random plasma glucose of 11.1mM), it represents severe hyperglycaemia, experienced in uncontrolled diabetes. It is approximately five times the physiological baseline, so represents a high stress environment for ECs and is well established experimental standard in literature (215-218). This model elevates this standard approach by incorporating microfluidics, ECs are cultured in a physiological environment, reducing confounding effects arising from the artificial nature of static cell culture.

This model evolved into a more refined approach whereby glucose was oscillated between extreme, but within physiological reason, hypo and hyperglycaemic levels to more closely reflect conditions experienced by ECs in situ. Termed ambulatory glucose, this model was designed to mimic daily behaviours of eating meals at regular intervals and sleeping during the night. For comparison, the reflected changes to blood glucose experienced in ‘healthy’ control conditions and under diabetic conditions were presented. Glucose levels were chosen to represent the highest (control 10mM, diabetic, 20mM) and lowest (control 5.5 mM, diabetic, 2.5mM) possible blood glucose levels extrapolated from continuous glucose monitoring data of diabetic patients and healthy controls taken from Battelino et al 2019 (208). This model ran for 48hrs, for 12hrs per day glucose was oscillated from low to high glucose every 2hrs to represent a meal and subsequent peak or drop in blood glucose.

HUVECs are a robust model of WPBs, reliably synthesising populations suitable for analysis. As such, they were selected at the cellular subject for treatments within the *in vitro* models of diabetes developed in this study.

3.2 Results: Model 1: Chronic exposure of ECs to hyperglycaemia

I identified one characteristic element of diabetes that I could both control and manipulate as a starting point: blood sugar. The fundamental treatment of diabetes is to achieve optimal glycaemic control, i.e. keep blood sugar within 'healthy' range. Defined by NICE guidelines, a healthy range for blood glucose is between 4 mmol/litre and 7 mmol/litre fasting and between 5 mmol/litre and 9 mmol/litre after eating (219). When blood sugar spikes in diabetes to hyperglycaemic levels, it can have pathogenic repercussions (220).

3.2.1. Validation of mannitol as a hyperglycaemic cell model control

A glucose concentration of 25mM was used as a high glucose condition, a widely accepted experimental standard (221-225). Glucose concentration affects osmolality of the environment; therefore, a sugar control was required for comparison. Mannitol is a simple sugar, not well metabolised by the human body, meaning it can be used as an osmotic control. To confirm this, standard EGM-2 media (5.5mM glucose) was compared to EGM-2 media with 19.5mM mannitol added to raise the overall sugar concentration to a comparable 25mM. Osmolality of media was assessed, alongside EC alignment under flow and the profile of WPBs.

3.2.1.1 Mannitol supplementation does not impact osmolality

When assessed by osmometer, there was a minor variation between EGM-2 and the mannitol control media recorded osmolality, but readings were consistent overall with no statistically significant difference (See **Table 3.1**).

3.2.1.2 Mannitol supplementation does not impact EC alignment to flow

ECs, which are constantly under the influence of blood flow, align with the direction of shear stress. Therefore, the ability of cells to align under flow was assessed as a marker of 'normal' cell function in cells cultured in normal glucose EGM2 or mannitol supplemented media. Following culture for 48hrs, ECs cultured under static conditions displayed the expected 'cobblestone' morphology in which cells grow in a seemingly random pattern with no identifiable directionality (**Figure 3.2**). Under the HSS condition ECs lost this morphology, adopting one of elongated cells aligning with the direction of flow (**Figure 3.2**). These phenotypes were consistent across all conditions. When assessed using **macro 1**, the images of the cells are converted into data that can be plotted to quantify this visual difference (see **Figure 3.2**). ECs under HSS culture form a peak at 0°, indicating that the majority of cells are horizontally aligned i.e. are following the direction of shear

stress. Conversely, the static lines are flat, showing there is no pattern or clustering of cells at any specific angle, indicating there is no measurable alignment. Given that this behaviour is observed regardless of media condition, it provides a good foundation for the argument that mannitol is a likely appropriate control for glucose as it is mirroring the standard EGM2 condition.

Table 3.1. Osmolality of standard media and mannitol supplemented do not significantly differ. Average osmolality of standard EGM2 media and mannitol supplemented normo-glucose control EGM2 media. Three averages taken with osmometer and standard error of the mean calculated. n/N=3/3

Media Condition	Average Osmolality mOsm/kg ±SEM
EGM2	295±0.33
Mannitol	301±1.76

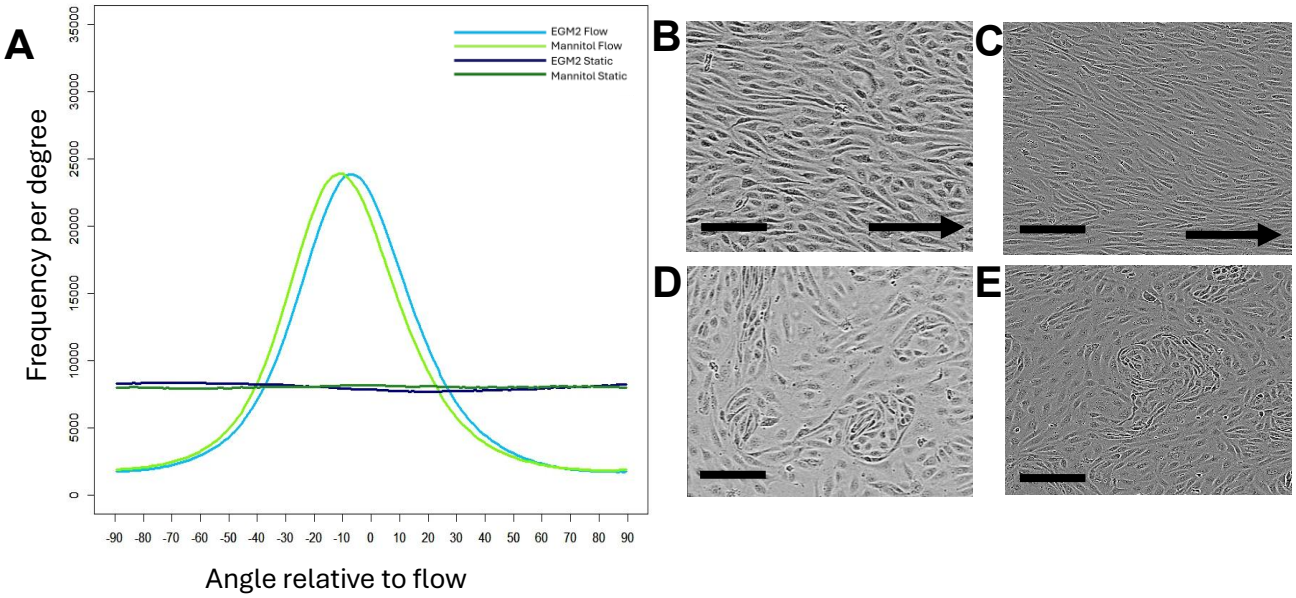

Figure 3.2. ECs cultured for 48 hours under static or physiological flow conditions in either standard 5.5 mM glucose EGM2 or mannitol supplemented media do not show significant variation in alignment.

Images taken using IncuCyte and analysed in FIJI. Scale bar is 100µm.

- **A.** Graph plots the degree of orientation of the cell along the x axis with the number of cells recorded at this angle on the Y. n/N=3/3
- **B.** Representative image of ECs cultured under directional high shear stress and standard EGM-2. Arrow depicts direction of flow.
- **C.** Representative image of ECs cultured under directional high shear stress and mannitol EGM-2. Arrow depicts direction of flow.
- **D.** Representative image of ECs cultured under static conditions in standard EGM-2.
- **E.** Representative image of ECs cultured under static conditions in mannitol EGM-2.

3.2.1.3 Mannitol does not impact the number, size or polarity of WPBs

As indicated by the literature and supported by the transcriptomic data shown in **Figure 3.1**, VWF is evidently elevated in diabetic populations, both for T1DM and T2DM (192-195, 198). Given that VWF is the only known ubiquitous cargo of WPBs I hypothesised that cells cultured in a diabetic environment would likely contain a higher number of WPBs, this notion is also supported by the *in vivo* studies as detailed by Anderson et al (191). Moreover, the length of WPBs is another indicator of thrombotic potential and is determined by the quantity of VWF bolus's being incorporated into WPBs when forming at the Golgi. Both the number and length of WPBs can be viewed as a proxy to measure the thrombotic potential of the EC population within the environment. This is because a greater quantity of WPBs should equate to a larger yield of VWF, and the longer the WPB, the greater the quantity of VWF and the greater thrombotic potential as there is a larger surface area for 'catching' platelets.

Therefore, to validate mannitol as a control I first ensured that WPB number and size was comparable in ECs cultured in mannitol to ECs cultured in normoglycemic EGM-2 to create a uniform profile in each environment. WPBs were visualised in ECs by immunostaining VWF as a marker for WPBs using high resolution microscopy. An average of 10 images per condition were taken per biological repeat and 3x biological repeats were performed. An example of images obtained is shown in **Figure 3.3**. From this, WPBs were measured to ascertain: 1) the number of WPBs per field of view (FOV), this gives us the total number of WPBs but it does not account for the number of cells; 2) the number of nuclei observed in each FOV; 3) the average number of WPBs per cell, this is the total WPB number divided by the number of (cells) determined by counting the nuclei in the FOV; 4) the average length of WPBs in each condition; 5) the percentage of cells that are expressing WPBs; 6) the polarity of the WPBs, recorded as the angle of the WPBs as imaged. An angle of 0° or 180° indicates horizontal orientation while values between these extremes represent increasing deviation towards vertical, peaking at 90°, the most vertically aligned position. As established above, ECs under shear stress align to the direction of flow, the same has been observed with WPBs.

3.2.1.4 WPB number is not affected by introduction of mannitol to media

The validity of mannitol as a control is dependent on its inertness, ensuring no impact on experimental outcomes. This would be reflected by comparable WPB profiles between ECs cultured in both normoglycemic EGM-2 and mannitol supplemented EGM-2. ECs were cultured under HSS and static in either normoglycemic EGM-2 or mannitol

supplemented EGM-2 media. There was no significant difference in the total number of WPBs observed per FOV between either media type or shear stress exposure (see **Figure 3.4 a**) (*p*=0.8472). There was an average of 1193±314 WPBs observed per FOV in the EGM2 static condition in the mannitol there was 1109±290. Under HSS in normoglycemic conditions there was 1391±149 and 1175±128 in the mannitol condition. To evaluate the potential impact of mannitol on cell proliferation, the number of nuclei per FOV was counted (**Figure 3.4 b**). EGM2 static had an average of 34±3, mannitol static was 33±3, EGM2 HSS was 37±2 and finally mannitol HSS was 31±5. There was no significant difference between these conditions in terms of cell growth (*p*= 0.6692). I used this to calculate the number of WPBs per cell as a more accurate measure than the gross total (Fig 4.4 x). There were no significant differences observed between the EMG2 media and mannitol supplemented media under either static (34±7, 32±6) or HSS (39±6, 40±5) conditions (see **Figure 4.4 c**) (p = 0.6878).

3.2.1.5 Length of WPBs is not affected by introduction of mannitol to media

Feret length in relation to WPBs is the longest measurable distance of the object observed by the imaging software; this represents length of the organelle. Length of WPBs is another indicator of thrombotic potential, it is determined by the quantity of VWF being stored within, incorporated when formed at the Golgi. For mannitol to be considered an appropriate control I would expect no deviations in the length of WPBs in ECs cultured in mannitol versus ECs in normoglycemic EGM-2 media conditions.

WPBs length did not significant change with exposure to mannitol (see **Figure 3.4 d**), a two-way ANNOVA was used to assess the impact of both the media environment and flow condition. Media environment did not significantly affect results (*p* = 0.8818) whereas HSS exposure did (*p* =0.0204). WPBs in the HSS condition were significantly shorter (EGM2 1.03±0.05μM, mannitol 1.02±0.02μM) than those from the static culture condition (EGM2 1.15±0.5μM, mannitol 1.15±0.04μM), this is in line with the expected outcome based on the flow phenotype created by our lab group (54). The absence of significant variation between conditions is a favourable outcome, supporting the consistency of the system.

3.2.1.6 WPB polarity is not affected by introduction of mannitol to media

As established above, when ECs are exposed to shear stress they align with the direction of flow, conferring an appropriate elongated morphology. Analysis of VWF immunofluorescent images it was observed that WPBs also aligned to flow (see **Figure 3.3**). Quantification of ferret angle was used to assess the effects in this intercellular context.

The angle of WPBs was measured using a particle analysis macro (**macro 1)**. The angle of WPBs indicate that they were perpendicular (i.e. at 0° or 180°) and therefore aligned with the direction of shear stress. This was observed at a greater frequency under flow conditions compared to static conditions. The static conditions show a greater population of WPBs clustered towards the centre of the distribution graphs, demonstrating that there was no directional alignment. Under high shear stress, the WPBs cluster more to the extreme ends of the graph, indicating a higher frequency of WPBs that follow perpendicular orientation, following directional alignment with flow (see **Figure 3.5**). This was true of both control (5.5mM glucose) and mannitol supplemented media conditions.

3.2.1.7 Number of ECs expressing WPBs is not affected by introduction of mannitol to media

Prior studies suggest that different cell types and/or conditions may have a different proportion of cells expressing WPBs (59). For example, hAECs produce a lower overall number of WPBs without the number of nuclei (number of cells) being impacted. This is expressed as a percentage of 'WPB positive' cells. There is no significant difference between any of the conditions (see **Figure 3.6**). The percentage of static for both control and mannitol are rounded to 96% whilst under for the control is 98% and the mannitol is 99%, almost every cell in each FOV was expressing WPBs.

These data suggest that mannitol can be used as an appropriate control for our hyperglycaemic model

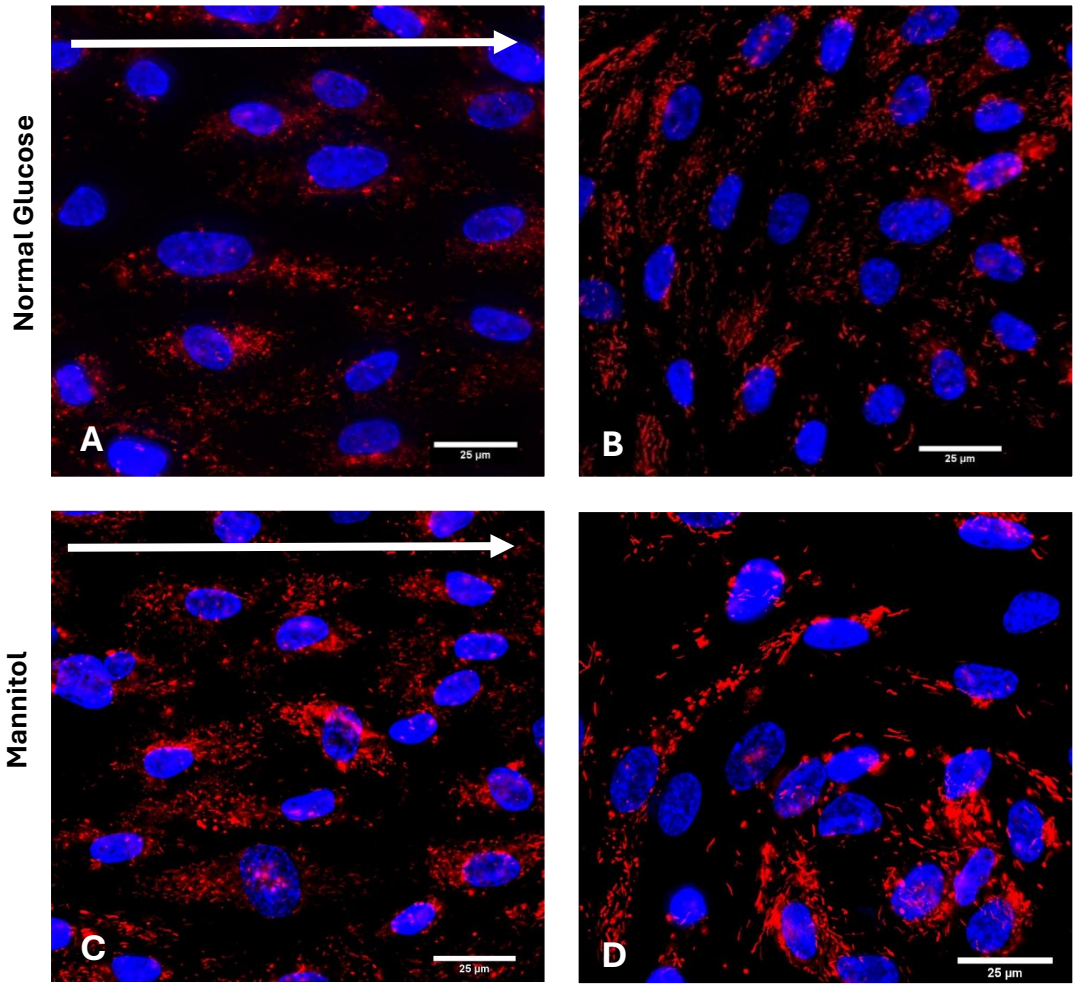

Figure 3.3. Representative images (x60 objective) of WPBs (red) in HUVECS cultured in mannitol supplemented EGM-2 and normoglycemic EGM2 media in both static and HSS culture conditions.

Endothelial cells (Hoechst blue) with expressed WPBs (VWF red).

A. HUVECs exposed to HSS under normoglycemic EGM2 conditions

B. Static HUVECs under normoglycemic EGM2 conditions

C. HUVECs exposed to HSS under mannitol supplemented conditions

D. Static HUVECs under mannitol supplemented conditions

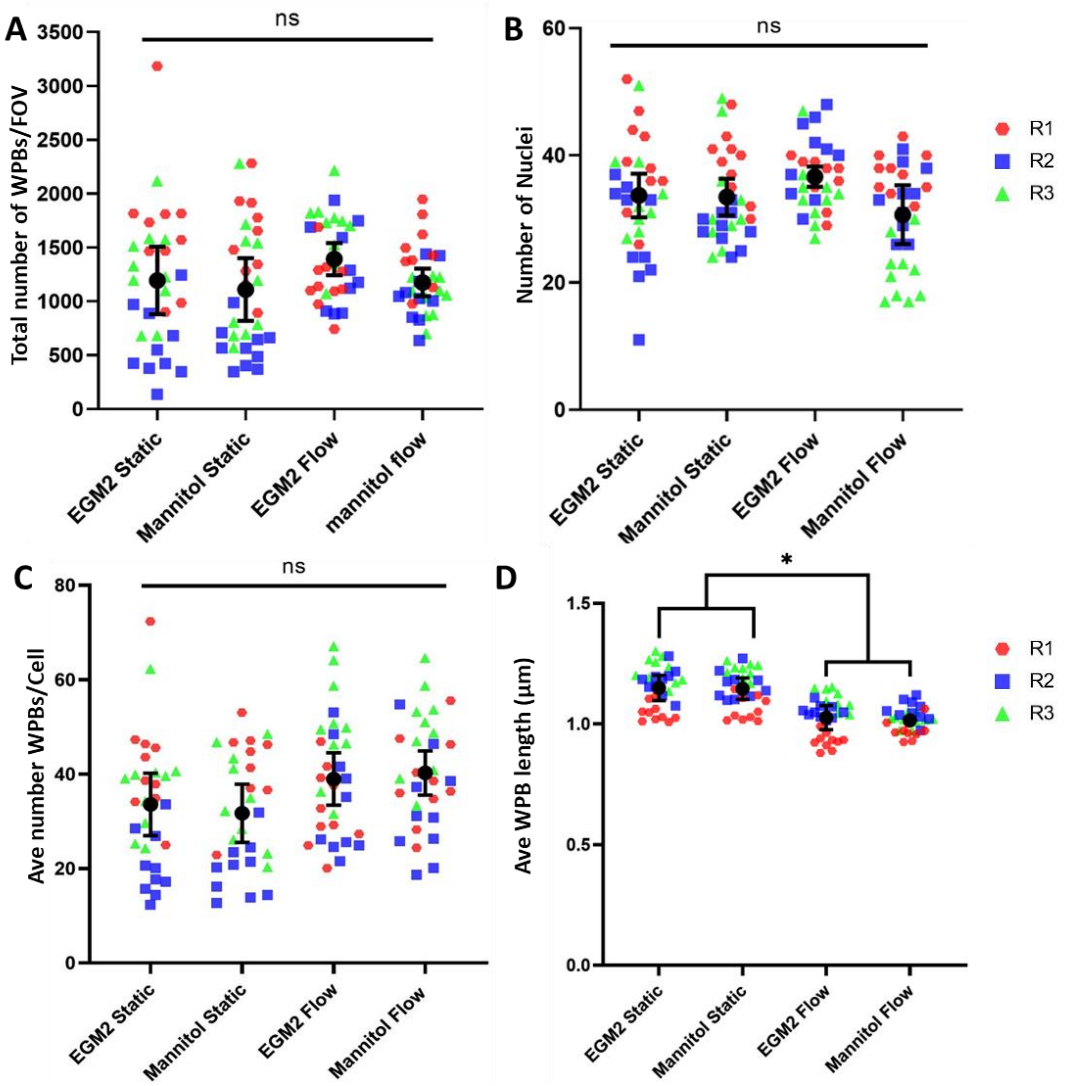

Figure 3.4. ECs cultured in either normoglycemic EGM2 or supplemented with mannitol have no significant differences in WPB numbers or size.

A. Mean data of the total number of WPBs observed in each FOV per condition ±SEM n/N=3/30. Each data point represents a mean of all WPBs counted in an image. Colours/shapes represent technical repeats (R1 red hexagon, R2 blue square, R3 green triangle)

B. Mean data of number of nuclei counted in each FOV ±SEM n/N=3/30 Each data point represents a mean of all nuclei counted in an image. Colours/shapes represent technical repeats (R1 red hexagon, R2 blue square, R3 green triangle)

C. Mean number of WPBs per nuclei calculated in each FOV n/N=3/30. Each data point represents a mean of WPBs per cell in an image. Colours/shapes represent technical repeats (R1 red hexagon, R2 blue square, R3 green triangle).

D. Mean length of WPBs in each FOV n/N=3/30. Each data point represents a mean of WPB length per cell in an image. Colours/shapes represent technical repeats (R1 red hexagon, R2 blue square, R3 green triangle).

Two-way ANOVA ns= non-significant, * = p <0.05

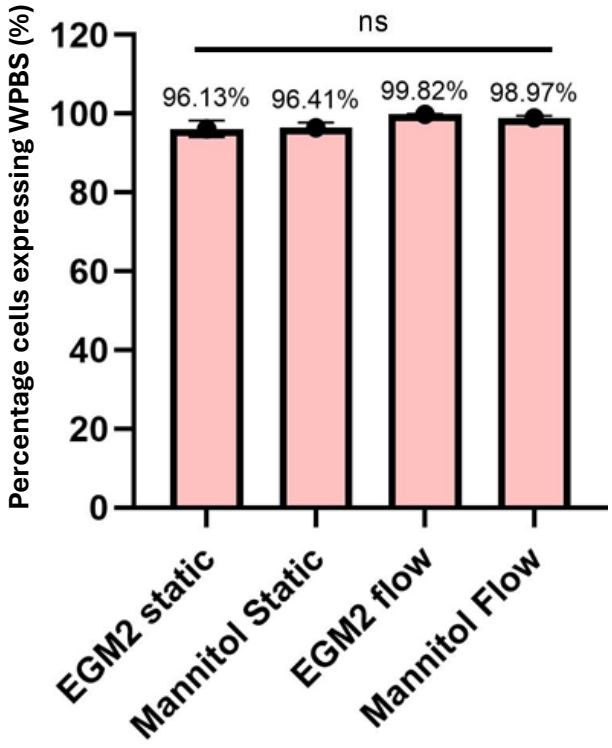

Figure 3.5. Mannitol does not induce a significant difference in the percentage of cells expressing WPBs.

Average percentage of WPB 'positive' cells ±SEM n/N=3/30. A cell area was defined around a nucleus and was assessed to see if WPBs were present within. Cell that did not were considered to not be producing WPBs. The cells were subtracted from WPB 'positive' cells and a percentage calculated.

One-way ANOVA with repeated measures p= 0.1827 ns = non-significant

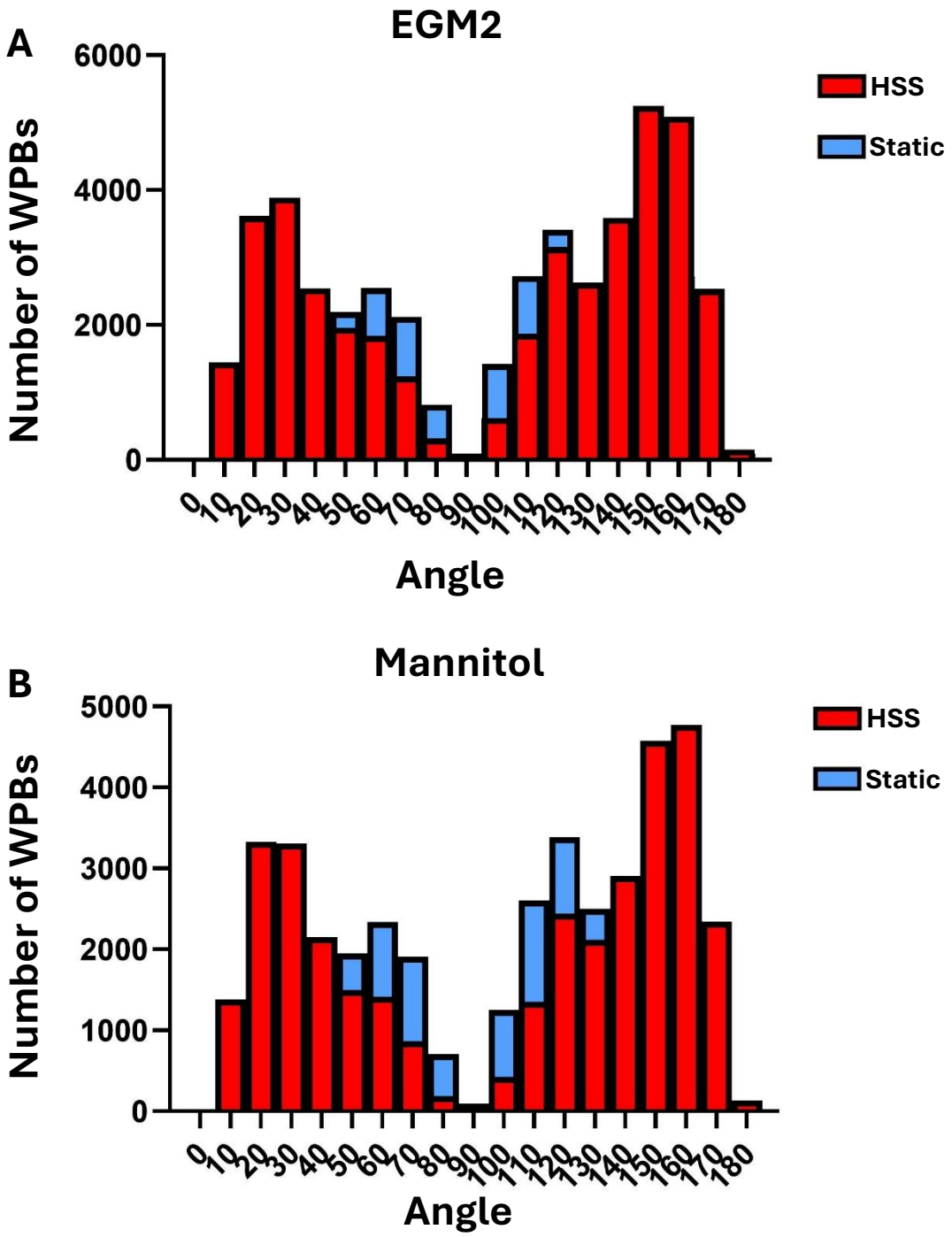

Figure 3.6. WPBs in cells in static culture (blue) are more randomly orientated compared with those from flow culture (red) overlayed in both normo-glucose EGM2 and mannitol environments.

- **A.** Angles of WPBs in cells cultured in normoglycemic EGM2 media for 48hrs under static or HSS conditions n/N=3/30
- **B.** Angles of WPBs in cells cultured in mannitol supplemented media for 48hrs under static or HSS conditions n/N=3/30

3.3 The impact of chronic exposure of hyperglycaemia on ECs

The hyperglycaemic model uses ECs cultured in EGM2 supplemented with 25 mM glucose as a severe condition to establish if constant exposure to chronic hyperglycaemia triggers a reactive shift in cellular behaviour as compared to our inert control mannitol. The ECs are cultured under HSS (10 dynes) for 48hrs and then fixed with PFA and immunostained for WPBs using VWF as a marker. The same measurements were conducted as seen in section **3.2** above.

3.3.1 Hyperglycaemia impacts the profile of ECs

3.3.1.1 Hyperglycaemia impacts phosphorylation of Akt and eNOS in ECs

The metabolic pathway responsible for the phosphorylation of AKT is disrupted in diabetes (8, 176). This was assessed via western blotting (data not shown) and densitometry.

ECs exposed to 48hrs of hyperglycaemia have an observed increased in phosphorylation of AKT but was not significantly different to the mannitol condition (1.00± 0.061, 1.466±0.258, p=0.0191). No difference was observed in tAKT between high glucose and mannitol (1.00±0.057, 1.08±0.158, p=0.6436) (**figure 3.7 b**). This suggests that exposure to a hyperglycaemic environment may be starting to disrupt phosphorylation activity of AKT in HUVECs but is not affecting the expression of tAKT, i.e., it is the phosphorylation process that is affected, not an increase in the total amount of AKT available to be phosphorylated.

There is a greater than 2-fold increase in phosphorylation of ENOS observed in the high glucose condition compared to that of the control (2.883±0.932, 1±0.352, p=0.0727), however this difference was not significant. Conversely there is close to 50% reduction in expression of tENOS recorded in the HG condition compared to the control but was also not a significant difference (0.5572±0.141, 1±0.161, p=0.0652). Once again, this implied that the increase observed in phosphorylation is a result of increased phosphorylation activity rather than an overall increase in the expression of the protein being phosphorylated.

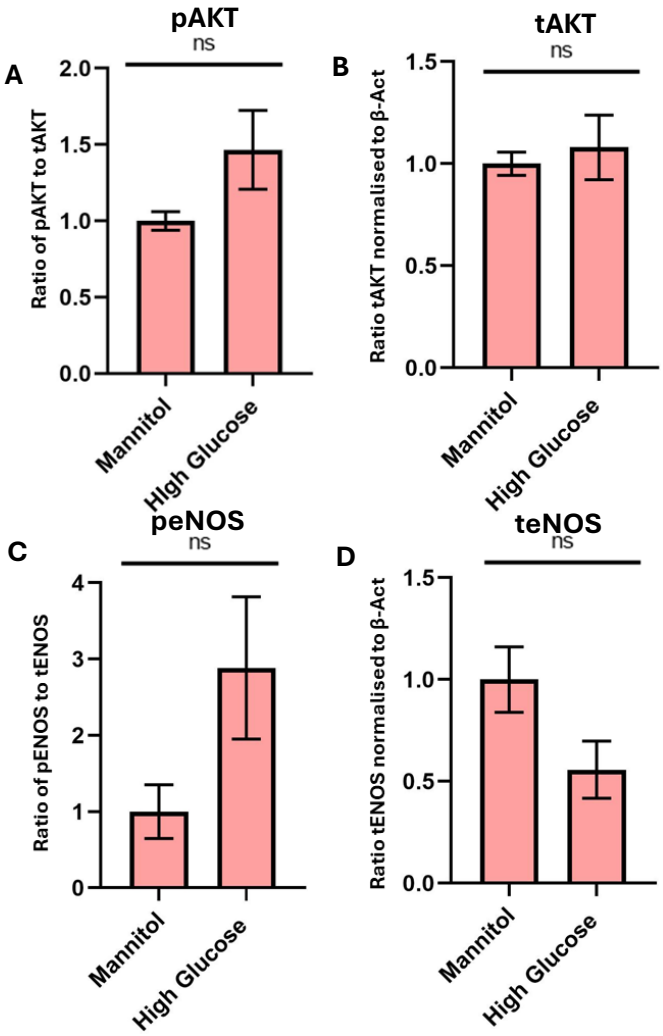

Figure 3.7. Densitometry analysis of western blotting identified that exposure of ECs to a high glucose environment does not change phosphorylation activity of AKT and ENOS or increase the level of total protein n/N=1/6

- **A.** Ratio of phosphorylated AKT to total AKT expressed in ECs in both control and high glucose environments.
- **B.** Total expression of AKT in in ECs in both control and high glucose environments.
- **C.** Ratio of phosphorylated ENOS to total ENOS expressed in ECs in both control and high glucose environments
- **D.** Total expression of ENOS in in ECs in both control and high glucose environments.

t-test ns = non-significant

3.3.1.2 Hyperglycaemia does not prevent EC alignment to flow

ECs under laminar high shear stress aligned in the direction of flow. ECs cultured under both mannitol and hyperglycaemic conditions align to HSS, under static conditions the characteristic cobblestone appearance is maintained, reflected by the flat line in **Figure3.8 a**. Although the ECs cultured using high glucose condition did align under flow, the peak at 0° is not as high as ECs cultured under the mannitol condition, indicating fewer cells fell within the angles that are associated with laminar stress. It can be seen in **Figure 3.8 b-e** that these cells did still display a flow phenotype, and the static displayed random cell placement. Osmolality was assessed between mannitol supplemented and high glucose media, there was no difference observed between media types (table 3.2).

Table 3.2. Average ±SEM osmolality of mannitol supplemented control media and high glucose (25mM) condition media.

Media Condition	Average Osmolality mOsm/kg ±SEM
Mannitol	301±1.76
Glucose	308±1.53

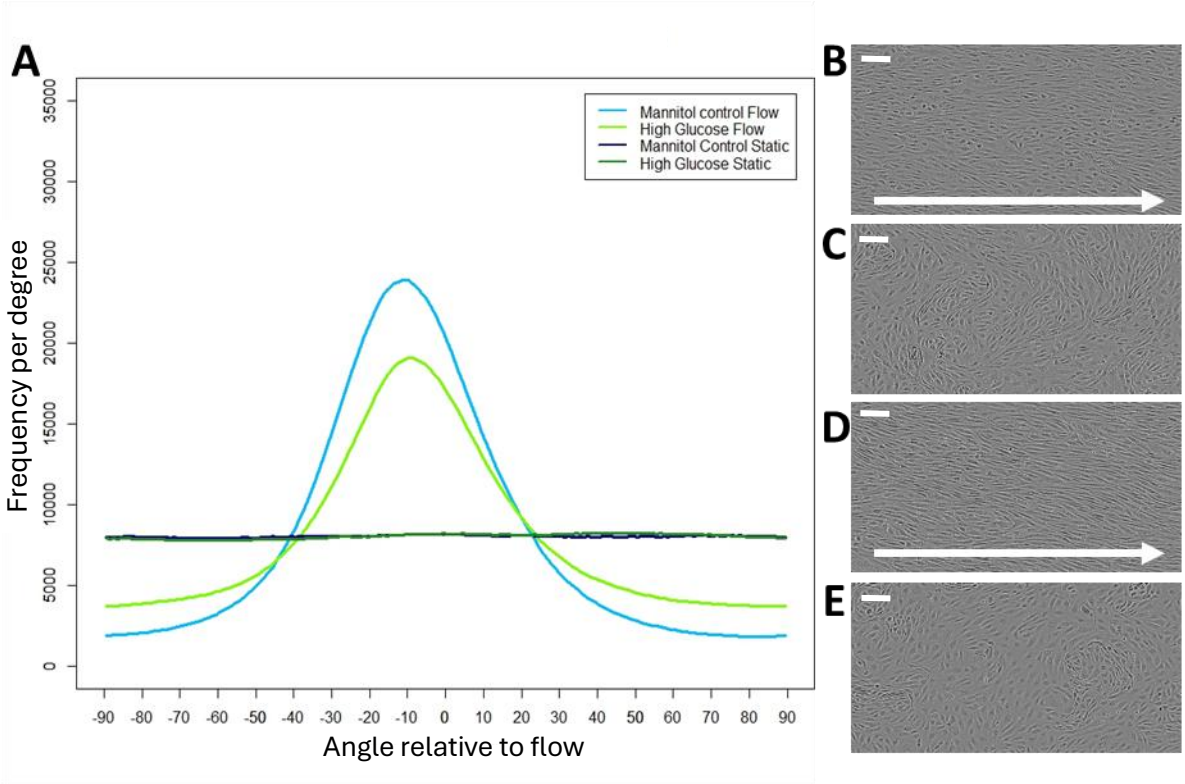

Figure. 3.8. Cells grown in both a mannitol and high glucose environment respond to shear stress and differ from those cultured statically

Scale bar is 100µm

A. Orientation analysis of cells cultured in both control and high glucose media and under static and HSS environments ±SEM n/N=3/30.

B. HUVECs cultured under HSS in a control environment

C. HUVECS cultured under static conditions cultured in a control environment

D. HUVECs cultured under HSS in a high glucose (25mM) environment

E. HUVECs cultured under static conditions in a high glucose (25mM) environment.

3.3.2. Constant hyperglycaemia has no effect on WPB numbers, size or polarity

3.3.2.1 Total number of WPBs was not affected by exposure to constant hyperglycaemia

The same measurements as detailed in **section 3.3.1** were taken to build a WPB profile. No significant differences were observed in the total number of WPBs per FOV between the mannitol control or hyperglycaemic conditions.

There was no significant impact of shear stress on the total WPB number, with consistent averages seen across all conditions (Mannitol static 1109±290, Glucose static 1182±229, Mannitol flow 1175±128 Glucose flow 1259±262) (see **Figure 3.10 a**) (p =0.9758, n/N=3/30). There is some variation between the different repeats, repeat 3 shows higher number of WPB in three of the four conditions.

The number of nuclei (number of cells) per FOV was consistent across all conditions (Mannitol static 33±3, Glucose static 31±2, Mannitol flow 31±5 Glucose flow 34±3) with no significant differences seen (see **Figure 3.10 b**) (p =0.8668, n/N=3/30). This implies that increasing the glucose concentration has not negatively impacted cell proliferation compared to the control condition, so the environment has not caused toxicity which would have confounded results.

3.3.2.2 Average number WPBs per cell was not affected by exposure to constant hyperglycaemia

The average number of WPBs per cell per FOV was consistent between the control and high glucose conditions under both static and high shear conditions (Mannitol static 32±6, Glucose static 37±5, Mannitol flow 40±5 Glucose flow 39±11; p =0.8474; n/N=3/30) (see **Figure 3.10 c**).

The number of cells expressing WPBs was consistent across all the conditions, no significant differences observed (p=0.1827). As observed in the control conditions when establishing the use of mannitol, there 1-2% fewer cells expressing WPBs when cultured in a static environment compared to the flow, this appears to be part of the flow phenotype of ECs being established (see **Figure 3.11**).

3.3.2.3 WPB length was not affected by exposure to constant hyperglycaemia

As expected, in control conditions (Mannitol), cells exposed to shear stress displayed a 'flow phenotype' whereby there were shortened WPBs (1.02±0.02) compared to static conditions (1.15±0.04; p =0.0342). This was also observed in cells exposed to hyperglycaemic (25mM Glucose) conditions under flow WPBs were shorter (1.00±0.05)

compared to those grown under static culture (1.08±0.04; p =0.0342). However, although there initially appeared to be a subtle trend between WPB length in Glucose conditions under flow, compared to control (mannitol) this was not significant (p = 0.3753) suggesting that there was no additive effect of flow and hyperglycaemia (see **Figure 3.10 d**).

3.3.2.4 WPB polarity was not affected by exposure to constant hyperglycaemia

In control (mannitol) media WPBs behaved as expected under high shear stress, the feret angle aligning with the elongation of the ECs with the direction of flow (peak clustering occurring at the 0° and 180° ends of the graph) which was distinct from EC grown under static conditions, that did not show this behaviour, with no distinct clustering, instead a full range of feret angles was observed denoting there is no distinct directionality in this environment. EC grown under hyperglycaemia also demonstrated polarity under flow conditions, however there was no compound effect of flow and hyperglycaemia see **Figure 3.12**).

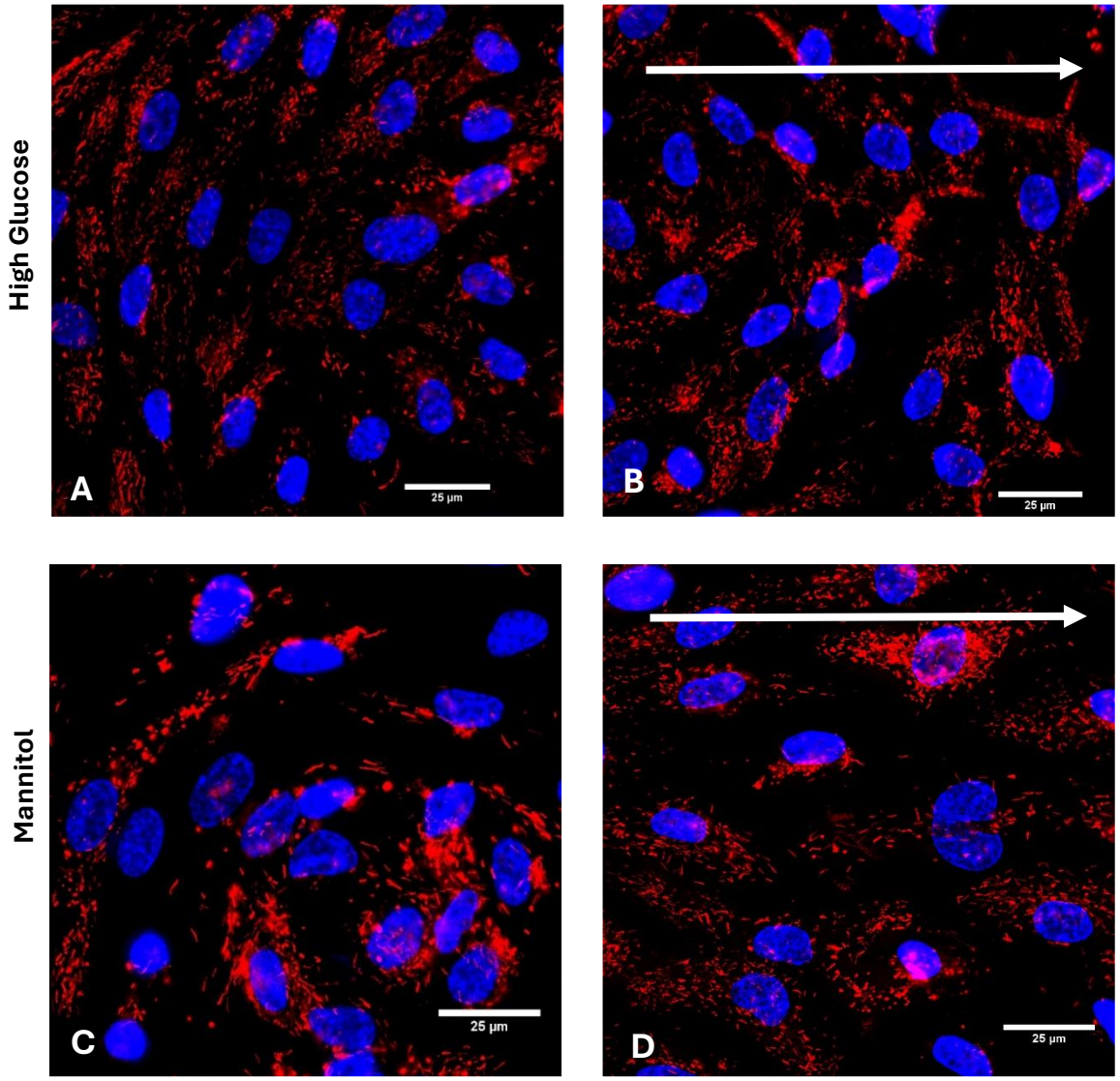

Figure 3.9. Representative images of HUVECS cultured in mannitol supplemented media and high 25mM glucose media in both static and HSS culture conditions for 48hrs.

Nuclei are in Blue (Hoechst) and WPBs are in red (VWF).

A. HUVECs cultured in static conditions in a high glucose environment

B. HUVECs cultured in HSS conditions in a high glucose environment

C. HUVECs cultured in static conditions in a mannitol supplemented environment

D. HUVECs cultured in HSS conditions in a mannitol supplemented environment

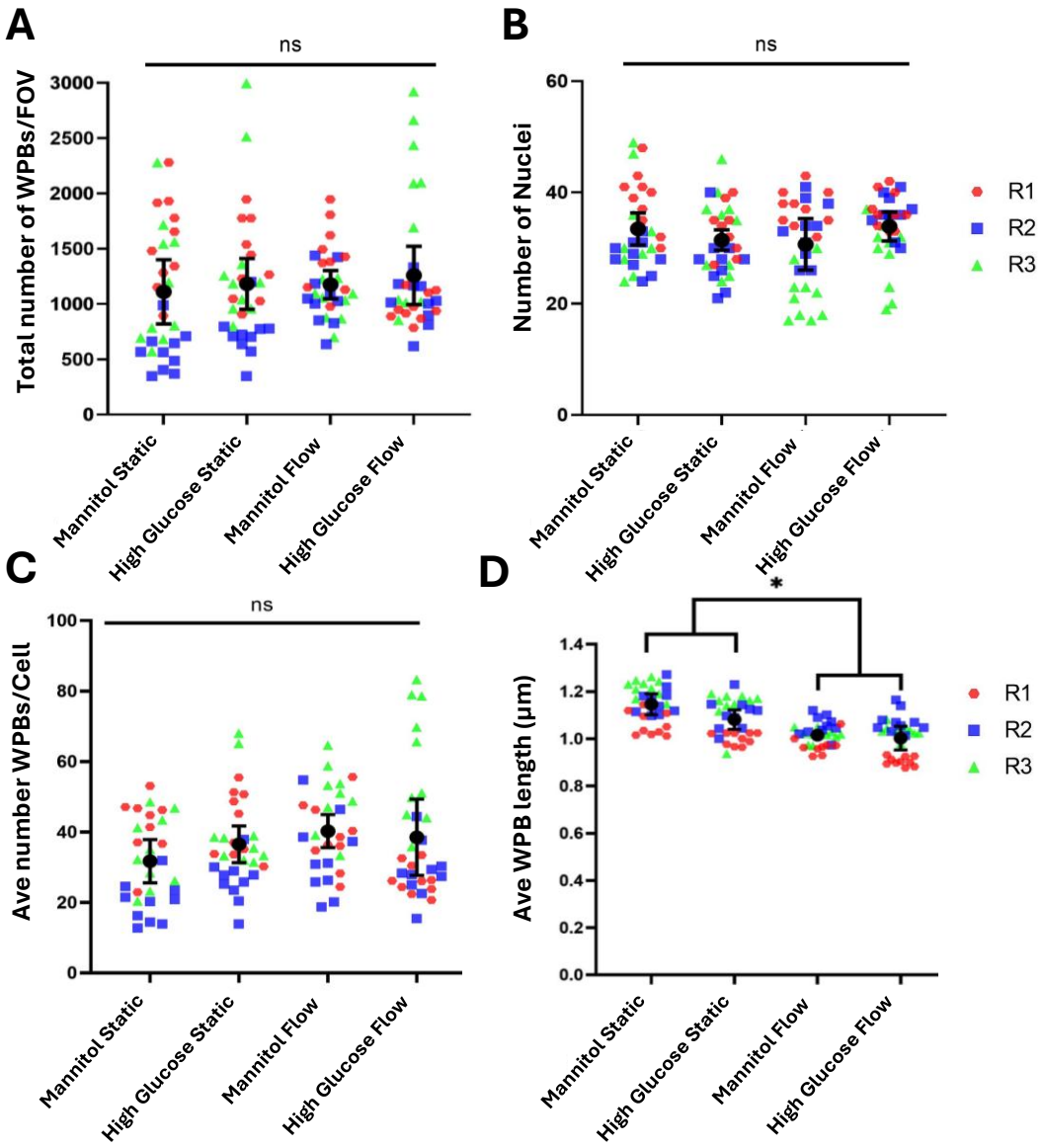

Figure. 3.10. The profile of WPBs does not significantly differ between mannitol and a high glucose environment.

A. Mean data of the total number of WPBs observed in each FOV per condition ±SEM n/N=3/30. Each data point represents a mean of all WPBs counted in an image. Colours/shapes represent technical repeats (R1 red hexagon, R2 blue square, R3 green triangle)

B. Mean data of number of nuclei counted in each FOV ±SEM n/N=3/30 Each data point represents a mean of all nuclei counted in an image. Colours/shapes represent technical repeats (R1 red hexagon, R2 blue square, R3 green triangle)

C. Mean number of WPBs per nuclei calculated in each FOV n/N=3/30. Each data point represents a mean of WPBs per cell in an image. Colours/shapes represent technical repeats (R1 red hexagon, R2 blue square, R3 green triangle).

D. Mean length of WPBs in each FOV n/N=3/30. Each data point represents a mean of WPB length per cell in an image. Colours/shapes represent technical repeats (R1 red hexagon, R2 blue square, R3 green triangle).

t-test * = p <0.05

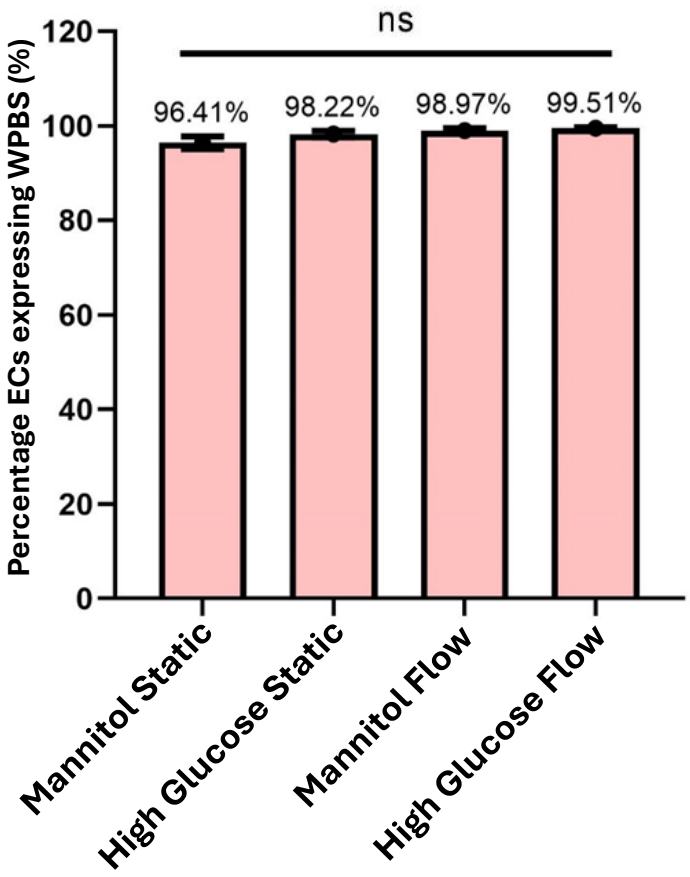

Figure 3.11. Constant hyperglycaemia does not impact the number of cells expressing WPBs.

Mean percentage of WPB 'positive' ECs ±SEM n/N=3/30. A cell area was defined around a nucleus and was assessed to see if WPBs were present within. Cell that did not were considered to not be producing WPBs. The ECs were subtracted from WPB 'positive' ECs and a percentage calculated.

ANOVA ns= non-signifiant

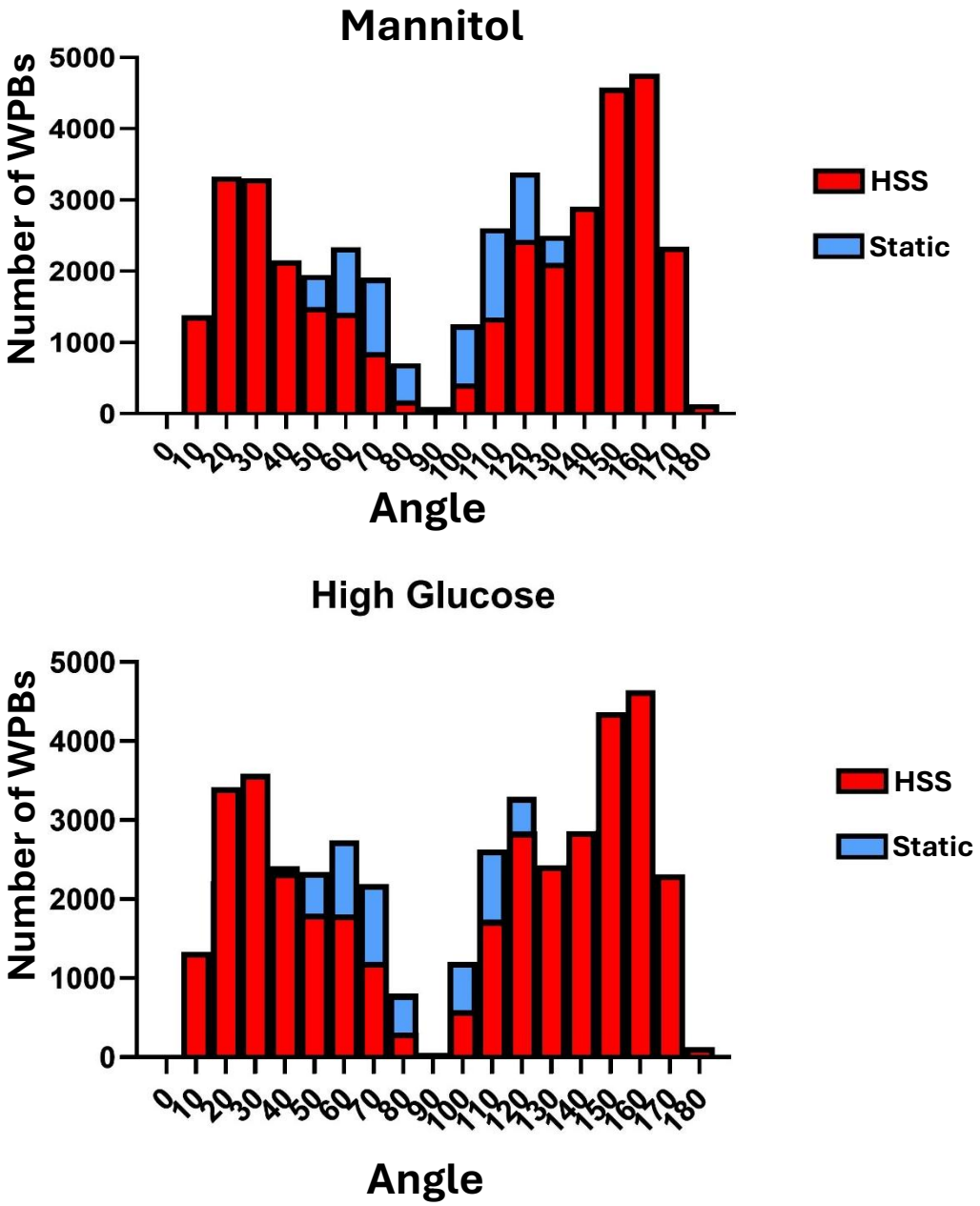

Figure 3.12. WPBs in cells in static culture (Blue) are more randomly orientated compared with those from flow culture (Red) overlayed in both mannitol and high glucose (25mM) environments.

A. Angles of WPBs in cells cultured in mannitol media for 48hrs under static or HSS conditions.

B. Angles of WPBs in cells cultured in high glucose supplemented media for 48hrs under static or HSS conditions.

3.3.3 Impact of hyperglycaemia on WPB Function

3.3.3.1 VWF Strings released from WPBs

When cells are stimulated by vascular injury or with a physiological agonist such as histamine, WPBs move and fuse to the cell membrane and exocytose their stored cargo. VWF is released as a bolus which, under flow, unravels and forms string-like structures, extending into the vessel lumen whilst remaining tethered to the endothelial cell itself (see **Figure 3.13**) (226). Binding sites are revealed that allow platelets and circulating VWF to attach and initiate the formation of the platelet plug necessary for primary haemostasis (23, 227). The length of these released strings is thought to be determined by the number of VWF 'quanta' stored within the WPB, this in turn also dictates the length of the WPB when formed (108). As such, the length of the VWF strings is thought to be correlated to the length of the observed WPBs. Longer strings have been shown to consist of higher molecular weight VWF (HMW), which is preferentially stored in WPBs and has an increased thrombotic capacity (94, 228). Diabetes is associated to thrombotic dysregulation, with patients more prone to increased thrombosis (229). I hypothesised that cells cultured under a high glucose or hyperglycaemic condition would display a phenotype favouring increased thrombosis, identified through the presence of longer exocytosed VWF strings.

4.3.3.2 Number of VWF strings was not affected by exposure to chronic hyperglycaemia

Similarly to analysis of WPBs, the number of strings observed in each FOV was assessed. The number of strings released in each condition was reasonably consistent with no significant differences observed between any of the conditions (Mannitol static 256±39, Glucose static 337±109, Mannitol flow 330±74 Glucose flow 331±114) (see **Figure 3.14 a** (p =0.9477). Nonetheless, a subtle trend persists in which the ECs in the hyperglycaemic condition yield a marginally greater volume of strings. This can be observed in both the static and flow conditions. So, it appears that culturing ECs in high glucose may have an influence on the exocytosed VWF.

4.3.3.3 Length of VWF strings was affected by consistent exposure to chronic hyperglycaemia.

Upon histamine stimulation, endothelial cells (ECs) cultured under both static and flow conditions released VWF from WPBs (**Figure 3.13**). Quantitative analysis revealed that VWF strings released under static conditions were significantly longer in the control group (Mannitol 10.21±0.78μM) compared to those from cells exposed to flow (Mannitol 6.79±0.43μM) (**Figure 3.14 b**; p = 0.0187). This finding aligns with the flow-mediated

endothelial phenotype consistent with previous studies, in which shear stress modulates WPB exocytosis and VWF string characteristics (59). ECs exposed were exposed to hyperglycaemic conditions, there was no significant difference between the static and flow conditions (10.13±1.37μM, 8.58±1.00μM; $p = 0.4124$).

My findings support a model in which static culture conditions, characterised by an absence of hemodynamic shear, promote a phenotype of increased thrombotic potential, with an increased capacity for platelet recruitment , reflected by the generation of longer VWF strings. These longer strings are associated with increased platelet binding and thrombogenic potential, a hallmark of endothelial dysfunction.

Although no statistically significant differences in VWF string length were observed between mannitol control and high glucose conditions in either static ($p= 0.9616$) or flow conditions ($p = 0.1767$), a trend toward longer strings in the high glucose group was noted. Importantly, the shortening of VWF strings typically induced by flow was no longer evident in the high glucose condition suggesting that hyperglycaemia attenuates the protective effects of flow on endothelial function.

These observations indicate that high glucose alters endothelial phenotypes, promoting a greater tendency towards thrombotic activation regardless of shear stress. Thus, hyperglycaemia appears to induce a pathogenic phenotype that disrupts the normal regulatory effects of flow on WPB-mediated VWF secretion.

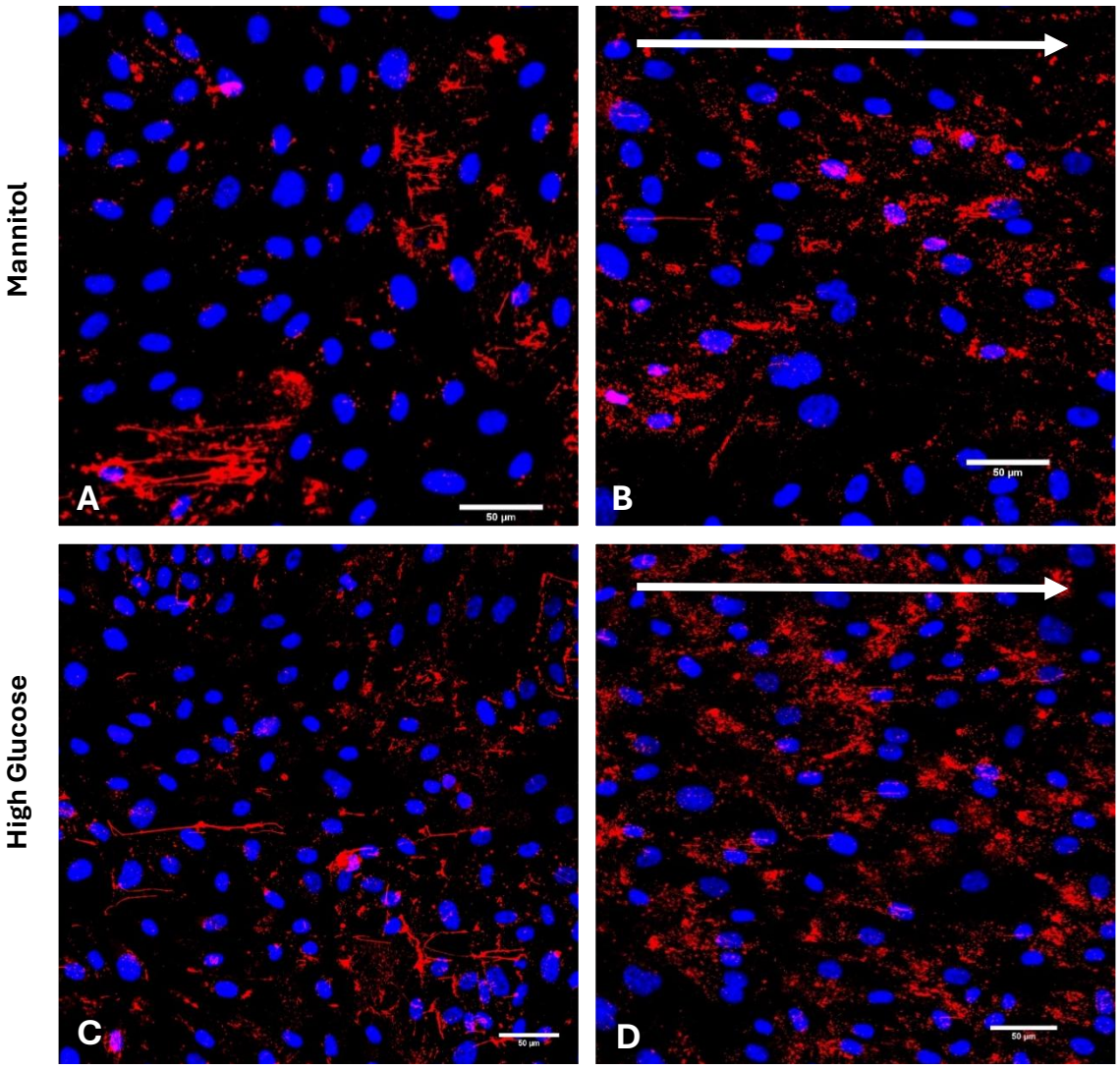

Figure 3.13. Representative images (x60) of HUVECS cultured in control media and high glucose media in both static and HSS culture conditions after acute exposure to histamine to stimulate WPB exocytosis and VWF string formation.

Nuclei are in Blue (Hoechst) and VWF strings are in red (VWF).

A. ECs cultured in mannitol media and grown under static conditions for 48hrs

B. ECs cultured in mannitol supplemented media and cultured under HSS for 48hrs

C. ECs cultured in high glucose supplemented media and grown under static conditions for 48hrs

D. ECs cultured in high glucose supplemented media and grown under HSS conditions for 48hrs

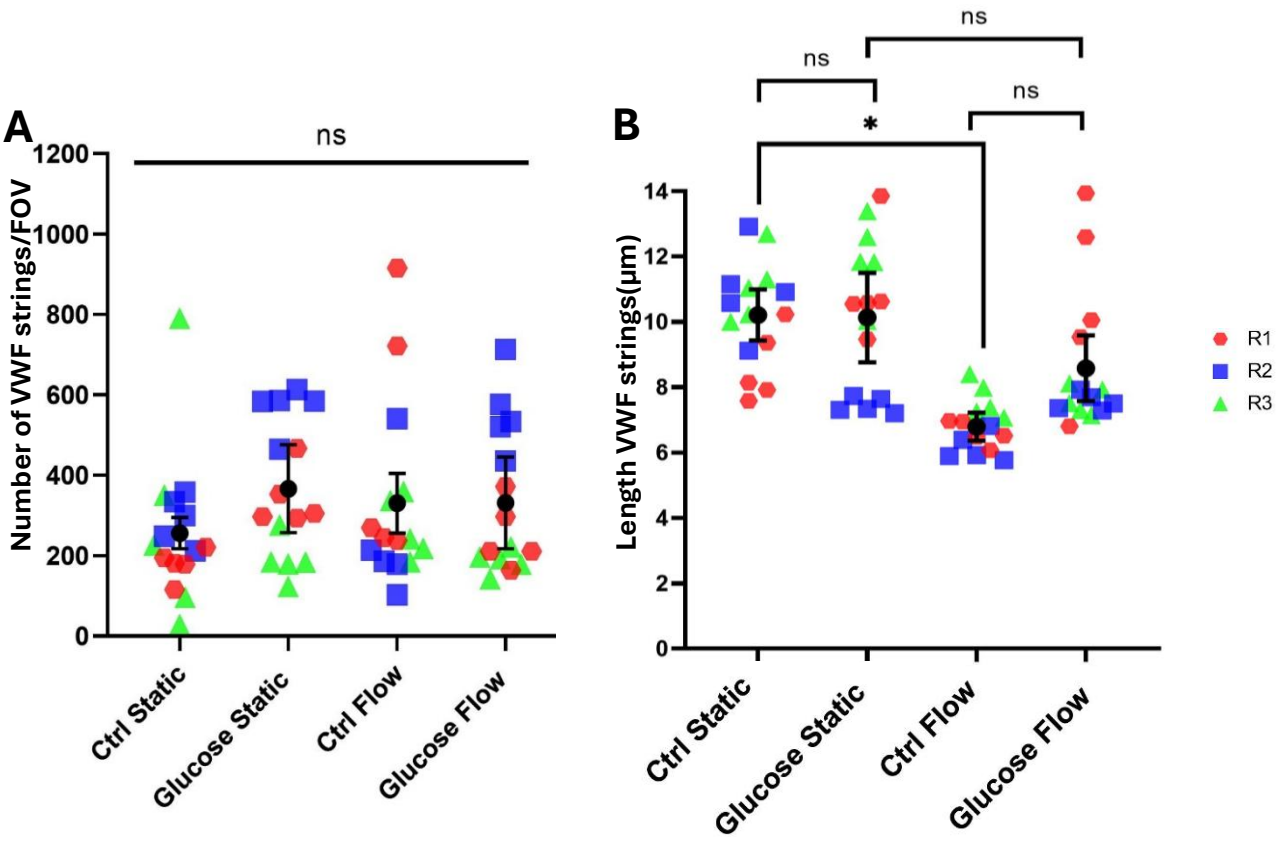

Figure 3.14. Cells from both normo-glucose EGM2 and high glucose environments release a similar number of VWF strings that differ in length.

A. Mean number of VWF strings released by ECs as shown in the images x ±SEM n/N=3/15. Each data point represents a mean number of all VWF strings counted in an image. Colours/shapes represent technical repeats (R1 red hexagon, R2 blue square, R3 green triangle)

B. Mean length of VWF strings released by ECs in each FOV in condition ±SEM n/N=3/15. Each data point represents a mean length of all VWF strings counted in an image. Colours/shapes represent technical repeats (R1 red hexagon, R2 blue square, R3 green triangle).

t-test * = p <0.05, ns = non-signifiant

3.4 Model 2: Ambulatory glucose cycles between hypo- and hyper-glycaemic environments for diabetes and a control counterpart

The high glucose model formed a springboard for the development of a more physiological relevant system, the ambulatory glucose model. ECs cultured in a consistent and non-physiological hyperglycaemic milieu elicited subtle changes, but HUVECs were robust enough to adapt to their environment. Recognising the limitations of static hyperglycaemia, I sought to develop a model that more accurately reflects the glycaemic fluctuations experienced *in vivo*. To achieve this, I used utilised continuous glucose monitoring (CGM) data to define representative glycaemic profiles for both diabetic and non-diabetic individuals (208). These profiles were then used to cycle ECs through alternating hyperglycaemic and hypoglycaemic glucose concentrations over a 48-hour period, simulating an average pattern of fluctuations in blood glucose levels. This dynamic approach aimed to capture the metabolic variability observe in daily life and to test the hypothesis that fluctuating glucose levels, rather than sustained hyperglycaemia, may elicit a more pronounced endothelial response.

The design of this model was informed by findings from other research groups indicating that cells are often more sensitive to physiologically relevant, modest fluctuations in glucose levels than to extreme or sustained exposures (230). By integrating these insights, the ambulatory glucose model offers a refined tool for investigating endothelial dysfunction in the context of diabetes and glycaemic variability.

To assess the impacts of this model, the same measurements were taken of WPBs as the previous consistent high glucose model.

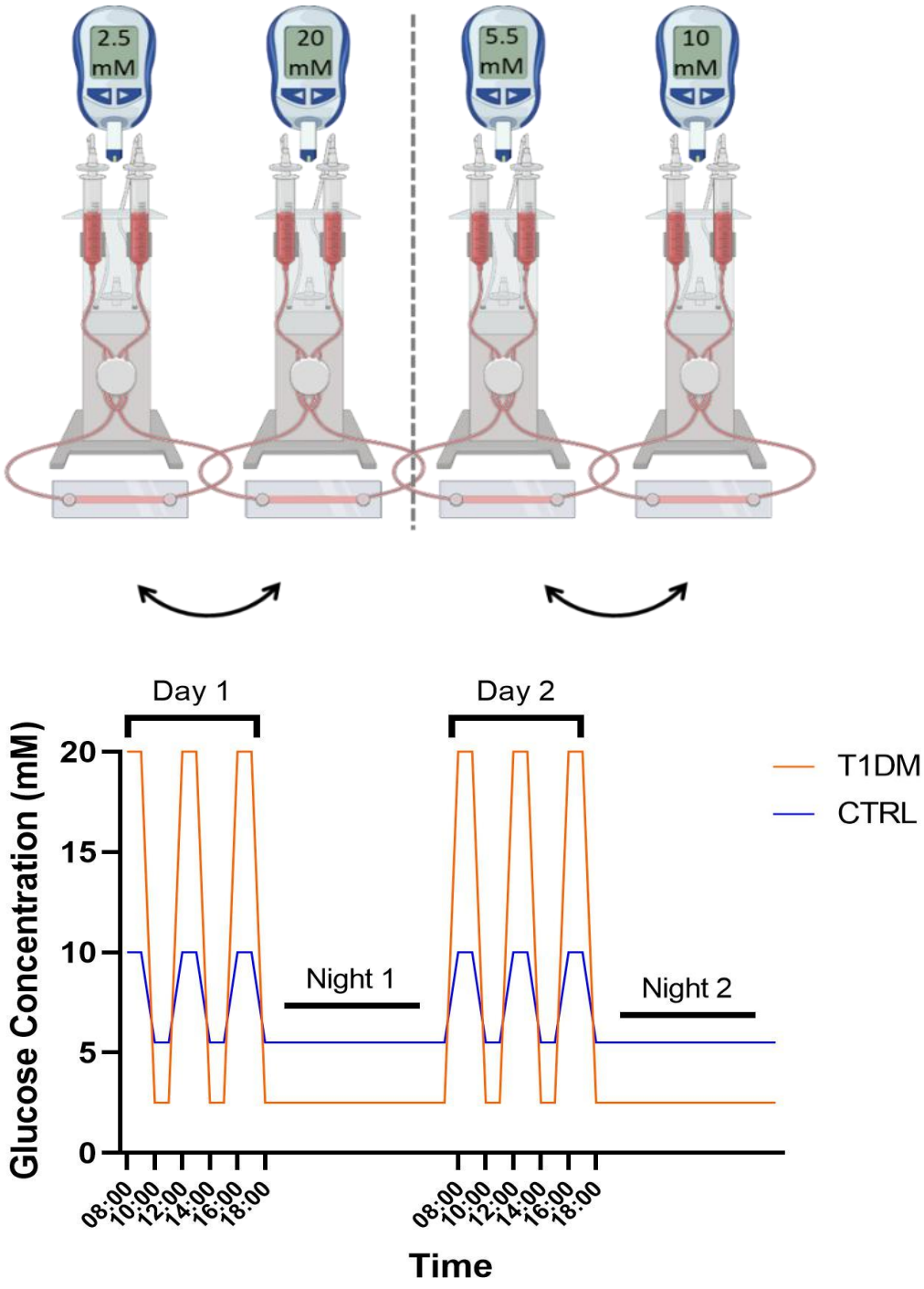

Figure 3.15. Ambulatory glucose model of diabetes with cells in both static and SS environments.

ECs were maintained for 48hrs, glucose was cycled between a hypo and hyperglycaemic environment for two twelve-hour periods to mimic an 'average' day of blood glucose fluctuations with eating. Concentrations of glucose were extrapolated from continuous glucose monitoring data from Battelino et al to maintain physiological relevance. Control hyperglycaemia was 10mM, hypoglycaemia was 5.5mM, diabetic hyperglycaemia was 20mM and hypoglycaemia was 2.5mM (208).

3.4.1 Ambulatory glucose exposure does not affect EC alignment

3.4.1.2 EC alignment shows no difference between diabetic and control glucose exposure

Following 48hrs of HSS exposure the alignment of the cells was assessed. There was no static counterpart to this model due to the switching nature of the glucose medias. To change the media, the slides were switched between different IBIDI perfusion kits in separate fluidic units, this was done as quickly and efficiently as possible, however it still introduces the possibility of disrupting the endothelial monolayer, so it was essential to investigate the cell alignment following treatment.

Both the diabetic and control conditions aligned with the direction of flow seen in both the data and the raw images of the cells (see **Figure 3.16**). The peaks overlay each other at the same angle of flow, which is right around 0° degrees indicating that they are horizontal, in line with the channel and flow direction. The control does have a peak that reaches slightly higher than that of the diabetic which may indicate a tighter alignment. This is a highly minimal effect, however as a greater variation was seen in the high glucose model as previously detailed, it is worth considering it as a potential result of exposure to extreme physiological glucose environments.

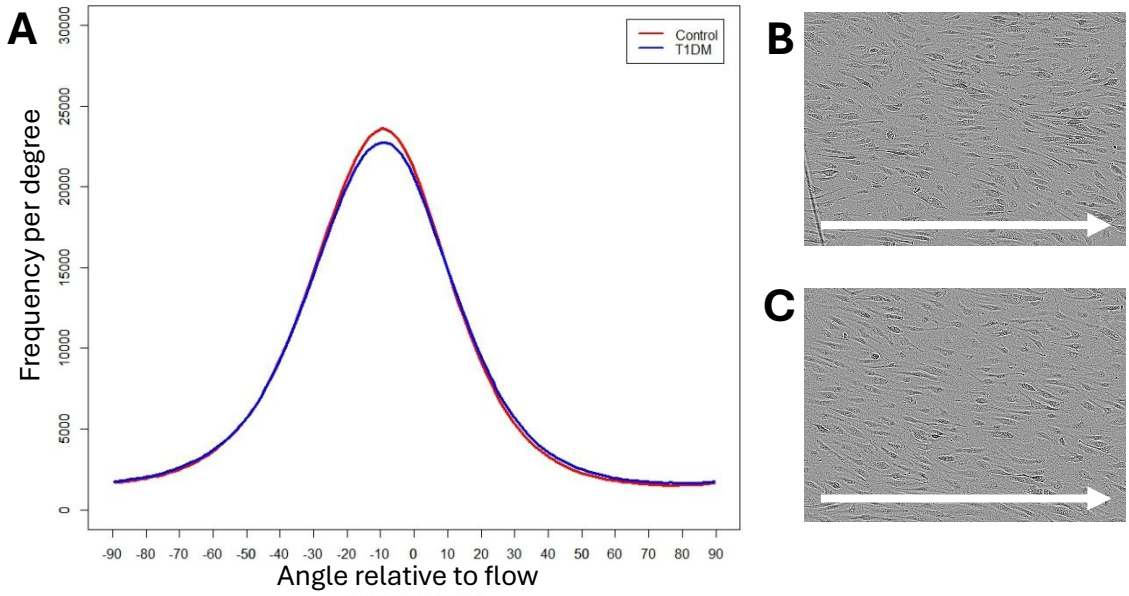

Figure 3.16. Cells from both the control and diabetic sides of the ambulatory model align with the direction of shear stress

A. Orientation analysis of cells cultured in both the control and diabetic models of the ambulatory model ±SEM n/N=3/30.

B. HUVECs cultured under HSS in the control side of the model

C. HUVECS cultured under HSS in the diabetic side of the model

3.4.2 Ambulatory glucose exposure has no impact on WPB Form

3.4.2.1 Total number of WPBS was not affected by exposure to oscillating glucose environments

As established, the number of WPBs observed relates to the thrombotic capacity, providing insights into the characteristics of a cell population. WPBs from each condition are illustrated in **Figure 3.17**. There were no significant differences between the total number of WPBs observed per FOV in the control and diabetic environments (Ctrl 1598±361, T1DM 1446±167) (see **Figure 3.18 a**) (p =0.7228). Both conditions showed variation between the repeats however the diabetic was more consistent which was reflected through smaller error bars. In contrast, the control condition showed a wider variation with a pattern of clustering between the three repeats. The repeats did still overlap with one another, but the result is a larger spread of data.

4.4.2.2 Number of Cells was not affected by exposure to oscillating glucose environments

The number of cells in each condition is a marker of their health, i.e. ability to proliferate. Ideally this parameter should be matched, or as close as possible, between conditions, as this indicates that the observed results are due to the treatment rather than a reduced number of cells. In this model there was no significant differences between the number of nuclei between the control and diabetic conditions (Ctrl 23±2, T1DM 21±22) (see **Figure 3.18 b**) (p =0.7231). Moreover, there was no clustering or distinction between repeats, indicating that the cells in both conditions were growing at a similar rate. This suggests that results found are not likely to be attributable to variations in cell viability.

4.4.2.3 Average number of WPBs per cell was not affected by exposure to oscillating glucose environments

There were no significant differences seen between either condition regarding the average number of WPBs per cell (Ctrl 73±17, T1DM 71±16) (see **Figure 3.18 c**) (p =0.9293). There is a fair degree of variation within the averages of both the diabetic and control environments with some clustering of repeats, which is more pronounced with the control condition.

4.4.2.4 WPB length was not affected by exposure to oscillating glucose environments

The length of WPBs, as established, is a marker of thrombotic potential, is hypothesised to be greater in diabetics. In both environments the clustering was very tight with no discernible differences between repeats. There were also no significant differences between the control and diabetic conditions (see **Figure 3.18 d**) (p = 0.9108). Both had an

average feret length in line with the expected flow phenotype (Ctrl 1.05±0.01, T1DM 1.04±0.01).

4.4.2.5 WPB Polarity was not affected by exposure to oscillating glucose environments

As established, ECs in both conditions aligned with the direction of flow, the directionality of WPBs within these cells was also assessed. Both diabetic and control ECs displayed alignment of WPBs in along the direction of flow (see **Figure 3.19**). Both show increased clustering at the 0° and 180° degree angles, indicating horizontal directionality. This is highlighted in the images of **Figure 3.17**.

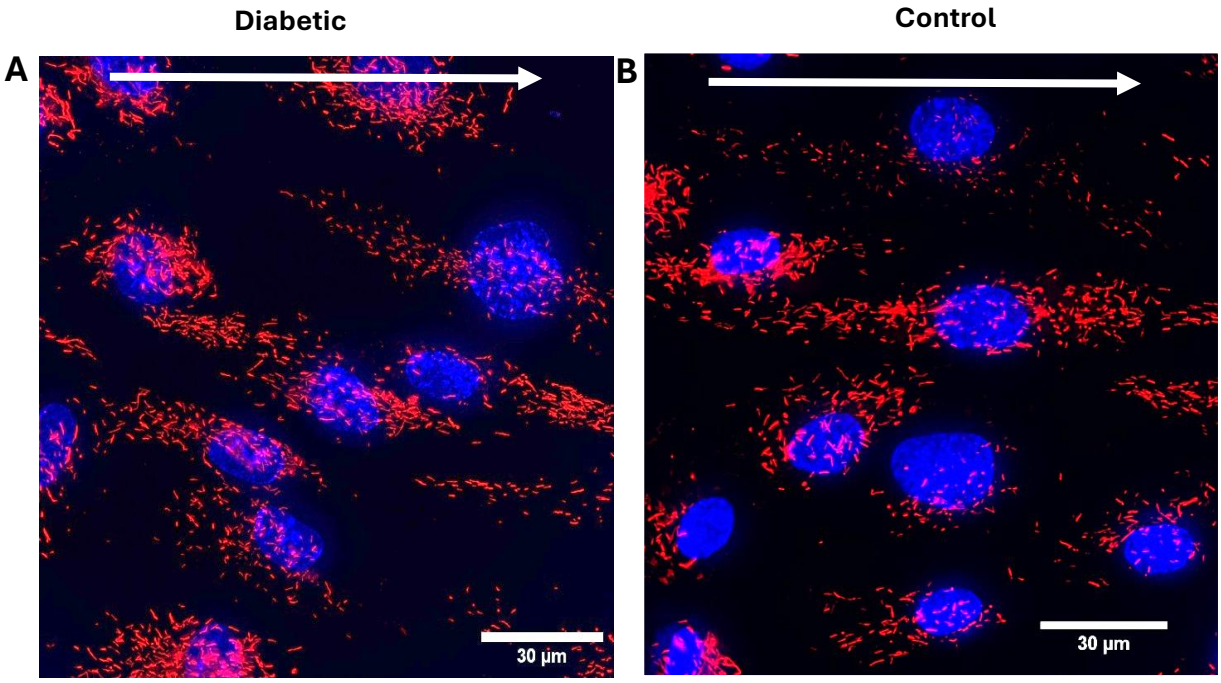

Figure 3.17. Representative images of HUVECS cultured in the ambulatory glucose model in a control and diabetic condition both under HSS culture for 48hrs.

(A) HUVECs (Hoechst blue) cultured under HSS in a diabetic condition with WPBs (VWF red), arrow denotes direction of flow.

(B) HUVECs (Hoechst blue) cultured under HSS in control condition with WPBs (VWF red) arrow denotes direction of flow.

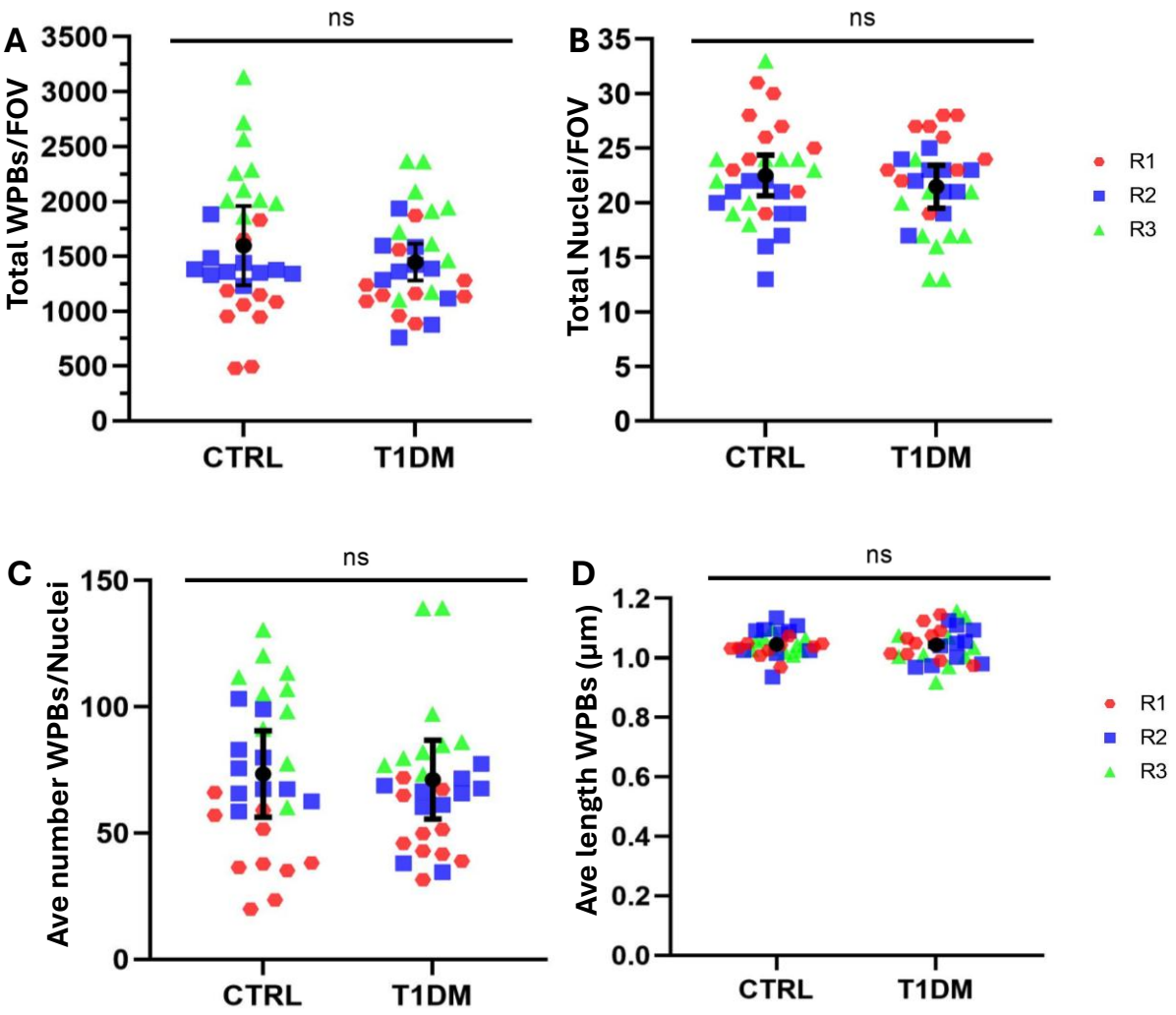

Figure 3.18. WPB profile of cells from a control and diabetic environment of an ambulatory glucose model don't differ from one another

A. Mean data of the total number of WPBs observed in each FOV per condition ±SEM n/N=3/30. Each data point represents a mean of all WPBs counted in an image. Colours/shapes represent technical repeats (R1 red hexagon, R2 blue square, R3 green triangle)

B. Mean data of number of nuclei counted in each FOV ±SEM n/N=3/30 Each data point represents a mean of all nuclei counted in an image. Colours/shapes represent technical repeats (R1 red hexagon, R2 blue square, R3 green triangle)

C. Mean number of WPBs per nuclei calculated in each FOV n/N=3/30. Each data point represents a mean of WPBs per cell in an image. Colours/shapes represent technical repeats (R1 red hexagon, R2 blue square, R3 green triangle).

D. Mean length of WPBs in each FOV n/N=3/30. Each data point represents a mean of WPB length per cell in an image. Colours/shapes represent technical repeats (R1 red hexagon, R2 blue square, R3 green triangle).

t-test ns = non-signifiant

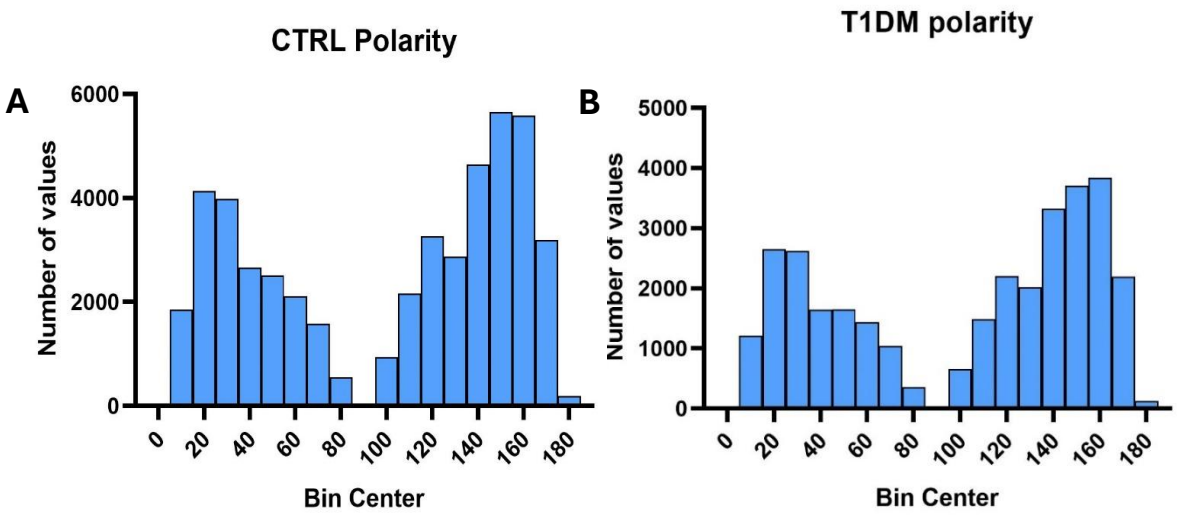

Figure 3.19. Angles of WPBs under both control and diabetic conditions align with shear stress.

Histogram of WPB angle across both control and diabetic conditions. Number of WPBs clustered at each angle forms the bar. The angle of each WPB is in reference to how horizontally it lies.

3.4.3 Ambulatory glucose exposure has no impact on WPB function

As above, the functionality of WPBs was assessed through investigation of expressed VWF strings following exocytosis triggered by stimulation with histamine. To ensure that the protocol was successful, a positive control was included, this constituted a control slide of cells cultured under static conditions exposed to PMA to induce an 'all-out- response from the ECs. Representative images of the control and high glucose condition, plus the positive control can be seen in **Figure 3.20**.

4.4.3.1 Number of VWF strings was not affected by exposure to oscillating glucose environments

The number of strings expressed in both diabetic and control conditions displayed a large variation with some separation observed between repeats. Within this, the diabetic does have a higher mean number of strings (362±210) compared to the control (248±108) however due to this variation, this difference is not significant (see **Figure 3.21 a**) (p =0.6566).

4.4.3.2 Length of VWF strings was not affected by exposure to oscillating glucose environments

Thrombotic potential of each environment was gauged through mean length of VWF strings. The length of strings in the diabetic environment are consistently longer than those in the control (6.91±0.60μM) vs (5.90±0.23 μM), however this difference was not significant (see **Figure 3.21 b**). There was clustering of the repeats in both conditions but no distinction between each one (p =0.1921). String structures were not truly observed as expected in the flow environments and the HSS conditions differ quite substantially from the positive control (see **Figure 3.20**). Smaller strings are expected under HSS, highlighting the pathogenic nature of static culture.

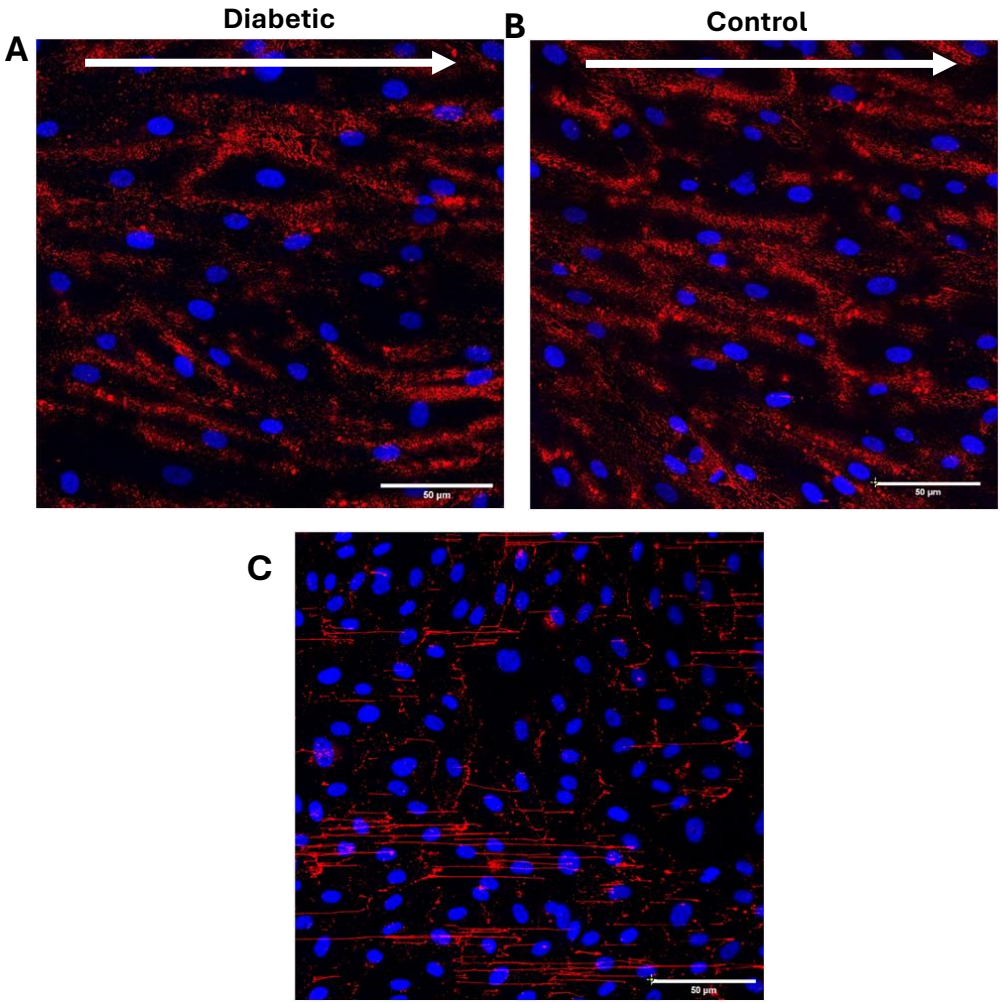

Figure 3.20. Representative images of HUVECS cultured in the ambulatory glucose model after acute exposure to histamine to stimulate WPB exocytosis in a control condition and diabetic condition both under HSS culture for 48hrs.

A. HUVECs cultured in a diabetic environment

B. HUVECS culture in a control environment

C. Positive control, HUVECS cultured in static conditions and under normo-glucose EGM2 conditions exposed to acute PMA stimulation to trigger exocytosis of WPBs. PMA is a non-physiological compound and acts as a positive control for the experiment. Nuclei are in Blue (Hoechst), and WPBs are in red (VWF).

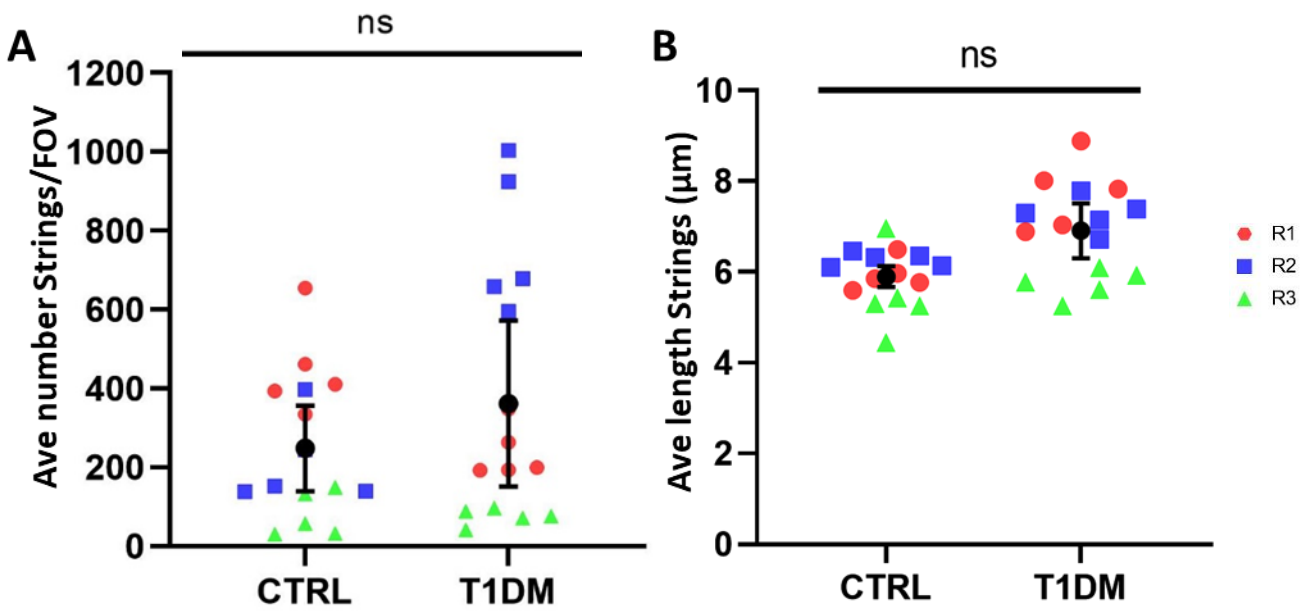

Figure 3.21. ECs cultured in an oscillating hyper- and hypoglycaemic diabetic environment showed no difference in number of strings and string length compared to those cultured under an oscillating glucose control environment

A. Mean number of VWF strings released by ECs in each FOV in condition ±SEM n/N=3/15. Each data point represents a mean number of all VWF strings counted in an image. Colours/shapes represent technical repeats (R1 red hexagon, R2 blue square, R3 green triangle)

B. Mean length of VWF strings released by ECs in each FOV in condition ±SEM n/N=3/15. Each data point represents a mean length of all VWF strings counted in an image. Colours/shapes represent technical repeats (R1 red hexagon, R2 blue square, R3 green triangle).

t-test ns = non-signifiant

3.5 Discussion

In this chapter I investigated whether pathological glucose dysregulation, synonymous with diabetes, alters the form and function of WPBs synthesized in healthy HUVECs. I successfully developed a model to assess physiologically relevant hyperglycaemic conditions using mannitol as a control. Using these models, I established that glucose had limited impact on WPBs form or function in HUVECs. Glucose is closely linked to diabetes, with hyperglycaemia serving as a hallmark of the disease and its associated complications (231). However, glucose levels can be precisely controlled in an *in vitro* setting allowing for targeted investigation of its effects. If there is no intervention, prolonged exposure to hyperglycaemia can lead to serious complications from acute damage such as osmotic or inflammatory stress to systemic issues such as neuropathy and retinopathy (232) (233) (234).

The high glucose and ambulatory glucose models highlighted that HUVECs are environmentally adaptable tolerating 48hrs of both chronic hyperglycaemia and cycles of extreme hypo- and hyperglycaemia while exposed to HSS. As such, there were more subtle differences observed between conditions. Mannitol was accepted as a suitable control to glucose as it was shown to have no effect on the ECs. Key characteristics including alignment of cells and WPB feret size were consistent between EGM2 and mannitol supplemented media environments and almost complete overlap of data points.

Under chronic hyperglycaemia, WPBs exhibited a morphological profile comparable to that observed in control conditions. However functional differences emerged in the length of VWF strings released upon stimulation, whereby under hyperglycaemic conditions, ECs did not exert the typical response to flow (shorter strings) as observed in control (mannitol) conditions. ECs exposed to high glucose did not display a flow-mediated phenotype, with no difference in string length between HSS and static culture, suggesting that exposure to hyperglycaemia may be beginning to disrupt WPB function. Given that a diabetic environment is regarded as a prothrombotic, the loss of the HSS phenotype is a promising indicator, suggesting the presence of longer strings and consequently increased thrombotic potential with a greater potential for platelet capture and clot formation. This observation aligns with existing literature which reports elevated VWF levels in diabetic populations (192-195, 235). The WPBs observed did not fully behave as expected with no significant differences in their length or number under diabetic conditions. This contrasts with findings from animal models which suggest that diabetes can influence both the size and abundance of WPBs in EC populations (191, 196, 197).

Longer length of VWF equates to increased thrombotic potential (greater capacity for platelet recruitment), typically associated with the pathological static environment (67, 228). These findings imply that chromic hyperglycaemia may compromise the atheroprotective effect of HSS. Comparable findings have been observed in similar studies; one such investigate EC morphology as a measure of response to shear and glucose. Their methodology is somewhat subverted to the models I have presented, with cells cultured static for 7 days under either a control (5mM) or hyperglycaemic (22mM) environment (236). ECs were subsequently exposed to 10 dyne/cm^2 shear stress for a brief period of up to 15 minutes (236). Notably, HUVECs subjected to prolonged hyperglycaemic conditions exhibited marked morphological changes compared to the controls including reduced elongation (as would be consistent with a shear stress phenotype) and evidence of cell shrinkage, suggestive of oxidative damage (236). These observations support the findings of my models, indicating that hyperglycaemia may attenuate endothelial responsiveness to shear stress and in doing so potentially compromise the atheroprotective effects conferred by blood flow.

To provide further context to the high glucose model, the internal biochemistry was assessed, investigating the effects of high glucose exposure phosphorylation of AKT and eNOS, both representative cellular process pathways commonly affected in diabetic patients (8, 237). Whilst visually it appeared that both pAKT and peNOS were elevated, numbers were too low to achieve significance. These findings may suggest that high glucose exposure influences the phosphorylation activity of both proteins. Increasing the sample size would help clarify this potential effect. Due to methodological constraints, protein analysis under HSS was not feasible, however, future studies could explore whether the observed variation persists within an atheroprotective flow environment. Incorporating ambulatory glucose conditions would also offer valuable insight into how oscillations between hyper- and hypoglycaemia affect AKT and eNOS signalling in HUVECs. Phosphorylation of eNOS in literature is reduced in diabetes, yet in the high glucose model it was increased (238). Unlike AKT, the level of total eNOS expressed was not consistent between conditions and decreased by half under high glucose than control. It is suggested that eNOS activity and expression may be proportional to duration of diabetes, with an increase noted in earlier stages of diagnosis and declining with disease duration progressing (239). As there is a clear if not significant difference between control and diabetic environments it would suggest that high glucose affects ECs metabolic activity, given the simplicity of the model, it does support moving towards a more nuanced approach.

The high glucose model was developed into the ambulatory glucose approach to increase physiological relevance. Once again, WPB morphology was consistent between the diabetic and control glucose environments, displaying minimal variation. Within this diabetic context, exposure to glucose dysregulation appear to influence WPB function as evidenced by release of longer VWF strings upon stimulation with histamine. As longer strings have a greater thrombotic capacity, this may be suggestive of pathological alterations. Both approaches indicate that glucose dysregulation may initiate modulation of VWF release from WPBs, albeit at a level currently below statistical detectability, providing a solid foundation to build upon.

In both T1DM and T2DM populations, VWF has been demonstrated to be significantly elevated and identified as a potential biomarker of CVD risk, compared to non-diabetic populations (192-194). Several studies have reported elevated levels of VWF in both its active and inactive forms alongside abnormalities in multimerization (202). These changes have also been observed in diabetes related complications such as retinopathies (240, 241). Based on this I hypothesised that exposure to hyperglycaemic conditions or persistent dysregulation of glucose would impact WPBs, the primary intracellular store of VWF in ECs. Given that increased VWF levels are a hallmark of diabetes in literature and that longer VWF strings have greater thrombotic potential (longer strings can bind to a greater number of platelets, increasing the likelihood of clot formation), I anticipated a potential increase in length and frequency of WPBs or release of longer VWF strings reflecting a shift towards a greater propensity for thrombus formation within the endothelial phenotype (228). The high glucose model showed no difference in the profile of WPBs between the mannitol supplemented and high glucose (25mM) environments. Several clinical investigations of diabetes and CVD have highlighted increased concentrations of VWF in plasma, which could correlate with an increase in WPBs. As this approach was conducted in isolated ECs, it excludes analysis of released VWF which may have resulted in higher extracellular levels of VWF. The high glucose and ambulatory glucose models developed in this study enable controlled investigation into the effects of hyper- and hypoglycaemic environments on the endothelium. To achieve this the models necessarily focus on a single facet of a multifactorial disease, representing a reductionist approach to replicating diabetes *in vitro.* As a result, they may lack certain systemic components required to elicit a full endothelial response and the stress imposed on HUVECS may not fully recapitulate the complexity of diabetic pathology. Critically investigation into isolated cells removes the contextual complexity of intact blood vessels

including cross talk between tissues, an important consideration when interpreting *in vitro* findings. ECs are continuously exposed to circulating and cycling glucose when in situ throughout a person's life span (242). Therefore, the absence of a marked morphological variation between control and HG environments is not an unforeseen outcome. The ambulatory model was designed to highlight and exaggerate the fluctuations in blood sugar processed by ECs daily. By switching from extreme but physiological hyper and hypoglycaemia I hoped to capture how this may impair endothelial function, resulting in changes to WPB populations. However, HUVECs adapted once again and processed the changes to their surroundings. Fluctuations of this magnitude would be uncommon in diabetic patients, long term especially with treatment. Other groups have identified that ECs may in fact have a harder time adapting to smaller glucose fluctuations than these extreme one in a 48hrs window, reporting changes to the expressed phenotype (230). Byford et al, demonstrated that fluctuations from normoglycaemia (5mM) to mild hyperglycaemia (7mM) elicited dysregulation in *ex vivo* human placental explants to vascular development pathways (230). While this is not specific to a cell line model, it does indicate the effects of more subtle, physiologically relevant glucose manipulation on human tissues. This presents another avenue of investigation as more frequent smaller oscillations in glucose may better reflect the glycaemic patterns seen in patients undergoing medical interventions for diabetes.

Comparative to the animal models discussed results from these models differed from the anticipated results. Study of WPBs in a diabetic context have been historically concentrated in animal models of disease (191, 196). Anderson et al demonstrated that within the retinas of dogs with induced diabetes, there was an increase in the total number of WPBs compare to control samples. Moreover, this result was amplified in venous tissue compare to aortic, illustrating the heterogeneity of WPBs across vascular beds (191). It was suggested that under a hyperglycaemic diabetic environment, there was an increase in VWF synthesis, resulting in a greater number of WPBs (191). Elevated counts of WPBs have been previously associated to diseases such as atherosclerosis and rheumatic disease, which suggests there may be a role for categorising WPBs are a diagnostic tool (191). The elevated VWF n plasma was thought to be the potential cause of diabetic complications such as diabetic retinopathy in this study. These findings have been reinforced in both mouse and hamster studies conducted by Popov et al. Within the aortic endothelium, 2.8-fold higher number of WPBs was observed in the diabetic mice compare to the control (196). In a model of diabetes in hamsters Popov and Simonsecu reported an 'observed abundance' of WPBs within the venular endothelium of the lungs

and posited themselves that diabetes may be responsible for the elevation of plasma concentrations of VWF previously reported in diabetic patients (197). While the animal models presented display a degree of discrepancy between findings related to WPBs in different vascular beds, the universal conclusion was an association between VWF and diabetes that could be assessed through study of WPBs. In line with these animal models, adaptations to WPBs were anticipated within the diabetes models I constructed for this investigation. Although none of the observed changes reached statistical significance, there were indications of early dysregulation of WPB morphology under high or fluctuating glucose conditions. Given that animal models typically span longer durations (6 weeks to 5 years) and allow for multiple facets of diabetes to develop, the absence of immediate alteration in WPB structure is not unexpected. Ribau et al demonstrated that the number of WPBs significantly elevated with the first week of diabetes being induced, this increase persisted up to two months, suggesting that duration of diabetes does impact WPB adaptation (243). This could be because of increased oxidative stress exposure. When compared to a human study, it as shown that plasma levels of VWF was significantly higher in older populations and moreover s higher proportion of it was active which contributes to an increased state of thrombosis. Indicating that extended durations of diabetes can be associated to more severe phenotypes of endothelial dysfunction (195). In fact, this may be encouraging, indicating that the healthy ECs used in my models have retained their ability to adapt to the acutely altered environment and functioned appropriately under stress without developing major pathological adaptations rapidly. It would be pertinent to explore if duration of exposure to hyperglycaemia could override the protection from HSS which could be achieved by extending the timeframe of my models of diabetes to being a week, based on (243), this would be an ideal starting point to see if ECs begin to display pathological alterations. Moreover, use of cells from a pathological environment i.e., a patient with a formal diagnosis of diabetes would allow for assessment of how a more comprehensive and physiological diabetic environment can impact an ECs phenotype.

Investigation into the relationship between WPBs and diabetes in human models remains limited, particularly with respect to morphometric analysis. Most human centric studies regarding diabetes and WPBs rely on an omics-based approaches, while morphometric analyses of WPBs are conducted in animal models. There are few exceptions to the limited human-focused morphometric studies on WPBs. One study examined activation of endothelial cells in insulin-dependent diabetes (now diagnosed as T1DM) using transmission electron microscopy (TEM) imaging to assess WPBs in in umbilical vein

samples. The analysis reported a significantly larger Nv value (number of subcellular components/cell cytoplasmic area), in diabetic samples compared to controls, suggesting a greater number of WPBs (244). Findings from both the high glucose and ambulatory model did not reflect this pattern. Given the methodological differences, whole tissue versus isolated endothelial cells, this discrepancy is not unexpected and does not substantially undermine the relevance of the current model. It does however support progression to a less reductionist approach.

In a more general regard, ECs in literature typically react to high glucose exposure (25mM) displaying a pathologically interrupted phenotype compared to that of a control counterpart (223, 224). With altered morphology, metabolic activity, increase release of inflammatory markers and a decrease in angiogenesis (236, 242, 245). Exposure of ECs to both high glucose and SS, is a less common practice than static culture but, use of microfluidics is increasing. One study demonstrated that human aortic endothelial cells (hAECs) cultured in 30.5MM glucose and exposed to 8 dynes/cm^2 of SS for 12hrs displayed significantly reduced alignment than the normal glucose control (246). However, this effect was mitigated with increased SS, elongation was comparable to the normal glucose ECs with 16 dynes/cm^2 (246). Previous optimisation steps within the McKeown lab showed that ECs exposed to less than 24hrs of SS under normoglycemic conditions displayed minimal alignment (59). The poor flow phenotype observed in the high glucose treated cells, while likely influenced by glucose exposure, which as seen in my own model can attenuate alignment, may be exaggerated by the short SS exposure period.

The observed increase in AKT phosphorylation contrasts with previous literature which typically reports a reduction under hyperglycaemic conditions associated with diabetic conditions (8, 176, 247). Insulin resistance in diabetes is the suspected trigger the reduction of pAKT, specifically due to insulin sensitive tissues impairing the PI3K/AKT pathway (247). In this study we observed the converse, an approximate 2-fold increase in phosphorylation, with no difference in total AKT. It is possible that pAKT can be upregulated in response to diabetes under certain environments such as increased inflammation (248). There may also be methodological explanation for this. Firstly, this experiment has a limited sample size hence the variability observed has a greater bearing. Secondly, ECs were cultured in static 6-well plates, this was a product of restriction, the IBIDI microslides needed for this microfluidics approach have a small growth area, constraining the number of ECs that can be grown. This in turn reduces the amount of protein that can be gathered to be tested. It is an insufficient quantity to run a successful western blot. As we have established, static culture significantly alters EC profiles and

WPB populations by extension, subsequently the results observed here may also be impacted. ECs when considered in abstract tissue culture is only exposed to growth media. In my model, this includes insulin-like growth factor as a supplement. Therefore, as the HUVECs utilised in the model are from healthy donors, they will not have experienced insulin resistance. Taken in combination with the pathologies associated with static cell culture, this may explain this increase in AKT phosphorylation. To gain meaningful insight into the impact of modulating glucose exposure within a physiologically relevant microfluidic context, assessing AKT phosphorylation would be feasible, providing sufficient cells could be cultured to yield adequate protein for western blot analysis. This may be achievable by adapting he current models to incorporate microslides in series allowing for increased surface area while maintaining controlled flow conditions. However initial attempts implement this approach has resulted in a cytotoxic environment further restraining protein yield.

While use of HSS strengthens the approach to studying WPBs by conferring increased physiological relevance to the model also affords HUVECs protection from the induced pathogenic environment. This may partly account for the divergence in WPB profiles observed between this model and the in vivo studies. In other in vitro studies, 25mM glucose is a widely accepted experimental analogue of diabetes, however it is applied to static cultured cells, which increases the pathology of an already pathogenic environment, potentially exaggerating or confounding results. These considerations highlight a need for caution when interpreting results derived from this environment, particularly in light of the relatively muted response of ECs within my models of persistent exposure to dysregulated glucose. Moreover, 48hrs of HSS exposure represents an optimised timeframe for ECs to adopt a phenotype more reflective of in situ conditions with a reported 17% increase in gene recovery compared to static culture (198). However, given that hyperglycaemia is a chronic feature of the diabetic microenvironment, this duration may be insufficient to elicit a full cellular response. Extending the exposure period within these models may allow for a transition from emerging trends to statistically significant outcomes, better capturing the sustained impact of diabetic conditions on endothelial behaviour.

HUVECs offer a robust model for studying WPBs, consistently synthesising large populations suitable for morphometric and functional analysis. This reliability makes them an optimal choice for developing *in vitro* models to assess the impact of stimuli on WPB dynamics. On the other hand, the origin of HUVECs creates a limitation within such models. HUVECs are derived from a highly specific vascular context, namely the umbilical

vein, they represent a transient endothelial population, unique to pregnancy (249). As such, they may not be truly representative of the broader physiological diversity found *in vivo* which may constrain the generalisability of findings. As venous ECs, HUVECs are not typically exposed to HSS, a well characterised regulator of endothelial behaviour both *in vitro* and *in vivo* settings (250). Moreover, literature indicates that WPB characteristics including cargo composition and responsiveness vary across vascular beds under healthy physiological conditions. This highlights the importance of contextualising WPB findings within the broader vasculature especially within a diabetic context where complications affecting the microvasculature and macrovasculature can arise independently and exert distinct influences on endothelial behaviour.

As discussed, the findings present here contrast those seen in existing literature from various animal models, where induced diabetes has been associated with an increased volume of WPBs per FOV (191). Interestingly, there is a distinct lack of published studies examining the impact of diabetes on WPB morphology in a human context, in instances where WPBs have been studied in human cells, they have been maintained in static conditions, which is already representative of a pathological environment with a shift towards an increased pro-thrombotic state, likely to be more effective at clot formation. As such these models offer a novel perspective, shifting focus from the commonly explored WPB cargo in human studies to structural and functional characteristics of the organelle.

Progression of these models requires an increase in physiological relevance. Rather than applying short term, pathological exposure to healthy ECs the approach will be inverted, cells derived from a pathological environment (confirmed diagnosis of diabetes) will be placed into a healthy normoglycaemia setting to assess whether they retain features of metabolic memory. This shift allows investigation into the persistence of diabetic imprinting and the potential for reversibility in endothelial dysfunction. Accounting for far more exposures and potential triggers for alterations of cell physiology and pathologies than simple glucose manipulation. Furthermore, this will provide expansion into other vascular beds which affords the capacity to compare and contrast WPBs throughout the vascular tree. Finally, WPBs while the primary source of VWF within ECs is only one of three pathways VWF is expressed within the vasculature, as levels of VWF are consistently elevated in diabetes it could also be pertinent to investigate the alternative pathways within a diabetic context. This can be achieved through analysis of patient derived plasma.

In summary, manipulation of glucose levels surrounding ECs is not sufficient to induce a truly pathogenic environment as associated with diabetes in a 48hr window. Nonetheless, the models proposed offer a foundational framework that can be expanded with additional pathological factors to enhance physiological relevance and investigative utility. There is evidence to suggest that it is enough to begin to alter the function of WPBs and impact the functionality of released VWF strings when stimulated. Both the consistent high glucose hyperglycaemia model and ambulatory glucose model impacted the length of VWF strings, with longer stings with increased thrombotic potential released in both. Under high glucose the VWF strings under HSS are not significantly different to the static environment, this shows the high glucose reduces the conferred atheroprotection from HSS, creating an environment that is more aligned with one considered to be pathogenic. The ambulatory condition did display a trend for longer VWF strings. Longer VWF strings are have a greater capacity for platelet aggregation, thus, suggests that the created diabetic environments are displaying a greater tendency towards thrombus activation than their control counterparts.

Both the high glucose and ambulatory model demonstrate that exposure to hyperglycaemia or dysregulated glucose control can initiate disturbances in WPB function, with VWF string morphology differing from control conditions. These findings provide a foundational platform upon which additional layers of disease complexity can be incorporated enabling deeper investigation into the effects of diabetes on the vasculature.

Chapter 4: Physiological model of diabetes

4.1 Introduction

Prevalence of diabetes is increasing; from 1985 to 2005 the population of diabetics rose to 30 million individuals affected globally (1). In the UK alone it is estimated that by 2030 diabetes treatment will cost the NHS £14 billion (2). Given the prevalence and projected cost of diabetes as a disease, it is large field of research, there are multiple accepted and preferentially selected models of investigation both *in vivo* and *in vitro* (251). While a reductionist strategy, deconstructing multifaceted diseases such as diabetes into isolated components, remains a widely used framework for *in vitro* disease modelling, enabling assessment of cellular and molecular characteristics (251), my findings (see **chapter 3**) suggest that this approach may be overly simplistic (252). Specifically, such models often fail to elicit significant responses from healthy cells when exposed to isolated pathological stimuli within a contained experimental system. Diabetes is a multifactorial disease, while hyperglycaemia is a defining characteristic, it is not the only pathogenic hallmark. Endothelial dysfunction is a well-documented component of diabetic pathology and is thought to contribute to the progression of both microvascular and macrovascular complications, as well as increasing the risk of atherosclerosis (253-255).

To quantify the impact of diabetes and the multiple assaults it incurs in the endothelium, I investigated the concept of 'metabolic memory' the concept that prior exposure to a stimuli will incur persistent alterations in gene expression through epigenetic modification, the molecular mechanisms behind which are not truly elucidated (204). It has been demonstrated within the vasculature (204). Therefore, I will assess if ECs isolated from defined environment, in this case from a patient diagnosed with T2DM retain the characteristics acquired from exposure to that environment will persist after removal of stimuli.

EC dysfunction is a disturbance of the quiescent state that is normally essential for maintaining homeostasis in blood vessels (256). It is characterised by dysregulation of vasoactive components responsible for preserving an appropriate microenvironment, they are often released at inappropriate times, when not required, and at unregulated levels (256). This dysregulation reflects a shift in the endothelial phenotype, denoted by impaired vasodilatory capacity and an increase in inflammatory and thrombotic markers (257). A key feature is the reduced bioavailability of compounds such as nitric oxide (NO), which diminishes NO-dependant signalling pathways and contributes to oxidative stress within

the vasculature (258). This increased oxidative stress can inhibit transcription factors e.g. nuclear factor kappa-light-chain-enhancer of activated B cells (NFκB), while increasing expression of adhesion molecules such as intercellular adhesion molecule-1 (ICAM-1) and vascular cell adhesion molecule-1 (VCAM-1)(259, 260). These abnormalities compromise endothelial function disrupting vascular health and shifting the atheroprotective nature of these agents shifts towards a pathological profile. Under disease states such as diabetes, regulation of these compounds becomes increasingly irregular (253). Replicating this complexity *in vitro* remains challenging.

Aortic cells (AECs) are a more physiologically relevant EC model compared to HUVECs by nature of their origin. This approach enables the development of a model with greater applicability for investigating functional characteristics of WPBs under conditions that more closely resemble the *in vivo* environment. While HUVECs provide a robust and reliable model for studying WPBs, they are a foetal derived cell not endogenous to adult vasculature (261, 262). This in conjunction with their venous origin raises concerns about the ability of HUVECs to replicate EC features most affected by diabetes. Intrinsic differences between venous and arterial cells have been documented; one previous study demonstrated significant variation in cell morphology, process and protein synthesis, between the two vascular beds (263). These findings highlight that HUVECs may not fully represent EC behaviours across mature tissue, particularly in disease-relevant contexts.

To advance my investigation, I elected to use ECs from the aortic vascular bed. This enabled direct evaluation of the physiological impact of diabetes on individual patient-derived ECs, providing a platform to test the metabolic memory principle outlined above. By combining ECs from relevant human donors (commercially acquired) within the established HSS model, which more accurately replicates the flow conditions experienced *in vivo*, this approach offers enhanced functionality for modelling disease-tissue interactions with greater fidelity.

Therefore, to assess the impact of diabetes on WPBs, I observed ECs isolated from the aortic bed of patients with a formal diagnosis of diabetes. The aim was to determine if these cells retained a pathological phenotype even when cultured under ‘healthy’ conditions, specifically, consistent exposure to normoglycemic glucose range. As previously established, static cell culture can amplify features of a pathological phenotype, therefore, HSS use was maintained throughout to preserve physiological relevance (54, 59).

Commercially available hAECs and dhAECs were 'paired' by sex and age as per **tables 2.1 and 2.2** in **section 2.1** and were exposed to HSS or static culture for 48hrs in a normo-glucose environment. Based on available clinical data, three matched pairs of patient derived ECs were acquired each consisting of one control and one diabetic counterpart (see set up in **figure 4.1**). Initially it was understood that there were four female derived cell lines and two males, as such this formed the basis of pairing cell lines. Post-analysis it was discovered that one cell line had been mis-recorded as female and was actually derived from a male donor. Given the stage this was discovered, analysis structure was maintained. This paring strategy was shaped by logistical, financial and time constraints.

Initially, Pair A, was used as a pilot study to establish a model of diabetes before proceeding to the remaining two pairs. Each pair was treated as a separate independent experiment with three technical repeats conducted per condition. Following individual analysis, all data were compiled and reanalysed as a combined dataset to strengthen statistical power and identified any consistent trends.

Hypothesis: ECs isolated from a donor with a confirmed diagnosis of diabetes and maintained under normoglycemic conditions will display an altered WPB phenotype to those from non-diabetic donors.

Aim 1: To create a model of diabetes using dhAECs and hAECs to establish is metabolic memory has a role in WPB morphology and function.

Aim 2: To expand the physiological EC model by incorporating additional patient samples thereby increasing the patient variability.

4.2 Results: Physiological cell model of diabetes

ECs used for these experiments were purchased from Promocell, limiting the selection to available stock. Pair A (see table 2.2) was used to conduct a pilot study to give insight into the use of a diabetic cell model.

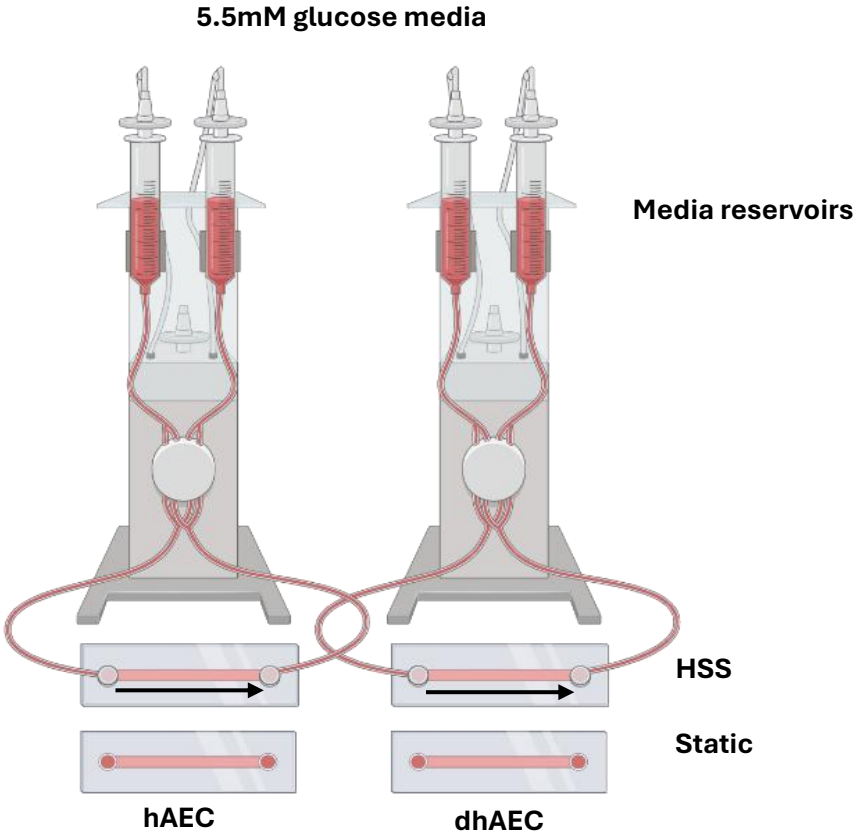

Figure 4.1 Schematic of the physiological cell model for control (hAEC) and diabetic (dhAEC) endothelial aortic cells.

ECs were plated onto IBIDI channels and were maintained for 48hrs in normoglycemia 5.5mM glucose media under HSS with a static counterpart. Arrow indicated direction of flow in HSS conditions.

4.2.1 dhAECs represent a diabetic phenotype

4.2.1.1 Phosphorylated Protein kinase B (AKT) is altered in dhAECs

To determine if the hAECs and dhAECs displayed differential metabolic profiles, I assessed levels of both phosphorylation of AKT and eNOS and their total protein expression.

ECs under static conditions were lysed and lysates used for WB analysis to create a baseline profile prior to cell exposure added to the microfluidics model. Insulin resistance usually confers a decrease in phosphorylation of AKT (pAKT), particularly in T2DM presentation (264). Hence, I assessed the levels of pAKT in the hAECs and dhAECs as a proxy measurement to confirm a diabetic phenotype in the cells.

There was significantly less pAKT (p= 0.0324) in the dhAECs (0.211±0.1) than in the hAECs (1.00±0.224) (see **figure 3.2**) There was no significant difference in total AKT (tAKT) between hAEC and dhAECs (1.00±0.152, 0,987±0.224, p= 0.9647). This aligns with data published on reduction of pAKT in a diabetic environment (264-267). The dhAECs displayed a greater variety than the hAECs.

4.2.1.2 Endothelial Nitric Oxide Synthase (eNOS) is altered in dhAECs

The phosphorylation of eNOS is susceptible to dysregulation in a diabetic environment, typically resulting in reduced enzymatic activity (268). There was no significant difference between the hAECs and dhAECs (1.00±0.386, 0.831±0.26, p= 0.7373) in peNOS but there was a significant increase in the amount of teNOS in the dhAECs compared to the hAECs (1.998±0.280, 1.00±0.131 p= 0.032), the level of protein is approximate 2-fold greater. Expression of eNOS is not widely considered in isolation, it is more typical to assess the phosphorylation activity rather than the overall quantity of the protein. An increase in eNOS activity would likely be translated through observation of an increase in peNOS, in a healthy condition this would allow regulation of nitric oxide (NO), a reduction in NO is tied to the foundation of ED (269). However, we did not see an increase in peNOS with the dhAECs in this model, which as an alternative measurement for eNOS activity suggests the increase in total eNOS observed is not protective in diabetes. It has been demonstrated that under high glucose (synonymous with diabetes) eNOS can uncouple, this results in the production of a superoxide rather than NO, which aggregates and encourages ED (153). From this data the dhAECs were deemed to be displaying an appropriate diabetic phenotype.

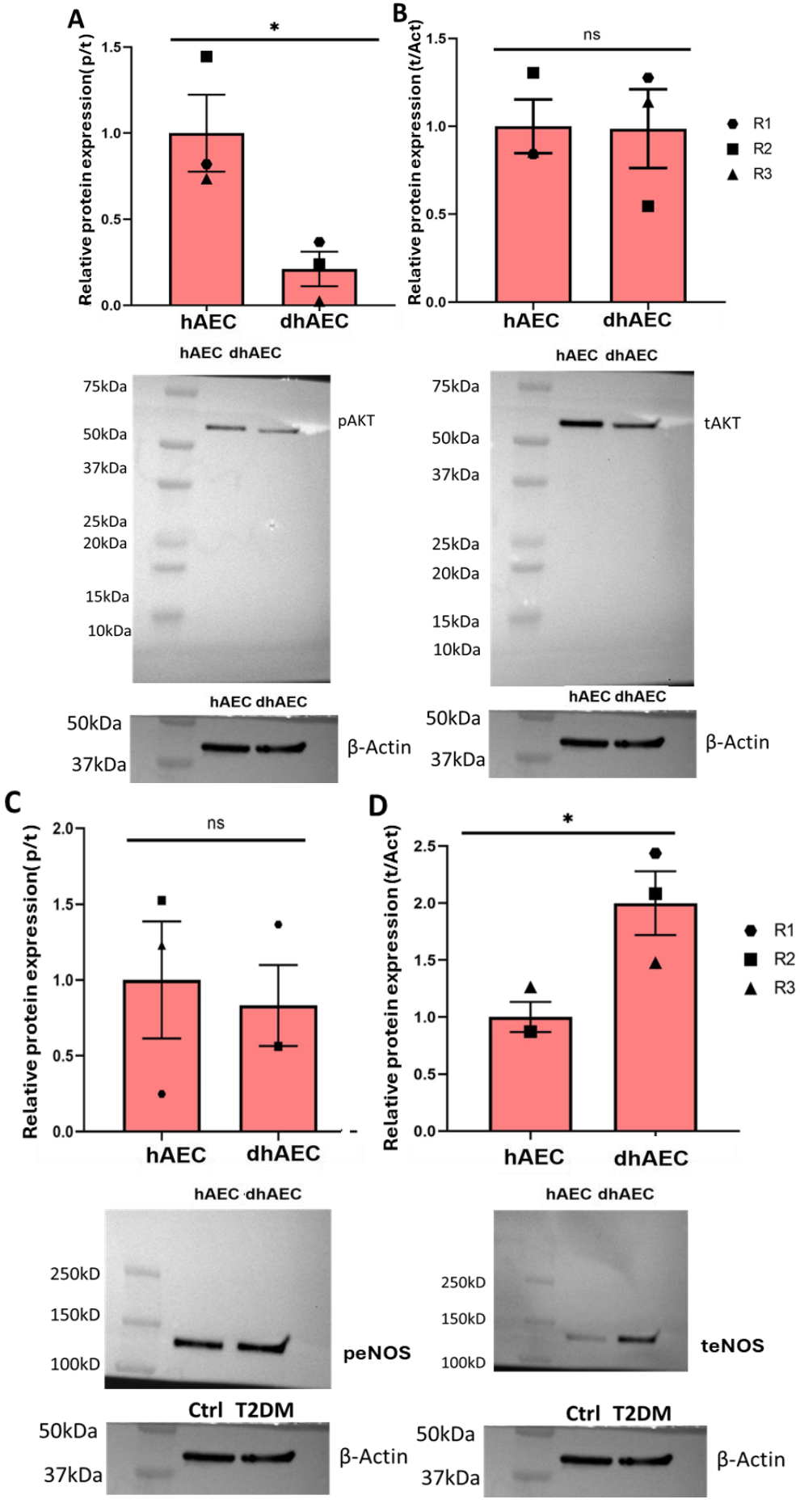
A
*
Relative protein expression(p/t)
1.5
1.0
0.5
0.0
hAEC
dhAEC
B
ns
Relative protein expression (t/Act)
R1
R2
R3
hAEC dhAEC
75kDa
50kDa
37kDa
25kDa
20kDa
15kDa
10kDa
pAKT
tAKT
β-Actin
C
ns
Relative protein expression(p/t)
2.0
1.5
1.0
0.5
0.0
D
*
Relative protein expression (t/Act)
2.5
250kD
150kD
100kD
peNOS
teNOS
Ctrl T2DM

Figure 4.2 dhAEC have reduced phosphorylation of AKT and increased total eNOS.

B- Actin representative as running control for all as proteins measured from same samples and stripped between.

- **A.** Mean phosphorylated AKT expression measured in hAECs and dhAECs normalised to total Akt. Mean ±SEM. n/N=3/3
- **B.** Mean total AKT expression normalised to beta actin measured in hAECs and dhAECs. Mean ±SEM n/N=3/3
- **C.** Mean phosphorylated eNOS expression measured in hAECs and dhAECs ±SEM n/N=3/3
- **D.** Mean total eNOS expression normalised to beta actin measured in hAECs and dhAECs. Mean ±SEM n/N=3/3

Unpaired t-test* = $p < 0.05$

4.2.2 hAECs and dhAECs show differential WPB profiles

To understand the impact of diabetes on WPBs I have undertaken several measurements as described in **chapter 3 section 3.2**.

4.2.2.1 Total number WPBs was affected by diagnosis of diabetes

Total number of WPB per FOV can be seen in in the representative images in **figure 4.3**. This was reflected in the quantification of the images in **figure 4.4**. There was statistically less WPBs in dhAECs compared to hAEC (298±78, 1734±195 p= 0.0024) cultured under static conditions. Under HSS, there was no significant difference between the dhAEC and hAECs (256±68, 632±159 p= 0.0947). The hAECs did demonstrate a flow effect, with a significant difference between static and HSS conditions (p= 0.0117), no difference was observed within the dhAECs.

4.2.2.2 Number of Nuclei was not impacted by diagnosis of diabetes

The number of nuclei can be used to represent the number of cells in each FOV which can represent the growth rate of cells. There was a significantly greater number of cells counted in the dhAEC static condition compared to the hAEC static counterpart (29±, 21±2 p= 0.0282). A similar trend was observed in the HSS condition, but this difference was not significant (26±1,17±3, p=0.0503). No other significance was seen between any of the other conditions, see **figure 4.4**.

4.2.2.3 There was a significant decrease in the number of WPBs per cell in dhAECs compared to hAECs

This parameter gives more of a quantified insight into the above data, informing how many WPBs are associated on average to each cell. The increased number of nuclei in dhAECs may indicate an increase in growth rate or cell confluency, however there was a significant decrease in the number of WPBs in dhAECs under both static (16±8, 68±92 p=0.0008) and HSS (17±5, 39±p=0.0067) conditions, comparative to the hAECs (**figure 4.**). There was no significant difference in the number of WPBs generated in dhAECs between static or HSS conditions, suggesting that the atheroprotective phenotype that HSS can convey could not salvage the dhAEC physiology, see **figure 4.4**.

*4.2.2.4 dhAECs demonstrated no differences in WPB l*ength under HSS

WPB length can be considered an illustration of thrombotic potential of a population of WPBs. Longer WPBs denotes a greater number of ‘quanta’ of VWF being inserted into the newly forming WPB, which therefore generate longer VWF strings when secreted. In this instance, WPBs responded as expected to shear stress in both the hAEC and dhAEC

conditions, with those under HSS significantly smaller than their static counterpart (p< 0.0001; p= 0.0007). The WPBs in dhAECs were significantly short than those in hAEC cultured under static conditions (1.245±0.02 µm, 1.183±0.007 µm, p= 0.0463), but under HSS conditions there was no significant difference (0.764±0.043 µm, 0.826±0.012 µm, p=0.2376) **figure 4.4**. The length of WPBs in hAECs, regardless of flow exposure, were consistent across different repeats with tight clustering of data points. Conversely the WPBs observed in the dhAEC displayed a greater variation and spread of data point across the repeats in both conditions, there is no distinct clustering of a particular individual repeat suggesting that the dhAECs in general were less uniform in behaviour than the hAECs.

4.2.2.5 WPB Polarity was not impacted by diabetes

WPBs, in a manner like ECs, align to the direction of flow **see section 3.2**. In both hAECs and dhAECs, the expected static and HSS phenotypes were observed. Under static, no distinct clustering was seen with the angles WPBs were recorded. Whereas under HSS clustering was observed with the highest proportion of WPBs being recorded at the 0° and 180° ends. This indicates that WPBs were at an angle close to being horizontal i.e. aligned with flow. The most distinct observation from **figure 4.5** is a reduction in volume of WPBs in the dhAECs compared to the hAEC with the max being 1200 compared to 5000.

4.2.2.6 The number of ECs expressing WPBs is reduced in dhAECs

Despite being classed as the same cell type, ECs throughout the vasculature are specialised to their environment and differences can be observed between ECs taken from different origins. WPBs have been shown to adhere to this concept too. Money et al demonstrated that a lower proportion of hAECs synthesise WPBs compared to HUVECs (in which almost every cell expresses WPBs) (59). In this model, no significant difference was observed in the number of hAECs that expressed WPBs between the static and HSS conditions in the static on average every cell (100%) expressed WPBs compared to 96% under flow. However, the number of cells expressing WPBs were significantly reduced in the dhAECs, where only 64% expressed WPBs under static conditions (64.38±2.12% p= 0.0316) and 76% under HSS (76.44±4.98% p=0.0316) see **figure 4.6**.

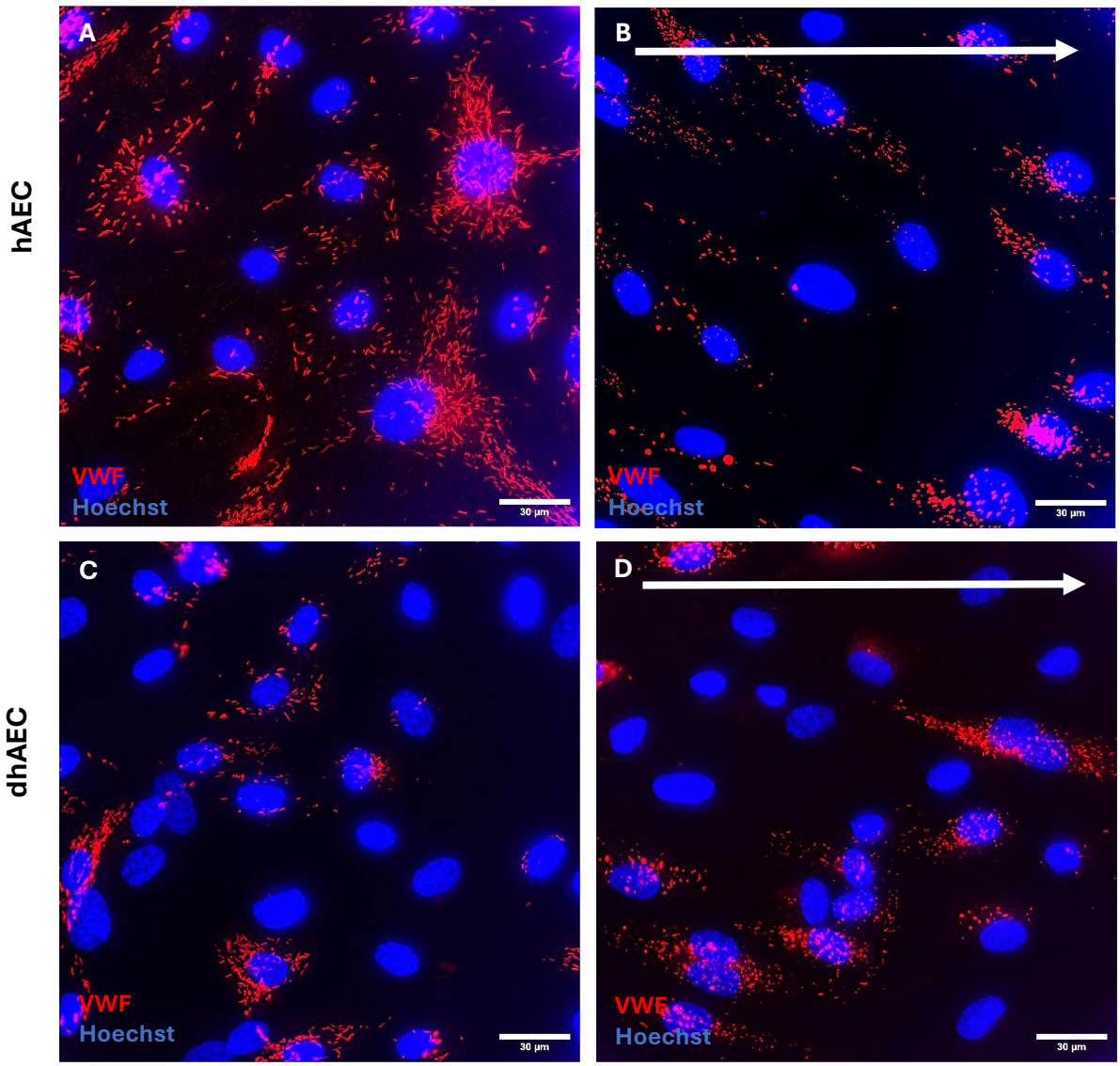

Figure 4.3 Representative images (x60) of hAECs and dhAECs in static and HSS conditions.

Nuclei are in blue (Hoechst), and WPBs are in red (VWF). Arrow denotes direction of flow for cells under HSS. Images with no arrow represent cells under static conditions. hAECs = control ECs. dhAECs = ECs extracted from diabetic patients

A. hAECs cultured in a static environment. Consistent expression of WPBs and no clear directionality to cells.

B. hAECs cultured in a HSS environment. Fewer WPBs expressed compared to the control static condition. Nuclei have aligned to the direction of flow.

C. dhAECs cultured in a static environment. Irregular and reduced expression of WPBs across cells, no clear directionality of cells.

D. dhAECs cultured in a HSS environment, irregular expression of WPBs across cells that have aligned along with cells in the direction of flow.

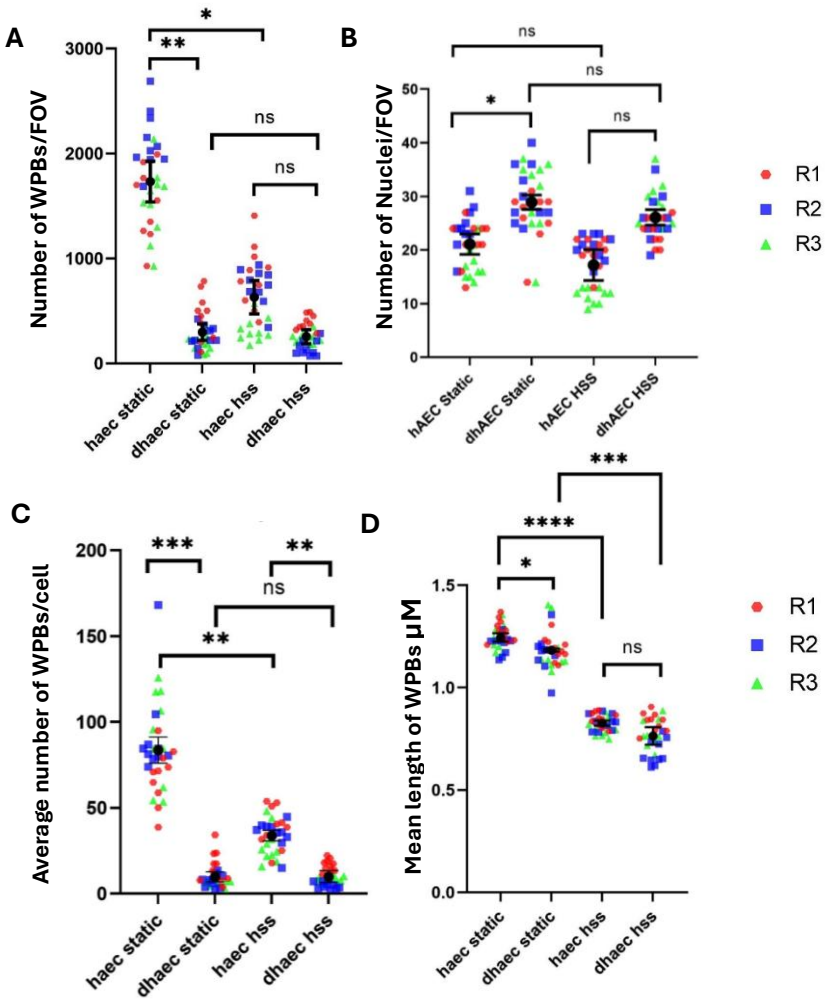

Figure 4.4 The profile of WPBs is significantly different in dhAECs compared to hAECs

- **A.** Mean data of the total number of WPBs observed in each FOV per condition ±SEM n/N=3/30. Each data point represents a mean of all WPBs counted in an image. Colours/shapes represent technical repeats (R1 red hexagon, R2 blue square, R3 green triangle)
- **B.** Mean data of number of nuclei counted in each FOV ±SEM n/N=3/30. Each data point represents a mean of all nuclei counted in an image. Colours/shapes represent technical repeats (R1 red hexagon, R2 blue square, R3 green triangle)
- **C.** Mean number of WPBs per nuclei calculated in each FOV n/N=3/30. Each data point represents a mean of WPBs per cell in an image. Colours/shapes represent technical repeats (R1 red hexagon, R2 blue square, R3 green triangle).
- **D.** Mean length of WPBs in each FOV n/N=3/30. Each data point represents a mean of WPB length per cell in an image. Colours/shapes represent technical repeats (R1 red hexagon, R2 blue square, R3 green triangle).

Unpaired *t*-test * = p <0.05, ** = p <0.01 *** = p <0.001

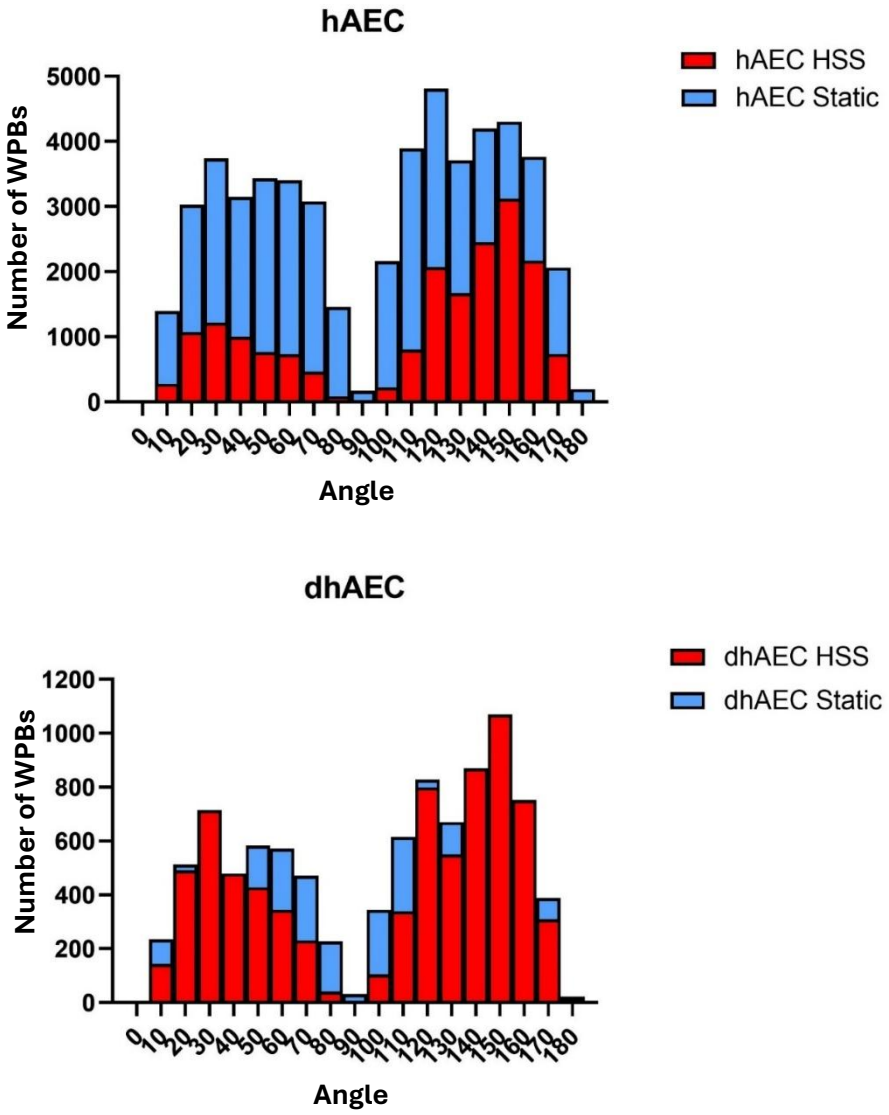

Figure 4.5 WPBs from both hAECs and dhAECs align with the direction of shear stress.

The angle of WPBs was assessed and plotted into a histogram for both HSS (red) and static (blue) conditions. The higher the bar the greater the number of WPBs clustered at that angle.

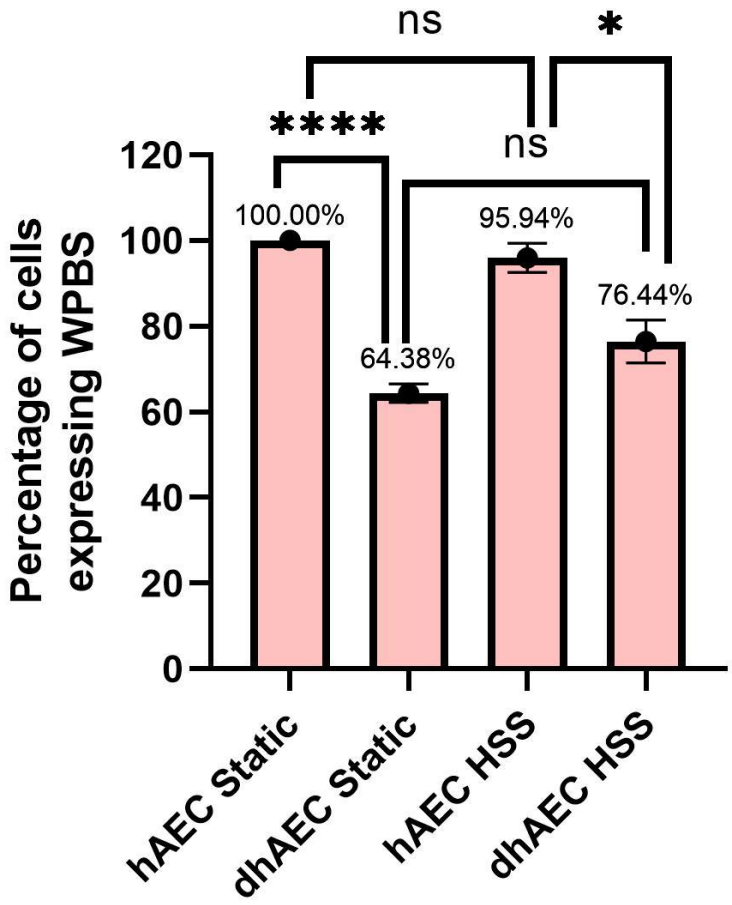

Figure 4.6 The mean percentage of cells expressing WPBs is significantly lower in dhAECs than in hAECs in both static and HSS conditions

Average percentage of WPB 'positive' cells ±SEM n/N=3/30. A cell area was defined and assessed to see if WPBs were present within. Cells that did not were considered to not be producing WPBs. The cells were subtracted from WPB 'positive' cells and a percentage calculated.

Unpaired *t*-test * = p <0.05, **** = p < 0.00001

4.2.3 Impact of diabetes on WPB function

hAECs and dhAECs were stimulated to exocytose their WPBs and release the VWF contained within as strings. It was observed that in hAECs strings do not present in the same manner as those released from HUVECs under the same high dosage of histamine (see **section 3.3.3**). This can be seen in the representative images in **figure 4.7**.

4.2.3.1 Number of VWF strings is not affected by diabetes

Substantial variability was observed between repeats in the number of strings released by hAEC and to a lesser degree by dhAECs. No significant differences were observed in the number of strings released by hAECs and dhAECs in either static (93±28, 69±9, p=0.4473) or HSS conditions (173±29, 93±14, p=0.0694).

4.2.3.2 Length of VWF strings is reduced in diabetes

VWF sting length is proportional to function, longer strings have a greater thrombotic potential, and can bind to a greater volume of platelets etc. Strings released from hAECs were significantly longer than those released from dhAECs under both static (14.00±0.61 µm,8.98±1.63 µm p=0.0447) and HSS (11.41±0.47µm,7.54±0.65 µm p=0.0083) conditions. As reported previously, hAECs released significantly shorter strings in the HSS condition compared to the cells cultured under static conditions (p= 0.0271). The dhAECs did not follow this pattern, there was no significant difference in the length of the strings between static and HSS environments (p= 0.4573), see **figure 4.7**.

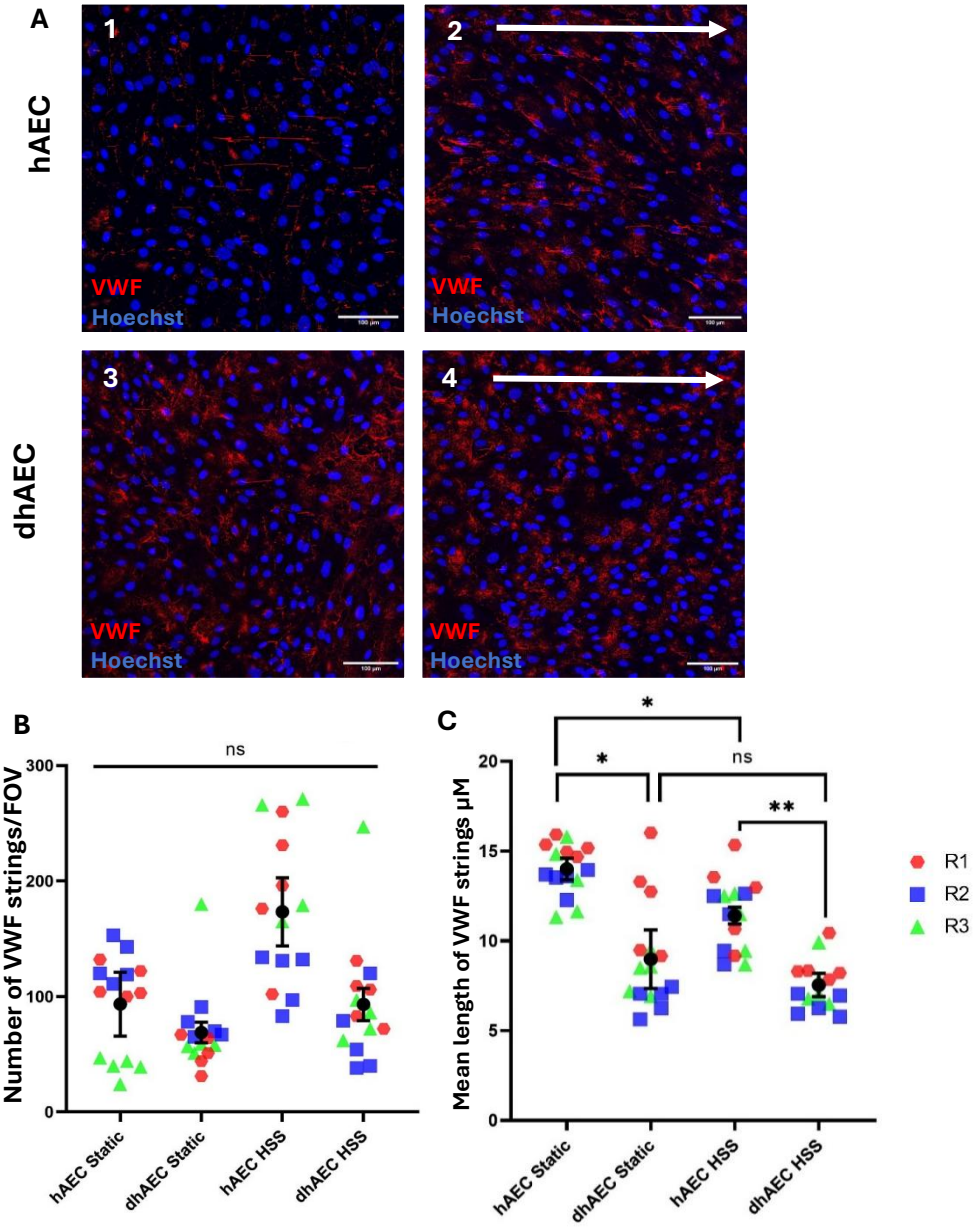

Figure 4.7. The length but not the number of VWF strings is significantly different between hAECs and dhAECs in both static and HSS conditions.

Arrow denotes direction of flow for cells under HSS. Images with no arrow represent cells under static conditions. hAECs = control ECs. dhAECs = ECs extracted from diabetic patients

A. Representative images (x40) of VWF strings (red) released from ECs (blue nuclei) following stimulation with histamine in static hAECs, HSS hAECs, static dhAECs and HSS dhAECs.

B. Mean number of VWF strings released by ECs in each FOV in condition ±SEM n/N=3/15. Each data point represents a mean number of all VWF strings counted in an image. Colours/shapes represent technical repeats (R1 red hexagon, R2 blue square, R3 green triangle)

C. Mean length of VWF strings released by ECs in each FOV in condition ±SEM n/N=3/15. Each data point represents a mean length of all VWF strings counted in an image. Colours/shapes represent technical repeats (R1 red hexagon, R2 blue square, R3 green triangle).

Unpaired *t*-test * = p <0.05, ** = p <0.01 *** = p <0.001

4.3 Expansion of sample size in the physiological cell model

4.3.1 Statistical power was increased with addition of new cell lines

Commercially available hAECs originate from a single donor (270) and therefore the observed differences in WPB characteristics could be due to diabetes or merely due to physiological variability. There is an overall need to increase the biological representation of aortic samples. Two pairs of hAECs and dhAECs were matched according to the clinical data available (see **table 2.1 and 2.2 in section 2.1**), thereby. This allowed me to increase the sample size within the diabetic model. Subsequently elevating the statistical power of the model and increasing confidence in any pronounced discernible trends in cellular responses. Pairs B and C were assessed in the same manner as Pair A, as distinct, individual pairs.

4.3.2 Pair B: WPB profiles in dhAECs and hAECs were similar

4.3.2.1 Phosphorylated Protein kinase B (AKT) is not affected in dhAECs

Metabolic profile of ECs was created from static lysates of dhAECs and hAECs. There was no significant difference in phosphorylation of AKT between the hAEC and dhAECs (1±0.183,0.468±0.123, p=0.0735) (**figure 4.8a**). Nor was there a different in the expression of tAKT (1±0.142, 1.158±0.085, p=0.395), despite a close to 2-fold decrease in pAKT in the dhAEC condition (**figure 4.8b**).

4.3.2.2 Endothelial Nitric Oxide Synthase (eNOS) is not affected in dhAECs

Similarly, while eNOS phosphorylation varied between the dhAEC and hAEC conditions no significant difference was observed (2.172±0.831,1±0.322, p=0.2591) despite a close to 2-fold increase in peNOS observed in the dhAECs (**figure 4.9a**). There was also variation in the teNOS between dhAECs and hAECs, but this too was not significant (0.636±0.127,1±0.098, p=0.085) (**figure 4.9b**).

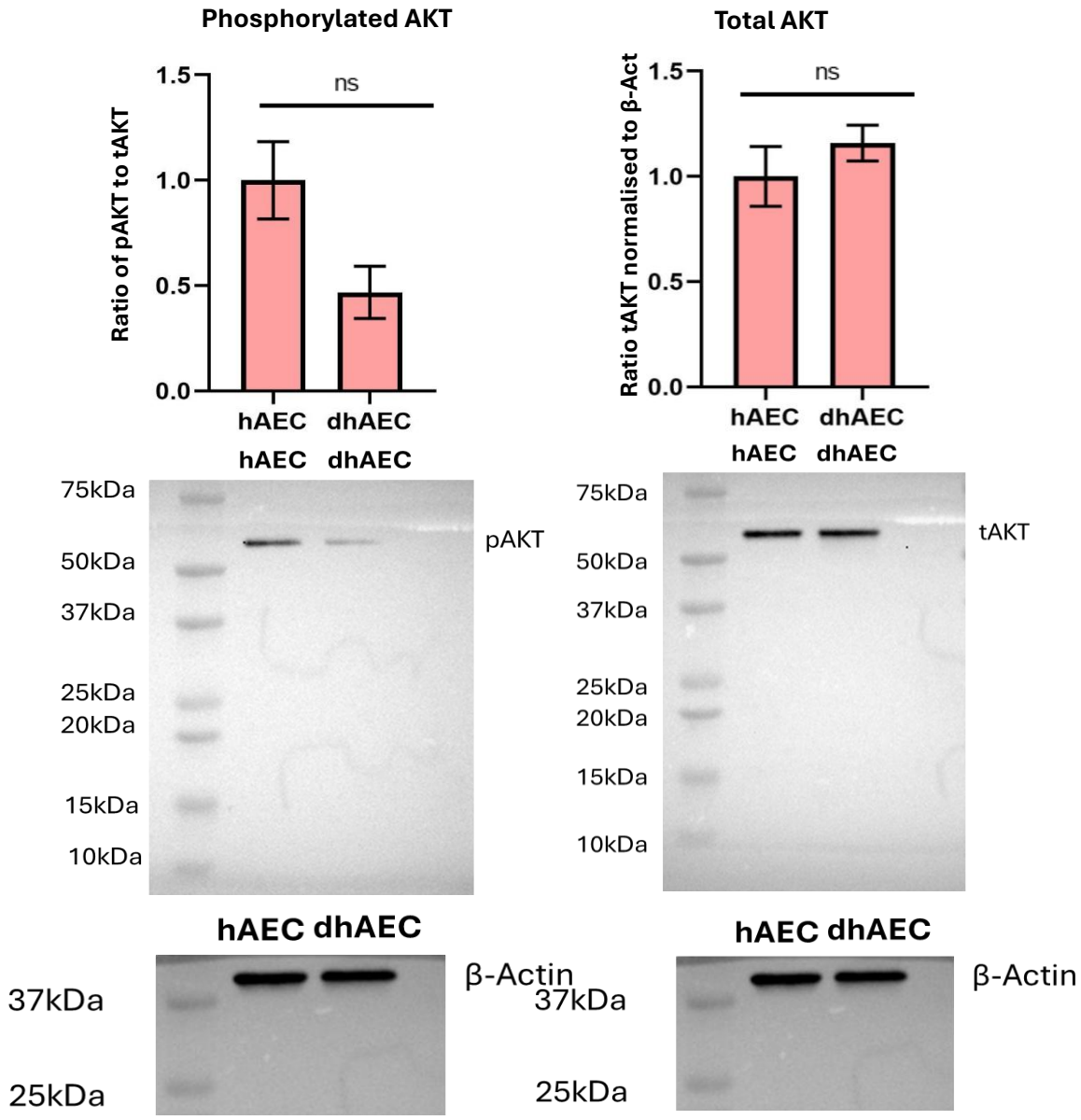

Figure 4.8 There are no differences between hAEC and dhAEC phosphorylation of AKT and total AKT.

- **A.** Mean phosphorylated AKT expression measured in hAECs and dhAECs normalised to total Akt. Mean+/- SEM. n/N=3/3
- **B.** Mean total AKT expression normalised to beta actin (running control) measured in hAECs and dhAECs ±SEM n/N=3/3

Unpaired t-test ns=non-significant

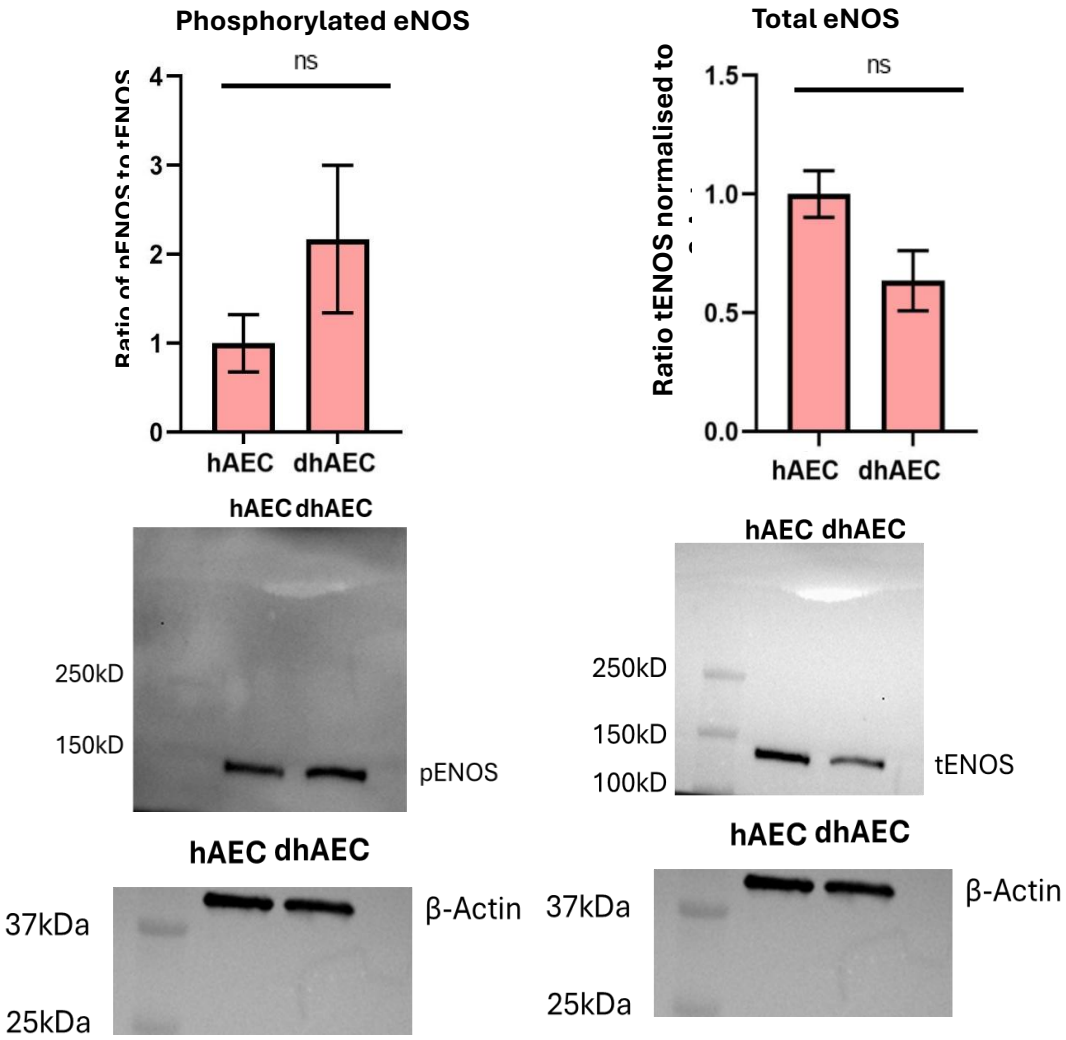

Figure 4.9 There are no differences between hAEC and dhAEC phosphorylation of eNOS and total eNOS.

- **A.** Mean phosphorylated eNOS expression measured in hAECs and dhAECs ±SEM n/N=3/3
- **B.** Mean total eNOS expression normalised to beta actin measured in hAECs and dhAECs ±SEM n/N=3/3

Unpaired t-test ns=non-significant

4.3.2.1 Total number of WPBs is reduced in dhAECs

In the static condition, there were significantly fewer WPBs in the dhAECs than in the hAECs (**figure 4.11a** p=0.041). The total number of WPBs per FOV did not significantly differ between static and HSS conditions in either hAECs (1777±150,1822±299, p=0.899) or dhAECs (1224±109, 972±235, p=0.384)

4.3.2.2 Number of nuclei is significantly affected by diabetes

The number of cells observed in each FOV is represented by the number of nuclei. Within Pair B there was a significantly higher number of hAECs per FOV in both the static (43±1, 27±5 p= 0.027) and HSS (40±2, 24±4 p= 0.0169) conditions compare to the dhAECs. This was a consistent result as the error bars and spread of data is much tighter in the hAECs, suggesting greater variation within the dhAECs. This can be observed both through the data in **figure 4.11b** but also literally the images of **figure 4.10**.

4.3.2.3 Average number of WPBs per cell is not affected by diabetes

Despite disparities in the number of cells between conditions, there were no significant differences in the average number of WPBs per cell across the model. There was no difference in the average number of WPB per cell between static and HSS exposure in either hAECs (42±3, 45±5, p=0.532) or dhAECs (47±6, 39±6, p=0.416). Nor was there a difference between hAECs and dhAECs within the static (p=0.459) or HSS condition (p=0.475) (**figure 4.11c**).

*4.3.2.4 WPB l*ength is affected by SS but not diabetes

WPB length responded to flow conditions as reported previously, i.e. contained significantly longer WPBs under static conditions and shorter when exposed to HSS in both the hAECs (1.007±0.017, 0.901±0.021, p=0.0172) and dhAECs (1.079±0.025, 0.912±0.053, p= 0.0471). There are no significant differences in WPB length observed between hAECs and dhAECs within either static (p=0.079) or HSS (p=0.859) conditions. There is a greater degree of variation seen with larger SEM in the dhAECs indicating less consistency albeit minor in the diabetic cells compared to the hAECs (**figure 4.11d**).

4.3.2.5 WPB polarity is not impacted by diabetes

WPB in both hAECs and dhAECs behaved as expected under HSS. A full range of angles was recorded under the static condition and clustering was seen at the extreme end of the HSS indicating angles close to horizontal (**figure 4.12**).

4.3.2.6 Number of cells expressing WPBs was reduced by diabetes

Variability was observed in the number of cells expressing WPBs in all ECs and conditions. This was consistent with previous findings on aortic ECs. However, there were no significant differences between hAECs and dhAECs under HSS (p=0.305) or static (p=0.588) conditions. There were no significant differences within dhAECs (p=0.852) or hAECs (p=0.628) with exposure to HSS. Approximately 1-2% fewer dhAECs in both static and HSS were positive for WPBs compared to the hAEC counterpart (**figure 4.13**).

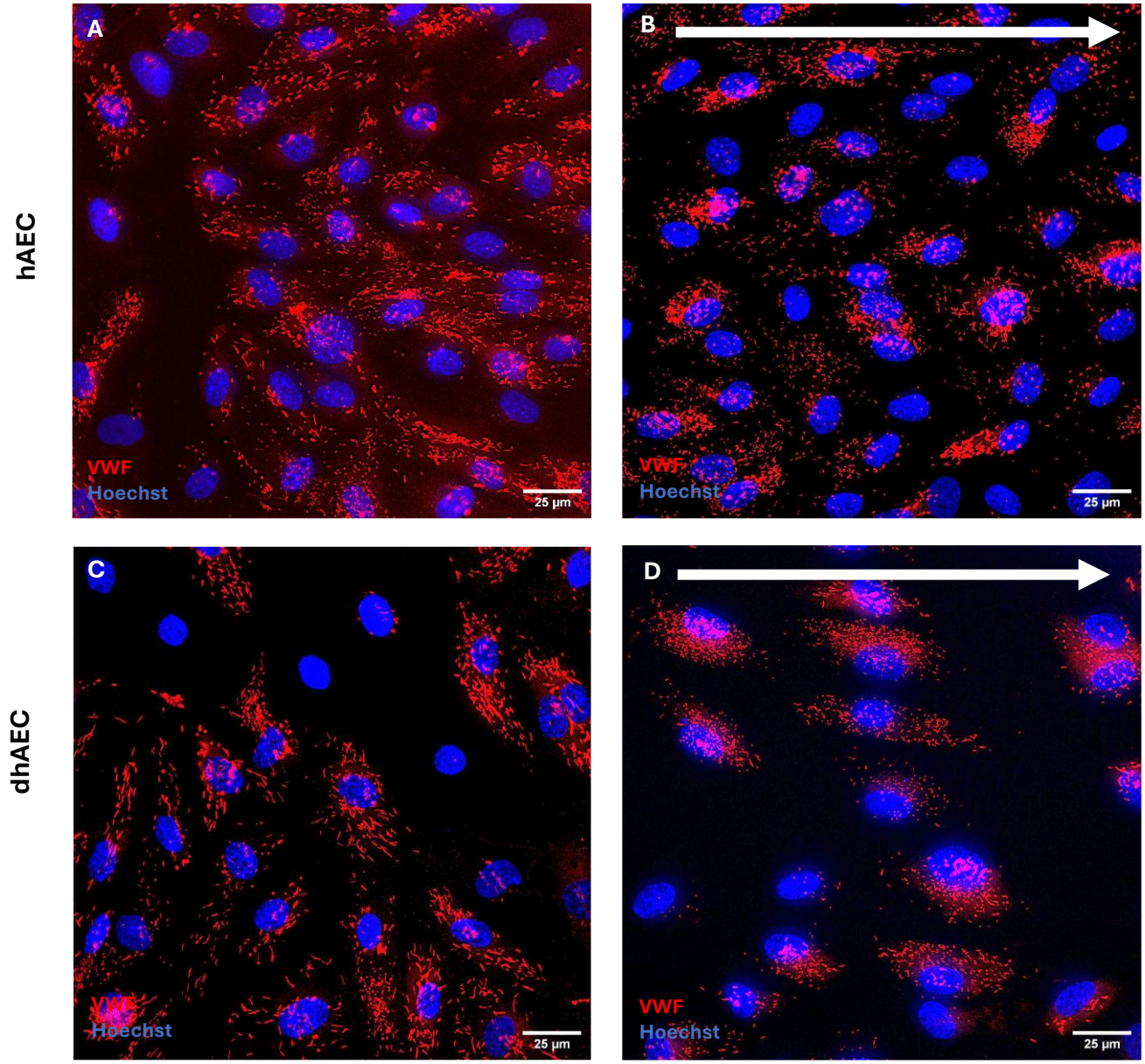

Figure 4.10 Representative images (x60) of WPBs in hAECs and dhAEC cultured under static and HSS conditions.

Nuclei are in blue (Hoechst), and WPBs are in red (VWF), direction of shear stress is white arrow where appropriate.

A. hAECs from pair B cultured in a static environment show consistent expression of WPBs. Nuclei are disordered displaying no clear directionality.

B. hAECs from pair B cultured in a HSS environment show consistent expression of WPBs aligned with cells. Nuclei have aligned to direction of flow.

C. dhAECs from pair B cultured in a static environment show relatively even WPB expression and no alignment of nuclei.

D. dhAECs from pair B cultured in a HSS environment show a relatively even expression of WPBs aligned with nuclei in direction of flow.

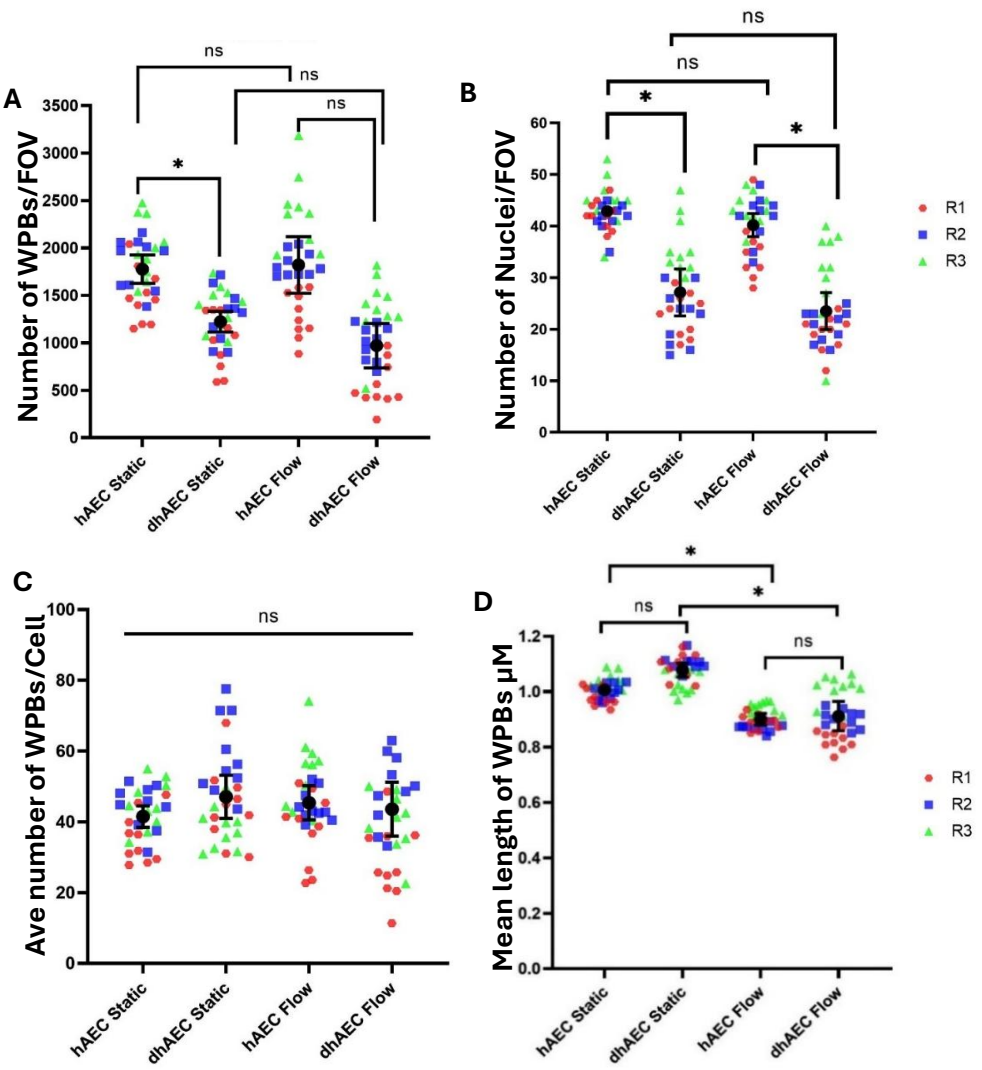

Figure 4.11 The profile of WPBs from dhAECs within pair B do no differ significantly from the hAEC counterpart in all conditions. The total number of WPBs and number of nuclei are reduced.

A. Mean data of the total number of WPBs observed in each FOV per condition ±SEM n/N=3/30. Each data point represents a mean of all WPBs counted in an image. Colours/shapes represent technical repeats (R1 red hexagon, R2 blue square, R3 green triangle)

B. Mean data of number of nuclei counted in each FOV ±SEM n/N=3/30 Each data point represents a mean of all nuclei counted in an image. Colours/shapes represent technical repeats (R1 red hexagon, R2 blue square, R3 green triangle)

C. Mean number of WPBs per nuclei calculated in each FOV n/N=3/30. Each data point represents a mean of WPBs per cell in an image. Colours/shapes represent technical repeats (R1 red hexagon, R2 blue square, R3 green triangle).

D. Mean length of WPBs in each FOV n/N=3/30. Each data point represents a mean of WPB length per cell in an image. Colours/shapes represent technical repeats (R1 red hexagon, R2 blue square, R3 green triangle).

Unpaired t-test * = p <0.05

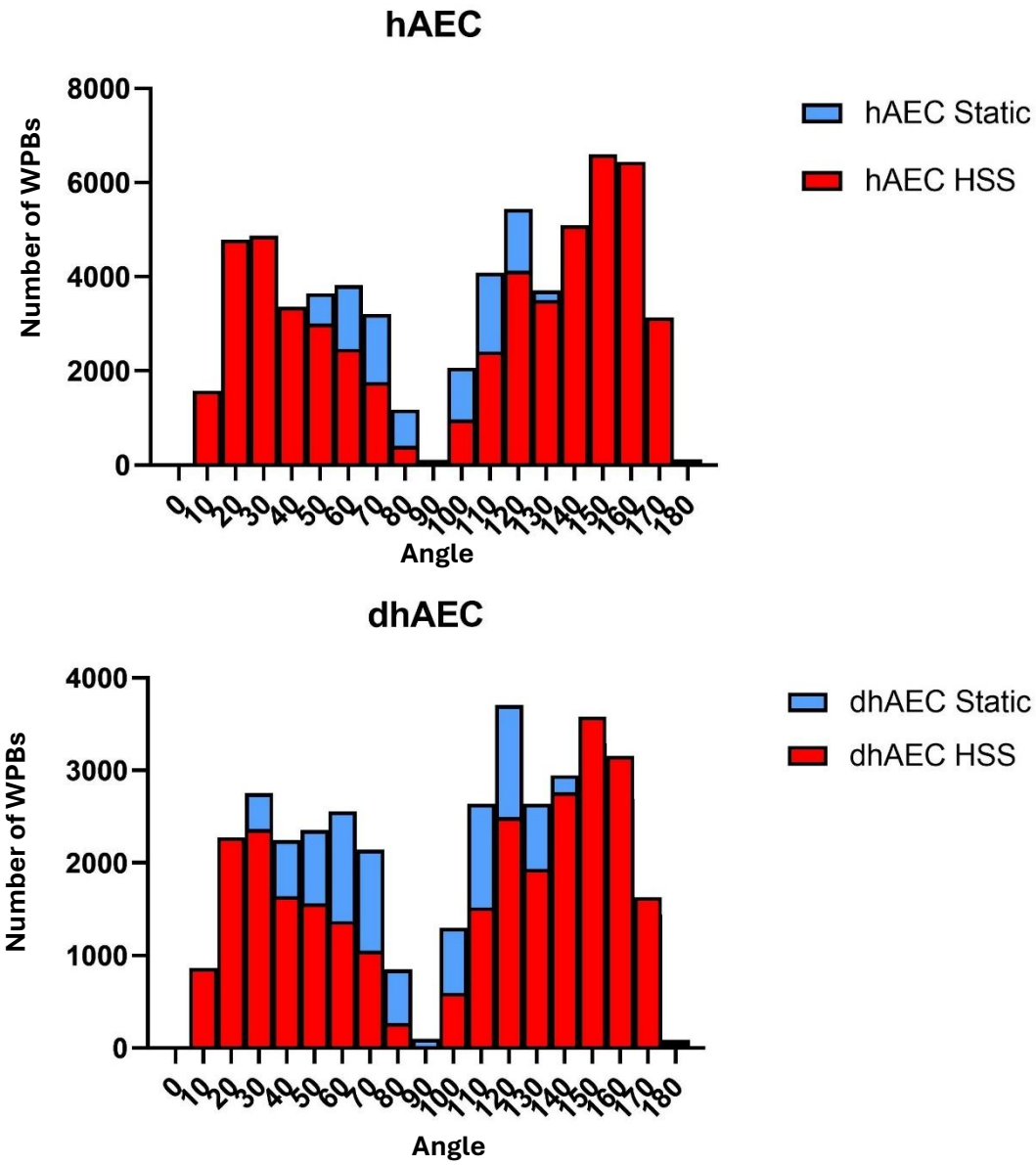

Figure 4.12 WPBs in both hAECs and dhAECs respond to HSS and align with the direction of flow.

The angle of WPBs was assessed and plotted into a histogram for both HSS (red) and static (blue) conditions. The higher the bar the greater the number of WPBs clustered at that angle.

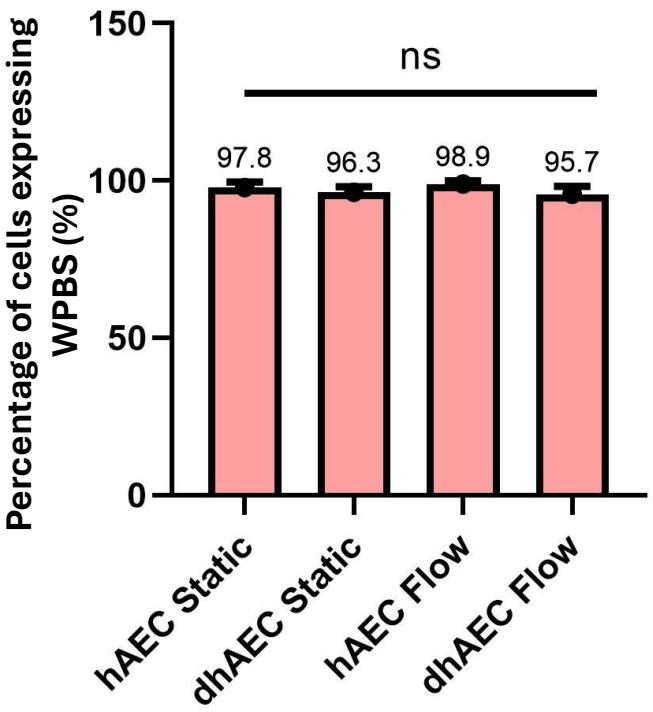

Figure 4.13 The mean number of cells expressing WPBs is consistent across both hAECs and dhAECs irrespective of shear exposure.

Average percentage of WPB 'positive' cells ±SEM n/N=3/30. A cell area was defined around a nucleus and was assessed to see if WPBs were present within. Cell that did not were considered to not be producing WPBs. The cells were subtracted from WPB 'positive' cells and a percentage calculated.

4.3.3 Pair C: WPB profile of dhAECs and hAECs exhibits distinct differences

4.3.3.1 Phosphorylated Protein kinase B (AKT) is not affected in dhAECs

Phosphorylation of AKT shows an approximate to 2-fold decrease in dhAECs to hAECs (0.612±0.330,1±0.801, p=0.678), this however was not a significant difference (**figure 4.14a**). There was little variation between hAECs and dhAECs regarding tAKT with no significant difference observed (1±0.249, 0.997±0.153, p=0.991) (**figure 4.14b**).

4.3.3.2 Endothelial Nitric Oxide Synthase (eNOS) is affected in dhAECs

There was a significant 3-fold increase in eNOS phosphorylation in the dhAECs compared to the hAECs (3.315±0.639,1±0.202, p=0.259) (**figure 4.15a**). Very little variation was seen between dhAECs and hAECs in teNOS levels with no significant difference (1.084±0.206,1±0.261, p=0.814) (**figure 4.15b**). This suggested that differences seen in peNOS are because of an increase phosphorylation rather than an increase in substrate.

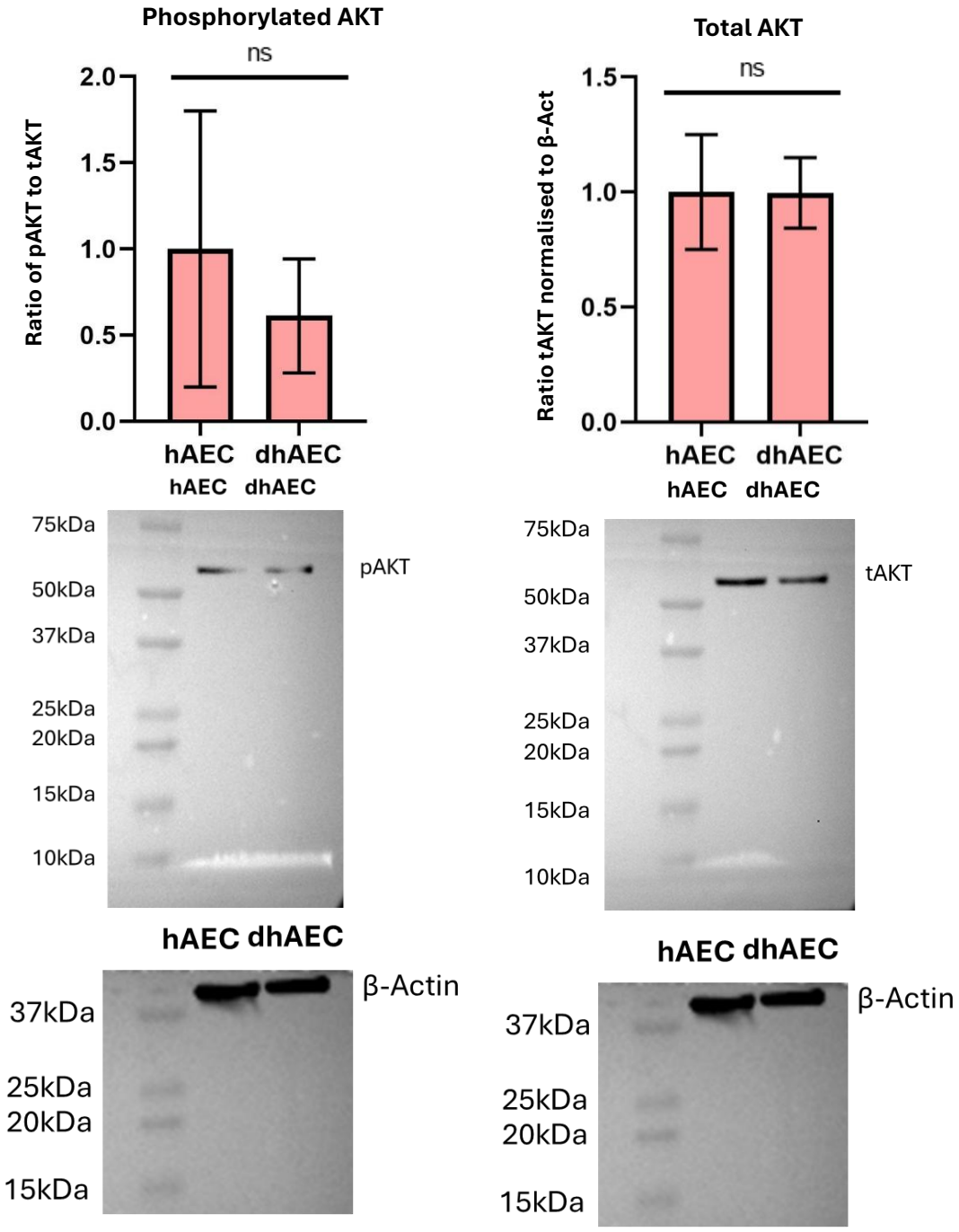

Figure 4.14 There are no differences between hAEC and dhAEC phosphorylation of AKT and total AKT.

- **A.** Mean phosphorylated AKT expression measured in hAECs and dhAECs normalised to total Akt. Mean+/- SEM. n/N=3/3
- **B.** Mean total AKT expression normalised to beta actin measured in hAECs and dhAECs ±SEM n/N=3/3

Unpaired t-test ns= non-significant

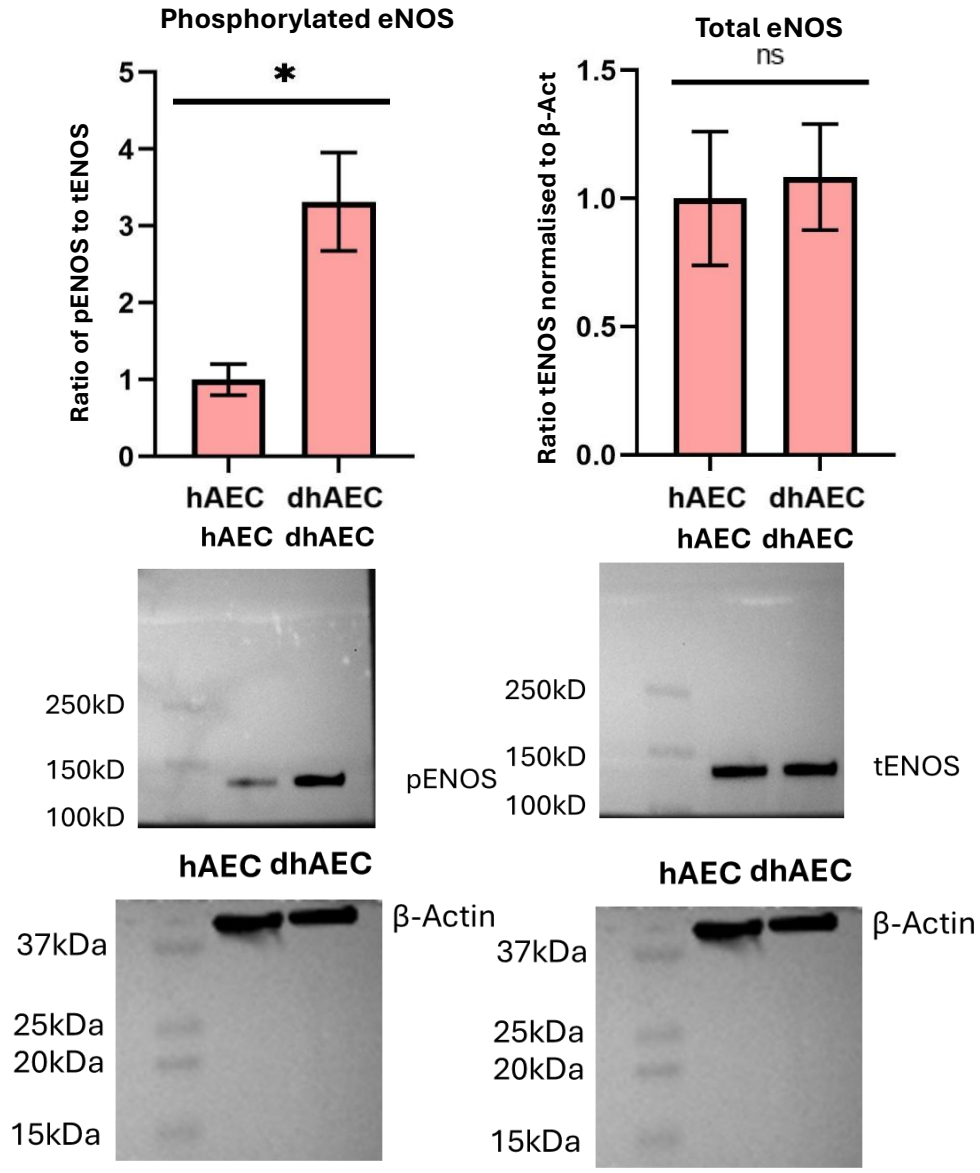

Figure 4.15 There is increased phosphorylation of eNOS in dhAECs compared to hAECs but no change in total eNOS.

- **A.** Mean phosphorylated eNOS expression measured in hAECs and dhAECs ±SEM n/N=3/3
- **B.** Mean total eNOS expression normalised to beta actin measured in hAECs and dhAECs ±SEM n/N=3/3

Unpaired t-test* = p <0.05

4.3.3.1 Total WPB Number was reduced by diabetes

In both static and HSS culture there were significantly fewer WPBs per FOV in the dhAECs than hAECs (301±98, 1947±239, *p*= 0.009; 300±106, 2696±401, *p*= 0.009), visible in **figure 4.16**. Number of WPBS was not impacted by exposure shear stress in either hAECs or dhAECs (*p*= 0.343, *p*= 0.225) **figure 4.17a**.

4.3.3.2 Number of Nuclei was reduced by diabetes

The hAECs were consistent across static (41±2) and HSS (38±2) conditions with no significant difference observed (*p*= 0.3428). There were also no significant differences between the dhAECs in either the static (19±2) or HSS (16±1) (*p*=0.2247) conditions **figure 4.17b**. The number of cells in the dhAECs did significantly differ from the hAECs in both the static (*p*=0.0009) and HSS (*p*=0.0009) with a significant reduction from the number of cells observed.

4.3.3.3 Average number of WPBs Per Cell was reduced by diabetes

There was no significant difference between the average number of WPBs per cell in hAECs cultured under static or HSS (48±5, 71±8, *p*= 0.1836). The was also observed in dhAECs, (16±5, 19±6, *p*=0.9958) **figure 4.17c**. There was a significant difference in the average number of WPB per cell between the hAECs and dhAECs in both static (48±5, 16±5, *p*= 0.0093) and HSS (71±8, 19±6, *p*= 0.0058) environments.

*4.3.3.4 WPB L*ength was affected by diabetes

WPBs in hAECs displayed a flow phenotype with significantly smaller WPBs in the HSS condition compared to those in static (0.852±0.015µm, 0.935±0.009µm, *p*= 0.059). This was also observed in the dhAECs, with significantly shorter WPBs in the HSS condition compared to static (0.816± 0.028µm, 1.055±0.006µm, *p*= 0.0011). Within the static environment, the WPBs in the dhAECs were significantly longer than those from hAECs (*p*= 0.0093) (**figure 4.17d**). This is indicative of a potentially enhanced thrombotic population of WPBs even within an expected 'pro-thrombotic' environment. No significant difference was seen between the dhAECs and hAECs under HSS.

4.3.3.5 WPB Polarity is not affected by diabetes

WPBs in both hAECs and dhAECs responded to HSS with clustering at the extreme 'horizontal' angles 0° and 180°. At first glance the patterns seen in both are very similar (see **figure 4.18)** however, the difference in the number of WPBs is highlighted as a tenfold difference between the dhAECs and hAECs can be observed.

4.3.3.6 Number of cells expressing WPBs was affected by diabetes

Neither hAECs nor dhAECs displayed a flow effect when exposed to HSS, with no significant difference in the number of cells expressing WPBs to their static counterpart (**figure 4.19**). However, there was significantly fewer dhAECs expressing WPBs in both the static (p= 0.0017) and HSS (p= 0.0371) conditions compared to the hAECs, indicating diabetes did have an effect. Under static 99% of hAEC were expressing WPBs compared to 60% of dhAECs. Under HSS 99% of hAECs were expressing WPBs compared to 71% of dhAECs.

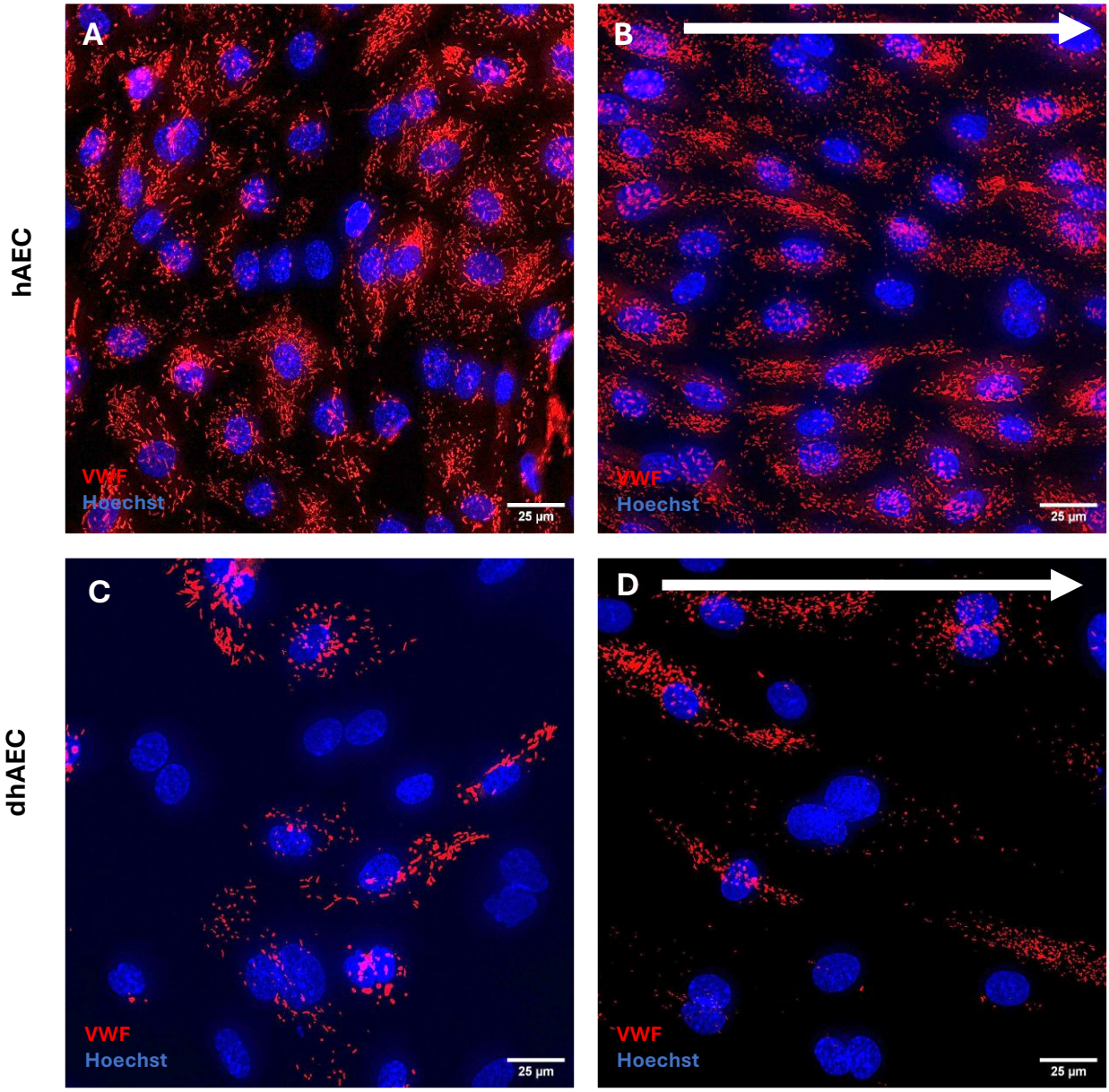

Figure 4.16 Representative images (x60) of hAECs and dhAECs in static and HSS conditions.

Nuclei are in blue (Hoechst), and WPBs are in red (VWF).

A. hAECs from pair C cultured in a static environment show consistent expression of WPBs. Nuclei are disordered displaying no clear directionality.

B. hAECs from pair C cultured in a HSS environment show consistent expression of WPBs aligned with cells. Nuclei have aligned to direction of flow.

C. dhAECs from pair C cultured in a static environment show relatively even WPB expression and no alignment of nuclei.

D. dhAECs from pair C cultured in a HSS environment show a relatively even expression of WPBs aligned with nuclei in direction of flow.

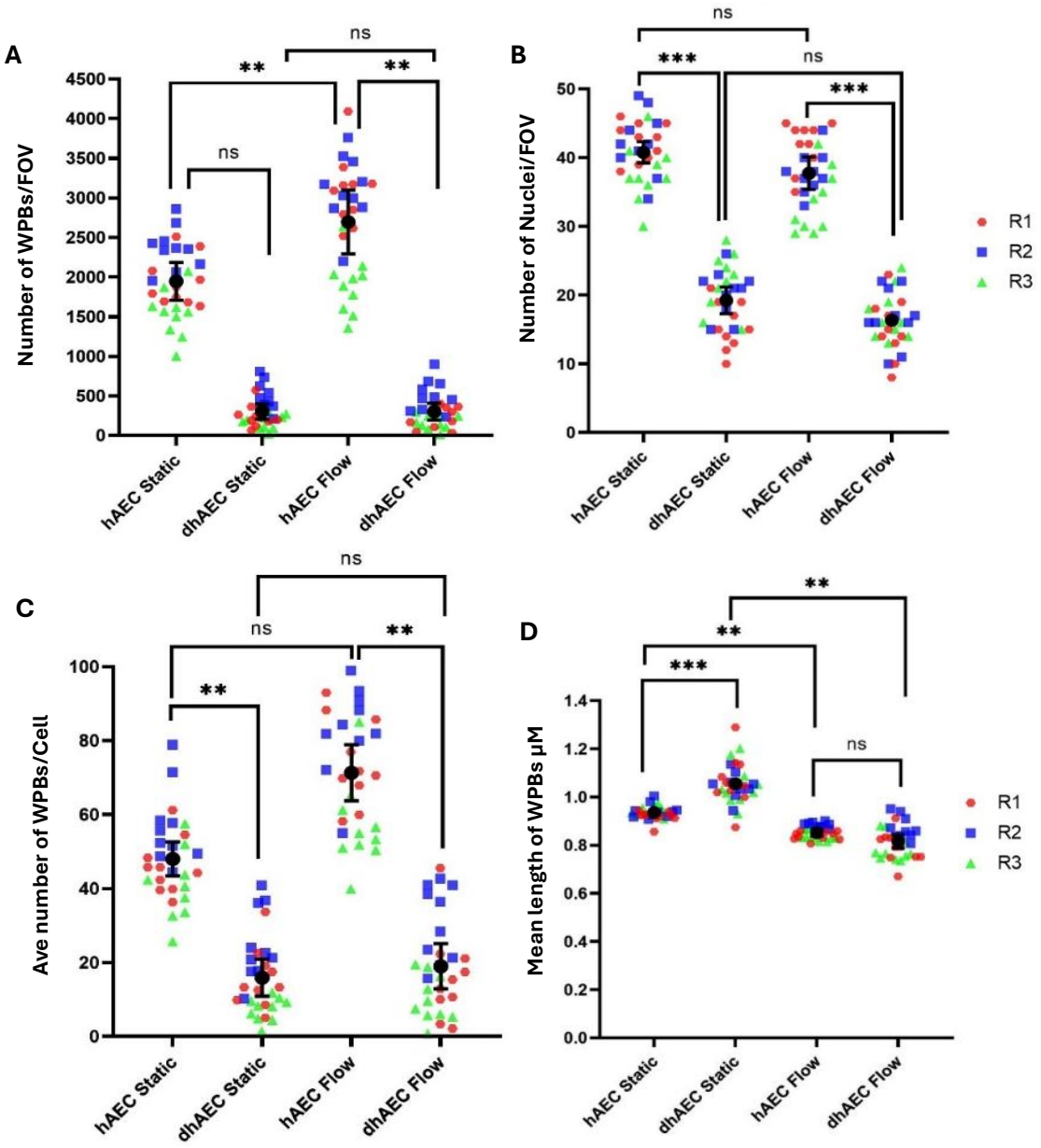

Figure 4.17 The profile of WPBs from cells in pair C are significantly different between hAECs and dhAECs cultured under both HSS and static conditions.

- **A.** Mean data of the total number of WPBs observed in each FOV per condition ±SEM n/N=3/30. Each data point represents a mean of all WPBs counted in an image. Colours/shapes represent technical repeats (R1 red hexagon, R2 blue square, R3 green triangle).
- **B.** Mean data of number of nuclei counted in each FOV ±SEM n/N=3/30 Each data point represents a mean of all nuclei counted in an image. Colours/shapes represent technical repeats (R1 red hexagon, R2 blue square, R3 green triangle).
- **C.** Mean number of WPBs per nuclei calculated in each FOV n/N=3/30. Each data point represents a mean of WPBs per cell in an image. Colours/shapes represent technical repeats (R1 red hexagon, R2 blue square, R3 green triangle).
- **D.** Mean length of WPBs in each FOV n/N=3/30. Each data point represents a mean of WPB length per cell in an image. Colours/shapes represent technical repeats (R1 red hexagon, R2 blue square, R3 green triangle).

Unpaired t-test * = p <0.05, ** = p <0.01 *** = p <0.001

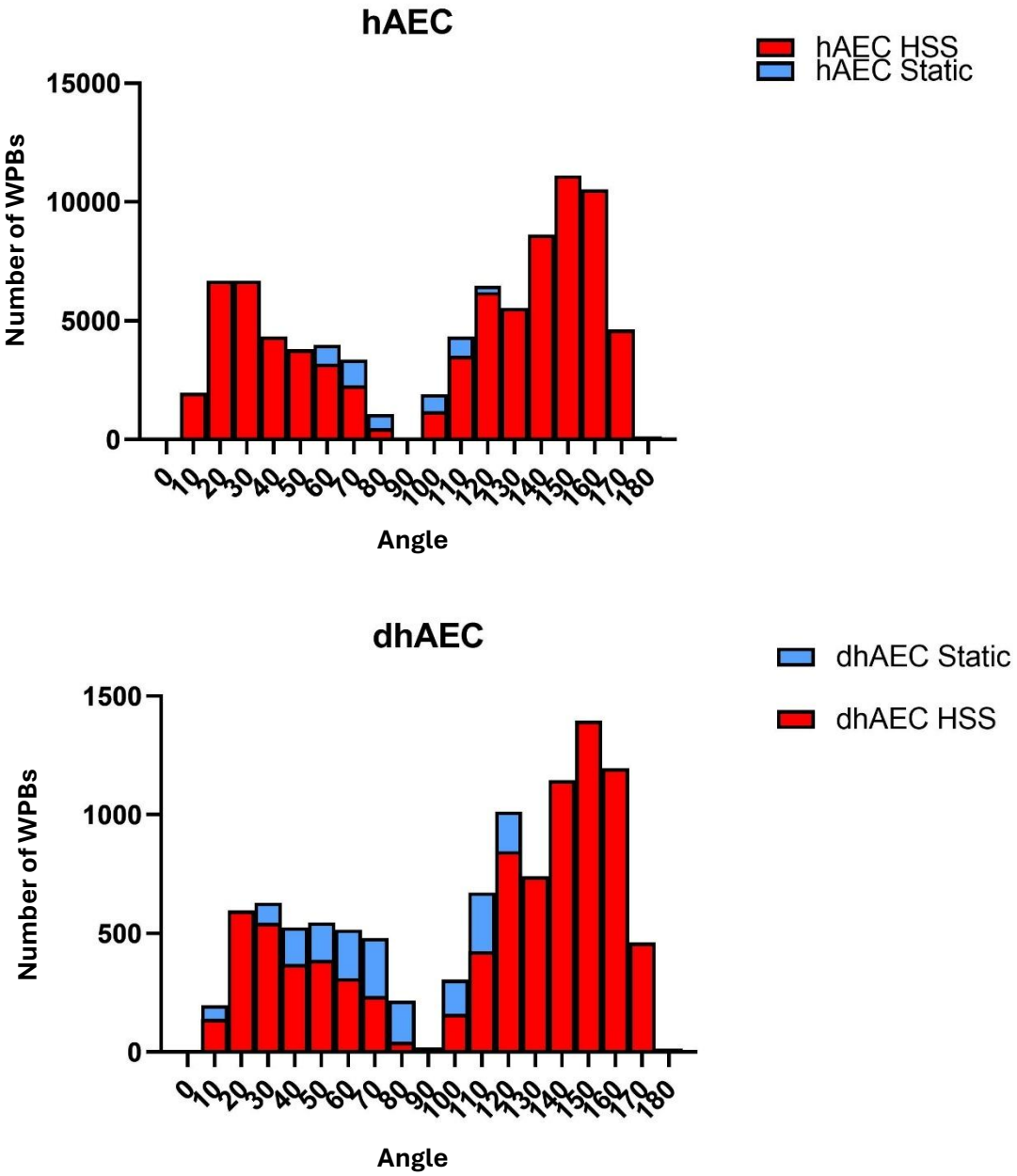

Figure 4.18 WPBs in both hAECs and dhAECs respond to HSS and align with the direction of flow.

The angle of WPBs was assessed and plotted into a histogram for both HSS (red) and static (blue) conditions. The higher the bar the greater the number of WPBs clustered at that angle.

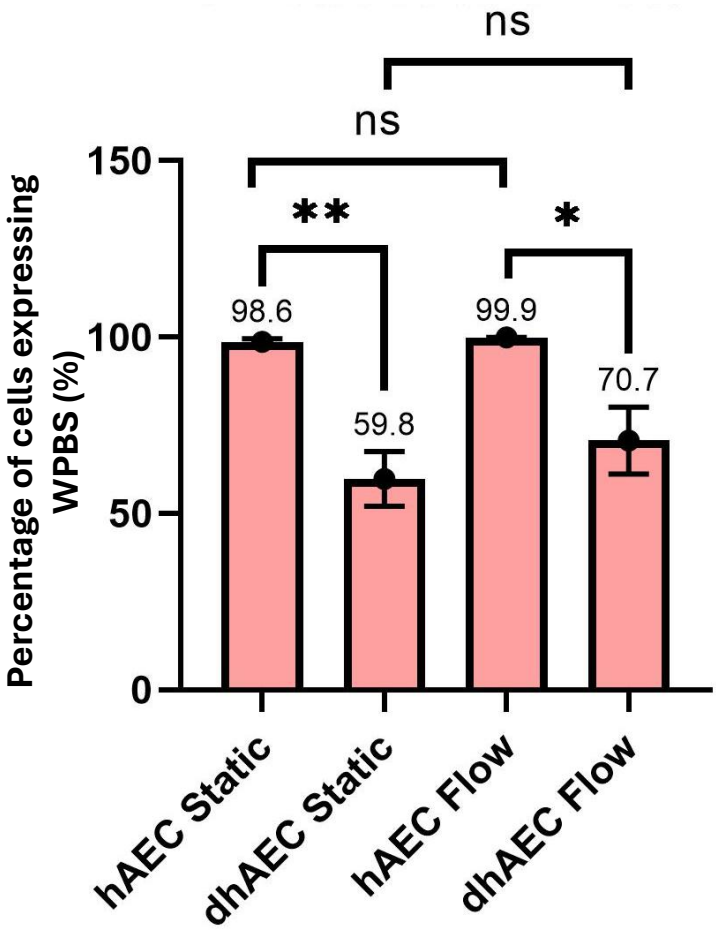

Figure 4.19 The mean percentage of cells expressing WPBs was significantly lower in dhAECs that hAECs in both static and HSS conditions.

Average percentage of WPB 'positive' cells ±SEM n/N=3/30. A cell area was defined assessed to see if WPBs were present within. Cell that did not were considered to not be producing WPBs. The WPB 'negative' cells were subtracted from the total number of cells and a percentage calculated.

Unpaired t-test * = p <0.05, ** = p <0.01

4.4 Comparative analysis of patient characteristics

I analysed several parameters within each of the paired samples, but the outcomes showed variability between the pairs. The ECs assessed in this study were derived from individual donors, suggesting that the observed differences may reflect patient-specific variability. In particular, distinguished differences in donor profiles, especially age and sex, could influence the measured outcomes. This is why the ECs were paired initially: to preserve the integrity of comparative analysis and account for potential confounding variables.

Here I combined the pairs and assessed the data as a compete set to ascertain if any significant differences were observed between the hAECs and the dhAECs.

4.4.1 dhAECs have a different metabolic profile to hAECs

4.4.1.1 Phosphorylated Protein kinase B (AKT) is not affected in dhAECs

To illustrate the impact of amalgamating the three pairs into one data set, I assessed AKT phosphorylation. When assessed in discrete pairs significance was identified however when the datasets were combined this was lost.

All dhAECs displayed a reduced phosphorylation in AKT compared to the hAECs, but significance was only determined in Pair A (p= 0.0324) (see **figure 4.21a**). Upon analysis of the data as a whole set the dhAECs displayed approximately 50% less pAKT compared to hAECs (1±0.352, 0.425±0.122) (**figure 4.20a**). However, due to the variability in hAECs display this difference was not found to be significant. This highlights the need for greater n numbers in cell-based experiments, this was not something that was physically possible to achieve in this study however it does provide a strong springboard from which to continue.

To differentiate between changes in phosphorylation and protein abundance, total AKT was quantified. There was no significant difference between the hAECs and dhAECs both overall (1±0.212, 1.047±0.055, p=0.442) (see **figure 4.20b**) or in individual pairings (see **figure 4.21b**). When pairs are considered independently, both pair A and C show almost no difference in tAKT in the dhAECs compared to the hAECs. Pair B conversely shows a noticeable but insignificant elevation of tAKT in diabetic cells. The lack of significance across the three pairs supports the interpretation that dysregulation of pAKT observed in dhAECs is specific to phosphorylation activity rather than reflecting changes in total AKT expression. As compiling pairs into one large data set obscured significant differences in pairs, they have been analysed as discrete sets from here forward.

4.4.1.2 Endothelial Nitric Oxide Synthase (eNOS) is affected in dhAECs

Phosphorylation of eNOS displayed considerable heterogeneity across the three pairs of ECs (**figure 4.21c**). In pair A, there no significant difference in peNOS abundance in the dhAECs compared to the hAECs (0.831±0.267,1.00±0.386, p=0.7373). Pair B showed close to a 2-fold difference peNOS abundance in the dhAECs compared to the hAECs (2.172±0.831, 1.00±0.322, p=0.2591), this was not a significant difference as the variability within the condition was too great. Pair C displayed a result in line with pair B, with a close to 3-fold increase in peNOS in dhAECs than in hAECs (3.315±0.639, 1.00±0.202, p= 0.026) resulting in a significant difference (**figure 4.21c**).

Total levels of eNOS (tENOS) were assessed to provide context, distinguishing if observed results are due to altered phosphorylation activity or increased abundance of eNOS. Pair A showed a significant difference of tENOS with an approximately 2-fold higher abundance in dhAECs than in the hAECs (1.998±0.280, 1.00±0.131, p=0.0320). There was no significant difference between hAECs and dhAECs (1.00±0.261, 1.084±0.206, p=0.8138) in pair C. Pair B did not have a significant difference between hAECs and dhAECs (1.00±0.127, 0.636±0.0127, p=0.0854), but did show the opposite trend to A with a decrease in tENOS in the dhAECs compared to the hAECs (**figure 4.21d**). Given the degree of variability seen in ENOS data for cell pairing was not combined as it cancelled out these significant changes seen.

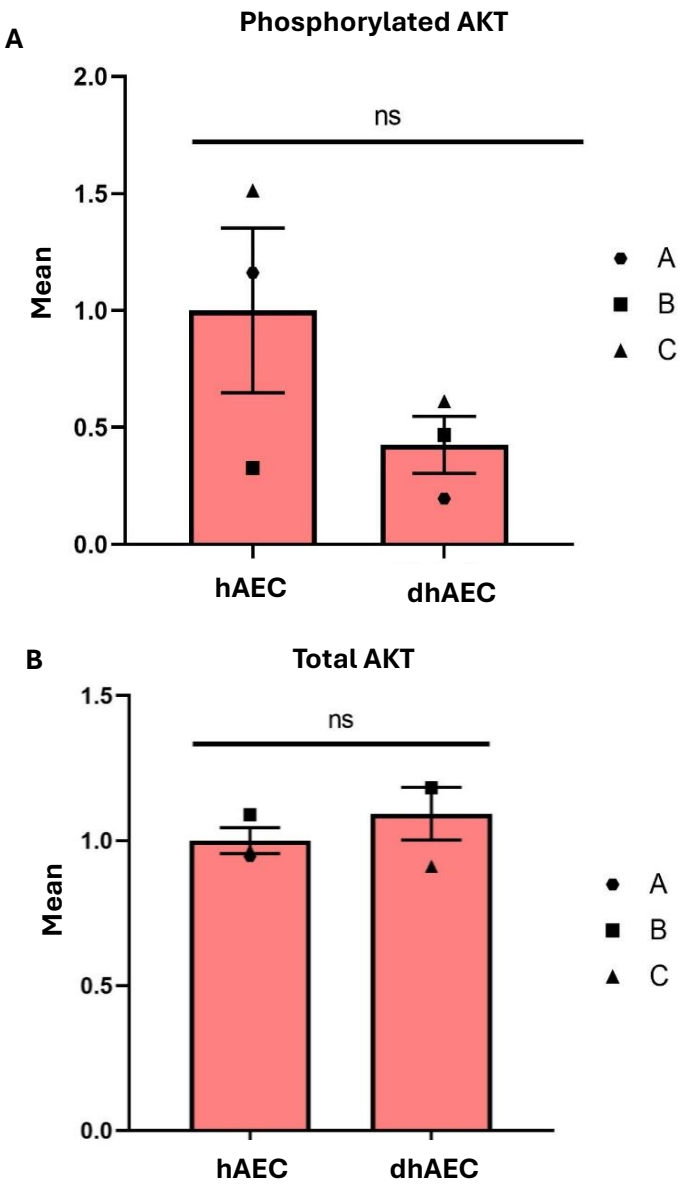

Figure. 4.20 No difference was observed between hAECs and dhAECs in phosphorylated or total AKT when assessed by densitometry of Western blot.

A. Mean amount of pAKT ±SEM n/N=3/3 taken from mean pAKT expressed combined results of all three pairs (hAEC 1.00±0.352 and dhAEC 0.425±0.122). Less phosphorylation was seen in the diabetic ECs than the control, but this difference was not significant.

B. Mean amount of tAKT ±SEM n/N=3/3 taken from mean tAKT expressed in each condition (hAEC and dhAEC) of each pair A, B and C. There was a slightly elevated amount in the diabetic condition compared to control, but no significant difference was observed.

Unpaired t-test * = p <0.05

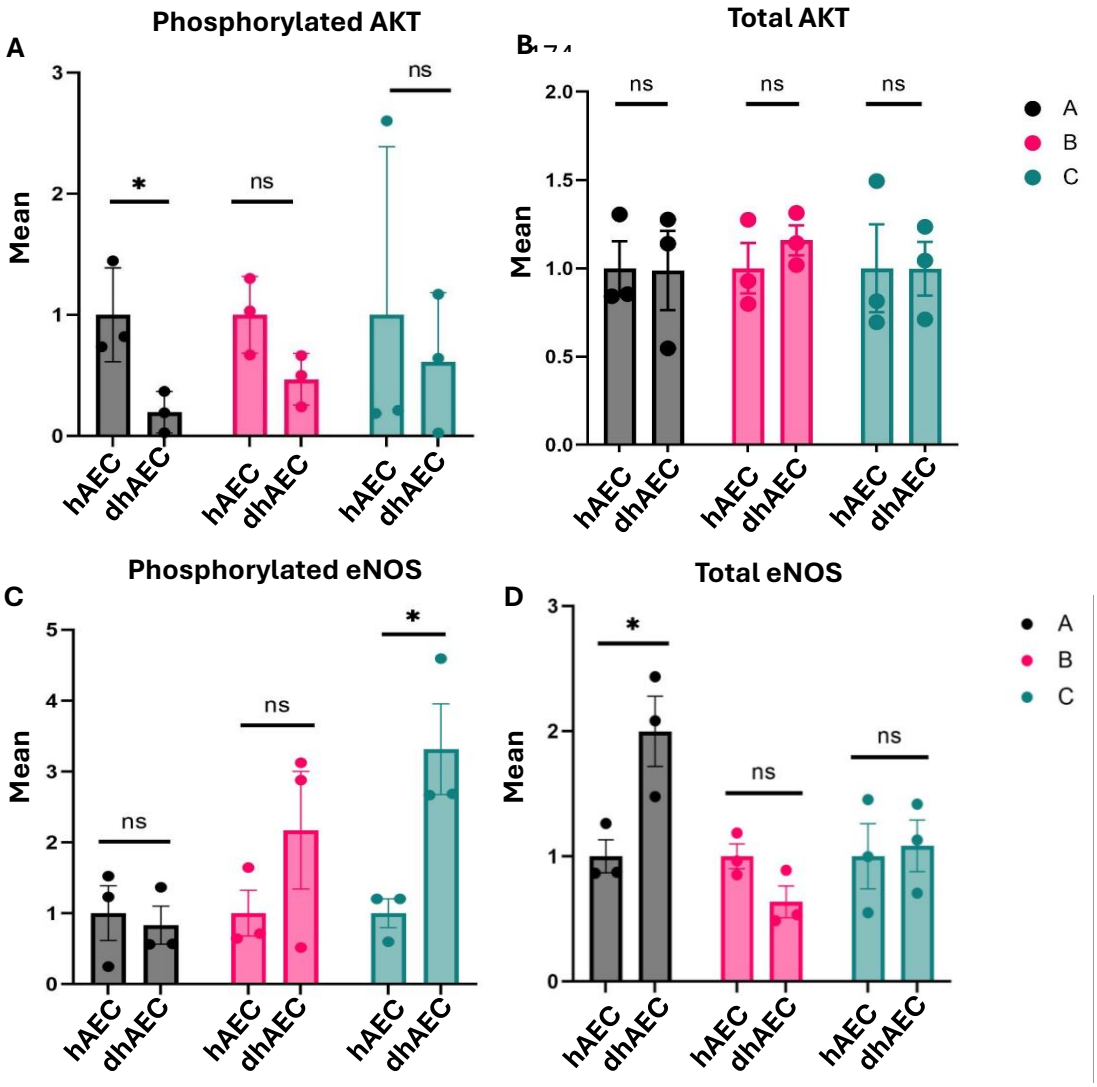

Figure 4.21 Phosphorylation of AKT and eNOS was assessed across all three pairs individually, variation was seen between each pair and within each pair. Total levels of AKT and eNOS were also assessed total AKT showed consistency between each pair whereas total eNOS was more varied.

- **A.** Mean amount of pAKT ±SEM n/N=3/3 taken from mean pAKT expressed in each condition (hAECs and dhAECs) separated into each pair A, B and C. Less phosphorylation was seen in the hAECs and dhAECs, in all pairs this was significant in A but this difference was not significant in B and C.
- **B.** Mean amount of pAKT ±SEM n/N=3/3 taken from mean pAKT expressed in each condition (hAECs and dhAECs) separated into each pair A, B and C. There were no significant differences in any pair in total amount of AKT.
- **C.** Mean amount of peNOS ±SEM n/N=3/3 taken from mean peNOS expressed in each condition (hAECs and dhAECs) separated into each pair A, B and C. Less phosphorylation was seen in the hAECs and dhAECs, in all pairs this was significant in A, but this difference was not significant in B or C.
- **D.** Mean amount of tENOS ±SEM n/N=3/3 taken from mean tENOS expressed in each condition (hAECs and dhAECs) separated into each pair A, B and C. Less phosphorylation was seen in the hAECs and dhAECs, in all pairs this was significant in A, but this difference was not significant in B and C.

Unpaired t-test * = p <0.05

4.4.2 Statistical dispersion of WPB Feret Length

There were significant differences seen between hAECs and dhAECs in each of the three pairs. As the cell lines were obtained from a commercial source they were matched by sex and age, but the lack of clinical data means more robust criteria could not be included. As such, it was pertinent to compare each of the six cell lines to one another.

Data in **figure 4.22a** presents mean of WPB length for hAECs and dhAECs. The average represents the combined data for each cell type under static or HSS culture conditions. When presented and analysed in this manner, any significance seen in patient pairs repeats is lost. As pair A and pair C showed diametrically opposing significant differences (static dhAEC WPBs were longer in C and shorter in A) it is reasonable to infer that this effect may be obscured under the given conditions. The dhAECs from pair A and B display opposing trends, suggesting divergent responses within the diabetic environments. Heterogeneity is more pronounced in the dhAECs especially exposure to HSS. Under HSS hAECs cells have lost any discernible heterogeneity with near total overlap of all three hAEC donors. This is illustrated by the overlay of means for each patient (see **figure 4.22b**) HSS has had the predicted protective effect on each of the cell lines used regardless of diabetes diagnosis. In the hAEC this was not a significant effect (static 1.063±0.093, HSS 0.860±0.022 p= 0.1025), this was significant in the dhAECs (static 1.106±0.039, HSS 0.831±0.043). There were however no significant differences between the hAECs and dhAECs within static (p=0.6922) or HSS (p=0.5785) exposure.

For the dhAECs, they follow a trend of having shorter WPBs under flow ever further than the hAECs the only exception to this is pair C where the trend is an increase in length, suggesting these cells may be resisting the protection afforded by HSS. The opposite trend is observed in the static dhAECs with both pair B and C trending to have longer (and a theoretically greater thrombogenic profile) WPB populations whereas A is decreasing in length. The hAECs for assigned to pair A is however displaying the longest phenotype of all three possible controls. As these are not results of a true matched pair experimental design, it becomes valuable to note that all the hAECs are shorter than those in pair A in a static environment. Similarly, dhAECs in pair A are longer than the hAECs in both pair B and pair C, could it therefore be the hAECs n pair A causing this standout deviation?

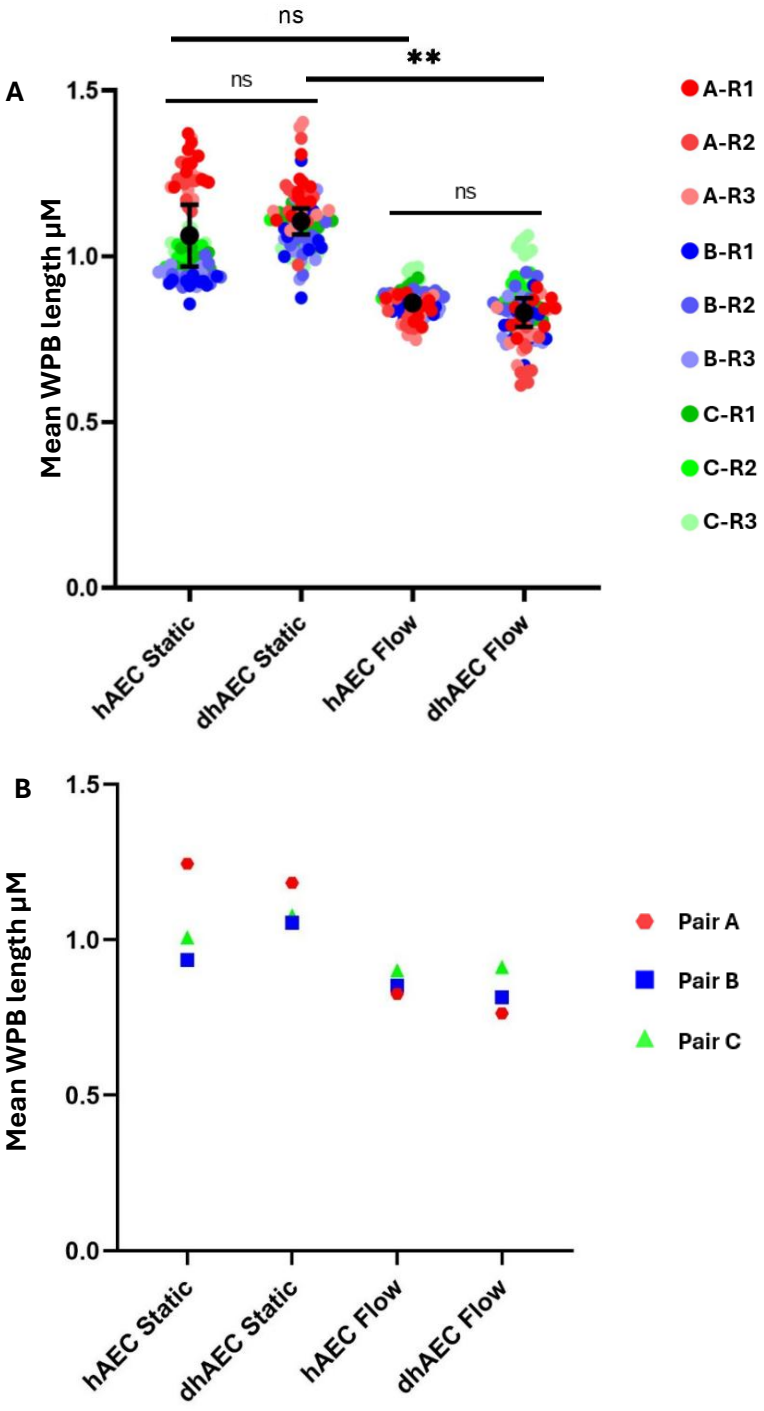

Figure 4.22 There are patient to patient differences in WPB length in both hAECs and dhAECs from different pairs in both static and HSS conditions.

- **A.** Mean length of WPBs in hAECs and dhAECs in both static and HSS conditions, all three repeats of all three pairs (A, B and C) combined in each ±SEM n/N=3/90.
- **B.** Mean of WPB length for individual pairs for each condition shows the variability within each environment n/N=3/3. ECs cultured under HSS are the most consistent. Diabetic cells cluster consistently showing a lower length trend in HSS.

4.4.3 Statistical dispersion of the average number of WPBs per cell

Compared to WPB length, the average number of WPBs per cell displays greater variability. Clear distinctions are evident between cell lines under each condition, even within matched pairs. In **figure 4.23a**, the hAECs and dhAECs show minimal variance, with data points tightly clustered within each condition and substantial overlap between conditions. Pairs A and C further illustrate this showing consistent clustering of replicates with each donor. No significant differences were identified between hAECs and dhAECs in static culture (58±13, 24±10, p=0.128) or HSS (50±11, 24±10, p=0.158). No differences were recorded between dhAECs (p=0.9952) or hAECs (p=0.6830). This highlights the inherent variability when comparing individual patient samples. While increasing the number of donors has strengthen the argument that diabetes influences WPB characteristics the variation observed between pairs suggests that additional factors such as duration of diabetes may contribute (**figure 4.23b**). This information was not available from Promocell.

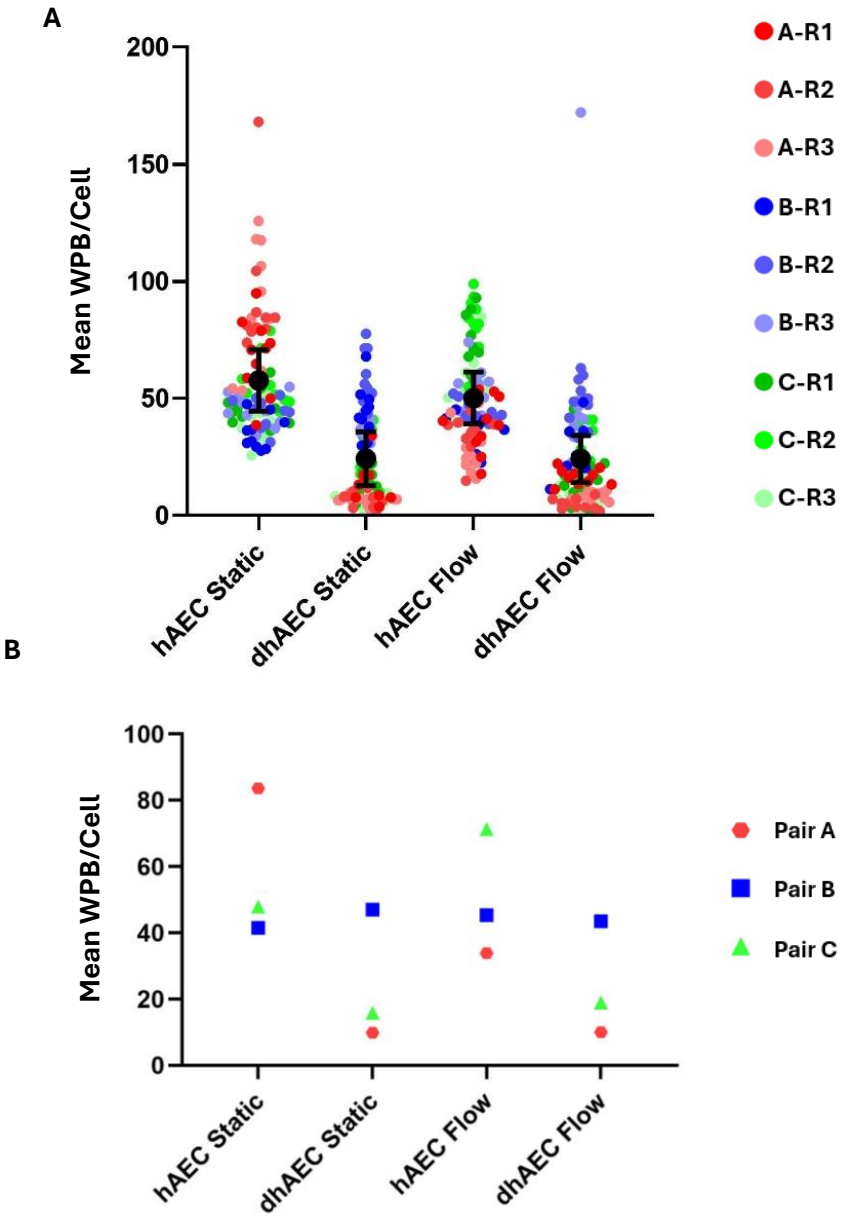

Figure 4.23 There are patient to patient differences in the average number of WPBs per cell in both dhAECs and hAECs from different pairs in both static and HSS conditions.

A. Mean number of WPBs/cell in dhAECs and hAECs in both static and HSS conditions, all three repeats of all three pairs (A, B and C) combined in each ±SEM n/N=3/90.

B. Spread number of WPBs/cell data points without mean. Each pair shows some distinctive clustering of repeats more obvious in the static than HSS condition.

C. Mean of individual pairs number of WPBs/cell for each condition shows the variability within each environment n/N=3/3. ECs cultured under HSS are the most consistent. Diabetic cells cluster consistently showing a lower length trend in HSS.

4.5 Discussion

This model of investigating the impact of diabetes on WPBs was designed to create a more physiological representation of diabetes in an *in vitro* context. Aortic cells were utilised as they are an EC found within the mature vasculature and have greater physiological relevance than HUVECs. Both hAECs and dhAECs were maintained in a normo-glycaemic environment of 5.5 mM. As dhAEC were taken from patients with a confirmed diagnosis of diabetes this model enabled exploration the concept of metabolic memory, whereby cells extracted from an environment where they have had exposure to pathogenic cues, have been placed into a 'healthy' environment (204). As aortic ECs were available as only individual donors, unliked pooled HUVECs, it limits sample diversity. This was addressed here by utilising multiple single donor samples to increase biological variability. This model demonstrated the importance of including a broad range of donor characteristics. When data from all three pairs were pooled into a single dataset, significant differences were obscured, highlighting the need to assess samples individually in this context but also increasing the sample size further.

There was a persistent phenotypic shift in the dhAECs compared to the hAECs, despite removal of pathogenic environmental cues associated to diabetes e.g., hyperglycaemia. As both EC lines were cultured in identical in vitro conditions it allows us to infer that these differences can be attributed to exposure to stimuli observed with diabetes. This suggests that there is an intrinsic cellular imprint, consistent with the metabolic memory concept. Pair A revealed significant differences in WPB populations between dhAECs and hAECs. Based I these initial findings, the model was expanded to include additional commercially sourced donor samples. This increased the number of biological replicates to n=3 and introduced greater donor variability, enhancing the robustness and reproducibility of the results.

Comparison of the three pairs shows pair A and pair C display similar phenotypes to one another regarding WPB population. Among the three pairs, A and C pairs exhibited shared trends that distinguish them from pair B. Both A and C presented a significantly lower average number of WPB per cell in the dhAECs compared to the hAECs irrespective of HSS exposure. Furthermore, there was fewer dhAECs expressing WPBs than the hAECs in both pairs. Both pairs displayed similarities in their metabolic fingerprint with a decrease in phosphorylation of AKT in the diabetic ECs, this difference was only significant in pair A but there was a trend in pair C. Neither of the pairs displayed a significant change in the total expression of AKT in the diabetic ECs indicating that this increase was in fact due to

raised phosphorylation activity than increase production of the AKT protein. These results deviate from the findings of the previous models of diabetes presented in **chapter 3** however it does align more to expectations from literature as diabetes is impacting WPB and by extension VWF. However, the relationship is the converse of that predicted in this context as a reduction in WPBs translated to a reduction in VWF. Literature suggests that VWF should d be increased in diabetic patients (192, 199, 200). There are several possibilities to explain this discrepancy. As these dhAECs were derived from a single donor, the observed phenotype may reflect a donor specific characteristic, however as 2 of 3 donors have displayed comparable WPB populations this is less likely. Alternatively, an event affecting VWF synthesis, packaging or exocytosis may be disrupting its expected storage within WPBs, resulting in the reduced WPB number observed. This could be an increased constitutive release of VWF (from unstimulated WPBs), elevated basal secretion or impaired synthesis of HMW VWF limiting its availability for packaging into WPBs.

Pair B differs in the trend of reduced WPB numbers in dhAECs compared to hAECs. The divide between B from A and C resides primarily in WPB biogenesis. Pair B displays variation between the hAEC and dhAEC WPB populations, for example there is significantly fewer WPB in the diabetic static conditions. There are also significantly fewer nuclei counted in the dhAEC conditions regardless of shear stress (SS) exposure compared the hAECs condition. This does not translate to a difference in the adjusted expression of WPBs, between the dhAEC and hAEC in any condition in the average number of WPBs per cell. The percentage of cells expressing WPBs is near identical in each condition, the opposite of the pattern of expression seen in A and C. This is not to say that A and C are a perfectly matching pair. Critically both dhAEC from both A and C are significantly different in static culture to the hAEC counterpart, there is no significance seen in pair B. However, in pair A the WPBs are significantly shorter in the dhAEC in static than the hAECs, the converse is true of pair C whereby the dhAEC display WPBs that are significantly longer than the hAECs. Thus, when data is combined, the majority of trends are lost. The only significant difference retained is the flow effect observed in the dhAEC WPB length. WPBs produced in static cultured ECs are the longest of all conditions tested, this may suggest that with the combined pathological exposures of static culture and diabetes results in longer WPBs with increased thrombotic potential. This also serves to highlight that both hAEC and dhAEC respond to HSS exposure and there is a rescue effect afforded by the atheroprotection associated.

This physiological EC model of diabetes aligns more to literature than the high glucose and ambulatory models in respect to AKT and eNOS behaviour. Phosphorylation of AKT in each pair displayed a decrease in dhAECs. There was variability between pair A, B and C with the greatest decrease seen in A and the least in pair C. Concurrently, the expression of total AKT remained consistent across the hAEC counterpart of each pair. This would suggest that the activity of phosphorylation is the process that is impacted under diabetes rather than the expression of AKT. This aligns with the published literature which indicates a reduction in pAKT should be expected in a diabetic context (8, 176). Insulin resistance associated to diabetes has been linked to a reduced phosphorylation of AKT due to impairment of the PI3K signalling pathway (8, 247). In my previous models, healthy ECs were utilised and only glucose was manipulated (see **chapter 3**). As such these ECs would not have experience insulin resistance. The dhAECs used in this model were derived from donors with a confirmed diagnosis of diabetes and are therefore likely to have been exposed to insulin resistance alongside a broader spectrum of diabetic-associated stimuli. The persistent reduction in AKT phosphorylation observed in dhAECs compared to hAECs supports the concept of metabolic memory. This suggest that even under normoglycemic conditions dhAECs do not fully revert to normal insulin/glucose responsiveness and maintain the reduction in phosphorylation activity.

Converse to AKT, eNOS generally displayed an increase in phosphorylation in the dhAEC compared to the hAECs. There is very minimal variation in data in pair A between hAECs and dhAECs, with a minor decrease observed in dhAECs. From here phosphorylation increases, with a 2-fold higher expression of peNOS in pair B dhAECs and a 3-fold increase in the dhAECs of pair C. This contrasts with the prevailing trend seen in literature which typically reports a reduction in eNOS phosphorylation under diabetic conditions (237, 271). Diabetes-associated hyperglycaemic has been linked to increased phosphorylation of eNOS at the Ser 1177 site (the site assessed via western blotting in my model) in a rat model (214). There is considerable variation across studies examining eNOS phosphorylation, in part, due to the fact eNOS can be phosphorylated at multiple regulatory sites (177). Notably hyperglycaemic conditions have been reported to increase phosphorylation at specific sites such as Thr495, which may exert inhibitory effects on eNOS activity (238). Unlike the deviation from established literature observed in eNOS phosphorylation patterns, teNOS expression in the physiological model aligns more closely with reported trends. Prolonged high glucose exposure has been shown to upregulate both eNOS gene and protein expression in hAECs (272). Consistently, two out

of three hAEC donors demonstrated increased teNOS levels, with pair A exhibiting an approximate 2-fold elevation in the dhAECs.

Two of three pairs of ECs displayed a reduction in WPB numbers (both total and per cell), which may be broadly translated into a reduction in VWF (as that is the primary constituent of WPBs). This interpretation would be contrary to the literature which suggests that VWF is elevated in diabetic patients (192, 193, 199, 200). A critical consideration when interpreting VWF levels in diabetic patients is that measured increases in VWF concentration are typically derived from blood plasma (193, 201, 202). Given the nature of circulating blood, it interacts with diverse vascular beds and is exposed to multiple sources and pathways of VWF release. WPBs represent stored UHMW/HMW VWF that is released via the regulatory pathway, requiring stimulation, constitutive is unstimulated release of WPBS and basal is the continuous secretion of LMW VWF (94). As such, concentrations of plasma VWF reflect contributions beyond WPBs alone. Therefore, a reduction in WPB number within dhAECs may be insufficient to conclude that these ECs contradict the broader literature on elevated VWF levels in diabetic patients. As constitutive release of VWF involves unstimulated exocytosis of WPBs, this would reduce the number of observable WPBs (as is seen in pairs A and C) (94). Consequently, it would be pertinent to widen the scope of this investigation to investigate these such pathways, which will be explored later. Pair B differed from this trend of reduced WPBs, if VWF release is altered basally, this would not be observable through this method of investigation. Another possible explanation for this deviation is patient variability. Alterations in VWF levels among diabetic patients have been linked to co-morbidity with CVD; notably in one study, elevated VWF was observed only in individuals with both diabetes and CVD (192). This suggests that VWF upregulation may reflect a more advanced state or cumulative pathogenic burden, which may not apply to the donor of dhAECs in pair B.

Regarding *in vivo* models there is a degree to which results of this model support and contrast findings from literature. In diabetes induced dogs, Anderson et al demonstrated that the number of WPBs varies between vascular beds, with venous ECs displaying a higher WPB count than aortic ECs, a trend consistent with observations in this study (191). However, their data showed that diabetes specific differences were only significant in venous-driven ECs when compared to controls. Given that the physiological cell model employed here uses aortic-derived ECs, the WPB reduction observed in two of three donor pairs may be attributable in part to vascular bed origin and therefore not necessarily indicative of deviation from established diabetic trends. In T1DM induced mice, Popov et

al presented a 2.8-fold increase in WPBs compared to the control mice endothelium (196). This was further supported by Ribau et al using a mouse model of genetically induced spontaneous T1DM which reported that hyperglycaemia was induced in mice and that in aortic ECs at 1 week and 2 months the diabetic condition contained a higher number of WPBs compared to the equivalent control (243). As with any approach there were limitations to this, for one, only male mice were used. In comparison, the AECs used in my physiological model used ECs from both males and females, which is more likely to increase the variability in the results. An interesting observation from the study by Ribau et al was that mice with diabetes for 2 months exhibited structural deformations of WPBs, suggesting a possible disruption in the biosynthesis of WPBs within the diabetic context (243). They also report that VWF abnormalities in humans precede clinical or histological signs of vascular disease (243). This supports the interpretation that the lack of morphological differences in WPBs from pair B may reflect an early stage of diabetes, capturing a snapshot prior to overt pathology within the vasculature developing.

Commercially acquired cells (hAECs and dhAECs) are typically more reliable regarding growth rate than experimentally isolated patient samples, which can be more prone to contamination with unwanted cell types due to the isolation and harvesting processes (273, 274). ECs in this model both hAECs, and dhAECs needed to be cultured in tandem keeping the environment as similar as possible and ensuring equal passage numbers, to reduce confounding factors. The reliability of commercial cell lines aids in this but ECs maintain a degree of fluctuation between one another regarding growth, pair C in this model proved to have a slower growth rate compared to the other pairs, particularly the diabetic cells. This created a challenge when utilising these cells as each had to be grown to confluence prior to plating into IBIDI channels. Confluence is a critical factor in studying ECs and WPBs, when cells are confluent, they are more reflective of a true endothelium so there is a physiological argument, but it also affects the expression of WPBs. In ECs that are not confluent, WPB will be reduced (275). Knowing this and seeing a reduction in WPB expression in A and C confluency was a concern and was assessed manually prior to and post exposure to HSS, ECs appeared to grow as normal in a monolayer throughout experiments. As the static culture, that experience no additional external stresses displayed the same reduction in WPB expression in the diabetic counterpart of both A and C this increased confidence that the displayed expression was truly a result of diabetes rather than confounding interference from cell growth.

Use of commercial cell lines also meant I had limited information regarding each donor in terms of sex, age and diagnosis of diabetes status. Diabetes is a complex disease, with

many factors that can vary across a population that may inform the presentation and effects of the disease and subsequently impair the production of WPB populations, resulting in variation. Duration of diabetes, and consequently, the length of exposure of ECs to a pathological environment should be considered when investigating whether temporal differences are reflected in WPB physiology. Prolonged exposure may influence organelle biogenesis, VWF processing or secretion dynamics, potentially contributing to altered endothelial function.

Similarly, treatment of diabetes may alter the microenvironment ECs experience in the vasculature (276). If patients are compliant with medication/treatments and they are effective, in theory, it will limit the exposure of ECs to pathological stimuli such as spikes and falls in hyperglycaemia and insulin resistance (277). Factors such as this may contribute to variability seen ECs used in this model. To account for this ideally the number of biological samples would be increased, this was not possible using more commercially available cells. Aortic cells are not simple to acquire from patients, I considered expansion to include use of umbilical artery cells as a middle ground, extracted from donated umbilical cords, however, time constraints prevented the development of this method into practice as a model. Despite this cavate, as has been highlighted in literature, there is a gulf between what has been observed in in vivo animal experiments i.e. significant alterations in WPB profiles in diabetes induced models when compared to control and attempts to assess these effects in human tissue in vitro, this model allows us to begin to bridge our understanding of WPBs *in situ* in humans.

This model in comparison to the previous high glucose and ambulatory glucose models highlights the heterogeneity of vascular beds throughout the vasculature. HUVECs and hAECs represent two different vascular beds each specialised to different functions, as such the microenvironment within each is different. We know that this impacts WPBs, they are heterogeneous and have cargo that varies with vascular bed (98). Given the demonstrated and documented heterogeneity in WPBs across vasculature, there could be a difference in the expression of VWF that follows the same pattern (101). In the aorta, blood pressure is far greater than that experience in veins, as such, the response to vascular injury, while universal may have small adaptations suited to each environment (58). This could be reflected by the difference seen in VWF string length, in veins pressure is lower and therefore less likely to damage the fragile structure of the strings, in arteries, particularly in the aorta, the pressure is far greater, increasing the likelihood of mechanical damage to the VWF string structure. Hence it would be of an evolutionary advantage to

save energy by manufacturing smaller but stronger VWF strings to use in case of vascular injury.

WPB functionality can be measured by a proxy measure of the length of VWF strings released from ECs when stimulated. This was carried out for pair A, which showed that VWF strings were significantly shorter from the dhAECs regardless of shear exposure. One explanation for this may be the reduced number of WPBs observed in the dhAECs, as there are fewer WPBs present to release strings, there will be fewer interactions occurring, VWF self-associates and will bind to itself, which aids in the formation of the characteristic long strings (278). There was a clear difference between the hAEC and HUVEC response to stimulation with histamine, under static HUVECs release long strings, thought to be highly thrombotic. This behaviour was not observed in the hAECs, there were defined structures released by ECs in the static environment but not to the same degree, hAECs were also more prone to an adverse reaction to histamine exposure, resulting in cell senescence. As a result, a second approach is needed, VWF once synthesised is separated by molecular weight, low, medium and high (including ultra-large) weight (228). Each class is associated to different distinguished roles and to one of three exocytosis pathways (94). Thus, use of a western blot like approach allows separation of the different MWs of VWF contained in each cell, like a fingerprint, provided more information on the composition of VWF contained in each cell line. This will allow for assessment of the effects of diabetic stress on VWF synthesised by hAECs.

Expansion of the population would be optimal to account for the variability observed between individual donors, particularly within control and diabetic cohorts. While this was beyond the scope of the present study, several strategies could be employed to achieve broader representation. Increasing the number of hAEC and dhAECs would offer improved consistency with the current model, though this approach is limited by cost and the restricted availability of diabetic donors in commercial cell stocks. Alternative methods, although more time consuming may be more cost-effective and allow for the integration of patient demographic data into the analysis. For instance, ECs derived from diabetic patient's saphenous vein ECs or HUVECs/HUAECs from umbilical cords could be used. Isolation of these cells in house would provide greater control over patient demographics and population size, enhancing the relevance and interpretability of future findings.

Given that ECs offer only a partial view of VWF dynamics when assessed in this context, expanding the study to include diabetic patient plasma would enhance patient diversity, increasing the applicability of findings to a broader clinical context. Moreover, it would

provide insight into basal and constitutive VWF release which are not captured in the presented ECs models. This could help determine whether an overactivation of these pathways is masking or interfering with regulated secretion, potentially explaining the discrepancy between dhAECs findings in this model and the directionality of the relationship between diabetes and VWF reported in existing literature.

The use of physiologically relevant ECs under normoglycemic conditions reveals that diabetes exerts enduring effects on WPBs even in the absence of acute pathological stimuli. This supports the paradigm of metabolic memory. Overall, this model highlights the importance of incorporating sufficient sample sizes when using donor-derived ECs. While differences were evident between hAECs and dhAECs within individual donor pair, these became obscured when data were combined due to inter-donor variability. Nonetheless, the findings provide a strong foundation for further investigation. The use of commercial ECs offered a well-characterised baseline but future studies could build on this by developing larger donor-derived models. Although this would be challenging for aortic ECs due to tissue availability, alternative sources such as HUVECs could be used to establish a curated donor pool. Finaly, the reduction in WPBs observed in donor pars A and C suggest a diabetes-specific effect on VWF regulation, contrasting with trends typically reported in the literature and highlighting an important direction for future research.

Chapter 5: von Willebrand Factor Multimerization

5.1 Introduction

My previous data demonstrates that there is a significant reduction in WPBs numbers in ECs derived from diabetic patients. The biosynthesis of WPBs is critically dependent on the synthesis of VWF and its subsequent packaging at the Golgi apparatus (106). ECs with depleted VWF fail to generate WPBs, whereas non-ECs engineered to artificially express VWF will form pseudo-WPBs (99, 100). Therefore, to investigate whether diabetes disrupts VWF biosynthesis I utilised multimer gel analysis. In parallel, I explored the structure of the Golgi apparatus to identify any diabetes-associated adaptations that might impair VWF packaging and consequently affecting WPB synthesis.

Molecular weight is central for VWF function and determines how it is released from cells (94, 279). VWF is a multimeric protein produced in various weights which allows formation of different multimeric profiles (65, 70). Broadly, VWF can be divided into low, medium, high and ultra-high molecular weight (LMW, MMW, HMW, UHMW), each with specific functions relating to size (228). LMW VWF ranges from 500-2500 kDa, MMW 3000-5000kDa, HMW 5500-10,000 and UHMW >10,000 (228). WPBs are the site for storage of HMW to UHMW VWF, which is necessary for VWF string formation upon WPB exocytosis (regulated release pathway requiring stimulation) (228). In multimer gel analysis, a normal patient pooled plasma sample is used in place of a ladder due to the size of this protein. Exocytosed VWF strings are unravelled permitting platelet binding and initiation of haemostasis and wound healing, without VWF this process is compromised (70, 228).

An absence or reduction of VWF is termed von Willebrand disease (VWD), which is the most commonly inherited bleeding disorder, it highlights the central role of VWF in haemostasis and as a wound healing agent (88). VWD is classified into three types, type 1 is a partial deficiency of VWF resulting in a mild/moderate bleeding phenotype. Type 2 (which can be further subcategorised, into 2A, 2B, 2M and 2M) is characterised by structural abnormalities to VWF which often impair function (88). This often results in heavier and more frequent bleeding, than that observed with type 1resembling that of haemophilia as it is coupled with impaired interaction with factor VIII (88, 280). Type 3 VWD, the most severe classification, is marked by the near-total depletion of VWF within circulation (88). Together, these classifications highlight the critical importance of VWF in mediating haemostatic responses to vascular injury and wound healing.

Upon release from WPBs UHMW VWF remains anchored to EC surface and unravels into the lumen of blood vessels, uncovering bindings sites for circulating (LMW) VWF and platelets (281). The facilitates the formation of a platelet plug in response to a vascular injury and represents the first stage of primary haemostasis (21). HMW release is maintained by basal expression, whereby VWF is released from WPBs in the absence of stimulation, from the apical side of ECs into the bloodstream (92). In contrast, LMW circulates as a component of plasma under physiological conditions (typically in a range of 50 to 200 IU/dL), however may also be secreted by ECs, via constitutive pathways (92, 282). In this instance, VWF is released basolaterally into the subendothelial matrix without stimulation (92, 282).

A multimer index analysis will facilitate visualisation of the MW distribution of VWF multimers across different samples allowing identification of specific multimeric forms that may be absent in the disease model. The structure of VWF can be inferred from its MW, as high and ultra-high multimers are preferentially sorted and packaged into WPBs (109). Therefore, the absence of high-weight bands may explain the significant reduction of WPBs observed in the dhAECs as reported in in **chapter 3.** It is important to note that the only other source of HMW VWF is the alpha granules of platelets, where it is packaged during megakaryocyte development (283, 284). Release from these granules is typically stimulated by vascular injury and is tightly regulated within local microenvironments to support adhesion of platelets (283, 284).

Another key factor influencing the biosynthesis of WPBs is the structure of the Golgi apparatus. As discussed in **chapter 1**, VWF is packaged into WPBs at the Golgi, which determines WPB morphological characteristics and the number of quanta packaged into each (108). The Golgi architecture can be fundamentally reconfigured, for example statin treatment has been shown to transform its structure from long ribbon structures to small rounded structures (120). This structural adaptation directly influences WPB morphology with WPBs adopting forms that mirror the Golgi configuration (59). The McKeown lab group has further demonstrated plasticity within the Golgi, the structure differing significantly in ECs cultured under HSS and static environments resulting in WPBs with altered morphology (54).

As such, I sought to determine whether a diabetic environment impacted the WPB manufacturing process, beginning with assessment of the structure of the Golgi structure. This could help to explain the reduction in WPB numbers observed in diabetic ECs outlined in **chapter 3**. Conversely, if no significant structural changes are detected in the

Golgi architecture, this would suggest that the disruption originates elsewhere in the biosynthetic pathway.

WPBs are a reflection of their environment. They exhibit heterogeneity and specialisation across different vascular beds (98). Venous and aortic vessels fulfil vastly different roles within the circulatory system and are structurally adapted to these functions. Aortic ECs are exposed to high pressure, oxygenated blood, whereas venous ECs return deoxygenated blood under significantly lower pressure (33, 50, 285). Through experiments conducted in **chapter 3** it was revealed that hAECs produced shorter VWF string structures compared to HUVECs, supporting the concept that WPB morphology reflects the surrounding environmental conditions.

Having established that hAECs express fewer WPBs than HUVECS in **chapters 2 and 3,** I next investigated whether VWF expression and structure was altered in these cells. To do so, I conducted a multimeric analysis of each cell line seen in **chapter 3** to determine which MWs of VWF were present and subsequently whether any were absent. This analysis provides insight into potential functional impairments, as VWF multimer size is closely linked to haemostatic activity.

Multimer gels were employed to achieve this, providing a comprehensive quantification of VWF multimer distribution across each sample. Total protein was quantified prior to gel loading in multimer analysis and equal protein concentrations were applied to ensure that the intensity of bands could be used as a measure for the abundance of VWF via densitometry analysis. Unlike conventional western blotting, which cannot be used to reliably resolve UHMW VWF due to its size and aggregation tendencies, multimer gel analysis circumvents these limitations. The unique composition of the multimer gel allows enhanced separation and clearer visualisation of individual VWF bands, making it a more suitable technique for assessing VWF structure.

To investigate how diabetes may be impacting VWF synthesis and storage I chose two elements to focus on, multimeric composition of VWF in ECs and morphology of Golgi architecture. Both factors play a central role in the biosynthesis of WPBs serving as key drivers in shaping the WPB profile.

Firstly, I quantified the multimeric composition of VWF to establish whether the diabetic ECs within the model in **chapter 3** exhibited a reduced universal presence of VWF, potentially explaining the reduction in WPB numbers observed. The multimeric ‘fingerprint’ of VWF was identified for each EC line, revealing the range of MWs present

(revealed by the number of multimers) and provides insight into the functional capacity of VWF within these ECs. This analysis was extended to encompass a cohort of 22 pairs of diabetic and control plasma samples, creating a VWF multimer profile for comparison with the cell-based model. As previously established, VWF is governed by MW, with distinct release pathways and subcellular destinations depending on physiological context. A deeper understanding of the distribution of VWF multimers across these samples may offer mechanistic insight into the diversity and variation observed in diabetic samples. Which may help localise the origin of the VWF dysregulation.

Secondly, I visualised and quantified the Golgi architecture of each cell line used in the physiological model pairings. Given that Golgi plasticity in response to environmental cues can influence WPB morphology and biosynthesis in ECs, I sought to replicate the assessment conducted by Money et al. to determine whether similar structural adaptions were present in these diabetic ECs (59, 108).

Hypothesis: Diabetes alters the multimeric profile of VWF in endothelial cells and affects circulating VWF levels in plasma.

Aim 1: To determine how the multimeric profile and abundance of VWF differs between the paired hAECs and dhAECs (seen in **chapter 3**).

Aim 2: To assess paired plasma samples from diabetic and control patients and compare VWF profiles and patient population demographics.

5.2 Results: VWF Multimer profiles vary between different vascular beds

Previous research into the vascular bed specific generation of VWF has yielded inconclusive results, necessitating further investigation, here I have assessed how the vascular bed of origin influences the synthesised VWF. As a secondary consideration, I accounted for cell passage number. All experiments were conducted using non-immortalised commercial ECs between passages 1-5 as their phenotype is known to drift with increased passaging (286).

To assess the impact of vascular bed and passage on VWF structure, I utilised HUVECs at passages 1-3, beyond which our lab has observed VWF structure to be altered. Profiles of VWF were generated using multimer gels. Equivalent sampling and analysis were performed using hAECs to enable comparison across vascular beds. Multimeric banding patterns were assessed, bands 1-5 are classified as LMW VWF any bands 5< fall into MMW, HMW or UHMW VWF (287).

The VWF multimer banding profile is shown in **figure 5.1** and is represented as a multimeric profile in **figure 5.1 b**, the proportion of HMW multimers to LMW is recorded as the multimeric index **figure 5.1 c**. The reference plasma denotes all the possible VWF multimer banding patterns as expected, plasma has VWF from multiple excretion pathways and vascular beds, thus, it is consistent to see the most diverse fingerprint as it shows the totality of physiological VWF expression compared to limited, cell line models. Moreover, reference plasma utilised is a commercially available option derived from multiple different donors to create a pooled sample (normal pooled plasma (NPP)), increasing the likely diversity observed in the multimer profile. This is used in place of a ladder as seen in a traditional western blot.

The presence of HMW VWF is more pronounced in HUVECs harvested at passage 1 (P1) where 7 bands can be confidently identified compared to those at passage 3 (P3) where 5 bands are discernible. Comparatively fewer bands are present in the profile of the hAECs irrespective of passage, averaging 4-5 bands per sample compared to 5-7 bands in the HUVECs. Despite exhibiting fewer VWF bands overall compared to HUVECs, hAECs also demonstrated a passage-dependant effect. Band expression is lowest at P1, increases at _2 and declines again at P3. Specifically, P1 hAECs display 4 identifiable bands, P2 show 5 and P3 return to 4. Notably no HMW VWF is detectable in P1 samples, whereas medium to high molecular weight VWF is present at P2.

HUVEC harvested a P1display the greatest diversity of VWF multimers in the banding profile (**figure 5.1 a**) with 7 identifiable bands, there are both LMW and HMW multimers present. In terms of functionality, it is suggestive that there is a greater capacity for platelet aggregation in this environment. . The trend evident in the hAEC is a distinct reduction in banding past the 5th band (as read from the right-hand side) indicating that there are fewer HMW multimers seen in these samples which is reflected in the multimer index in **figure 5.1 b**. The index value for P1 HUVECs was almost double that of the P1 hAEC at 0.210±0.084 compared to 0.114±0.006. In later passages the multimer index of the hAECs remains lower than that observed in the HUVECs, at P2 an index of 0.127±0.042 was observed and at P3 0.113±0.048.

Samples in these gels were run to gather pilot data and as such, the concentration of protein was not calculated prior to preparing samples. Each sample was run in an equal proportion (same fold dilution) to one another. While this means intensity of banding cannot be reliably quantified here, it does not mean it should be ignored. P1 HUVECs has the darkest intensity across all bands, indicating the highest presence of VWF. What is common across all cell samples is the lowest bands and subsequently the lowest weight VWF is the most intense. This would suggest that proportionately there is a higher concentration of less multimerised lower weight VWF in these samples. This implies that these ECs don't contain the expected HMW and UHMW VWF associated to WPBs.

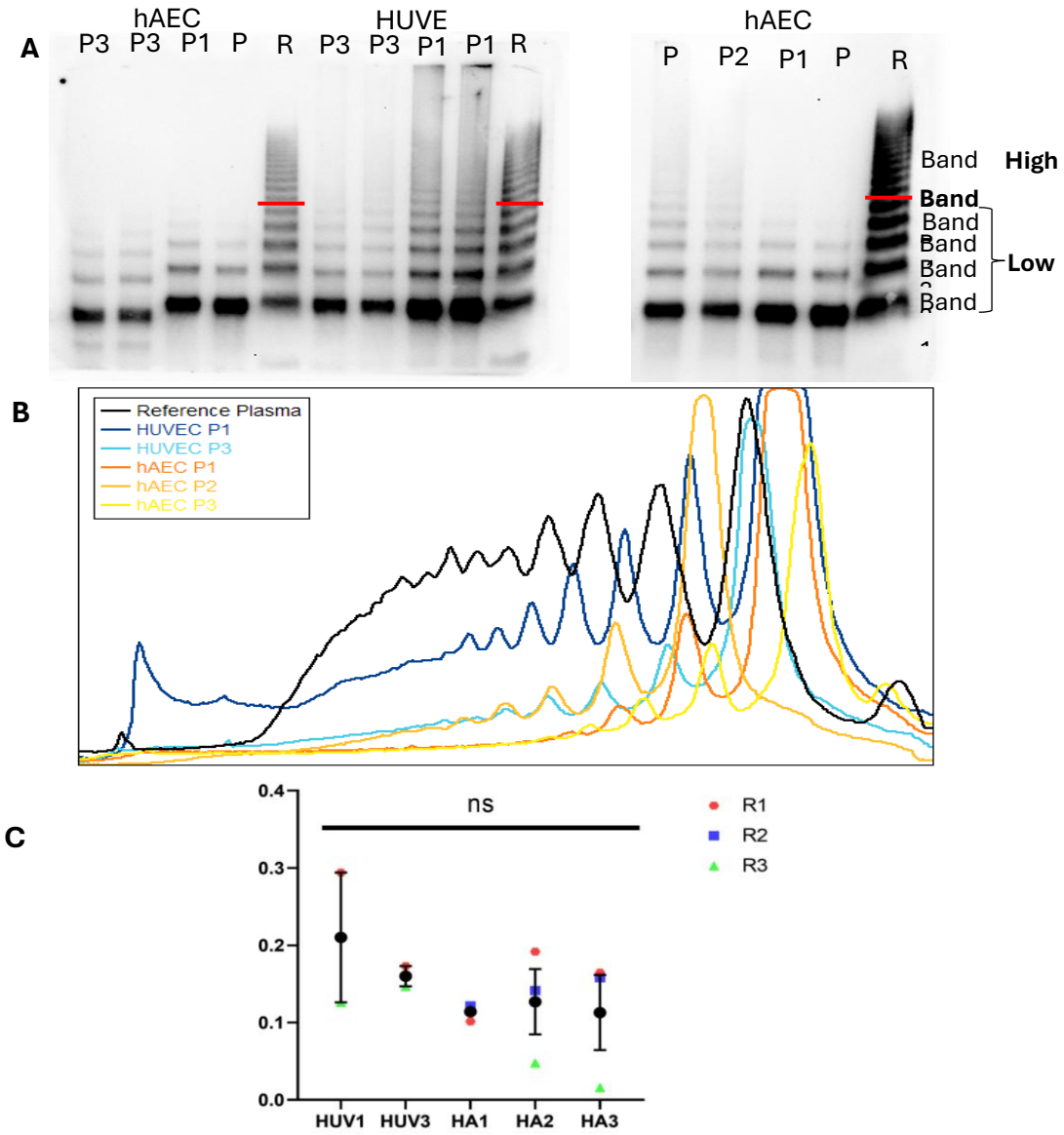

Figure 5.1. Multimer profiles are different across endothelial cell beds and are affected by the number of times cells have been passaged.

- **A.** Multimer gels showing the VWF multimers present in HUVECs and hAECs at the stated passage numbers (P1, P2, P3). The bands are categorised into HMW/MMW to LMW as per the red line as compared to reference plasma (RP; Normal Pool Plasma). The number of bands varies according to both cell type and passage number.
- **B.** Visualised VWF banding, seen as a profile of the intensity peaks. The measurements are depicted from left to right showing HMW to LMW multimers. HUVECs demonstrate a larger range of MW VWF than hAEC, lower passages have a similar characteristic.
- **C.** Multimer ratio index ±SEM showing the proportion of high molecular weight band to low/medium bands normalised to the reference plasma. HUVECs show a greater proportion of HMW to LMW, lower passages show a higher index score. hAECs reduced compared to HUVECs, passage also has an effect, P1 is lower than P2 but then the index declines after this. n/N= 3/3

NS = non-significant

5.3 Diabetes affects the multimeric profile of VWF released from endothelial cells

Since the hAECs have demonstrated inter-passage variability, the established EC pairs were maintained and assessed in isolation from one another as done previously in **chapter 4**. Pairs A, B and C were each assessed to create a VWF multimer profile. Control and diabetic plasma samples were run in a specialised gel alongside the NPP, allowing the various molecular weight multimers to separate out as seen above (**section 5.2**). An example of the gel can be seen in **figure 5.2 a** this was then visualised in a profile graph (**figure 5.2 b**) which allows each sample to be overlayed, highlighting any similarities or variations between them, moreover it allows counting of the bands and further quantification by calculation of the index of HMW VWF to medium/low MW multimers (**figure 5.2 d**). The final quantification conducted was an adaptation to the original multimer gel method that permits analysis more akin to western blots. Protein was quantified prior to samples being loaded into the gel to ensure equal loading by concentration. As samples were uniformly imaged this allowed the intensity of each band to be read and quantified, each sample was normalised to the NPP reference and provides an interpreted amount of protein in each condition (**figure 5.2 c**). This analysis was conducted for each EC pair to generate the most comprehensive possible profile of VWF multimers, enabling meaningful comparison between groups. It also allows for comparison to WPB data compiled in **chapter 4**.

5.3.1 Pair A

The multimeric profile of the reference NPP is an example of a 'complete spectrum' of VWF. The profiles for both hAECs and dhAEC differ to this profile. Cell lysates from those both hAECs and dhAECs do not display the distinct HMW bands (any present above band 5). There are a greater overall number of bands in the hAEC lysates compared to dhAEC lysate, meaning higher MW VWF can be observed **figures 5.2 a**. hAECs showed a greater range of multimers than the dhAEC counterpart within pair A, (i.e. there are a greater number of bands (5 compared to 4)) observed in the VWF fingerprint in **figure 5.2 b**.

As protein samples were quantified and proportionally loaded, intensity can be assessed. The hAECs have a higher intensity of banding, indicating a greater quantity of VWF in these cells than in the dhAEC lysate from Pair A (0.304±0.064 vs 0.173±0.011) this is evident in **figure 5.2 c**. Whist there is a visible difference, it is not significant (p=0.361). Compared to hAECs the dhAECs showed reduced variability across repeats, indicating a more

consistent pattern in their expression, or lack, of VWF multimers. There was no significant difference seen in the multimer gel ratio between the hAECs and dhAEC (0.35±0.035, 0.32±0.057, p=0.091) (**figure 5.2 d**).

As the reference NPP bands cluster around the HMW multimer region, individual banding becomes increasingly difficult to distinguish. In this gel, there are approximately 14 bands that are identifiable for comparison. This pattern suggests that HMW VWF bands are 'missing' from the hAEC lysates, with a more pronounced reduction in the dhAEC multimer profile. As established in **chapter 4** there is a variation to be expected between the VWF profile of ECs from different vascular beds. Each pair was conducted with the control and diabetic cells at the sample passage (cultures maintained in parallel), so we may account for variation between repeats but not between conditions.

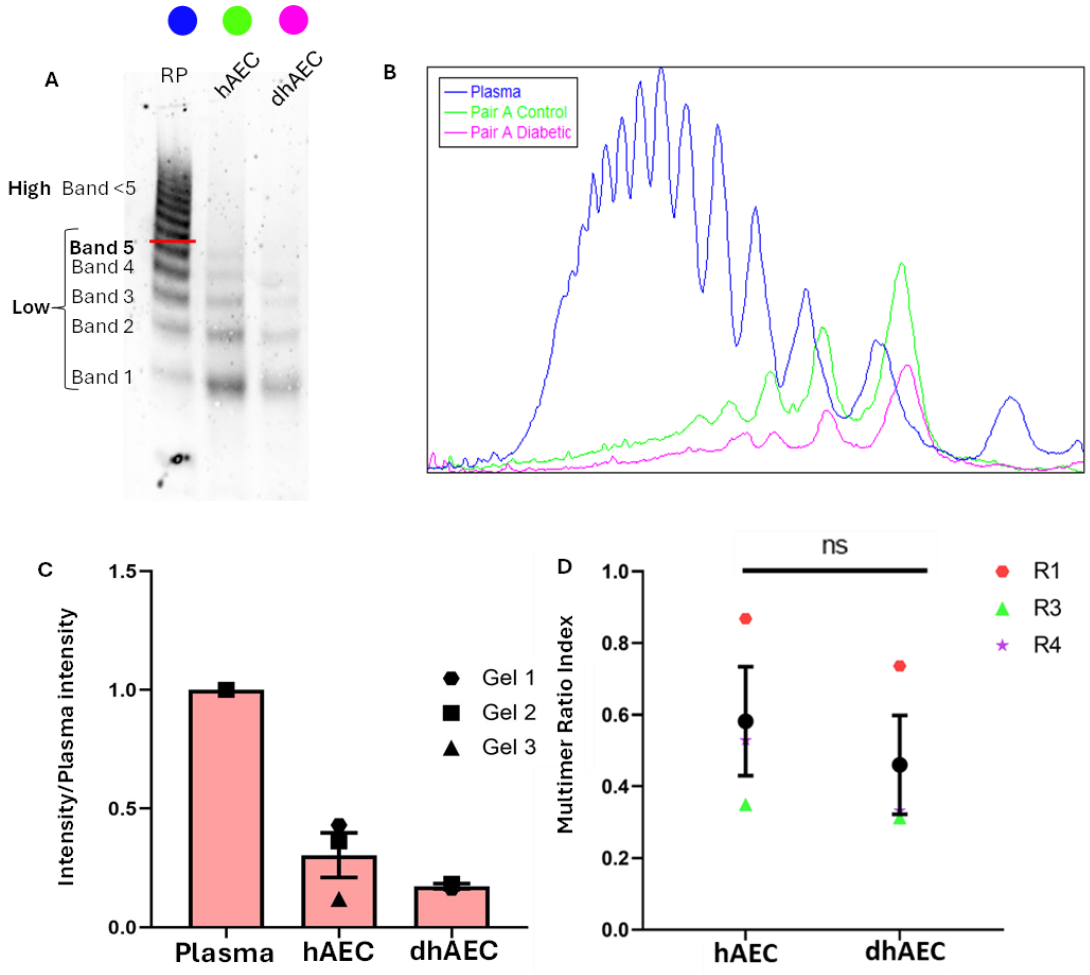

Figure 5.2 Multimer gel profiles for Pair A control hAEC shows a greater diversity of VWF bands than the dhAEC counterpart.

A. Multimer gel of reference plasma (RP), hAEC and dhAEC lysate. Neither the control nor diabetic ECs showed HMW bands (observable in the reference plasma). Colours refer to conditions in figure B (blue: reference plasma, green: hAEC control, pink: dhAEC diabetic)
B. Quantified multimer profile of multimer gel. There is a higher quantity of VWF in the control ECs than the diabetic. There is approximately one band at a higher MW seen in the hAEC not seen in the dhAEC (band 5).
C. Samples were run at a uniform concentration to allow intensity to be measured and quantified. Cell lysates were normalised to the reference plasma. hAECs had a higher intensity and therefore quantity of VWF than dhAECs. *t-test* was not significant.
D. Multimer Index of high to medium/low MW VWF multimers. hAEC had a higher proportion of HMW bands to low compared to dhAEC.

NS = non-significant

5.3.2 Pair B

Pair B present with a similar VWF multimeric banding pattern in both hAECs and dhAECs. In hAECs, there are 6 bands that are identifiable and the dhAEC shows 9 bands. As noted, band 5 marks the threshold between LMW and HMW VWF multimers. In pair B, both dhAECs and hAECs exhibit bands beyond this point, indicating the presence of HMW VWF in both cell types. The profile analysis (**figure 5.3 a**) demonstrates that there are VWF bands in the HMW category, the heaviest fail to differentiate from one another (above red line) indicating more HMW bands could be resolved, this is not observed in hAECs.

The dhAECs exhibits greater intensity than the hAECs visually in the multimer gel displaying the banding profile **figure 5.3 b**. The intensity of VWF is reduced in the hAECs compared to dhAECs (0.357±0.225, 0.551±0.254). While this apparent difference is visually discernible in the figure, when quantified and analysed there was no significant difference detected (p=0.5971) (**figure 5.3 c**)**.**

The multimer index is reflective of these differences, the diabetic had the higher of the pair with 0.582±0.152, as expected the control was lower with 0.460±0.138 (**figure 5.3 d**). This translates to the dhAECs having a higher proportion of HMW VWF multimers to LMW, with the converse being true for the control , this difference was not significant (p=*0*.5843).

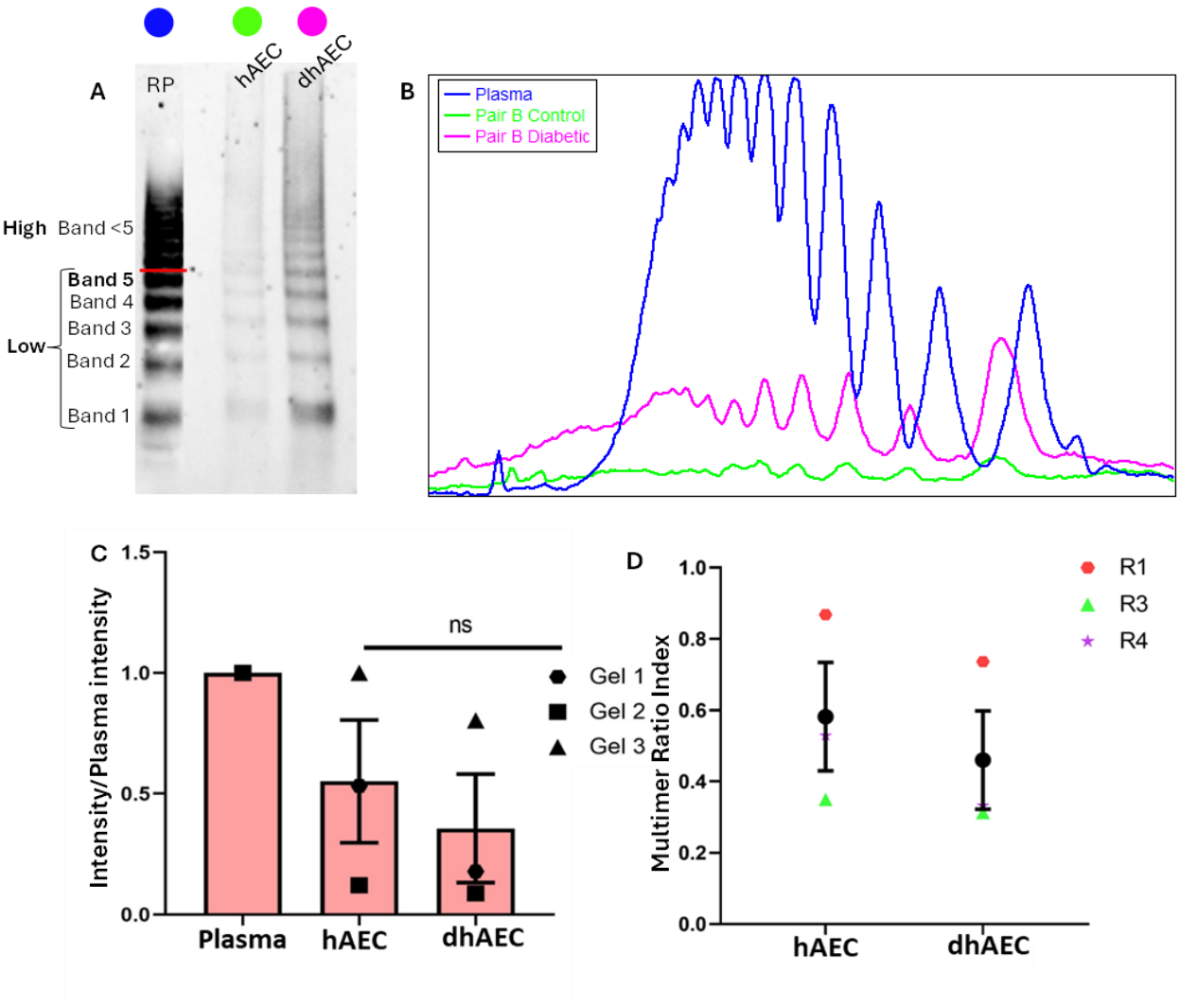

Figure 5.3. Multimer gel profiles for Pair B control hAEC shows a greater diversity of VWF bands than the dhAEC counterpart.

A. Multimer gel of reference plasma (RP), hAEC and dhAEC lysate. Neither hAECs nor dhAECs showed HMW bands (observable in the reference plasma).

B. Quantified multimer profile of multimer gel. There is a higher quantity of VWF in the control ECs than the diabetic. There were approximately two bands at a higher MW seen in the hAEC not seen in the dhAEC (bands 6 and 7).

C. Samples were run at a uniform concentration to allow intensity to be measured and quantified. Cell lysates were normalised to the reference plasma. hAECs had a higher intensity and therefore quantity of VWF than dhAECs.

D. Multimer Index of high to medium/low MW VWF multimers. hAEC had a higher proportion of HMW bands to low compared to dhAEC.

NS = non-significant

5.3.3 Pair C

In both hAECs and dhAECs of this pair, there are very few discernible multimers seen in each respective VWF profile **figure 5.4 a**. The control has 4 identifiable bands, and the diabetic has 3 bands in the profile graph **figure 5.4 b**. Neither reaches the 5-band threshold to move out of the LMW category. As the reference plasma has run and created a full profile (12 bands) we can be confident that this was all that was present within these cells.

Despite this similarity in profile, the intensity and subsequent quantity of VWF differs. There is a greater than 2-fold increase the intensity of VWF in the hAECs (0.542±0.152) compared to the dhAECs (0.129±0.078). Despite this, there was not a significant difference identified between conditions (p=0.1369) (**figure 5.4 c**). The multimer index of LMW to MMW/HMW multimers have minimal diversity between the pair (control 0.345±0.168, diabetic 0.311±0.138, p=0.885) (**figure 5.4 d**).

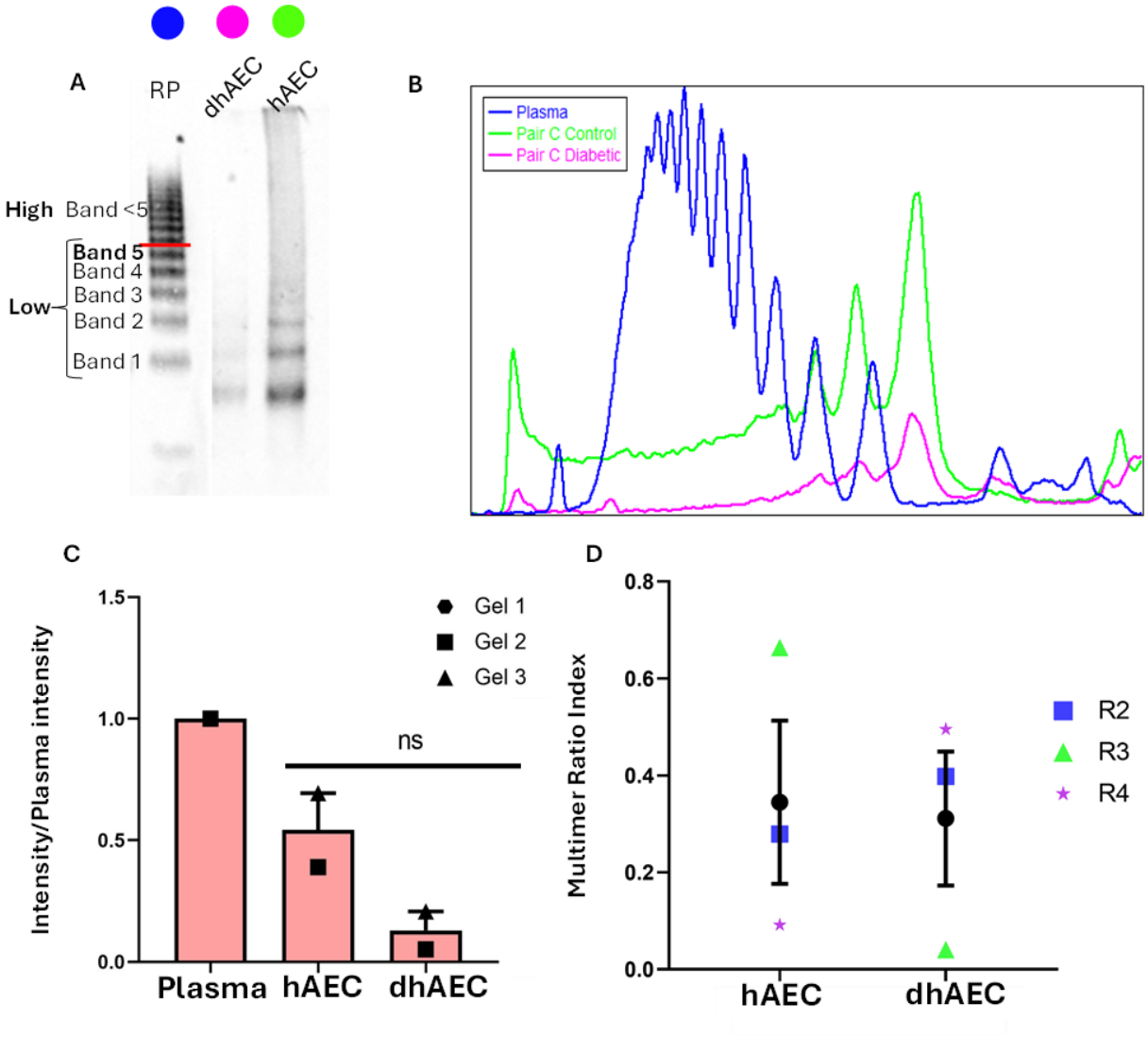

Figure 5.4. Multimer gel profiles for Pair C control hAEC shows a greater diversity of VWF bands than the dhAEC counterpart.

A. Multimer gel of reference plasma, hAEC and dhAEC lysate. Neither the control nor diabetic ECs showed HMW bands (observable in the reference plasma).
B. Quantified multimer profile of multimer gel. There is a higher quantity of VWF in the control ECs than the diabetic.
C. Samples were run at a uniform concentration to allow intensity to be measured and quantified. Cell lysates were normalised to the reference plasma. hAECs had a higher intensity and therefore quantity of VWF than dhAECs.
D. Multimer Index of high to medium/low MW VWF multimers. hAEC had a higher proportion of HMW bands to low compared to dhAEC.

NS = non-significant

5.3.4 Diabetes expression is heterogeneous across pairs

Analysis of dhAECs and hAECs was done maintaining discrete pairings given the variation observed in **chapter 2**. Like previous findings seen in **chapter 4**, there was inter-donor variation seen between the hAEC (controls) of each pair. When considering EC pairs against each other, pair C present with the lowest number of VWF bands (4 bands), followed by pair A (5 bands) and then pair B with the greatest number (9 bands). This is likely a result of patient variability as each control is from a single donor origin. Interestingly, despite this variation in the VWF multimers observed, the intensity of the VWF bands and the multimer index ratio follows the same pattern across all three pairs. The hAEC of each pair display a higher intensity of VWF than its dhAEC equivalent.

The multimeric banding profile for dhAECs and hAECs appear proportionally alike, though each pair exhibits a degree of heterogeneity. In pairs A and C, dhAECs exhibited one fewer detectable band than the hAEC counterpart, while pair B showed a greater difference, with three bands absent in the dhAEC profile.

The reference plasma in all three of the gels (**figure 5.2, figure 5.3** and **figure 5.4**) have a faint band appearing below band 1 that could be misinterpreted as an imaging artefact. This is a satellite dimer band of VWF, which represents cleavage of VWF by ADAMTS13. This band is not present in any of the six analysed cell lysates.

Although each pair exhibited variation between the dhAECs and hAECs, none of these differences reached statistical significance. To preserve contextual integrity sample pairs were treated as discrete analytical units. Given the observed heterogeneity, likely stemming from patient variability, data aggregation would not guarantee significance, as seen in **chapter 4**. Therefore, diabetic plasma samples were employed to assess the impact of diabetes on the VWF multimeric profile to enhance statistical power and gain further insight on the interaction.

5.4 Diabetic patient plasma

Across this investigation, variation has been demonstrated in the VWF and WPBs between the hAECs and dhAECs. In some areas, significant differences have emerged however the cohort size has been a limitation the overall power of the study. The underlying trend that has been identified points to be a reduction in VWF in dhAEC populations which is the inverse of the trend to that seen in the literature which suggests an increase in VWF in diabetic cohorts compared to control (192, 193, 195, 202, 210). To mitigate the effects of reduced statistical power, I next developed an experiment to investigate the impact of diabetes by assessing patient plasma samples. Unlike isolated ECs, plasma samples consolidate contributions of VWF from multiple vascular beds and expression pathways, thereby offering an extracellular perspective on VWF multimeric composition. Plasma samples were utilised from a pre-existing study of diabetes and consequently there was patient data available. I used frozen plasma samples from T2DM patients and control patients (with no formal diagnosis of diabetes). These were compared to a normal pooled plasma (NPP) running control. All samples were freeze thawed (no more than two cycles), with thawing performed at 37°C to maintain sample integrity.

This approach offered greater control over sample size compared to experiments using ECs. To achieve statistical significance a power calculation was necessary. As this was a new study without preliminary data, I relied on o previously published findings to guide sampling. Based on these data, a sample size of 22 patients per condition was selected as it permitted detection of a 59% difference in means, allowing for a 95% confidence interval and statistically different results (235). A cohort was constructed comprising of 44 samples was made up of 22 control and 22 diabetics from pre-existing available samples of both control and diabetic patients and were matched on sex and age to the greatest feasible extent (see **table 5.1** below). Approximate demographic equivalence following the methodology applied to the cell pairings seen in **chapter 2** This was a post-hoc matching process and not part of the original experimental design when the samples were first collected. Smokers and those with autoimmune conditions were excluded where possible but as samples were secondary to my study this was not entirely possible while maintaining a sufficient n number. There were limited numbers of female samples, I chose this diversity measure as a priority over excluding females that were flagged in the exclusion criteria.

The paired plasma samples were run in multimer gels allowing VWF bands to separate out and create a VWF banding profile for each an example of each can be seen in **figure 5.5 a**.

From this a multimeric fingerprint could be elucidated (**figure 5.5 b**). This visualises a representative sample of diabetic and control plasma samples. In this experiment, equal proportions of plasma were loaded per lane to ensure consistency across samples. However, total protein was not quantified prior to loading, as a result band intensity cannot be interpreted as a quantitative measure of VWF abundance. What is evident is that, regardless of diabetes diagnosis, all samples express LMW, MMW and HMW VWF in within their profiles.

While it was not possible at this stage to conduct a fully comparative analysis of plasma with total protein quantified there is a visual increase in intensity of banding in the diabetic compared to the control samples (**figure 5.5 a**), Suggestive of potentially higher VWF concentrations. When assessing the multimer index, the diabetic plasma samples show a marginal increase (1.372±0.066) than the control (1.285±0.048) seen in **figure 5.5c**, indicative that there is a slightly increased proportion of HMW multimers to LMW multimers in the diabetic patient samples than in the control.

An important consideration is that individuals with controlled diabetes may present with lower HbA1C values. Which could influence the perceived relationship with the multimer index value. Similarly, diabetes duration should be interpreted alongside symptom management, as effective control may alter the tissue microenvironment in ways that affect the observed interaction at this stage.

Table 5.1. Patient demographics of control and diabetic plasma samples including factors used as exclusion criteria

	Control	Diabetic
Age (Years)	48±3.47	60±1.76
Female	41%	41%
Male	59%	59%
DM duration (Months)	0±0	128±17.42
Smoking	3	6
Autoimmune	2	2
HbA1C (mmol/mol)	37.42±0.85	70.14±4.96

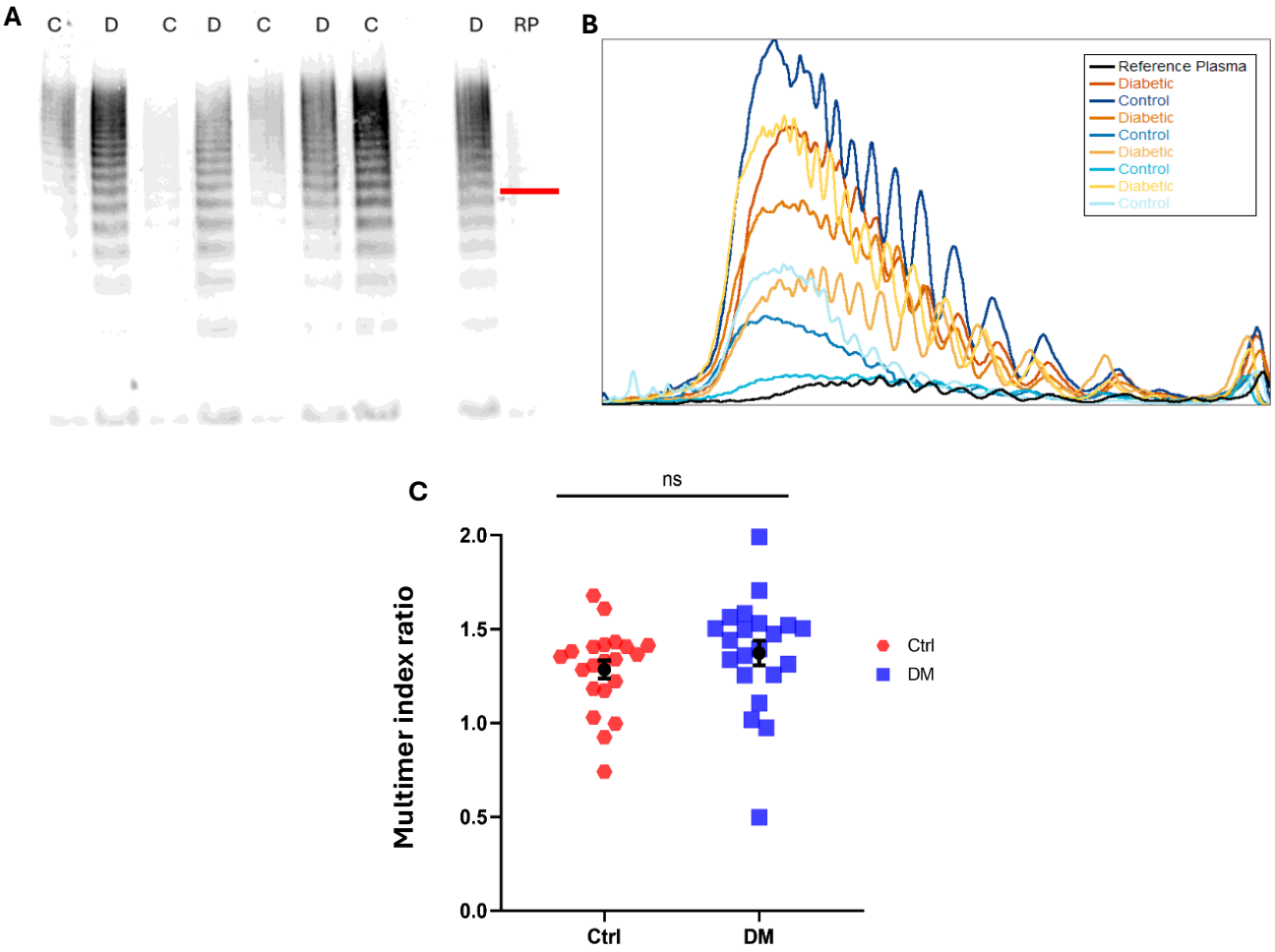

N=21

Figure 5.5. Multimer gel profile for control plasma and diabetic plasma shows a greater diversity of VWF bands than the cell lysates.

A. Multimer gel of reference plasma (RP), control (C) and diabetic (D) plasma samples (sample of four pairs) showing the VWF banding profile for each. Showing the banding structure of 4 pairs of plasma samples (two diabetic two control).
B. Quantified of multimer gel to create multimer profile of 4 pairs of plasma samples (two diabetic two control). All contain the same proportion of plasma.
C. Multimer Index (±SEM) of high to medium/low MW VWF multimers. No significance was detected using t-test.

NS= non-significant

5.5 Golgi Fragmentation

The Golgi is the site at which VWF is packaged into WPBs, it has been shown by Money et al and Ferraro et al that the microenvironment of cells can modulate the morphology of the Golgi, which in turn affects the structure of the WPBs synthesised (59, 108). The presence of HSS disrupted the ribbon like structure of the Golgi, creating increased fragmentation with a greater number of smaller fragments, resulting in significantly smaller WPBs being produce

As there were significant differences identified between the WPB populations in diabetic and control cells at both intra-pair and inter-pair levels, I assessed the effects of diabetes on the Golgi architecture. This provides the contextual background for WPB formation.

Both pairs A and C exhibited significantly fewer WPBs than their respective control counterparts (see **chapter 4**). One line of investigation pursued was whether diabetes alters the Golgi architecture, specifically examining if reduced fragmentation is present and potentially contributing to diminished availability of the biosynthetic machinery required for WPB production. I assessed the total number of Golgi fragments, the average number of fragments per cell and the average area of the Golgi fragments for each of the pairs.

5.5.1 Pair A

There were no significant differences in the Golgi morphology across any condition with pair A. This is not to say there was no variation between conditions that impacted Golgi fragmentation. Irrespective of diabetes diagnosis, the number of Golgi fragments was impacted by SS exposure. HSS-exposed hAECs displayed a greater number of smaller fragments (11.0±0.8) than the static culture conditions (10.5±0.8). The mean number of fragments for the dhAEC in the static was 8.5±0.6 and was 7.4±1.8 in the HSS condition. Moreover, in both static and HSS environments the dhAECs show a lower number of Golgi fragments per cell compared to the hAECs. However given the variability within the data sets, there was no significant difference observed.

The average area of Golgi fragments remained consistent across both cell types and culture environments, with only minor variation in the SEM. However, individual data points showed a wide range, indicating variety within groups. No significant differences were observed between HSS and static conditions in either hAEC or dhAEC samples, nor between hAEC and dhAEC overall. Under static conditions, the area of the Golgi fragments was similar in both the hAEC (3.15±2.37μm^2) and dhAEC environments (2.75±2.81μm^2) the same observation can be seen in ECs exposed to HSS with hAECs (3.40±3.02 μm^2) and with dhAECs (3.92±3.13 μm^2). In both the static and HSS conditions, the dhAECs Golgi area is on average lower than that of the hAEC, this is more pronounced in the static condition, which is already representative of a pathological environment. HSS appears to cause an increase in fragment area in both hAEC and dhAEC environments.

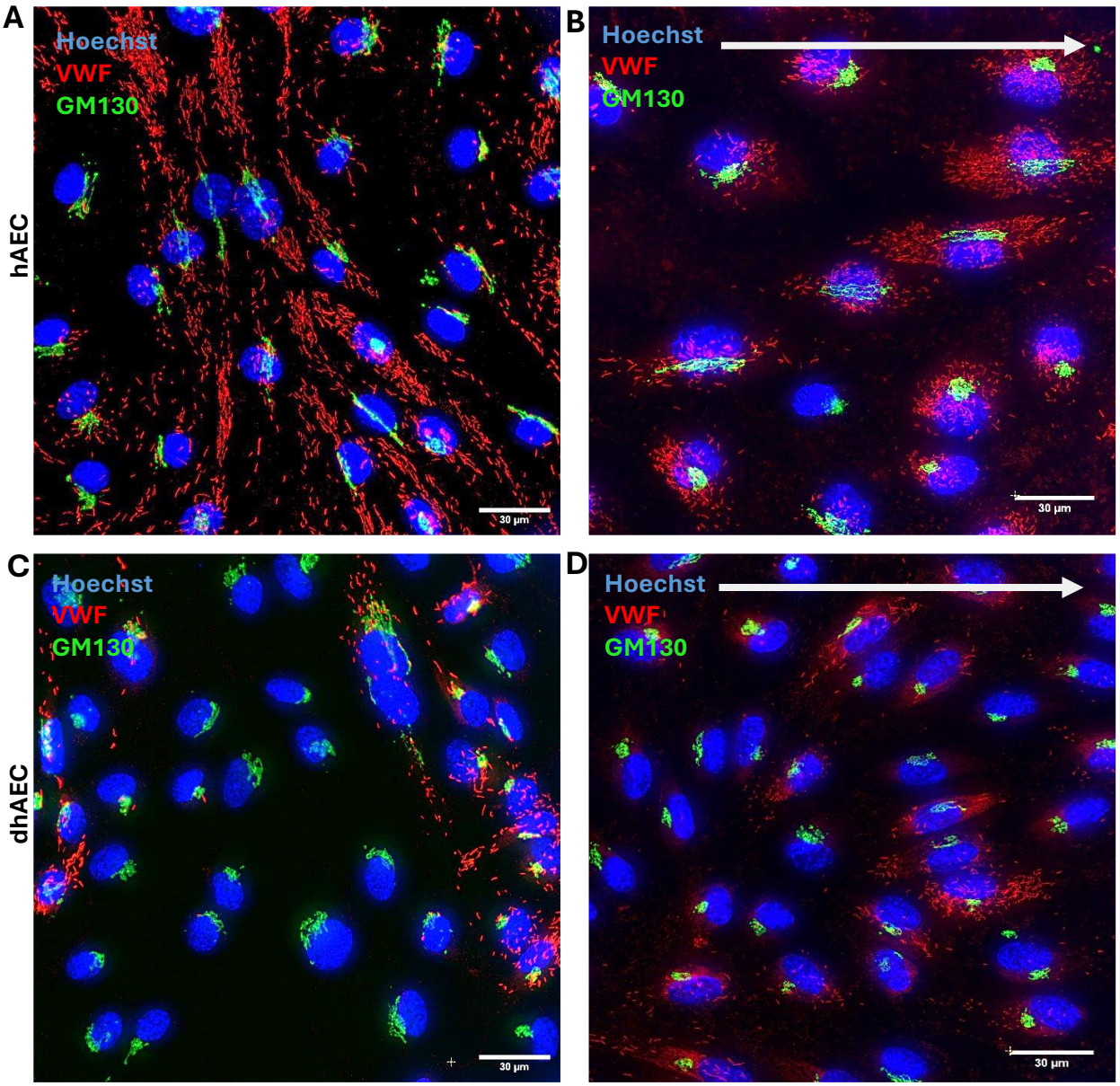

Figure 5.6. Representative images (x60 objective) of pair A WPBs (red) and Golgi (green) in hAEC and dhAEC (nuclei blue) both static and HSS culture conditions.

- **A.** hAEC after 48hrs in a static culture environment. Endothelial cell (Hoechst blue) with their expressed WPBs (VWF red) and Golgi (GM130 green).
- **B.** hAEC after 48hrs in a HSS environment. Endothelial cells (Hoechst blue) with their expressed WPBs (VWF red) and Golgi (GM130 green).
- **C.** dhAEC after 48hrs in a static culture. Endothelial cells (Hoechst blue) with their expressed WPBs (VWF red) and Golgi (GM130 green).
- **D.** dhAEC after 48hrs in a HSS environment. Endothelial cells (Hoechst blue) with their expressed WPBs (VWF red) and Golgi (GM130 green).

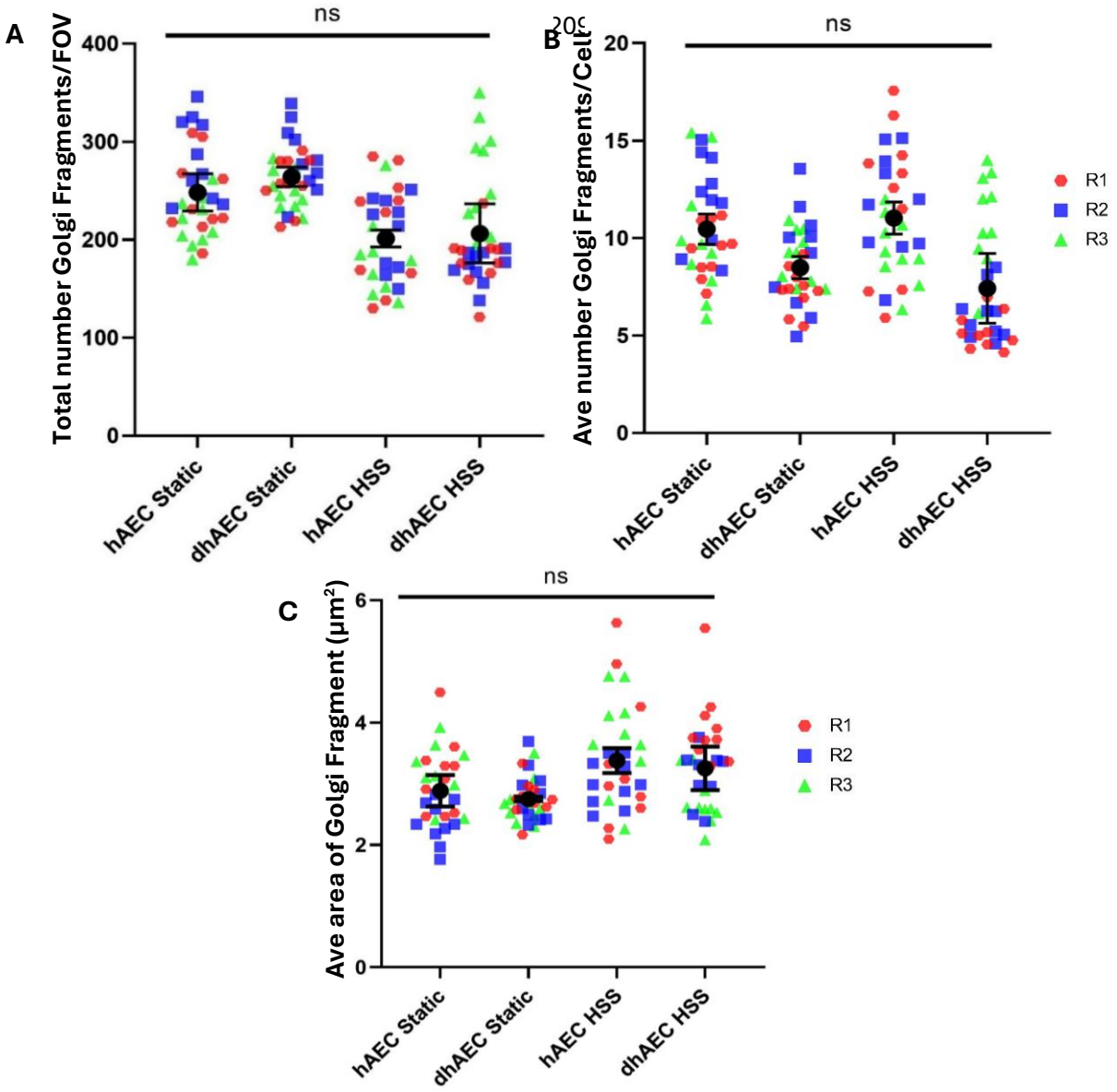

Figure 5.7. Diagnosis of diabetes and exposure to shear stress does not affect the Golgi in the ECs used in Pair A.

A. Mean of the total number of Golgi fragments observed per FOV ±SEM n/N=3/30. Each data point represents a mean of all WPBs counted in an image. Colours/shapes represent technical repeats (R1 red hexagon, R2 blue square, R3 green triangle).

B. Mean number of Golgi fragments observed per cell ±SEM n/N=3/30. Each data point represents a mean of all WPBs counted in an image. Colours/shapes represent technical repeats (R1 red hexagon, R2 blue square, R3 green triangle).

C. Mean area of Golgi fragments per FOV ±SEM n/N=3/30. Each data point represents a mean of all WPBs counted in an image. Colours/shapes represent technical repeats (R1 red hexagon, R2 blue square, R3 green triangle).

NS = non-significant

5.5.2 Pair B

When assessing the number of Golgi fragments per cell, diabetes diagnosis does significantly alter results, under the increased pathological environment of static cell culture, hAECs displayed significantly fewer fragments (6.12±0.91) than the diabetic counterpart (10.87±0.81). This difference persists under HSS with the average fragments in hAEC (3.40±0.19) and dhAEC (5.62±0.28), however the atheroprotective nature of this environment salvages some of the pathological effects and reduces the difference, preventing a significant difference. Notably, there is no significant difference in the average fragments per cell between the static and HSS hAECs, both are lower than the dhAEC under equivalent environments.

This phenotype of increased fragmentation is expected for the Golgi in ECs under HSS. This effect is elevated in dhAECs, demonstrating an even greater fragment count than would be predicted under the static conditions resulting in a marked reduction in fragmentation and significantly fewer counted in the HSS condition.

Irrespective of diabetes, there was a detectable flow response in the mean area of the Golgi fragments. Area of the Golgi was significantly higher in the HSS condition for both the hAECs (4.52±0.32 μm^2) and the dhAECs (4.27±0.06 μm^2) that the static counterparts (2.91±0.32 μm^2 and 2.12±0.14 μm^2 respectively), showing that cells responded to flow. No significant difference arose related to diabetes diagnosis; however, a more pronounced trend can be observed within the static environment wherein dhAECs exhibit Golgi fragments that are smaller compared to their hAEC counterparts.

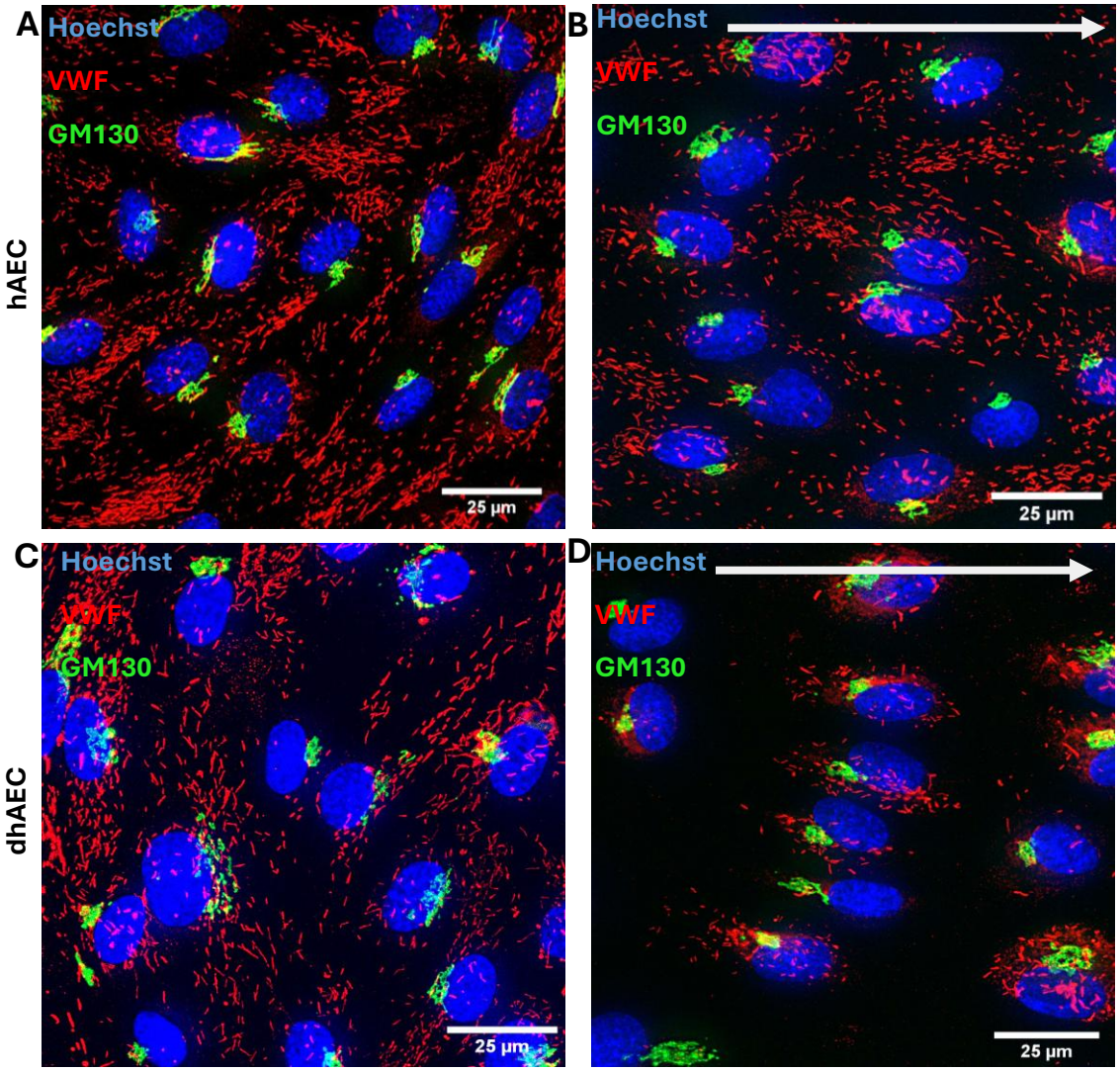

Figure 5.8. Representative images (x60 objective) of Pair B hAEC and dhAEC both static and HSS culture conditions

Endothelial cells (Hoechst blue) with their expressed WPBs (VWF red) and Golgi (GM100 green).

A. hAEC under static culture Endothelial cells (Hoechst blue) with their expressed WPBs (VWF red) and Golgi (GM100 green).
B. hAEC under HSS Endothelial cells (Hoechst blue) with their expressed WPBs (VWF red) and Golgi (GM100 green).
C. dhAEC under static culture Endothelial cells (Hoechst blue) with their expressed WPBs (VWF red) and Golgi (GM100 green).
D. dhAEC under HSS Endothelial cells (Hoechst blue) with their expressed WPBs (VWF red) and Golgi (GM100 green).

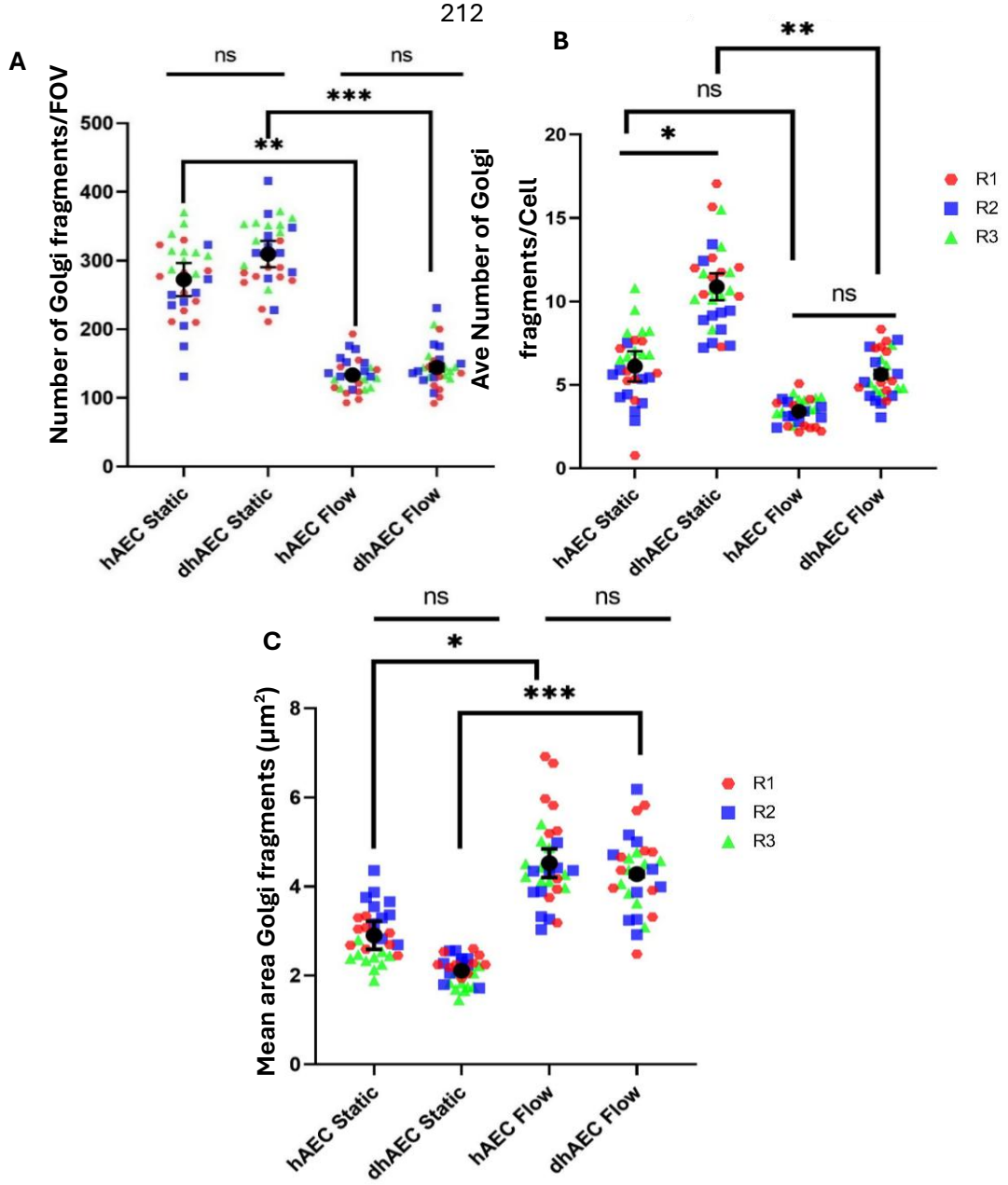

Figure 5.9. Diagnosis of diabetes affects the average number of Golgi fragments in Pair B ECs and shear stress impacts the area of observed fragments.

A. Mean of the total number of Golgi fragments observed per FOV ±SEM n/N=3/30. Each data point represents a mean of all WPBs counted in an image. Colours/shapes represent technical repeats (R1 red hexagon, R2 blue square, R3 green triangle).

B. Mean number of Golgi fragments observed per cell ±SEM n/N=3/30. Each data point represents a mean of all WPBs counted in an image. Colours/shapes represent technical repeats (R1 red hexagon, R2 blue square, R3 green triangle).

C. Mean area of Golgi fragments per FOV ±SEM n/N=3/30. Each data point represents a mean of all WPBs counted in an image. Colours/shapes represent technical repeats (R1 red hexagon, R2 blue square, R3 green triangle).

* = p <0.05 ** = p <0.01 *** = p <0.001

5.5.3 Pair C

In similar vein to pair A, there were no significant differences seen in the total number of Golgi fragments expressed in either cell line under either condition. Generally, there is an overall increase in fragmentation in the diabetic conditions in both HSS and static environment but there is a wide spread of data and subsequent overlapping between conditions.

Diabetes appears to affect the mean number of Golgi fragments per cell. There is a significant difference in the average number of Golgi fragments between the hAEC and dhAEC in both static and HSS conditions. Under static conditions there is a significantly greater number of Golgi fragments in the dhAECs (11.93±1.81) than the hAECs (5.27±0.65), close to double the fragmentation. This is also true in the HSS condition with dhAEC (10.88±1.81) displaying a significantly greater number of fragments than hAEC (4.04±0.18), in this instance more than double the fragmentation. Control ECs are displaying variation, more so in static, HSS is comparatively concise. The dhAECs show a similar degree of variation regardless of environment. Average number of Golgi fragments per cell does not display a significant flow effect with no differences recorded between ECs of either diabetes status in static or HSS environments. As there are significant changes in between diabetic and control it suggests the diabetic phenotype is strong, preventing the atheroprotective effects of shear from taking full effect. This mirrors what was observed in the morphology of WPBs in **section 5.3.3**.

The area of the fragments did not show any significant changes between any combination of factors. There is a trend in the static environment whereby the dhAEC Golgi fragments (2.28±0.32 μm^2) have a smaller area than the hAEC (3.15±0.22 μm^2) in the same environment. This trend can also be seen under HSS with the diabetic ECs being slightly larger than under static (3.23±0.80 μm^2) but still shorter than those from the control ECs (3.61±0.61 μm^2).

It is worth noting that differences were observed within each pair of cells, reflecting individual patient variation. This variability has been noted throughout the investigation of ECs and informed the decision to broaden the scope of the investigation by incorporating a larger cohort of patient plasma samples, thereby enhancing the robustness and generalisability of findings seen above.

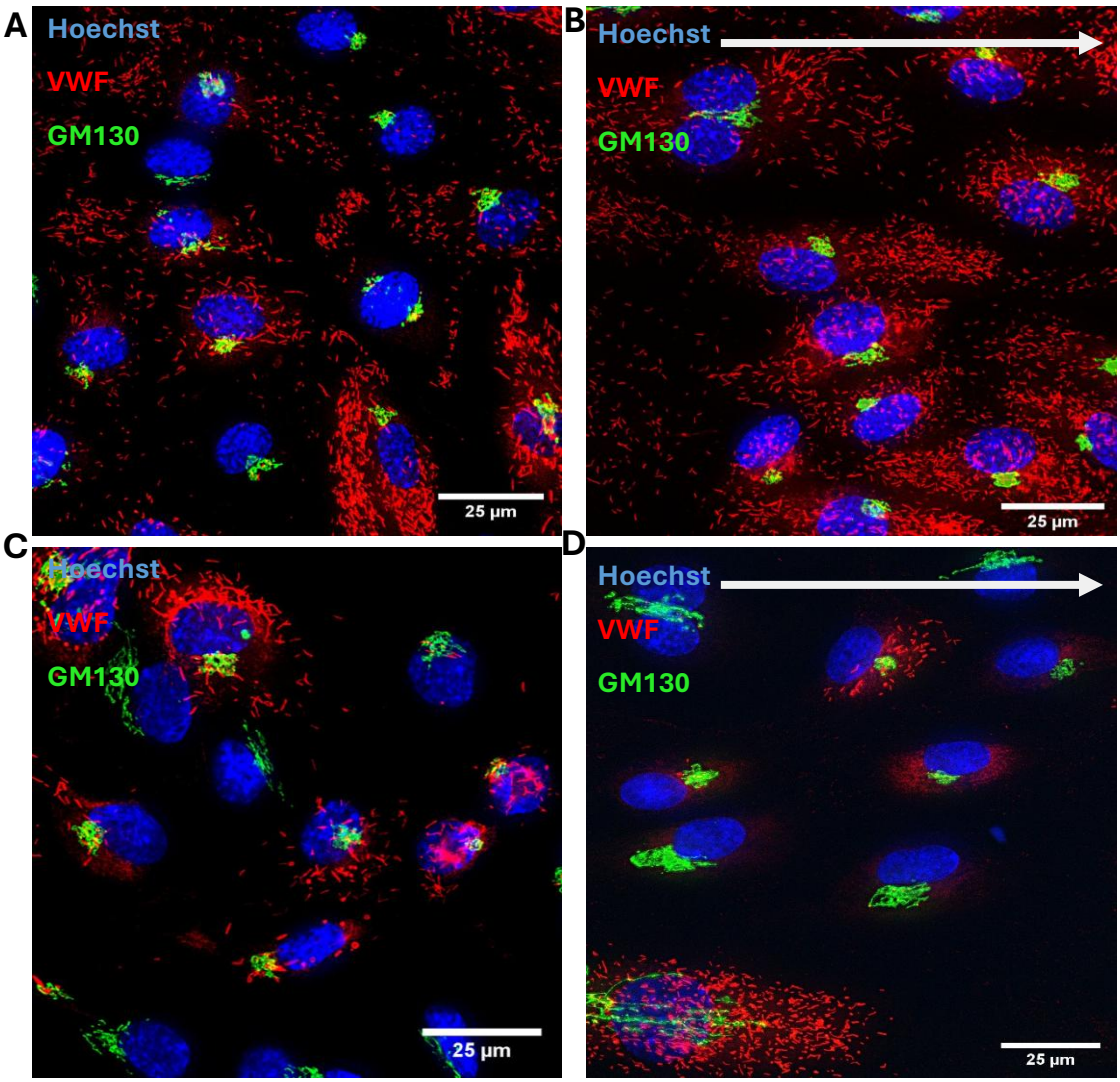

Figure 5.10. Representative images (x60 objective) of Pair C hAEC and dhAEC both static and HSS culture conditions.

A. hAEC under static culture Endothelial cells (Hoechst blue) with their expressed WPBs (VWF red) and Golgi (GM100 green).
B. hAEC under HSS Endothelial cells (Hoechst blue) with their expressed WPBs (VWF red) and Golgi (GM100 green).
C. dhAEC under static culture Endothelial cells (Hoechst blue) with their expressed WPBs (VWF red) and Golgi (GM100 green).
D. dhAEC under HSS Endothelial cells (Hoechst blue) with their expressed WPBs (VWF red) and Golgi (GM100 green).

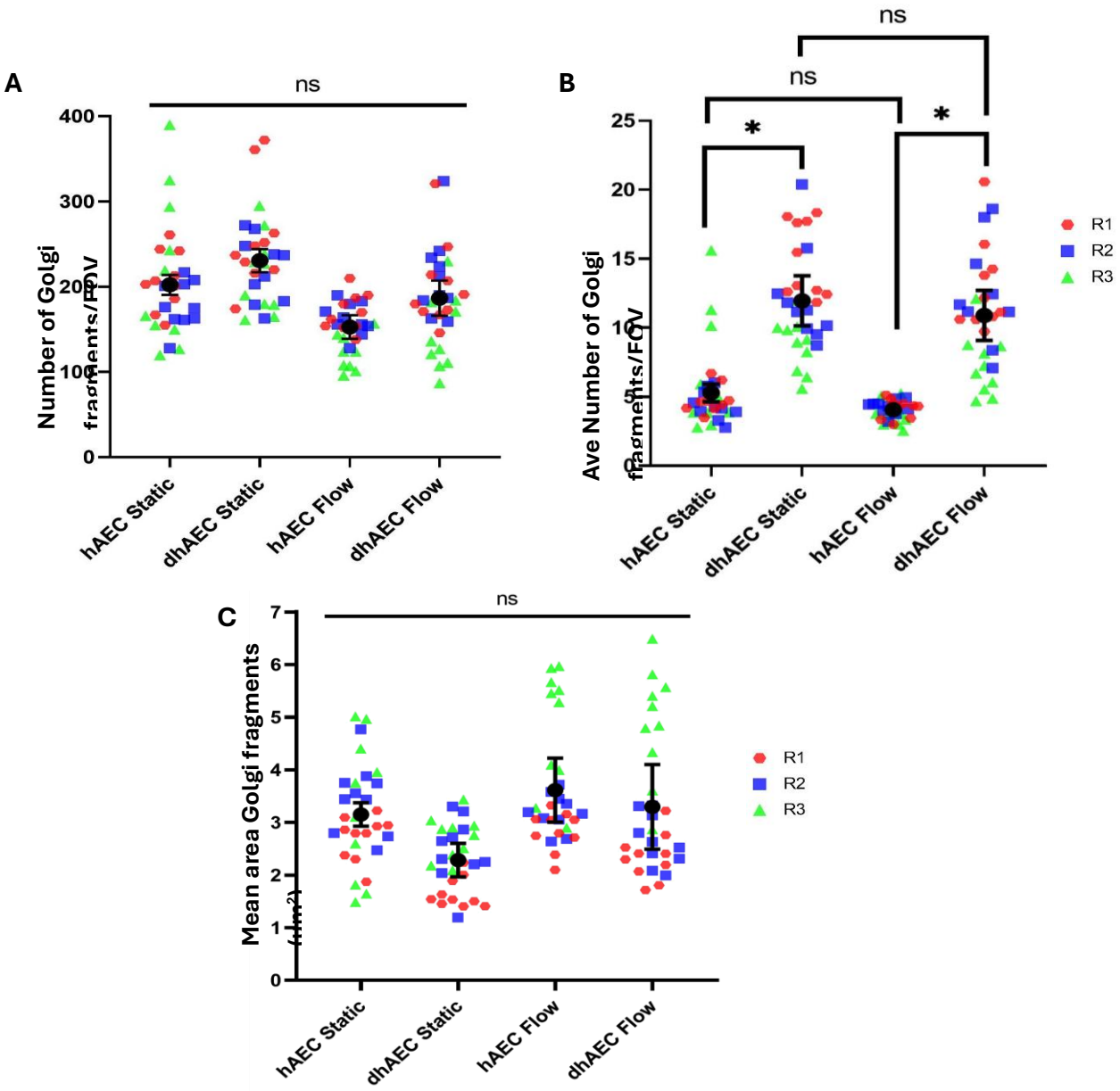

Figure 5.11. Diagnosis of diabetes affects the average number of Golgi fragments in the ECs used in Pair C, exposure to shear stress does not affect the Golgi.

A. Mean of the total number of Golgi fragments observed per FOV ±SEM n/N=3/30. Each data point represents a mean of all WPBs counted in an image. Colours/shapes represent technical repeats (R1 red hexagon, R2 blue square, R3 green triangle).
B. Mean number of Golgi fragments observed per cell ±SEM n/N=3/30. Each data point represents a mean of all WPBs counted in an image. Colours/shapes represent technical repeats (R1 red hexagon, R2 blue square, R3 green triangle).
C. Mean area of Golgi fragments per FOV ±SEM n/N=3/30. Each data point represents a mean of all WPBs counted in an image. Colours/shapes represent technical repeats (R1 red hexagon, R2 blue square, R3 green triangle).

t-test * = p <0.05

5.6 Discussion

Cells are the foundational units of all tissues and organs each programmed and specialised to function optimally in their native environment (288). ECs which line the vasculature and organ systems exhibit functional diversity shaped through their local physiological context (289, 290). As demonstrated in this study, WPB populations are heterogeneous carrying specialised cargo tailored to the demands of their vascular bed. VWF, the structural backbone of WPBs, is expressed in all ECs and may similarly reflect these environmental cues (98, 291). Through comparative analysis I observed that HUVECs displayed a more diverse multimeric fingerprint and larger multimer index, indicative of an increased thrombotic phenotype, compared to that observed in the hAECs. This is telling of HUVECs having a phenotype that has an increased thrombotic potential, with enhanced capacity for aberrant clot formation. These finding suggest that, alongside WPB composition being controlled by the vascular environment, VWF structure may also be influenced. This reinforces the importance of context-specific models when studying endothelial function. Data presented in this chapter also demonstrate the importance of matching cell passage rates across experimental conditions within each repeat. Both HUVECs and hAECs exhibited variation in multimeric profiles depending on the cell passage number, which may contribute to the variability observed between experimental repeats. To mitigate this, all cells were maintained and matched at the same passage throughout, ensuring consistency and reducing confounding effects attributable to passage-dependent changes in VWF expression.

Chapter 4 showed that when pairs of ECs were considered as discrete experimental conditions, there were significant differences in the number of WPBs observed with a reduction in the dhAECs in two of three pairs. As such, this pairwise approach was maintained in investigating VWF multimeric profiles in this chapter.

Both pairs A and C, which previously displayed a reduction in WPB the dhAECs in **chapter 4**, also exhibited a lower quantity of VWF and diminished multimeric fingerprint compared to the matched hAEC counterparts. This reduction in VWF diversity is reflected in the multimeric index which is consistently reduced in dhAEC conditions compared to the hAEC in pairs A and C. These changes subsequently translated into a higher proportion of low molecular weight VWF multimers in the dhAECs, suggesting a shift in VWF composition that may contribute to impaired or reduced WPB biosynthesis. Interestingly, Pair B deviated from this pattern. No significant differences observed in the average number of WPBs per cell between hAECs and dhAECs in **chapter 4**. However,

investigation into the VWF composition revealed a reduction in the total VWF expression and the multimeric diversity in the dhAECs, with a predominance of LMW VWF multimers. Although this did not result in a significant decrease in WPB number in **chapter 4** it does indicate that VWF biosynthesis and processing are none the less altered in dhAECs, potentially affecting their functional capacity.

A key observation of this investigation is that the observed reduction in intracellular VWF in dhAECs contradicts the patterns established in the literature. While this study presents a novel analysis of the multimeric composition of VWF from hAEC samples in a diabetic model, previous studies have primarily focused on quantifying plasma levels of VWF in diabetic populations (193, 210). Based on this literature, it was initially hypothesised that VWF levels would also be elevated within dhAECs. Specifically, it was speculated within the literature that VWF expression was so much greater in a diabetic population, it could be used as a predictive biomarker in diabetic patients for risk of developing CVD (192). When taken in context with data presented from this investigation, findings suggests that a more nuanced approach may be required to assess endothelial function in diabetes. Specifically, one that distinguishes between intracellular stores of VWF and circulating plasma levels of VWF. The primary difference in studies in literature and this investigation regarding VWF is that plasma is 'holistic', samples will contain VWF expressed through all three pathways (basal, constitutive and regulated) (94). This project has been focused exclusively on WPBs and subsequently on regulated VWF release, which while a primary source of VWF, does not encompass all VWF associated with ECs (86, 99).

Such focus inherently centres on regulated VWF secretion mediated through storage in WPBs, overlooking basal and constitutive pathways. These alternative routes mediate unregulated release of VWF and contribute to extracellular VWF levels in the plasma and subendothelial matrix (94). If these pathways were modified by diabetes, it could explain the increase in VWF reported in multiple studies in literature (80, 192, 199, 243). An increase in constitutive release may also account for the reduction in the number of WPBs observed in two out of three of the dhAEC samples, as this pathway comprises of VWF released from WPBs without stimulation (279). The inclusion of diabetic plasma samples provided the opportunity to explore these alternative release mechanisms as well as addressing the hypothesised limitation identified in **chapter 4,** namely that the EC-based investigation was underpowered. Expanding the cohort and increasing the biological diversity strengthened the analysis and offered broader insight into mechanisms underlying VWF dysfunction in diabetes.

Plasma samples used were paired based on available patient's profiles provided; however, as this was not a primary investigation, pairing was a secondary occurrence, and exact matching was not feasible. Confounding factors were used as exclusion criteria including smoking and autoimmune disease. Due to the limited number of female participants in both the control and diabetic cohorts, all female samples were included regardless of confounder static to enhance overall cohort diversity. The quantity of protein in each plasma sample was not quantified in this experiment due to time constraints. Instead, the primarily the focus was on the multimer profile of each sample and comparing these profiles to those observed from the dhAECs, with particular attention to the absence or presence of specific bands.

Multimer profiles seen in diabetic patients showed broad similarity to those from control patients. Comparative to the dhAEC and hAEC samples, profiles exhibited a greater diversity of multimer weights present. While no statistical differences in multimer index were observed between diabetic and control plasma samples, the diabetic group displayed a shift towards a higher index value, suggestive of increased variation and a greater presence of HMW VWF.

The diabetic plasma samples appeared to exhibit greater band intensity compared to those from control patients. However, as total protein content was not quantified prior to gel loading, these results may be skewed despite equal loading of plasma across samples. To improve accuracy in future analyses, it would be beneficial to quantify both total protein and the specific quantity of VWF in each plasma sample prior to multimer analysis. Which would allow for more precise normalisation and enable clear interpretation of differences in VWF abundance. Overall, these findings do suggest that data from this investigation may be beginning to align with patterns reported in literature. The visually increased expression of VWF in the diabetic samples was so great, it posed technical challenges to capture the control samples, implying elevated circulating VWF levels in the diabetic environment, consistent with previous reported findings of patient studies (192, 195, 210, 243, 292). Taken together with the reduction in WPB number observed in ECs in **chapter 4**, this begins to establish a foundation for the hypothesis that diabetes drives overactivity of unregulated VWF release. If substantiated through further investigation, this mechanism could not only support use of VWF as a predictive biomarker for CVD in diabetic patients but also highlight a potential therapeutic target to mitigate or prevent vascular complications associated with diabetes.

Given the apparent dysregulation of VWF and reduction in WPB numbers observed under diabetic conditions, I began to attempt and elucidate a mechanism driving this, starting with analysis of the Golgi, the site of WPB biosynthesis (108, 110). As we have seen, under specific stresses such as differential shear stress, the Golgi morphology can be modulated, which in turn promotes modification of the resultant WPBs. Once again, significant findings varied between each of the pairs.

There was no significant difference in the Golgi morphology between control and diabetic ECs in pair A. Pair B exhibited a greater number of Golgi fragments in the diabetic environment under static culture, a phenotype that was eradicated under exposure to HSS. While the mean area of Golgi fragments did not show any effects of diabetes, a clear flow-dependant effect was observed: ECs cultured under static conditions displayed significantly smaller Golgi fragments compared to those maintained under flow. Pair C did not show any significant in the number total number of fragments or in the mean area of fragments. However, there was an effect of diabetes in the average number of Golgi fragments per cell in both static and HSS cultured ECs.

Golgi morphology in hAECs responded in contrast to the trend identified in HUVECs as reported by Money et al and Ferraro et al, where exposure to HSS led to increased Golgi fragmentation and a reduction in fragment volume (59, 108). In the presented study, hAECs did not exhibit a comparable response to HSS; Golgi structure remained largely unchanged under flow conditions. This discrepancy may reflect a cell type specific effect as findings from Money et al and Ferraro et al both are derived from HUVECs, whereas this study focused on hAECs (59, 108). Further highlighting the importance of vascular bed specific models when assessing endothelial responses. Given the variation seen across pairs and the absence of consistent correlations, it is unlikely that alterations in Golgi morphology and consequent effects on packaging account for the observed disturbances to WPB populations and VWF expression.

Studies surrounding this mechanism of Golgi modulation in ECs is lacking in a diabetic context. There is evidence to demonstrate that the Golgi is disturbed in pancreatic β-Cells in a diabetic environment (293). If insulin was inhibited, it induced morphological changes in the Golgi apparatus architecture, resulting in increased fragmentation into ministacks, deformation and swelling of the apparatus (293). Furthermore, in a broader mechanistic context, diabetes is associated with elevated oxidative stress, which has been shown to promote fragmentation of the Golgi apparatus (294). This relationship may help explain the variation in Golgi morphology observed between EC pairs in the study. Differences in

oxidative stress levels, potentially influenced by factors such as diabetes duration, glycaemic control or treatment compliance, could contribute to the heterogeneity in Golgi structure observed. These findings suggest that Golgi fragmentation may not be a uniform feature of endothelial diabetic dysfunction, but rather a variable phenotype resulting from an individual's profile and disease progression.

A recognised concern of tissue culture and cell maintenance is emphasized here, the inherent artificiality of the *in vitro* environment. Despite efforts to replicate physiological conditions, systems remain vulnerable to artefactual influences that may persist despite use of methods such as microfluidics to salvage physiological replicability. It has been documented that increased serial passaging of cells may induce changes to biochemical properties of cells, impairing ability to proliferate, reducing NO production and increasing levels of oxidative stress (286). In that study, results were assessed in cells from across vascular beds and species (including both human and murine). However comparable findings have also been substantiated in human-derived ECs. Impairment to regeneration has been observed alongside disruption and dysregulation of VWF (295). One study utilising saphenous vein ECs showed that the composition of the surface ECs are cultured on can influence the phenotype of the cells, increased passage number correlates with a shift regardless of this, but effects may be mediated and curtailed (295). Evidence is conflicting regarding passage effects on VWF, with reported increase of extracellular release (295) but also reported decrease of VWF stores in HUVECs with increase in passage (296). These studies suggest that VWF storage may be progressively impaired with increased cell passage which potentially leading to overexpression of the protein via unstimulated pathways. While intriguing, this observation remains inferential and warrants further investigation.

Lopes et al raise a potential secondary complication of cell culture, suggesting that method of detachment of a HUVECs monolayer may specifically interfere with VWF pathways within ECs. Irrespective of method, VWF stores (i.e. WPBs) decreased with cell passage, however this reduction was increased 20-30% if trypsin was used as the detaching reagent in comparison to pancreatin complex (296). This is a process termed, trypsin-degranulation of WPBs, highlighting the negative impact on ECs to resynthesis VWF in culture (296). Conclusions drawn from this study align with my own observations regarding use of ECs to study VWF. Specifically, the recommendation to use cells up to but not exceeding passage 3 reinforces observations from my own investigation, in which HUVECs beyond passage 3 failed to release VWF in the expected string like structures. This convergence of evidence strengthens the rationale for limiting passage number to a

maximum of three when modelling WPB behaviour and specifically VWF secretion(296). A study focused on hAECs showed that ageing cells (increasing passage number) adversely affected endothelial function (297). This was evidenced by a reduction in eNOS expression and a consequent effect of disrupting dependant down-stream pathways (297). Interestingly, they demonstrated that immortalisation of the cell line mitigated these effects (297).

Ability to separate out each different molecular weight VWF multimer has been integral in defining the effects of diabetes in the context of WPBs. While this method is robust there has been a recent development to reduce the introduction of huma bias with regards to analysis technique. An automated image analysis pipeline has been devised aimed to increase the accuracy and reduce variability in analysis (298). This deep learning approach has demonstrated ability to accurately identify and classify patterns within VWF multimer pattern and gives scope to standardising the approach of analysis. The novelty of this technique means it is not fully at capacity for routine application, once the approach is streamlined this could be an essential addition to elevate analysis as done here (298). In multimer gels in **appendix** potential data or artefacts of imaging are evident, showing shadows in the HMW section of the lane where samples have run. These shadows are more defined in the dhAEC condition, given the low intensity and subsequent low resolution, it is not possible to discern if they are truly a result. The machine learning techniques outlined could be applied here to improve the reliability and accuracy of analysis while reducing bias of assessing manually for artefacts or shadows on the gel.

Plasma samples were accompanied by more comprehensive patient demographics than were provided with the commercial cell lines. This conferred several advantages including access to potential exclusion criteria, as previously discussed, and clinical metrics, such as HbA1C a standard measure blood glucose control (160, 163, 218, 299). The inclusion of these details enabled a more comprehensive characterisation of the patient cohort and facilitated comparison of factors both contributing to or reflective of a diabetic status. As expected, the average HbA1C value was elevated in the diabetic patient cohort. HbA1C and duration of diabetes was assessed for correlation with VWF levels in plasma samples, however, no significant associations emerged. It is important to note that the data set was incomplete in the control population, not all patients had a recorded HbA1C value, this may have introduced bias or limited the robustness of comparative analysis. Furthermore, both diabetes duration and HbA1C are influenced by diabetes treatment regimes, for which data were not available for this study.

This chapter has identified that dysregulation of VWF in diabetic individuals compared to the control counterparts observed consistently across both ECs and plasma samples. Critically, a discrepancy emerged between the VWF multimeric profiles of dhAECs and diabetic plasma suggesting a potential defect in VWF packaging or intracellular handling. One plausible mechanism is an overactive release of VWF into the extracellular environment via constitutive or basal VWF secretion pathways. The presence of UHMW VWF in diabetic plasma implies that synthesis of the protein itself is not impaired. However, when considered alongside the reduction in WPB number observed in the majority of dhAEC samples, these findings point towards a dysfunction in in the storage of VWF within WPBs. Rather than being retained for regulated release at an appropriate time and needed for primary haemostasis. If substantiated, this would represent a novel insight into endothelial dysfunction in diabetes, with potential for biomarker development and therapeutic intervention.

To further this investigation, it would be pertinent to consider treatment regimens of patients, including assessing adherence to prescribed plans and determine if individuals within the cohort were presenting with controlled to uncontrolled diabetes. This could offer valuable insight into the significance of treatment and help delineate which components of the diabetic environment act as key pathological triggers. Such indicators may hold potential for both therapeutic targeting and earlier identification of disease progression. Moreover, quantification of total protein content and specifically VWF expression in plasma samples would proffer deeper insight into the quantity of VWF in the diabetic environment. Such measurements would enable more accurate comparisons and help determine whether the elevated VWF levels observed in both literature and this model of diabetes are driven by overactivity in constitutive or basal release pathways. This additional layer of analysis could strengthen the hypothesis presented above, that unregulated secretion contributes to increased circulating VWF seen in diabetic patients and clarify the relationship between intracellular storage deficits and extracellular accumulation.

The investigation supports the notion that VWF is dysregulated in diabetic patients and warrants further investigation. While these findings reinforce that that ECs from individual patients exhibit considerable variability, even under comparable stress conditions, they also suggest that dysregulation of VWF may occur independently of Golgi mediated regulation. This points to the need for further investigation both up and downstream of this mechanism to identify a possible ignition point for this disruption. Understanding of these mechanisms could offer valuable insight into the endothelial environment in diabetes.

6: Overall Discussion

6.1 Summary of findings

While animal models have demonstrated that WPBs may be modulated by diabetes and human patient studies have highlighted that VWF is specifically elevated in diabetic plasma samples, studies establishing a link between the two have not been hugely explored. As a result, a gap has formed in our understanding of how diabetes can modulate the biogenesis and function of WPBs in humans with diabetes. Given VWF is a well characterised protein further elucidation of its dysregulation in diabetes may offer critical insights into therapeutic strategies. Moreover, its potential utility as a biomarker could enable predictive assessment of vascular complications of diabetes such as CVD and diabetic retinopathy. This thesis has highlighted that diabetes has the capacity to interfere with storage of VWF with a noted reduction in WPB numbers in dhAECs. Findings here also underscore a critical therapeutic consideration by reinforcing and supporting the concept of metabolic memory. The physiological cell model revealed that even under normoglycemic conditions, as would be observed in patients with well-controlled blood glucose, a pathological vascular phenotype may persist. This highlights the necessity for early intervention aimed at preventing or mitigating the initial vascular damage resultant from hyperglycaemia exposure and other triggers associated with diabetes. These such measures may be pivotal in reducing the risk of long-term vascular complications. Furthermore, the reduction in WPBs, essential for the rapid wound healing response of ECs, observed within dhAECs suggest they may have diminished reparative capacity. This in turn may contribute to the delayed or compromised wound healing commonly observed in diabetic patients. Data presented highlight the importance of investigating the association of VWF impairment and diabetes.

A recurring theme in this investigation has been an alteration to the VWF profile in ECs cultured in environments mimicking diabetic conditions. These alterations have manifested through changes in a reduction in WPB numbers and, variation in both the quantity and the multimeric profile of VWF. Markedly, healthy ECs exposed to a manufactured diabetic environment, such as exposed to extreme hyperglycaemia, demonstrated an adaptive response to a prolonged *in vitro* exposure period (48hrs). In contrast, when ECs originating from a diabetic environment are subsequently placed in a normoglycemic (healthy) condition, the functional impairments gained persist. This asymmetry highlights the enduring impact of pathological conditioning and reinforces metabolic memory as a concept of causing potentially irreversible endothelial dysfunction

in diabetes. While findings in EC lysates indicated reduction in total VWF in diabetic conditions, analysis of VWF in the plasma from diabetic patients highlighted an opposite result.

The presented multimer gels cannot be used to conclusively state that VWF concentration was higher in the diabetic plasma samples compared to the controls, however; in several instances, the control signal was obscured or difficult to capture reliably due to being overshadowed by the diabetic sample intensity. This supports the concepts identified in the literature regarding elevated VWF levels in diabetes (192, 210, 243). This suggests in a diabetic microenvironment; dhAECs are not able to synthesise the same high number of WPBs as were observed in hAECs. Given the seemingly elevated levels of VWF in plasma and presence of high/ultra-high MW VWF multimers that are absent from the cell lysates, it implies that there may be either a 'leak' of VWF into the lumen of the blood vessel from cells or an increase in constitutive release of VWF where WPBs exocytose without stimulation. Moreover, the observed reduction in WPB number in dhAECs may offer an initial mechanistic insight into why this phenomenon is commonly reported, suggesting a potential link between WPB depletion and altered VWF release in diabetic endothelial environment.

Several key findings have been identified in this thesis.

WPBs in pooled ECs:

- HUVECs exposed to a combination of high glucose and high shear stress can adapt to their environment for prolonged exposure (48hrs).
- HUVECs exposed to prolonged extreme hyperglycaemia begin to exhibit pathogenic traits, primarily release of longer VWF strings indicating a reduction in the atheroprotective effects of high shear stress.
- Exposure of healthy HUVECs to 48hrs of controlled fluctuations between hyper and hypoglycaemia did not impact the production of WPBs nor their morphology.

These models demonstrated that pooled HUVECs were capable of withstanding both extreme hyperglycaemic conditions and HSS. Exposure of ECs to HSS demonstrates a continuation of the argument put forward by Money et al that WPBs should not be studied in a static culture (54, 59). As WPBs morphology is significantly regulated by SS, static is representative of a pathological environment. The critical advantage of using HUVECs was that they reliably synthesise a large population of WPBs, making them a good model for assessing the organelle. Being pooled from multiple donors increases the diversity of the

cell model and aids growth reliability. This dependability allowed the advancement of the constant high glucose model to the ambulatory model. Regardless of the glucose exposure, HUVECs were too efficient at adapting to the microenvironment. Following 48hrs of culture, some pathological effects of aberrant glucose exposure became more apparent, but the stimuli was insufficient to result in significantly altered phenotypes. In order to assess the prolonged effects of diabetes pathology on ECs, the model was inverted and ECs from donors with a confirmed clinical diagnosis were utilised, strengthening the approach by raising the physiological relevance of the cell line. HUVECs are foetal in origin, representing a transient vascular state, comparatively hAECs are taken from mature tissue that experience long term stresses. The diversity of donors is sacrificed as hAECs used were from individual donors, not pooled, however the physiological relevance provided novel insight into WPB populations as influenced by diabetes.

WPBs from physiologically relevant patient ECs:

- ECs from a patient with a diagnosis of diabetes display a metabolic memory when isolated and placed into a normoglycemic environment.
- Expression or manufacture of WPBs appears to be dysregulated and decreased by diabetes in ECs.
- Commercial ECs taken from individual donors (not pooled) display individual patient characteristics and subsequently vary between one another even in the same condition.
- Diagnosis of diabetes results in variation and dysregulation of metabolic profiles of ECs regarding AKT and eNOS and subsequent phosphorylation.
- Multimeric profile and quantity of VWF is diminished in dhAECs as compared to hAECs.
- Plasma from both control and diabetic patients presents a ‘full’ expression of VWF multimers.
- Diabetic patient plasma displayed a more intense VWF signal compared to control samples.
- The Golgi apparatus exhibits patient-specific alterations, with no distinct pattern, in response to diabetes, suggesting it is unlikely to be the primary cause of WPB reduction in ECs.

Use of hAECs from a physiological origin allowed for more holistic assessment of the cumulative effects of diabetes and the associated dysfunction of ECs. Furthermore, it allows the concept of metabolic memory to be assessed. When this EC model is

combined with the plasma sample data it suggests that there is an imbalance between the VWF stored within ECs and the VWF released into the plasma under exposure to diabetes. As well as increasing the contextual information surrounding VWF and diabetes, use of plasma samples provides patient data including diagnostic criteria of diabetes. This allows for population characteristics to be compared between control and diabetic donors, including HbA1c readings, used for diagnosis of diabetes. Providing further physiological perspective of how this data can be utilised in a therapeutic context.

The reduction in WPB numbers observed in this investigation contrasts with the observations recorded in models of induced diabetes in animals. On balance, animal models report an increase in the number of WPBs in vascular tissue harvested from diabetic subjects compared to the control (191, 196, 197). Whereas data from the diabetic plasma presented in this thesis, while not fully conclusive, does imply that there is a potential increase in VWF concentration in diabetic patient plasma comparative to control individuals. If quantified successfully, this would agree with the paradigm established in the literature whereby the concentration of VWF in diabetic populations is elevated (192, 193, 195, 210). This would reinforce the foundation of using VWF as a biomarker for elevated risk of vascular complications in diabetic cohorts.

Similar findings were presented by Xiang et al who demonstrated that VWF plasma concentrations in T2DM patients were twofold higher and T1DM were 1.6-fold higher than matched healthy controls (300). It was also demonstrated that high weight VWF multimers, that have the highest affinity for platelets, were at an elevated prevalence within the diabetic samples (300). Moreover, the risk of a vascular-associated complication of diabetes was correlated to VWF concentration within the T2DM population (300). Using a streptozotocin induced diabetic mouse model, Xieng et al assessed the effects of hyperglycaemia induced VWF elevation, as expected mRNA expression of VWF increased 2-fold and plasma VWF increased 1.4 fold compared to control mice (300). Xiang et al also sought to elucidate a mechanism for this increase in VWF, mIR-24 was identified as significantly associated to regulation of VWF (300). If under expressed, mIR-24 is correlated to a significant decrease in plasma VWF, subsequently conferring an increased bleeding phenotype, however further investigation is required to identify the signalling mechanism responsible (300). This study supports use of VWF as a biomarker in vascular complications associated to diabetes while also highlighting the requirement for further investigation to identify the mechanisms responsible for the observed dysfunction of the protein.

The cause of this discrepancy in stored VWF in WPBs and plasma VWF concentrations requires further investigation to elucidate a mechanism. Through the investigation laid out in this thesis, modulation of the Golgi body is not the apparent causal mechanism. One study investigating the role of diabetes in promoting tumour progression, an indirect result identified that there was increased expression of VWF in diabetic mice resulting from increased oxidative stress associated to hyperglycaemia (301). It was hypothesised that the elevated VWF expression may be as a result of an oxidative stress induced increase in calcium signalling which may stimulate exocytosis of WPBs (301). However, it was ultimately concluded that this mechanism is poorly understood and chronic diseases including diabetes may have long term effects on VWF regulation beyond this mechanism (301). I propose that assessment of the remaining two VWF release pathways, basal and constitutive, is required to identify if there is a defect in the regulation of either pathway. This may provide the missing explanation for the reduced number of WPB reported here and suggested increase in VWF plasma concentrations in diabetic individuals as alluded to here and observed within the literature.

Patella et al demonstrated that modulating WPB size through statin treatment has therapeutic potential in treating TTP, data presented in this thesis suggests revelation of the mechanism that results in elevated plasma VWF concentrations in diabetic populations could provide a target for therapeutic intervention (148). As raised VWF is becoming increasing strengthened as a marker of endothelial dysfunction and subsequently a biomarker for CVD progression within the context of diabetes, this would allow faster identification of vascular complications associated to diabetes. Altered handling of VWF within the vasculature has been reliably associated with increased inappropriate platelet activation, which contributes to the formation of thrombi in vascular conditions (302). Subsequently, increasing understanding of whether there is a fault in the formation of WPBs that is encouraging uncontrolled VWF release from ECs under a diabetic microenvironment would allow for earlier intervention which could slow or prevent progression of diabetes-associated vascular damage.

6.2 Limitations of this investigation

Whilst the data present in this thesis present a foundational bridge between research into WPBs and VWF dysregulation to humans, there are limitations with the approach. Primarily the use of commercial ECs, while this permits reliable and continuous study of WPBs, they are inherently artificial as they do not fully recapitulate the complexity of a blood vessel *in situ*. In particular, use of HUVECs which do not represent a true physiological EC, limits the application of findings to the more diverse vascular beds. As such, expansion of this project to incorporate a broader panel of ECs derived from characterised donors would enhance the physiological relevance and provide a more robust foundation to translate functional insights. Moreover, the number of WPBs expressed in each type of EC differs, HUVECs will synthesise a larger population of WPBs than hAECs. Likewise, data presented in this thesis and in literature demonstrate that the percentage of ECs that synthesis WPBs in each FOV is lower on average in hAECs than in HUVECs (54). This minor imbalance in populations, may result in the hAEC models being under powered in comparison. Therefore, it may be pertinent to increase the number of technical repeats of hAECs to achieve a comparable number of WPBs assessed to the HUVEC model.

In addition, the limited availability of patient-specific data further constrained the depth of this interpretation. While plasma samples were incorporated and permitted assessment of key patient characteristics, these samples were secondary in nature to this investigation, and lacked the definition required to fully contextualise the VWF and WPB response to diabetes. The absence of prospectively collected clinical data restricted the ability to account for confounding variables and limited the representativeness of the cohort. This was particularly evident in the hAEC and dhAECs populations, where diversity and donor characterisation were limited. Although inclusion of plasma samples partially mitigated this issue, it did not fully compensate from the loss of physiological nuance. Future studies would benefit from integrating well characterised donor derived ECs alongside matched clinical data. This would enable more comprehensive and physiologically relevant analysis of WPB behaviour and VWF dysregulation in the context of diabetes associated endothelial dysfunction.

As addressed throughout this thesis, the development of *in vitro* cellular models necessitates a reductionist approach, simplifying the vascular endothelium and diabetic environment into testable concepts. While this strategy has enabled the identification of significant differences in WPB behaviour, several mechanistic aspects remain unexplored.

One such area is the role of insulin and insulin resistance in modulating endothelial function. Insulin signalling is known to influence key metabolic pathways including AKT and its dysregulation may contribute to the changes observed in WPB characteristics under diabetic conditions. Investigating this axis could provide deeper insight into the molecular mechanisms driving endothelial dysfunction and WPB dysregulation and help clarify how metabolic imbalances translate into vascular pathology.

Ultimately, use of the IBIDI microfluidics system allowed for reliable and reproducible utilisation of HSS across multiple models of diabetes. While alternative microfluidics approaches exist, such as, orbital shakers and cone and plate systems, which expose cells to rotational flow in culture plates, these methods introduce both laminar and oscillatory stress making it difficult to isolate and analyse specific flow types. Similarly, the Masterflex system allows for cell culture on slides with a larger surface area, but the achievable shear stress is limited, and consistency falls short of the standards provided by the IBIDI system. The trade off in this investigation was clear, the IBIDI system offered superior consistency and control of shear stress but at the expense of growth area. As a result, protein-level analysis via western blotting was not feasible and key signalling factors such as AKT and eNOS could only be assessed under static conditions. There is scope to adapt the IBIDI system to support biochemical analysis and attempts were made during this investigation, for example by culturing multiple microslides per condition within a single experimental set up. However, initial attempts to implement this in series proved challenging moreover to add more slides individually is restricted by the available fluidic units and pump connections. A combined approach, integrating multiple microfluidic platforms and further optimisation of the IBIDI system could overcome these limitations. Enabling a more detailed investigation of the biochemical and metabolic responses of endothelial cells in diabetic environments.

Analysis and processing of immunofluorescent images throughout this thesis relied on a series of tailored ImageJ macros to ensure reliability, accuracy and minimal bias. While this approach was robust and reproducible, recent advances offer opportunities to further enhance image analysis. Two pipelines using CellProfiler software have been developed called OrganelleProfiler and OrganelleContentProfiler, which quantitatively analyse confocal fluorescent images and have been demonstrated to specifically identify WPBs within ECs (303). OrganelleProfiler enables profiling of EC and WPB populations, providing a cell count as well as the profile of WPB populations including the number, size and shape of the organelles (303). Use of the OrganelleContentProfiler pathway would provide a secondary approach to assessing the cargo contained within WPBs and therefore

provide insight into the effects of diabetes in WPBs alongside VWF (303). Incorporating these pipelines would enable faster, high-throughput analysis of raw images, ultimately allowing for more efficient overall analysis. It would also strengthen mechanistic understanding of endothelial dysfunction in diabetic environments, extending insight beyond VWF alone to encompass broader aspects of WPB biology including cargo composition and organelle dynamics. While similar to the method utilised in this investigation, incorporation of this approach would enhance analysis. However, the pipelines were published after my study was initiated, therefore could not be implemented into the current analysis of WPBs.

6.3 Future Directions

Expansion of vascular beds

A key future direction for this research is the incorporation of multiple vascular beds to enhance the physiological relevance. WPBs are heterogeneous organelles whose characteristics vary depending in the endothelial cell type and vascular context. Expanding the study to include a broader panel of ECs from well characterised donors, with improved sample diversity and robust cohort size, would allow for more representative analysis. This would permit investigation of diabetes-induced effects on WPB populations across distinct vascular environments providing a comprehensive overview of endothelial dysfunction and WPB behaviour beyond a single cell type. This would allow for a 'mapping' project whereby identification of dysfunction could be narrowed down to a specific subset of WPBs or tissue.

Identification of VWF pathway affected or mechanism behind alterations

Further analysis of plasma samples is required to fully elucidate the impact of diabetes on circulating VWF in patients. This could be achieved by quantifying total protein and specifically VWF levels prior to running multimer gel analysis, enabling assessment of differences in a more quantitative manner. A combination of BCA and ELISA assays would support this approach, though optimisation would be required to ensure sensitivity and reproducibility. Importantly, if a dysregulated pathway is responsible for excessive VWF release and could be identified, it could present a therapeutic target to modulated VWF secretion with potential to improve wound healing efficacy and reduce the pro-thrombotic pathology associated with diabetes. In parallel, analysis of ADAMTS13 activity would provide further insight into whether altered enzyme function contributes to the VWF profile observed in diabetic plasma, offering a more complete understanding of the regulatory mechanisms at play. This would be attainable through use of an ELISA assay and represents an important step in addressing current gaps in understanding the mechanisms that alter VWF multimerization in the context of diabetes.

Explore downstream repercussions of WPB modulation and VWF disruption

Models of diabetes presented here have demonstrated VWF and WPBs may be subject to dysregulation in this disease state. Further analysis of the downstream repercussions of this disruption could provide fundamental insight into how diabetes is affecting endothelial function and haemostasis. While no overall significant differences in WPB size were identified within the population, the dhAECs display a trend towards a reduction in WPB size compared to a non-diabetic donors and significance is identified in discrete

pairs. Utilisation of multimer gel analysis further demonstrated a relative reduction in VWF, including the absence of key HMW multimers. To determine if these structural changes translate into functional impairment, a VWF-platelet adherence assay would provide a basic quantitative assessment of the VWF released from the d/hAECs. Longer strings have greater capacity to bind to platelets; therefore, if HMW VWF is truly missing from the dhAECs, a measurable reduction in platelet adherence would be expected. An assay such as this would increase the physiological relevance of recent findings and offer insight into how diabetes may be influencing clot formation in response to vascular injury. These observations could then be integrated into broader understanding of the impact of diabetes on endothelial dysfunction and thrombosis within the vasculature. By extension this could have therapeutic applications.

Role or impact of treatment and medication in diabetes management

Finally, to enhance the real-world applicability of these findings, future models should include incorporation of medication or intervention data to assess the impact of treatment on endothelial function and WPB behaviour. In the current study, models largely assumed uncontrolled diabetes, particularly in the hyperglycaemia-based experiments. However, in clinical practice, diabetes management has advanced significantly and treatments such as metformin are widely used to mitigate complications, though these complications still develop and progress in many patients. To better evaluate how emerging to existing interventions might, minimise, delay to prevent vascular complications, it is important to integrate current therapeutic regimens into experimental models. For example, incorporating metformin treatment would allow for a more comprehensive assessment of its influence on the endothelial environment and determine whether it exerts detrimental or protective effects on WPBs or VWF. This approach would provide valuable insight into the interplay between pharmacological intervention and endothelial organelle dynamics in the context of diabetes.

Taken together, these future directions offer a clear path towards strengthening the physiological relevance, translational impact and mechanistic insight of this research. By expanding endothelial models, integrating patient-specific data, incorporating therapeutic interventions and adopting advanced imaging and analysis pipelines, future studies can more accurately reflect the complexity of diabetes-associated endothelial dysfunction and its impact of WPBs. This will not only deepen our understanding of WPB biology and VWF regulation but also support the development of targeted strategies to mitigate vascular complications in diabetic patients.

References

1. Matheus AS, Tannus LR, Cobas RA, Palma CC, Negrato CA, Gomes MB. Impact of diabetes on cardiovascular disease: an update. International journal of hypertension. 2013;2013:653789.
2. Galindo RJ, Trujillo JM, Low Wang CC, McCoy RG. Advances in the management of type 2 diabetes in adults. BMJ Medicine. 2023;2(1):e000372.
3. Shamsaldeen YA, Lione LA, Benham CD. Dysregulation of TRPV4, eNOS and caveolin-1 contribute to endothelial dysfunction in the streptozotocin rat model of diabetes. European Journal of Pharmacology. 2020;888:173441.
4. Zheng Y, Ley SH, Hu FB. Global aetiology and epidemiology of type 2 diabetes mellitus and its complications. Nature Reviews Endocrinology. 2018;14(2):88-98.
5. Kropp M, Golubnitschaja O, Mazurakova A, Koklesova L, Sargheini N, Vo TKS, et al. Diabetic retinopathy as the leading cause of blindness and early predictor of cascading complications-risks and mitigation. The EPMA journal. 2023;14(1):21-42.
6. Hippisley-Cox J, Coupland C. Diabetes treatments and risk of amputation, blindness, severe kidney failure, hyperglycaemia, and hypoglycaemia: open cohort study in primary care. BMJ (Clinical research ed). 2016;352:i1450.
7. Dymkowska D, Drabarek B, Podszywałow-Bartnicka P, Szczepanowska J, Zabłocki K. Hyperglycaemia modifies energy metabolism and reactive oxygen species formation in endothelial cells in vitro. Archives of biochemistry and biophysics. 2014;542:7-13.
8. Huang X, Liu G, Guo J, Su Z. The PI3K/AKT pathway in obesity and type 2 diabetes. International journal of biological sciences. 2018;14(11):1483-96.
9. Yang D-R, Wang M-Y, Zhang C-L, Wang Y. Endothelial dysfunction in vascular complications of diabetes: a comprehensive review of mechanisms and implications. 2024;Volume 15 - 2024.
10. Augustin HG, Koh GY. A systems view of the vascular endothelium in health and disease. Cell. 2024;187(18):4833-58.
11. Ricard N, Bailly S, Guignabert C, Simons M. The quiescent endothelium: signalling pathways regulating organ-specific endothelial normalcy. Nature Reviews Cardiology. 2021;18(8):565-80.
12. De Pablo-Moreno JA, Serrano LJ, Revuelta L, Sánchez MJ, Liras A. The Vascular Endothelium and Coagulation: Homeostasis, Disease, and Treatment, with a Focus on the Von Willebrand Factor and Factors VIII and V. International journal of molecular sciences. 2022;23(15).
13. Sachdev U, Lotze MT. Perpetual change: autophagy, the endothelium, and response to vascular injury. Journal of leukocyte biology. 2017;102(2):221-35.
14. Cooke JP. The endothelium: a new target for therapy. 2000;5(1):49-53.
15. Sandoo A, van Zanten JJ, Metsios GS, Carroll D, Kitas GD. The endothelium and its role in regulating vascular tone. The open cardiovascular medicine journal. 2010;4:302-12.
16. Pober JS, Sessa WC. Evolving functions of endothelial cells in inflammation. Nature Reviews Immunology. 2007;7(10):803-15.
17. Carmeliet P. Angiogenesis in health and disease. Nature medicine. 2003;9(6):653-60.
18. Martin P, Gurevich DB. Macrophage regulation of angiogenesis in health and disease. Seminars in Cell & Developmental Biology. 2021;119:101-10.
19. Chakroborty D, Goswami S, Basu S, Sarkar C. Catecholamines in the regulation of angiogenesis in cutaneous wound healing. FASEB journal : official publication of the Federation of American Societies for Experimental Biology. 2020;34(11):14093-102.
20. Cossutta M, Darche M, Carpentier G, Houppe C, Ponzo M, Raineri F, et al. Weibel-Palade Bodies Orchestrate Pericytes During Angiogenesis. 2019;39(9):1843-58.

21. Berndt MC, Metharom P, Andrews RK. Primary haemostasis: newer insights. 2014;20(s4):15-22.
22. Yu P, Zhang G, Hou B, Song E, Wen J, Ba Y, et al. Effects of ECM proteins (laminin, fibronectin, and type IV collagen) on the biological behavior of Schwann cells and their roles in the process of remyelination after peripheral nerve injury. 2023;Volume 11 - 2023.
23. Haginoya S, Thomovsky EJ, Johnson PA, Brooks AC. Clinical Assessment of Primary Hemostasis: A Review. Topics in Companion Animal Medicine. 2023;56-57:100818.
24. Zander CB, Cao W, Zheng XL. ADAMTS13 and von Willebrand factor interactions. Current opinion in hematology. 2015;22(5):452-9.
25. Clemetson KJ. Platelets and Primary Haemostasis. Thrombosis research. 2012;129(3):220-4.
26. Chapin JC, Hajjar KA. Fibrinolysis and the control of blood coagulation. Blood reviews. 2015;29(1):17-24.
27. Federici AB. The factor VIII/von Willebrand factor complex: basic and clinical issues. Haematologica. 2003;88(6):Erep02.
28. Bukkems LH, Heijdra JM, de Jager NCB, Hazendonk HCAM, Fijnvandraat K, Meijer K, et al. Population pharmacokinetics of the von Willebrand factor–factor VIII interaction in patients with von Willebrand disease. Blood advances. 2021;5(5):1513-22.
29. Terraube V, O'Donnell JS, Jenkins PV. Factor VIII and von Willebrand factor interaction: biological, clinical and therapeutic importance. Haemophilia : the official journal of the World Federation of Hemophilia. 2010;16(1):3-13.
30. Green D. Coagulation cascade. Hemodialysis international International Symposium on Home Hemodialysis. 2006;10 Suppl 2:S2-4.
31. Rossaint J, Margraf A, Zarbock A. Role of Platelets in Leukocyte Recruitment and Resolution of Inflammation. 2018;Volume 9 - 2018.
32. Dole VS, Bergmeier W, Mitchell HA, Eichenberger SC, Wagner DD. Activated platelets induce Weibel-Palade–body secretion and leukocyte rolling in vivo: role of P-selectin. Blood. 2005;106(7):2334-9.
33. dela Paz NG, D'Amore PA. Arterial versus venous endothelial cells. Cell and tissue research. 2009;335(1):5-16.
34. Flo K, Kulseng CPS, Peterson HF, Hillestad V, Sommerfelt S, Eskild A. Placental size and umbilical vein volume blood flow. 2025;104(6):1135-42.
35. Vega-Tapia F, Peñaloza E, Krause BJ. Specific arterio-venous transcriptomic and ncRNA-RNA interactions in human umbilical endothelial cells: A meta-analysis. iScience. 2021;24(6):102675.
36. Trimm E, Red-Horse K. Vascular endothelial cell development and diversity. Nature reviews Cardiology. 2023;20(3):197-210.
37. Wang Y, Nakayama M, Pitulescu ME, Schmidt TS, Bochenek ML, Sakakibara A, et al. Ephrin-B2 controls VEGF-induced angiogenesis and lymphangiogenesis. Nature. 2010;465(7297):483-6.
38. Yang C, Shu C, Wang L, Li X, He H, Li J, et al. EphB4 signaling maintains the contractile phenotype of adult venous smooth muscle cells. American journal of translational research. 2020;12(8):4522-31.
39. Chavkin NW, Genet G, Poulet M, Jeffery ED, Marziano C, Genet N, et al. Endothelial cell cycle state determines propensity for arterial-venous fate. Nature Communications. 2022;13(1):5891.
40. Icli B, Feinberg MW. Plasticity of Arterial and Venous Endothelial Cell Identity. Circulation Research. 2016;119(5):574-6.
41. Torres-Vázquez J, Kamei M, Weinstein BM. Molecular distinction between arteries and veins. Cell and tissue research. 2003;314(1):43-59.
42. Bloom SI, Islam MT, Lesniewski LA, Donato AJ. Mechanisms and consequences of endothelial cell senescence. Nature reviews Cardiology. 2023;20(1):38-51.

43. Eelen G, de Zeeuw P, Simons M, Carmeliet P. Endothelial cell metabolism in normal and diseased vasculature. Circ Res. 2015;116(7):1231-44.
44. Naderi-Meshkin H, Setyaningsih WAW. Endothelial Cell Dysfunction: Onset, Progression, and Consequences. 2024;29(6).
45. Chistiakov DA, Orekhov AN, Bobryshev YV. Effects of shear stress on endothelial cells: go with the flow. Acta physiologica (Oxford, England). 2017;219(2):382-408.
46. Cheng CW, Earle SL, Povstyan OV, Randall C, Smith KA, Debant M, et al. PIEZO1 variant implications for biological understanding and human health. Open biology. 2025;15(7):240345.
47. Chala N, Moimas S, Giampietro C, Zhang X, Zambelli T, Exarchos V, et al. Mechanical Fingerprint of Senescence in Endothelial Cells. Nano Letters. 2021;21(12):4911-20.
48. Malek AM, Alper SL, Izumo S. Hemodynamic Shear Stress and Its Role in Atherosclerosis. Jama. 1999;282(21):2035-42.
49. Traub O, Berk BC. Laminar Shear Stress. Arteriosclerosis, thrombosis, and vascular biology. 1998;18(5):677-85.
50. Lu D, Kassab GS. Role of shear stress and stretch in vascular mechanobiology. Journal of the Royal Society, Interface. 2011;8(63):1379-85.
51. Gogia S, Neelamegham S. Role of fluid shear stress in regulating VWF structure, function and related blood disorders. Biorheology. 2015;52(5-6):319-35.
52. Afshar Y, Ma F, Quach A, Jeong A, Sunshine HL, Freitas V, et al. Transcriptional drifts associated with environmental changes in endothelial cells. 2022:2022.07.08.499287.
53. Tamargo IA, Baek KI, Kim Y, Park C, Jo H. Flow-induced reprogramming of endothelial cells in atherosclerosis. Nature reviews Cardiology. 2023;20(11):738-53.
54. Money A, Todd HJ, Jo H, Beech DJ, McKeown L. Low oscillatory shear stress regulates Weibel-Palade body size and vWF release. 2023:2023.05.26.542527.
55. Spurway J, Logan P, Pak S. The development, structure and blood flow within the umbilical cord with particular reference to the venous system. Australasian journal of ultrasound in medicine. 2012;15(3):97-102.
56. Taylor DEM. BLOOD FLOW IN ARTERIES. 2nd ed. By D. A. McDonald. Edward Arnold, London, 1974. Pp. xviii+496. £12. 1975;60(1):65-.
57. Papaioannou TG, Karatzis EN, Vavuranakis M, Lekakis JP, Stefanadis C. Assessment of vascular wall shear stress and implications for atherosclerotic disease. International journal of cardiology. 2006;113(1):12-8.
58. Chatterjee S. Endothelial Mechanotransduction, Redox Signaling and the Regulation of Vascular Inflammatory Pathways. Frontiers in physiology. 2018;9:524.
59. Money A. The Effect of Shear Stress on Weibel-Palade Bodies: University of Leeds; 2023.
60. IBIDI. The Different Types of Flow [Available from: https://ibidi.com/content/286-the-different-types-of-flow#laminar.
61. Federici AB, Berntorp E, Lee CA. The 80th anniversary of von Willebrand's disease: history, management and research. Haemophilia : the official journal of the World Federation of Hemophilia. 2006;12(6):563-72.
62. Jaffe EA, Hoyer LW, Nachman RL. Synthesis of von Willebrand factor by cultured human endothelial cells. Proceedings of the National Academy of Sciences of the United States of America. 1974;71(5):1906-9.
63. Müller AM, Hermanns MI, Skrzynski C, Nesslinger M, Müller K-M, Kirkpatrick CJ. Expression of the Endothelial Markers PECAM-1, vWf, and CD34 in Vivo and in Vitro. Experimental and Molecular Pathology. 2002;72(3):221-9.
64. Hassan MI, Saxena A, Ahmad F. Structure and function of von Willebrand factor. 2012;23(1):11-22.

65. Yee A, Kretz CA. Von Willebrand factor: form for function. Seminars in thrombosis and hemostasis. 2014;40(1):17-27.
66. Pikta M, Vasse M, Smock KJ, Moser KA, van DM, Lejniece S, et al. Establishing reference intervals for von Willebrand factor multimers. Journal of medical biochemistry. 2022;41(1):115-21.
67. Favaloro EJ, Bonar R, Chapman K, Meiring M, Funk D. Differential sensitivity of von Willebrand factor (VWF) ‘activity’ assays to large and small VWF molecular weight forms: a cross‐laboratory study comparing ristocetin cofactor, collagen‐binding and mAb‐based assays. Journal of Thrombosis and Haemostasis. 2012;10(6):1043-54.
68. Zhou Y-F, Eng ET, Zhu J, Lu C, Walz T, Springer TA. Sequence and structure relationships within von Willebrand factor. Blood. 2012;120(2):449-58.
69. Voorberg J, Fontijn R, van Mourik JA, Pannekoek H. Domains involved in multimer assembly of von willebrand factor (vWF): multimerization is independent of dimerization. The EMBO journal. 1990;9(3):797-803.
70. Springer TA. von Willebrand factor, Jedi knight of the bloodstream. Blood. 2014;124(9):1412-25.
71. Csányi MC, Salamon P, Feller T, Bozó T, Hársfalvi J, Kellermayer MSZ. Structural hierarchy of mechanical extensibility in human von Willebrand factor multimers. Protein science : a publication of the Protein Society. 2023;32(1):e4535.
72. Zanardelli S, Chion AC, Groot E, Lenting PJ, McKinnon TA, Laffan MA, et al. A novel binding site for ADAMTS13 constitutively exposed on the surface of globular VWF. Blood. 2009;114(13):2819-28.
73. O'Brien HER, Zhang XF, Sanz-Hernandez M, Chion A, Shapiro S, Mobayen G, et al. Blocking von Willebrand factor free thiols inhibits binding to collagen under high and pathological shear stress. Journal of Thrombosis and Haemostasis. 2021;19(2):358-69.
74. Mobayen G, El-Mansi S, Chion A, Nightingale TD, McKinnon TAJ. Probing rare von Willebrand disease–causing mutations in the D4 and C-domains of von Willebrand factor. Research and practice in thrombosis and haemostasis. 2025;9(4).
75. Majerus EM, Anderson PJ, Sadler JE. Binding of ADAMTS13 to von Willebrand Factor*. Journal of Biological Chemistry. 2005;280(23):21773-8.
76. Ercig B, Arfman T, Hrdinova J, Wichapong K, Reutelingsperger CPM, Vanhoorelbeke K, et al. Conformational plasticity of ADAMTS13 in hemostasis and autoimmunity. The Journal of biological chemistry. 2021;297(4):101132.
77. Zanardelli S, Crawley JT, Chion CK, Lam JK, Preston RJ, Lane DA. ADAMTS13 substrate recognition of von Willebrand factor A2 domain. The Journal of biological chemistry. 2006;281(3):1555-63.
78. Akiyama M, Takeda S, Kokame K, Takagi J, Miyata T. Crystal structures of the noncatalytic domains of ADAMTS13 reveal multiple discontinuous exosites for von Willebrand factor. Proceedings of the National Academy of Sciences of the United States of America. 2009;106(46):19274-9.
79. Kokame K, Matsumoto M, Fujimura Y, Miyata T. VWF73, a region from D1596 to R1668 of von Willebrand factor, provides a minimal substrate for ADAMTS-13. Blood. 2004;103(2):607-12.
80. Kozlov S, Okhota S, Avtaeva Y, Melnikov I, Matroze E, Gabbasov Z. Von Willebrand factor in diagnostics and treatment of cardiovascular disease: Recent advances and prospects. Frontiers in cardiovascular medicine. 2022;9:1038030.
81. Wagner DD, Mayadas T, Marder VJ. Initial glycosylation and acidic pH in the Golgi apparatus are required for multimerization of von Willebrand factor. The Journal of cell biology. 1986;102(4):1320-4.
82. Ginsburg D. The von Willebrand Factor Gene and Genetics of von Willebrand's Disease. Mayo Clinic Proceedings. 1991;66(5):506-15.

83. Berber E, Pehlevan F, Akin M, Capan OY, Kavakli K, Çaglayan SH. A Common VWF Exon 28 Haplotype in the Turkish Population. 2013;19(5):550-6.
84. Bonthron DT, Handin RI, Kaufman RJ, Wasley LC, Orr EC, Mitsock LM, et al. Structure of pre-pro-von Willebrand factor and its expression in heterologous cells. Nature. 1986;324(6094):270-3.
85. Romani de Wit T, van Mourik JA. Biosynthesis, processing and secretion of von Willebrand factor: biological implications. Best Practice & Research Clinical Haematology. 2001;14(2):241-55.
86. Lenting PJ, Christophe OD, Denis CV. von Willebrand factor biosynthesis, secretion, and clearance: connecting the far ends. Blood. 2015;125(13):2019-28.
87. Haberichter SL, Jozwiak MA, Rosenberg JB, Christopherson PA, Montgomery RR. The Von Willebrand Factor Propeptide (VWFpp) Traffics an Unrelated Protein to Storage. 2002;22(6):921-6.
88. Seidizadeh O, Eikenboom JCJ, Denis CV, Flood VH, James P, Lenting PJ, et al. von Willebrand disease. Nature reviews Disease primers. 2024;10(1):51.
89. James P, Leebeek F, Casari C, Lillicrap D. Diagnosis and treatment of von Willebrand disease in 2024 and beyond. 2024;30(S3):103-11.
90. Weyand AC, Flood VH. Von Willebrand Disease: Current Status of Diagnosis and Management. Hematology/oncology clinics of North America. 2021;35(6):1085-101.
91. Tebo C, Gibson C, Mazer-Amirshahi M. Hemophilia and von Willebrand Disease: A Review of Emergency Department Management. The Journal of Emergency Medicine. 2020;58(5):756-66.
92. Giblin JP, Hewlett LJ, Hannah MJ. Basal secretion of von Willebrand factor from human endothelial cells. Blood. 2008;112(4):957-64.
93. Choi SJ, Lillicrap D. A sticky proposition: The endothelial glycocalyx and von Willebrand factor. Journal of thrombosis and haemostasis : JTH. 2020;18(4):781-5.
94. Lopes da Silva M, Cutler DF. von Willebrand factor multimerization and the polarity of secretory pathways in endothelial cells. Blood. 2016;128(2):277-85.
95. Keightley AM, Lam YM, Brady JN, Cameron CL, Lillicrap D. Variation at the von Willebrand Factor (vWF) Gene Locus Is Associated With Plasma vWF:Ag Levels: Identification of Three Novel Single Nucleotide Polymorphisms in the vWF Gene Promoter. Blood. 1999;93(12):4277-83.
96. Weibel ER, Palade GE. NEW CYTOPLASMIC COMPONENTS IN ARTERIAL ENDOTHELIA. The Journal of cell biology. 1964;23(1):101-12.
97. Krüger-Genge A, Blocki A, Franke RP, Jung F. Vascular Endothelial Cell Biology: An Update. International journal of molecular sciences. 2019;20(18).
98. Rondaij MG, Bierings R, Kragt A, Mourik JAv, Voorberg J. Dynamics and Plasticity of Weibel-Palade Bodies in Endothelial Cells. 2006;26(5):1002-7.
99. Metcalf DJ, Nightingale TD, Zenner HL, Lui-Roberts WW, Cutler DF. Formation and function of Weibel-Palade bodies. Journal of Cell Science. 2008;121(1):19-27.
100. Wagner DD, Saffaripour S, Bonfanti R, Sadler JE, Cramer EM, Chapman B, et al. Induction of specific storage organelles by von Willebrand factor propolypeptide. Cell. 1991;64(2):403-13.
101. Fiedler U, Scharpfenecker M, Koidl S, Hegen A, Grunow V, Schmidt JM, et al. The Tie-2 ligand Angiopoietin-2 is stored in and rapidly released upon stimulation from endothelial cell Weibel-Palade bodies. Blood. 2004;103(11):4150-6.
102. Erent M, Meli A, Moisoi N, Babich V, Hannah MJ, Skehel P, et al. Rate, extent and concentration dependence of histamine-evoked Weibel-Palade body exocytosis determined from individual fusion events in human endothelial cells. The Journal of physiology. 2007;583(Pt 1):195-212.
103. Nightingale T, Cutler D. The secretion of von Willebrand factor from endothelial cells; an increasingly complicated story. Journal of Thrombosis and Haemostasis. 2013;11:192-201.

104. Valentijn KM, Valentijn JA, Jansen KA, Koster AJ. A new look at Weibel–Palade body structure in endothelial cells using electron tomography. Journal of Structural Biology. 2008;161(3):447-58.
105. Wagner DD, Marder VJ. Biosynthesis of von Willebrand protein by human endothelial cells: processing steps and their intracellular localization. The Journal of cell biology. 1984;99(6):2123-30.
106. Valentijn KM, Sadler JE, Valentijn JA, Voorberg J, Eikenboom J. Functional architecture of Weibel-Palade bodies. Blood. 2011;117(19):5033-43.
107. Weibel ER. Fifty years of Weibel-Palade bodies: the discovery and early history of an enigmatic organelle of endothelial cells. Journal of thrombosis and haemostasis : JTH. 2012;10(6):979-84.
108. Ferraro F, Kriston-Vizi J, Metcalf Daniel J, Martin-Martin B, Freeman J, Burden Jemima J, et al. A Two-Tier Golgi-Based Control of Organelle Size Underpins the Functional Plasticity of Endothelial Cells. Developmental Cell. 2014;29(3):292-304.
109. Schillemans M, Karampini E, Kat M, Bierings R. Exocytosis of Weibel–Palade bodies: how to unpack a vascular emergency kit. 2019;17(1):6-18.
110. Mourik MJ, Faas FGA, Zimmermann H, Voorberg J, Koster AJ, Eikenboom J. Content delivery to newly forming Weibel-Palade bodies is facilitated by multiple connections with the Golgi apparatus. Blood. 2015;125(22):3509-16.
111. Philippe M, Léger T, Desvaux R, Walch L. Discs Large 1 (Dlg1) Scaffolding Protein Participates with Clathrin and Adaptator Protein Complex 1 (AP-1) in Forming Weibel-Palade Bodies of Endothelial Cells. Journal of Biological Chemistry. 2013;288(18):13046-56.
112. Bonnemaison M, Bäck N, Lin Y, Bonifacino JS, Mains R, Eipper B. AP-1A controls secretory granule biogenesis and trafficking of membrane secretory granule proteins. Traffic (Copenhagen, Denmark). 2014;15(10):1099-121.
113. Lui-Roberts WW, Collinson LM, Hewlett LJ, Michaux G, Cutler DF. An AP-1/clathrin coat plays a novel and essential role in forming the Weibel-Palade bodies of endothelial cells. The Journal of cell biology. 2005;170(4):627-36.
114. Naß J, Terglane J, Gerke V. Weibel Palade Bodies: Unique Secretory Organelles of Endothelial Cells that Control Blood Vessel Homeostasis. Frontiers in cell and developmental biology. 2021;9:813995.
115. Mobayen G, Smith K, Ediriwickrema K, Starke RD, Solomonidis EG, Laffan MA, et al. von Willebrand factor binds to angiopoietin-2 within endothelial cells and after release from Weibel–Palade bodies. Journal of Thrombosis and Haemostasis. 2023;21(7):1802-12.
116. Di Pietro SM, Falcón-Pérez JM, Tenza D, Setty SR, Marks MS, Raposo G, et al. BLOC-1 interacts with BLOC-2 and the AP-3 complex to facilitate protein trafficking on endosomes. Molecular biology of the cell. 2006;17(9):4027-38.
117. Sharda AV, Barr AM, Harrison JA, Wilkie AR, Fang C, Mendez LM, et al. VWF maturation and release are controlled by 2 regulators of Weibel-Palade body biogenesis: exocyst and BLOC-2. Blood. 2020;136(24):2824-37.
118. Doyle EL, Ridger V, Ferraro F, Turmaine M, Saftig P, Cutler DF. CD63 is an essential cofactor to leukocyte recruitment by endothelial P-selectin. Blood. 2011;118(15):4265-73.
119. Conte IL, Hellen N, Bierings R, Mashanov GI, Manneville J-B, Kiskin NI, et al. Interaction between MyRIP and the actin cytoskeleton regulates Weibel–Palade body trafficking and exocytosis. Journal of Cell Science. 2016;129(3):592-603.
120. Ferraro F, da Silva ML, Grimes W, Lee HK, Ketteler R, Kriston-Vizi J, et al. Weibel-Palade body size modulates the adhesive activity of its von Willebrand Factor cargo in cultured endothelial cells. Scientific Reports. 2016;6(1):32473.
121. Fiedler U, Reiss Y, Scharpfenecker M, Grunow V, Koidl S, Thurston G, et al. Angiopoietin-2 sensitizes endothelial cells to TNF-alpha and has a crucial role in the induction of inflammation. Nature medicine. 2006;12(2):235-9.

122. Pergolizzi M, Bizzozero L, Riccitelli E, Pascal D, Samarelli AV, Bussolino F, et al. Modulation of Angiopoietin 2 release from endothelial cells and angiogenesis by the synaptic protein Neuroligin 2. Biochemical and Biophysical Research Communications. 2018;501(1):165-71.
123. Yuan HT, Khankin EV, Karumanchi SA, Parikh SM. Angiopoietin 2 is a partial agonist/antagonist of Tie2 signaling in the endothelium. Molecular and cellular biology. 2009;29(8):2011-22.
124. Harrison-Lavoie KJ, Michaux G, Hewlett L, Kaur J, Hannah MJ, Lui-Roberts WWY, et al. P-Selectin and CD63 Use Different Mechanisms for Delivery to Weibel–Palade Bodies. 2006;7(6):647-62.
125. Hol J, Wilhelmsen L, Haraldsen G. The murine IL-8 homologues KC, MIP-2, and LIX are found in endothelial cytoplasmic granules but not in Weibel-Palade bodies. Journal of leukocyte biology. 2010;87(3):501-8.
126. Wang H-B, Wang J-T, Zhang L, Geng ZH, Xu W-L, Xu T, et al. P-selectin primes leukocyte integrin activation during inflammation. Nature Immunology. 2007;8(8):882-92.
127. Kanwar S, Woodman RC, Poon MC, Murohara T, Lefer AM, Davenpeck KL, et al. Desmopressin Induces Endothelial P-Selectin Expression and Leukocyte Rolling in Postcapillary Venules. Blood. 1995;86(7):2760-6.
128. Norman KE, Moore KL, McEver RP, Ley K. Leukocyte rolling in vivo is mediated by P-selectin glycoprotein ligand-1. Blood. 1995;86(12):4417-21.
129. Doré M, Korthuis RJ, Granger DN, Entman ML, Smith CW. P-selectin mediates spontaneous leukocyte rolling in vivo. Blood. 1993;82(4):1308-16.
130. Merten M, Thiagarajan P. P-selectin in arterial thrombosis. Zeitschrift fur Kardiologie. 2004;93(11):855-63.
131. Wagner DD, Olmsted JB, Marder VJ. Immunolocalization of von Willebrand protein in Weibel-Palade bodies of human endothelial cells. The Journal of cell biology. 1982;95(1):355-60.
132. Chauhan AK, Kisucka J, Brill A, Walsh MT, Scheiflinger F, Wagner DD. ADAMTS13: a new link between thrombosis and inflammation. Journal of Experimental Medicine. 2008;205(9):2065-74.
133. Arribas M, Cutler DF. Weibel-Palade body membrane proteins exhibit differential trafficking after exocytosis in endothelial cells. Traffic (Copenhagen, Denmark). 2000;1(10):783-93.
134. Kiskin NI, Hellen N, Babich V, Hewlett L, Knipe L, Hannah MJ, et al. Protein mobilities and P-selectin storage in Weibel–Palade bodies. Journal of Cell Science. 2010;123(17):2964-75.
135. Mayadas TN, Johnson RC, Rayburn H, Hynes RO, Wagner DD. Leukocyte rolling and extravasation are severely compromised in P selectin-deficient mice. Cell. 1993;74(3):541-54.
136. Wolff B, Burns AR, Middleton J, Rot A. Endothelial cell "memory" of inflammatory stimulation: human venular endothelial cells store interleukin 8 in Weibel-Palade bodies. The Journal of experimental medicine. 1998;188(9):1757-62.
137. Zeiher AM, Goebel H, Schächinger V, Ihling C. Tissue endothelin-1 immunoreactivity in the active coronary atherosclerotic plaque. A clue to the mechanism of increased vasoreactivity of the culprit lesion in unstable angina. Circulation. 1995;91(4):941-7.
138. Chen Y, Mahata M, Rao F, Khandrika S, Courel M, Fung MM, et al. Chromogranin A regulates renal function by triggering Weibel-Palade body exocytosis. Journal of the American Society of Nephrology : JASN. 2009;20(7):1623-32.
139. Russell FD, Skepper JN, Davenport AP. Evidence using immunoelectron microscopy for regulated and constitutive pathways in the transport and release of endothelin. Journal of cardiovascular pharmacology. 1998;31(3):424-30.

140. Vischer UM, Wagner DD. CD63 is a component of Weibel-Palade bodies of human endothelial cells. Blood. 1993;82(4):1184-91.
141. van Breevoort D, van Agtmaal EL, Dragt BS, Gebbinck JK, Dienava-Verdoold I, Kragt A, et al. Proteomic screen identifies IGFBP7 as a novel component of endothelial cell-specific Weibel-Palade bodies. Journal of proteome research. 2012;11(5):2925-36.
142. Nightingale TD, Pattni K, Hume AN, Seabra MC, Cutler DF. Rab27a and MyRIP regulate the amount and multimeric state of VWF released from endothelial cells. Blood. 2009;113(20):5010-8.
143. Miteva KT, Pedicini L, Wilson LA, Jayasinghe I, Slip RG, Marszalek K, et al. Rab46 integrates Ca(2+) and histamine signaling to regulate selective cargo release from Weibel-Palade bodies. The Journal of cell biology. 2019;218(7):2232-46.
144. Mietkowska M, Schuberth C, Wedlich-Söldner R, Gerke V. Actin dynamics during Ca2+-dependent exocytosis of endothelial Weibel-Palade bodies. Biochimica et Biophysica Acta (BBA) - Molecular Cell Research. 2019;1866(7):1218-29.
145. Babich V, Meli A, Knipe L, Dempster JE, Skehel P, Hannah MJ, et al. Selective release of molecules from Weibel-Palade bodies during a lingering kiss. Blood. 2008;111(11):5282-90.
146. Kiskin NI, Babich V, Knipe L, Hannah MJ, Carter T. Differential cargo mobilisation within Weibel-Palade bodies after transient fusion with the plasma membrane. PLoS One. 2014;9(9):e108093.
147. Demolli S, Doebele C, Doddaballapur A, Lang V, Fisslthaler B, Chavakis E, et al. MicroRNA-30 mediates anti-inflammatory effects of shear stress and KLF2 via repression of angiopoietin 2. Journal of molecular and cellular cardiology. 2015;88:111-9.
148. Patella F, Vendramin C, Charles O, Scully MA, Cutler DF. Shrinking Weibel-Palade bodies prevents high platelet recruitment in assays using thrombotic thrombocytopenic purpura plasma. Research and practice in thrombosis and haemostasis. 2021;5(8):e12626.
149. Hadi HA, Carr CS, Al Suwaidi J. Endothelial dysfunction: cardiovascular risk factors, therapy, and outcome. Vascular health and risk management. 2005;1(3):183-98.
150. Haybar H, Shahrabi S, Rezaeeyan H, Shirzad R, Saki N. Endothelial Cells: From Dysfunction Mechanism to Pharmacological Effect in Cardiovascular Disease. Cardiovascular Toxicology. 2019;19(1):13-22.
151. Poredos P, Poredos AV, Gregoric I. Endothelial Dysfunction and Its Clinical Implications. 2021;72(7):604-15.
152. Endemann DH, Schiffrin EL. Endothelial dysfunction. Journal of the American Society of Nephrology : JASN. 2004;15(8):1983-92.
153. Zhou Z-W, Xie X-L, Zhou S-F, Li CG. Mechanism of reversal of high glucose-induced endothelial nitric oxide synthase uncoupling by tanshinone IIA in human endothelial cell line EA.hy926. European Journal of Pharmacology. 2012;697(1):97-105.
154. World Health O. Definition, diagnosis and classification of diabetes mellitus and its complications : report of a WHO consultation. Part 1, Diagnosis and classification of diabetes mellitus. Geneva: World Health Organization; 1999.
155. Khan RMM, Chua ZJY, Tan JC, Yang Y, Liao Z, Zhao Y. From Pre-Diabetes to Diabetes: Diagnosis, Treatments and Translational Research. Medicina (Kaunas, Lithuania). 2019;55(9).
156. Wang M, Li Y, Li S, Lv J. Endothelial Dysfunction and Diabetic Cardiomyopathy. Frontiers in endocrinology. 2022;13:851941.
157. Zaccardi F, Webb DR, Yates T, Davies MJ. Pathophysiology of type 1 and type 2 diabetes mellitus: a 90-year perspective. 2016;92(1084):63-9.
158. Mack LR, Tomich PG. Gestational Diabetes: Diagnosis, Classification, and Clinical Care. Obstetrics and gynecology clinics of North America. 2017;44(2):207-17.

159. Alejandro EU, Mamerto TP, Chung G, Villavieja A, Gaus NL, Morgan E, et al. Gestational Diabetes Mellitus: A Harbinger of the Vicious Cycle of Diabetes. International journal of molecular sciences. 2020;21(14).
160. BMJ. Type 1 diabetes Clinical Presentation [Available from: https://bestpractice.bmj.com/topics/en-gb/25/diagnosis-approach.
161. Galicia-Garcia U, Benito-Vicente A, Jebari S, Larrea-Sebal A, Siddiqi H, Uribe KB, et al. Pathophysiology of Type 2 Diabetes Mellitus. International journal of molecular sciences. 2020;21(17).
162. **BMJ**. Type 2 diabetes in adults Investigtions [Available from: https://bestpractice.bmj.com/topics/en-gb/24/investigations.
163. UK D. Diagnostic criteria for diabetes 2006 [updated 2011. Available from: https://www.diabetes.org.uk/for-professionals/improving-care/clinical-recommendations-for-professionals/diagnosis-ongoing-management-monitoring/new_diagnostic_criteria_for_diabetes.
164. The Lancet Regional Health – E. Misdiagnosis of type 1 and type 2 diabetes in adults. The Lancet Regional Health – Europe. 2023;29.
165. Fuchsjäger-Mayrl G, Pleiner J, Wiesinger GnF, Sieder AE, Quittan M, Nuhr MJ, et al. Exercise Training Improves Vascular Endothelial Function in Patients with Type 1 Diabetes. Diabetes care. 2002;25(10):1795-801.
166. Li J, Flammer AJ, Nelson RE, Gulati R, Friedman PA, Thomas RJ, et al. Normal vascular function as a prerequisite for the absence of coronary calcification in patients free of cardiovascular disease and diabetes. Circulation journal : official journal of the Japanese Circulation Society. 2012;76(11):2705-10.
167. Nappi F, Fiore A, Masiglat J, Cavuoti T, Romandini M, Nappi P, et al. Endothelium-Derived Relaxing Factors and Endothelial Function: A Systematic Review. 2022;10(11):2884.
168. Ranasinghe R, Mathai M, Alshawsh MA, Zulli A, Ranasinghe R. Predictive markers of early endothelial dysregulation in type-1 diabetes: a meta-analysis. Acta diabetologica. 2024.
169. Gallo G, Savoia C. New Insights into Endothelial Dysfunction in Cardiometabolic Diseases: Potential Mechanisms and Clinical Implications. International journal of molecular sciences. 2024;25(5).
170. NHS. High blood sugar (hyperglycaemia) 2022 [Available from: https://www.nhs.uk/conditions/high-blood-sugar-hyperglycaemia/.
171. Feng C-L, Chou H-C. Hyperglycemia initiates N-cadherin rearrangement and diabetic monocytes promote inflammatory responses in human microvascular endothelial cells. Biomarkers and Genomic Medicine. 2014;6(4):175-9.
172. Kopp EL, Deussen DN, Cuomo R, Lorenz R, Roth DM, Mahata SK, et al. Modeling and Phenotyping Acute and Chronic Type 2 Diabetes Mellitus In Vitro in Rodent Heart and Skeletal Muscle Cells. Cells. 2023;12(24).
173. Wang Q, Zhang X, Wang K, Zhu L, Qiu B, Chen X, et al. An In Vitro Model of Diabetic Retinal Vascular Endothelial Dysfunction and Neuroretinal Degeneration. 2021;2021(1):9765119.
174. Wang X, He B. Endothelial dysfunction: molecular mechanisms and clinical implications. MedComm. 2024;5(8):e651.
175. Hemmings BA, Restuccia DF. PI3K-PKB/Akt pathway. Cold Spring Harbor perspectives in biology. 2012;4(9):a011189.
176. Taheri R, Mokhtari Y, Yousefi AM, Bashash D. The PI3K/Akt signaling axis and type 2 diabetes mellitus (T2DM): From mechanistic insights into possible therapeutic targets. Cell biology international. 2024;48(8):1049-68.
177. Kukreja RC, Xi L. eNOS phosphorylation: a pivotal molecular switch in vasodilation and cardioprotection? Journal of molecular and cellular cardiology. 2007;42(2):280-2.

178. Lu Y, Wang W, Liu J, Xie M, Liu Q, Li S. Vascular complications of diabetes: A narrative review. Medicine (Baltimore). 2023;102(40):e35285.
179. Natarajan R. Epigenetic Mechanisms in Diabetic Vascular Complications and Metabolic Memory: The 2020 Edwin Bierman Award Lecture. Diabetes. 2021;70(2):328-37.
180. Hex N, MacDonald R, Pocock J, Uzdzinska B, Taylor M, Atkin M, et al. Estimation of the direct health and indirect societal costs of diabetes in the UK using a cost of illness model. Diabetic medicine : a journal of the British Diabetic Association. 2024;41(9):e15326.
181. Feldman EL, Callaghan BC, Pop-Busui R, Zochodne DW, Wright DE, Bennett DL, et al. Diabetic neuropathy. Nature reviews Disease primers. 2019;5(1):42.
182. Raghavan S, Vassy JL, Ho YL, Song RJ, Gagnon DR, Cho K, et al. Diabetes Mellitus–Related All-Cause and Cardiovascular Mortality in a National Cohort of Adults. Journal of the American Heart Association. 2019;8(4):e011295.
183. Huang D, Refaat M, Mohammedi K, Jayyousi A, Al Suwaidi J, Abi Khalil C. Macrovascular Complications in Patients with Diabetes and Prediabetes. 2017;2017(1):7839101.
184. Barnes JA, Eid MA, Creager MA, Goodney PP. Epidemiology and Risk of Amputation in Patients With Diabetes Mellitus and Peripheral Artery Disease. Arteriosclerosis, thrombosis, and vascular biology. 2020;40(8):1808-17.
185. Thipsawat S. Early detection of diabetic nephropathy in patient with type 2 diabetes mellitus: A review of the literature. Diabetes & vascular disease research. 2021;18(6):14791641211058856.
186. Wang Z, Li Z, Li K, Mu S, Zhou X, Di Y. Performance of artificial intelligence in diabetic retinopathy screening: a systematic review and meta-analysis of prospective studies. Frontiers in endocrinology. 2023;14:1197783.
187. Teo ZL, Tham Y-C, Yu M, Chee ML, Rim TH, Cheung N, et al. Global Prevalence of Diabetic Retinopathy and Projection of Burden through 2045: Systematic Review and Meta-analysis. Ophthalmology. 2021;128(11):1580-91.
188. Spampinato SF, Caruso GI, De Pasquale R, Sortino MA, Merlo S. The Treatment of Impaired Wound Healing in Diabetes: Looking among Old Drugs. Pharmaceuticals (Basel, Switzerland). 2020;13(4).
189. Pang T, Shao Y, Zhou L, Wang Z, Xi P, Zhang Y, et al. rhaFGF promotes acute diabetic wound healing by suppressing chronicity of inflammation. Scientific Reports. 2025;15(1):19085.
190. An Y, Kang Y, Lee J, Ahn C, Kwon K, Choi C. Blood flow characteristics of diabetic patients with complications detected by optical measurement. Biomedical engineering online. 2018;17(1):25.
191. Anderson HR, Stitt AW, Gardiner TA, Archer DB. Stereological estimation of Weibel-Palade bodies in the retinal vasculature of normal and diabetic dogs. Current Eye Research. 1994;13(9):705-10.
192. Frankel DS, Meigs JB, Massaro JM, Wilson PW, O'Donnell CJ, D'Agostino RB, et al. Von Willebrand factor, type 2 diabetes mellitus, and risk of cardiovascular disease: the framingham offspring study. Circulation. 2008;118(24):2533-9.
193. Seligman BG, Biolo A, Polanczyk CA, Gross JL, Clausell N. Increased plasma levels of endothelin 1 and von Willebrand factor in patients with type 2 diabetes and dyslipidemia. Diabetes care. 2000;23(9):1395-400.
194. Feng D, Bursell SE, Clermont AC, Lipinska I, Aiello LP, Laffel L, et al. von Willebrand factor and retinal circulation in early-stage retinopathy of type 1 diabetes. Diabetes care. 2000;23(11):1694-8.
195. Chen SF, Xia ZL, Han JJ, Wang YT, Wang JY, Pan SD, et al. Increased active von Willebrand factor during disease development in the aging diabetic patient population. Age (Dordrecht, Netherlands). 2013;35(1):171-7.

196. Popov D, Hasu M, Costache G, Stern D, Simionescu M. Capillary and aortic endothelia interact in situ with nonenzymatically glycated albumin and develop specific alterations in early experimental diabetes. Acta diabetologica. 1997;34(4):285-93.
197. Popov D, Simionescu M. Alterations of lung structure in experimental diabetes, and diabetes associated with hyperlipidaemia in hamsters. The European respiratory journal. 1997;10(8):1850-8.
198. Korhonen A, Gucciardo E, Lehti K, Loukovaara S. Proliferative diabetic retinopathy transcriptomes reveal angiogenesis, anti-angiogenic therapy escape mechanisms, fibrosis and lymphatic involvement. Scientific Reports. 2021;11(1):18810.
199. Rumley A, Lowe GDO, Sweetnam PM, Yarnell JWG, Ford RP. Factor VIII, von Willebrand factor and the risk of major ischaemic heart disease in the Caerphilly Heart Study. 1999;105(1):110-6.
200. Smith FB, Lee AJ, Fowkes FGR, Price JF, Rumley A, Lowe GDO. Hemostatic Factors as Predictors of Ischemic Heart Disease and Stroke in the Edinburgh Artery Study. 1997;17(11):3321-5.
201. Coller BS, Frank RN, Milton RC, Gralnick HR. Plasma cofactors of platelet function: correlation with diabetic retinopathy and hemoglobins Ala-c. Annals of internal medicine. 1978;88(3):311-6.
202. Pasi KJ, Enayat MS, Horrocks PM, Wright AD, Hill FG. Qualitative and quantitative abnormalities of von Willebrand antigen in patients with diabetes mellitus. Thrombosis research. 1990;59(3):581-91.
203. Porta M, Townsend C, Clover GM, Nanson M, Alderson AR, McCraw A, et al. Evidence for functional endothelial cell damage in early diabetic retinopathy. Diabetologia. 1981;20(6):597-601.
204. Riches K, Alshanwani AR, Warburton P, O'Regan DJ, Ball SG, Wood IC, et al. Elevated expression levels of miR-143/5 in saphenous vein smooth muscle cells from patients with Type 2 diabetes drive persistent changes in phenotype and function. Journal of molecular and cellular cardiology. 2014;74(100):240-50.
205. Yang T, Qi F, Guo F, Shao M, Song Y, Ren G, et al. An update on chronic complications of diabetes mellitus: from molecular mechanisms to therapeutic strategies with a focus on metabolic memory. Molecular medicine (Cambridge, Mass). 2024;30(1):71.
206. Darenskaya MA, Kolesnikova LI, Kolesnikov SI. Oxidative Stress: Pathogenetic Role in Diabetes Mellitus and Its Complications and Therapeutic Approaches to Correction. Bulletin of experimental biology and medicine. 2021;171(2):179-89.
207. Yao Y, Song Q, Hu C, Da X, Yu Y, He Z, et al. Endothelial cell metabolic memory causes cardiovascular dysfunction in diabetes. Cardiovascular research. 2022;118(1):196-211.
208. Battelino T, Danne T, Bergenstal RM, Amiel SA, Beck R, Biester T, et al. Clinical Targets for Continuous Glucose Monitoring Data Interpretation: Recommendations From the International Consensus on Time in Range. Diabetes care. 2019;42(8):1593-603.
209. IBIDI. ibidi Pump System [Available from: https://ibidi.com/pump-system/112-ibidi-pump-system.html.
210. Peng X, Wang X, Fan M, Zhao J, Lin L, Liu J. Plasma levels of von Willebrand factor in type 2 diabetes patients with and without cardiovascular diseases: A meta-analysis. 2020;36(1):e3193.
211. Wang X, Starodubtseva MN, Kapron CM, Liu J. Cadmium, von Willebrand factor and vascular aging. npj aging. 2023;9(1):11.
212. Horvath B, Hegedus D, Szapary L, Marton Z, Alexy T, Koltai K, et al. Measurement of von Willebrand factor as the marker of endothelial dysfunction in vascular diseases. Experimental and clinical cardiology. 2004;9(1):31-4.

213. Gimbrone MA, Anderson KR, Topper JN. The Critical Role of Mechanical Forces in Blood Vessel Development, Physiology and Pathology. Journal of vascular surgery. 1999;29(6):1104-51.
214. Shi Y, Vanhoutte PM. Macro- and microvascular endothelial dysfunction in diabetes. 2017;9(5):434-49.
215. Chen Y-H, Lin S-J, Lin F-Y, Wu T-C, Tsao C-R, Huang P-H, et al. High Glucose Impairs Early and Late Endothelial Progenitor Cells by Modifying Nitric Oxide–Related but Not Oxidative Stress–Mediated Mechanisms. Diabetes. 2007;56(6):1559-68.
216. Duffy A, Liew A, O'Sullivan J, Avalos G, Samali A, O'Brien T. Distinct effects of high-glucose conditions on endothelial cells of macrovascular and microvascular origins. Endothelium : journal of endothelial cell research. 2006;13(1):9-16.
217. Gray CS, Hildreth AJ, Alberti GKMM, O'Connell JE. Poststroke Hyperglycemia. Stroke. 2004;35(1):122-6.
218. NICE. When should I suspect type 2 diabetes in an adult? : NICE; [updated 07/202502/10/2015]. Available from: https://cks.nice.org.uk/topics/diabetes-type-2/diagnosis/diagnosis-in-adults/.
219. (NICE) NIfHaCE. Diabetes (type 1 and type 2) in children and young people: diagnosis and management 2015 [updated 11 May 2023. Available from: https://www.nice.org.uk/guidance/ng18.
220. Bin Rakhis SA, Sr., AlDuwayhis NM, Aleid N, AlBarrak AN, Aloraini AA. Glycemic Control for Type 2 Diabetes Mellitus Patients: A Systematic Review. Cureus. 2022;14(6):e26180.
221. Thakur V, Alcoreza N, Cazares J, Chattopadhyay M. Changes in Stress-Mediated Markers in a Human Cardiomyocyte Cell Line under Hyperglycemia. International journal of molecular sciences. 2021;22(19).
222. Jain SK, McVie R, Bocchini JA, Jr. Hyperketonemia (ketosis), oxidative stress and type 1 diabetes. Pathophysiology : the official journal of the International Society for Pathophysiology. 2006;13(3):163-70.
223. Sorooshian P, Metcalfe AD, Lali FV. In vitro modelling of disease-induced changes in the diabetic wound fibroblast. Journal of wound care. 2021;30(4):300-3.
224. Toma L, Stancu CS, Botez GM, Sima AV, Simionescu M. Irreversibly glycated LDL induce oxidative and inflammatory state in human endothelial cells; added effect of high glucose. Biochem Biophys Res Commun. 2009;390(3):877-82.
225. Chettab K, Zibara K, Belaiba SR, McGregor JL. Acute hyperglycaemia induces changes in the transcription levels of 4 major genes in human endothelial cells: macroarrays-based expression analysis. Thrombosis and haemostasis. 2002;87(1):141-8.
226. Michels A, Swystun LL, Mewburn J, Albánez S, Lillicrap D. Investigating von Willebrand Factor Pathophysiology Using a Flow Chamber Model of von Willebrand Factor-platelet String Formation. Journal of visualized experiments : JoVE. 2017(126).
227. Huang R-H, Wang Y, Roth R, Yu X, Purvis AR, Heuser JE, et al. Assembly of Weibel–Palade body-like tubules from N-terminal domains of von Willebrand factor. 2008;105(2):482-7.
228. Stockschlaeder M, Schneppenheim R, Budde U. Update on von Willebrand factor multimers: focus on high-molecular-weight multimers and their role in hemostasis. Blood coagulation & fibrinolysis : an international journal in haemostasis and thrombosis. 2014;25(3):206-16.
229. Vazzana N, Ranalli P, Cuccurullo C, Davì G. Diabetes mellitus and thrombosis. Thrombosis research. 2012;129(3):371-7.
230. Byford AR, Walsh K, Wang D, Baird-Rayner C, Pensabene V, Scott EM, et al. Physiological glucose levels associated with gestational diabetes impact the human placental transcriptome in an ex vivo model. Placenta. 2025;168:46-55.
231. Lyssenko V, Vaag A. Genetics of diabetes-associated microvascular complications. Diabetologia. 2023;66(9):1601-13.

232. Serikbaeva A, Li Y, Ganesh B, Zelkha R, Kazlauskas A. Hyperglycemia Promotes Mitophagy and Thereby Mitigates Hyperglycemia-Induced Damage. The American journal of pathology. 2022;192(12):1779-94.
233. Eid SA, Rumora AE, Beirowski B, Bennett DL, Hur J, Savelieff MG, et al. New perspectives in diabetic neuropathy. Neuron. 2023;111(17):2623-41.
234. Weng J, Ross C, Baker J, Alfuraih S, Shamloo K, Sharma A. Diabetes-Associated Hyperglycemia Causes Rapid-Onset Ocular Surface Damage. Investigative ophthalmology & visual science. 2023;64(14):11.
235. Okubo N, Sugawara S, Fujiwara T, Sakatsume K, Doman T, Yamashita M, et al. von Willebrand factor Ristocetin co-factor activity to von Willebrand factor antigen level ratio for diagnosis of acquired von Willebrand syndrome caused by aortic stenosis. Research and practice in thrombosis and haemostasis. 2024;8(1):102284.
236. Sulistyowati E, Permatasari N, Aris Widodo M. Combined effects of shear stress and glucose on the morphology, actin filaments, and VE-cadherin of endothelial cells in vitro. IJC Heart & Vasculature. 2017;15:31-5.
237. Li Q, Atochin D, Kashiwagi S, Earle J, Wang A, Mandeville E, et al. Deficient eNOS Phosphorylation Is a Mechanism for Diabetic Vascular Dysfunction Contributing to Increased Stroke Size. Stroke. 2013;44(11):3183-8.
238. He A, Guo Y, Xu Z, Yan J, Xie L, Li Y, et al. Hypoglycaemia aggravates impaired endothelial-dependent vasodilation in diabetes by suppressing endothelial nitric oxide synthase activity and stimulating inducible nitric oxide synthase expression. Microvascular Research. 2023;146:104468.
239. Takahashi T, Harris RC. Role of endothelial nitric oxide synthase in diabetic nephropathy: lessons from diabetic eNOS knockout mice. Journal of diabetes research. 2014;2014:590541.
240. Dal Canto E, Ceriello A, Rydén L, Ferrini M, Hansen TB, Schnell O, et al. Diabetes as a cardiovascular risk factor: An overview of global trends of macro and micro vascular complications. 2019;26(2_suppl):25-32.
241. Adamiec-Mroczek J, Oficjalska-Młyńczak J, Misiuk-Hojło M. Proliferative diabetic retinopathy—The influence of diabetes control on the activation of the intraocular molecule system. Diabetes Research and Clinical Practice. 2009;84(1):46-50.
242. Clyne AM. Endothelial response to glucose: dysfunction, metabolism, and transport. Biochemical Society transactions. 2021;49(1):313-25.
243. Ribau JC, Hatton MW, Richardson M. Changes in the aortic endothelium and plasma von Willebrand factor levels during the onset and progression of insulin-dependent diabetes in BB rats. Atherosclerosis. 1998;139(2):291-9.
244. Cester N, Rabini RA, Salvolini E, Staffolani R, Curatola A, Pugnaloni A, et al. Activation of endothelial cells during insulin-dependent diabetes mellitus: a biochemical and morphological study. European journal of clinical investigation. 1996;26(7):569-73.
245. Ciechanowska A, Gora IM, Sabalinska S, Ladyzynski P. The Effect of High and Variable Glucose on the Viability of Endothelial Cells Co-Cultured with Smooth Muscle Cells. International journal of molecular sciences. 2022;23(12).
246. Brower JB, Targovnik JH, Caplan MR, Massia SP. High glucose-mediated loss of cell surface heparan sulfate proteoglycan impairs the endothelial shear stress response. Cytoskeleton (Hoboken, NJ). 2010;67(3):135-41.
247. Tonks KT, Ng Y, Miller S, Coster AC, Samocha-Bonet D, Iseli TJ, et al. Impaired Akt phosphorylation in insulin-resistant human muscle is accompanied by selective and heterogeneous downstream defects. Diabetologia. 2013;56(4):875-85.
248. Zhao L, Hu H, Zhang L, Liu Z, Huang Y, Liu Q, et al. Inflammation in diabetes complications: molecular mechanisms and therapeutic interventions. MedComm. 2024;5(4):e516.

249. Chandel S, Kumaragurubaran R, Giri H, Dixit M. Isolation and Culture of Human Umbilical Vein Endothelial Cells (HUVECs). Methods in molecular biology (Clifton, NJ). 2024;2711:147-62.
250. Saw SN, Dawn C, Biswas A, Mattar CNZ, Yap CH. Characterization of the in vivo wall shear stress environment of human fetus umbilical arteries and veins. Biomechanics and Modeling in Mechanobiology. 2017;16(1):197-211.
251. Janapati YK, Junapudi S. Progress in experimental models to investigate the in vivo and in vitro antidiabetic activity of drugs. Animal models and experimental medicine. 2024;7(3):297-309.
252. Corrò C, Novellasdemunt L, Li VSW. A brief history of organoids. American journal of physiology Cell physiology. 2020;319(1):C151-c65.
253. Stokić E, Derić M, Radak D. [Endothelial dysfunction and diabetes]. Medicinski pregled. 2005;58(9-10):459-64.
254. Roustit M, Loader J, Deusenbery C, Baltzis D, Veves A. Endothelial Dysfunction as a Link Between Cardiovascular Risk Factors and Peripheral Neuropathy in Diabetes. The Journal of clinical endocrinology and metabolism. 2016;101(9):3401-8.
255. Wu H, Wu J, Zhou S, Huang W, Li Y, Zhang H, et al. SRT2104 attenuates diabetes-induced aortic endothelial dysfunction via inhibition of P53. The Journal of endocrinology. 2018;237(1):1-14.
256. Bonetti PO, Lerman LO, Lerman A. Endothelial Dysfunction. 2003;23(2):168-75.
257. Meza CA, La Favor JD, Kim DH, Hickner RC. Endothelial Dysfunction: Is There a Hyperglycemia-Induced Imbalance of NOX and NOS? International journal of molecular sciences. 2019;20(15).
258. Cyr AR, Huckaby LV, Shiva SS, Zuckerbraun BS. Nitric Oxide and Endothelial Dysfunction. Critical care clinics. 2020;36(2):307-21.
259. Jeon H, Lee D, Kim JY, Shim JJ, Lee JH. Limosilactobacillus reuteri HY7503 and Its Cellular Proteins Alleviate Endothelial Dysfunction by Increasing Nitric Oxide Production and Regulating Cell Adhesion Molecule Levels. International journal of molecular sciences. 2024;25(20).
260. Busse R, Fleming I. Endothelial Dysfunction in Atherosclerosis. Journal of Vascular Research. 2008;33(3):181-94.
261. Oettel A, Lorenz M, Stangl V, Costa S-D, Zenclussen AC, Schumacher A. Human Umbilical Vein Endothelial Cells foster conversion of CD4+CD25−Foxp3− T cells into CD4+Foxp3+ Regulatory T Cells via Transforming Growth Factor-β. Scientific Reports. 2016;6(1):23278.
262. Tan PH, Chan C, Xue SA, Dong R, Ananthesayanan B, Manunta M, et al. Phenotypic and functional differences between human saphenous vein (HSVEC) and umbilical vein (HUVEC) endothelial cells. Atherosclerosis. 2004;173(2):171-83.
263. Wagner WH, Henderson RM, Hicks HE, Banes AJ, Johnson G, Jr. Differences in morphology, growth rate, and protein synthesis between cultured arterial and venous endothelial cells. Journal of vascular surgery. 1988;8(4):509-19.
264. De Nigris V, Pujadas G, La Sala L, Testa R, Genovese S, Ceriello A. Short-term high glucose exposure impairs insulin signaling in endothelial cells. Cardiovascular Diabetology. 2015;14(1):114.
265. Hao J, Chen C, Huang K, Huang J, Li J, Liu P, et al. Polydatin improves glucose and lipid metabolism in experimental diabetes through activating the Akt signaling pathway. Eur J Pharmacol. 2014;745:152-65.
266. Hami J, Kerachian MA, Karimi R, Haghir H, Sadr-Nabavi A. Effects of streptozotocin-induced type 1 maternal diabetes on PI3K/AKT signaling pathway in the hippocampus of rat neonates. Journal of receptor and signal transduction research. 2016;36(3):254-60.

267. Tyagi S, Singh N, Virdi JK, Jaggi AS. Diabetes abolish cardioprotective effects of remote ischemic conditioning: evidences and possible mechanisms. Journal of physiology and biochemistry. 2019;75(1):19-28.
268. Katagiri D, Nagasaka S, Takahashi K, Wang S, Pozzi A, Zent R, et al. Endothelial eNOS deficiency causes podocyte injury through NFAT2 and heparanase in diabetic mice. Sci Rep. 2024;14(1):29179.
269. Kolluru GK, Bir SC, Kevil CG. Endothelial dysfunction and diabetes: effects on angiogenesis, vascular remodeling, and wound healing. International journal of vascular medicine. 2012;2012:918267.
270. PromoCell. Human Umbilical Vein Endothelial Cells (HUVEC) 2025 [cited 2025 09/09/25]. Available from: https://promocell.com/uk_en/human-umbilical-vein-endothelial-cells-huvec.html.
271. Du XL, Edelstein D, Dimmeler S, Ju Q, Sui C, Brownlee M. Hyperglycemia inhibits endothelial nitric oxide synthase activity by posttranslational modification at the Akt site. The Journal of clinical investigation. 2001;108(9):1341-8.
272. Cosentino F, Hishikawa K, Katusic ZS, Lüscher TF. High Glucose Increases Nitric Oxide Synthase Expression and Superoxide Anion Generation in Human Aortic Endothelial Cells. Circulation. 1997;96(1):25-8.
273. Hilderink S, van der Velden J, Kuster DWD. Endothelial identity not found – Beyond passage 38, commercial cardiac microvascular endothelial cells do not express CD31 and VE-cadherin. Journal of Molecular and Cellular Cardiology Plus. 2024;8:100071.
274. Henrot P, Laurent P, Levionnois E, Leleu D, Pain C, Truchetet ME, et al. A Method for Isolating and Culturing Skin Cells: Application to Endothelial Cells, Fibroblasts, Keratinocytes, and Melanocytes From Punch Biopsies in Systemic Sclerosis Skin. Frontiers in immunology. 2020;11:566607.
275. Liu A, Ng CJ. Quantitative analysis of Weibel-Palade bodies. PLoS One. 2022;17(12):e0278044.
276. Wang Y, Yao M, Wang J, Liu H, Zhang X, Zhao L, et al. Effects of Antidiabetic Drugs on Endothelial Function in Patients With Type 2 Diabetes Mellitus: A Bayesian Network Meta-Analysis. Frontiers in endocrinology. 2022;13:818537.
277. Sahoo J, Mohanty S, Kundu A, Epari V. Medication Adherence Among Patients of Type II Diabetes Mellitus and Its Associated Risk Factors: A Cross-Sectional Study in a Tertiary Care Hospital of Eastern India. Cureus. 2022;14(12):e33074.
278. Zhang C, Kelkar A, Neelamegham S. von Willebrand factor self-association is regulated by the shear-dependent unfolding of the A2 domain. Blood advances. 2019;3(7):957-68.
279. Sporn LA, Marder VJ, Wagner DD. Differing polarity of the constitutive and regulated secretory pathways for von Willebrand factor in endothelial cells. The Journal of cell biology. 1989;108(4):1283-9.
280. Nakajima Y, Nogami K, Yada K, Kawamura T, Ogiwara K, Furukawa S, et al. Evaluation of clinical severity in patients with type 2N von Willebrand disease using microchip-based flow-chamber system. International journal of hematology. 2020;111(3):369-77.
281. Tsai H-M. Platelet Activation and the Formation of the Platelet Plug. Arteriosclerosis, thrombosis, and vascular biology. 2003;23(3):388-96.
282. Lavin M, O'Donnell JS. How I treat low von Willebrand factor levels. Blood. 2019;133(8):795-804.
283. Noetzli LJ, Italiano JE. Unlocking the Molecular Secrete(s) of α-Granule Biogenesis. Arteriosclerosis, thrombosis, and vascular biology. 2018;38(11):2539-41.
284. Gralnick HR, Williams SB, McKeown LP, Magruder L, Hansmann K, Vail M, et al. Platelet von Willebrand factor. Mayo Clin Proc. 1991;66(6):634-40.
285. Wolf K, Hu H, Isaji T, Dardik A. Molecular identity of arteries, veins, and lymphatics. Journal of vascular surgery. 2019;69(1):253-62.

286. Liao H, He H, Chen Y, Zeng F, Huang J, Wu L, et al. Effects of long-term serial cell passaging on cell spreading, migration, and cell-surface ultrastructures of cultured vascular endothelial cells. Cytotechnology. 2014;66(2):229-38.
287. Mobayen G. The Importance of the Von Willebrand Factor D4 and C-terminal Domains for Expression and Function: Imperial College London; 2024.
288. Palikuqi B, Nguyen DT, Li G, Schreiner R, Pellegata AF, Liu Y, et al. Adaptable haemodynamic endothelial cells for organogenesis and tumorigenesis. Nature. 2020;585(7825):426-32.
289. Huveneers S, Phng LK. Endothelial cell mechanics and dynamics in angiogenesis. Current opinion in cell biology. 2024;91:102441.
290. Augustin HG, Koh GY. Organotypic vasculature: From descriptive heterogeneity to functional pathophysiology. Science (New York, NY). 2017;357(6353).
291. Mourik M, Eikenboom J. Lifecycle of Weibel-Palade bodies. Hamostaseologie. 2017;37(1):13-24.
292. Vischer UM. von Willebrand factor, endothelial dysfunction, and cardiovascular disease. Journal of thrombosis and haemostasis : JTH. 2006;4(6):1186-93.
293. Iwamoto T, Shimizu S, Tajima-Sakurai H, Yamaguchi H, Nishida Y, Arakawa S, et al. Inhibition of Insulin Secretion Induces Golgi Morphological Changes. Juntendo Iji zasshi = Juntendo medical journal. 2023;69(1):42-9.
294. Jiang Z, Hu Z, Zeng L, Lu W, Zhang H, Li T, et al. The role of the Golgi apparatus in oxidative stress: is this organelle less significant than mitochondria? Free Radical Biology and Medicine. 2011;50(8):907-17.
295. Prasad Chennazhy K, Krishnan LK. Effect of passage number and matrix characteristics on differentiation of endothelial cells cultured for tissue engineering. Biomaterials. 2005;26(28):5658-67.
296. Lopes AAB, Peranovich TMS, Maeda NY, Bydlowski SP. Differential Effects of Enzymatic Treatments on the Storage and Secretion of von Willebrand Factor by Human Endothelial Cells. Thrombosis research. 2001;101(4):291-7.
297. Matsushita H, Chang E, Glassford AJ, Cooke JP, Chiu C-P, Tsao PS. eNOS Activity Is Reduced in Senescent Human Endothelial Cells. Circulation Research. 2001;89(9):793-8.
298. Anand K, Olteanu V, Zhang C, Nelton K, Aakre E, Botero JP, et al. Automated Von Willebrand Factor Multimer Image Analysis for Improved Diagnosis and Classification of Von Willebrand Disease. International journal of laboratory hematology. 2025;47(4):730-7.
299. Forouhi NG, Wareham NJ. Epidemiology of diabetes. Medicine. 2010;38(11):602-6.
300. Xiang Y, Cheng J, Wang D, Hu X, Xie Y, Stitham J, et al. Hyperglycemia repression of miR-24 coordinately upregulates endothelial cell expression and secretion of von Willebrand factor. Blood. 2015;125(22):3377-87.
301. Jeong H-S, Lee D-H, Kim S-H, Lee C-H, Shin HM, Kim H-R, et al. Hyperglycemia-induced oxidative stress promotes tumor metastasis by upregulating vWF expression in endothelial cells through the transcription factor GATA1. Oncogene. 2022;41(11):1634-46.
302. Rurali E, Noris M, Chianca A, Donadelli R, Banterla F, Galbusera M, et al. ADAMTS13 predicts renal and cardiovascular events in type 2 diabetic patients and response to therapy. Diabetes. 2013;62(10):3599-609.
303. Laan SNJ, Dirven RJ, Bürgisser PE, Eikenboom J, Bierings R. Automated segmentation and quantitative analysis of organelle morphology, localization and content using CellProfiler. PLoS One. 2023;18(6):e0278009.

Appendix

ImageJ Macro 1: WPB number, angle and feret diameter

```
imageTitle=getTitle();//returns a string with the image title

run("Split Channels");

selectWindow("C1-"+imageTitle)

close();

selectWindow("C2-"+imageTitle);

setOption("ScaleConversions", true);

run("8-bit");

run("Subtract Background...", "rolling=3 sliding");

run("Auto Local Threshold", "method=Bernsen radius=15 parameter_1=0
parameter_2=0 white");

run("Analyze Particles...", "size=0.1-3.00 show=Masks clear add");

run("Set Measurements...", "area perimeter feret's redirect=None
decimal=9");

roiManager("Measure");

saveAs("Results", "C:\\".txt");

selectWindow("C2-"+imageTitle);

close();

selectWindow("Mask of C2-"+imageTitle);

close();

close("Results");

close("ROI Manager");
```

ImageJ Macro 2: Cell orientation angle

```
imageTitle=getTitle();

run("Rotate 90 Degrees Left");

run("Difference of Gaussians", "  sigma1=20 sigma2=1");

run("32-bit");

run("OrientationJ Distribution", "tensor=2.0 gradient=4
orientation=off radian=off histogram=off table=on min-coherency=0.0
min-energy=0.0 ");

selectWindow("OJ-Distribution-1");

//change the line below to a file of your choice

saveAs("Results", "C:\\ ".txt");

selectWindow("OJ-Histogram-1-slice-1");

close("*");
```

ImageJ Macro 3: VWF Strings

```
imageTitle=getTitle();//returns a string with the image title

run("Split Channels");

selectWindow("C1-"+imageTitle)

close();

selectWindow("C2-"+imageTitle);

setOption("ScaleConversions", true);

run("8-bit");

run("Subtract Background...", "rolling=0.5 sliding");

run("Auto Local Threshold", "method=Phansalkar radius=15 parameter_1=0
parameter_2=0 white");

run("Analyze Particles...", "size=2-Infinity circularity=0.00-0.20
show=Masks clear add exclude");

saveAs("Results", "C:\\ +".txt");

selectWindow("C2-"+imageTitle);

close();

selectWindow("Mask of C2-"+imageTitle);

close();

close("Results");

close("ROI Manager");
```

ImageJ Macro 4: WPB positive cell percentage

```
//open both series

//macro to create distance map

imageTitle=getTitle();//returns a string with the image title

run("Split Channels");

selectWindow("C2-"+imageTitle);

close();

selectWindow("C1-"+imageTitle);

close();

selectWindow("C3-"+imageTitle);

rename("nuclei");

run("Command From Macro",
"command=[de.csbdresden.stardist.StarDist2D], args=['input':'nuclei',
'modelChoice':'Versatile (fluorescent nuclei)',
'normalizeInput':'true', 'percentileBottom':'1.0',
'percentileTop':'99.8', 'probThresh':'0.5', 'nmsThresh':'0.4',
'outputType':'Both', 'nTiles':'1', 'excludeBoundary':'2',
'roiPosition':'Automatic', 'verbose':'false',
'showCsbdeepProgress':'false', 'showProbAndDist':'false'],
process=[false]");

selectWindow("Label Image");

run("Auto Threshold", "method=MinError(I) white");

setOption("BlackBackground", true);

run("Convert to Mask");

run("Invert");

run("Distance Map");

close("ROI Manager");

close("nuclei");

run("Brightness/Contrast...");

setMinAndMax(0, 150);

run("Apply LUT");

run("Size...", "width=2048 height=2048 depth=1 constrain average
interpolation=Bilinear"); //end up with distance map with nuclei
identified using StarDist (much more robust than previous method)
```

```
//macro to identify WPBs - make sure this is the same as used before
if measuring Feret/number

imageTitle=getTitle();//returns a string with the image title

run("Split Channels");

selectWindow("C2-"+imageTitle);

setOption("ScaleConversions", true);

run("8-bit");

//insert subtract background step here if necessary

run("Auto Local Threshold", "method=Bernsen radius=15 parameter_1=0
parameter_2=0 white");

run("Analyze Particles...", "size=0.1-3.00 show=Masks clear add");

run("Set Measurements...", "area perimeter feret's redirect=None
decimal=9");

roiManager("Measure");

selectWindow("Mask of C2-"+imageTitle);

close();

close("Results");

selectWindow("C2-"+imageTitle);

close();
```

ImageJ Macro 5: Golgi fragmentation and area

```
imageTitle=getTitle();

run("Split Channels");

selectWindow("C1-"+imageTitle)

close();

selectWindow("C2-"+imageTitle);

close();

selectWindow("C3-"+imageTitle);

setOption("ScaleConversions", true);

run("8-bit");

run("Grays");

run("Subtract Background...", "rolling=20");

run("Auto Threshold", "method=IsoData white");

run("Set Measurements...", "area perimeter feret's redirect=None
decimal=9");

run("Analyze Particles...", "size=0.20-Infinity display");

saveAs("Results", "C:\\Users\\umhjt\\OneDrive - University of
Leeds\\Research\\Image analysis\\Diabetic Repeats\\Pair c\\repeat
3\\golgi\\hAEC Static\\"+imageTitle+".txt");

close("Results");

selectWindow("C3-"+imageTitle);

close();
```

WPB associated genes significantly altered in diabetic retinopathy

Gene Symbol	Gene Name	Regulation
ACTG2	Actin, gamma-enteric smooth muscle	**UP**
AGFG2	Arf-GAP domain and FG repeat-containing protein 2	**UP**
ANGPT2	Angiopoietin-2	**UP**
ATP1A3	Sodium/potassium-transporting ATPase subunit alpha-3	**DOWN**
BGN	Biglycan	**UP**
CLU	Clusterin	**DOWN**
COL1A1	Collagen alpha-1((I) chain	**UP**
COL3A1	Collagen alpha-1(III) chain	**UP**
DHCR7	7-dehydrocholesterol reductase	**DOWN**
ECE1	Endothelin-converting enzyme 1	**UP**
EFEMP1	EGF-containing fibulin-like extracellular matrix protein 1	**DOWN**
FSCN1	Fascin	**UP**
GIMAP1	GTPase IMAP family member 1	**UP**
GIMAP7	GTPase IMAP family member 7	**UP**
GSTP1	Glutathione S-transferase P	**DOWN**
HEXA	Beta-hexosaminidase subunit alpha	**DOWN**
HSPD1	60 kDa heat shock protein, mitochondrial	**DOWN**
ICAM2	Intercellular adhesion molecule 2	**UP**

LNPEP	Leucyl-cystinyl aminopeptidase;Leucyl-cystinyl aminopeptidase, pregnancy serum form	**UP**
MAN2B1	Lysosomal alpha-mannosidase	**UP**
MAN2B2	Epididymis-specific alpha mannosidase	**DOWN**
MCAM	Cell surface glycoprotein MUC18	**UP**
MGP	Matrix Gla protein	**UP**
MMRN1	Multimerin-1	**UP**
MSN	Moesin	**UP**
MYH9	Myosin-9	**UP**
MYRIP	Rab effector MyRIP	**DOWN**
NACA	Nascent polypeptide associated complex subunit alpha	**DOWN**
NPC2	Epididymal secretory protein E1	**DOWN**
NPDC1	Neural proliferation differentiation and control protein 1	**UP**
PECAM1	Platelet endothelial cell adhesion molecule	**UP**
PKP1	Plakophilin-1	**DOWN**
PLVAP	Plasmalemma vesicle-associated protein	**UP**
PLXND1	Plexin-D1	**UP**
PODXL	Podocalyxin	**UP**
PREX1	Phosphatidylinositol-3,4,5-trisphosphate dependent Rac exchange factor 1	**UP**
PROCR	Endothelial protein C receptor	**UP**
RAB27A	Ras-related protein Rab-27A	**DOWN**
ROBO4	Roundabout homolog 4	**UP**
RPL7	60S ribosomal protein L7	**DOWN**

SELP	P-selectin	**UP**
SMAD1	Mothers against decapentaplegic homolog 1	**UP**
TMX1	Thioredoxin-related transmembrane protein 1	**UP**
TPM4	Tropomyosin alpha-4 chain	**UP**
VWF	von Willebrand factor	**UP**

Table of all WPB associated genes

All WPB cargo and associated proteins and genes as determined by the McKeown lab group.

wpb_associated_protein	gene_short_name
Golgi resident protein GCP60	ACBD3
Lysosomal acid phosphatase	ACP2
Long-chain-fatty-acid--CoA ligase 4	ACSL4
Beta-actin-like protein 2	ACTBL2
Actin, gamma-enteric smooth muscle	ACTG2
Alpha-actinin-1	ACTN1
Apha-actinin-4	ACTN4
Actin-related protein 3B	ACTR3B
Disintegrin and metalloproteinase domain-containing protein 9	ADAM9
Adenylosuccinate synthetase isozyme 2	ADSS2
Arf-GAP domain and FG repeat-containing protein 2	AGFG2
Alpha-2-HS-glycoprotein	AHSG
Alpha-2-HS-glycoprotein	AHSG
Retinal dehydrogenase 1	ALDH1A1
10-formyltetrahydrofolate dehydrogenase	ALDH1L1
Fructose-bisphosphate aldolase A	ALDOA
Fructose-bisphosphate aldolase C	ALDOC
AMP-activated protein kinase	AMPK
Angiopoietin-2	ANGPT2
Aminopeptidase N	ANPEP
Annexin A1	ANXA1
Annexin A2	ANXA2
Annexin A3	ANXA3
Annexin A4	ANXA4
Annexin A5	ANXA5
Annexin A6	ANXA6
Amyloid beta A4 precursor protein-binding family B member 2	APBB2
Amyloid-like protein 2	APLP2
Amyloid beta A4 protein;N-APP;Soluble APPalpha;Soluble APP-beta;C99;Beta-amyloid protein 42;Beta-amyloid protein 40;C83;P3(42);P3(40);C80;Gamma-secretase C-terminal fragment 59;Gamma-secretase C-terminal fragment 57;Gamma-secretase C-terminal fragment 50;C31	APP
ADP-ribosylation factor 1;ADP-ribosylation factor 3	ARF1;ARF3
ADP-ribosylation factor 5	ARF5
Brefeldin A-inhibited guanine nucleotide-exchange protein 1	ARFGEF1

Arfaptin-2	ARFIP2
Rho GTPase-activating protein 1	ARHGAP1
Rho guanine nucleotide exchange factor 1	ARHGEF1
ADP-ribosylation factor-like protein 1	ARL1
PRA1 family protein 3	ARL6IP5
Arylsulfatase A	ARSA
Arylsufratase B	ARSB
Acid ceramidase	ASAH1
ATPase family AAA domain-containing protein 3A	ATAD3A
Atlastin-3	ATL3
Sodium/potassium-transporting ATPase subunit alpha-3	ATP1A3
Calcium-transporting ATPase type 2C member 1	ATP2C1
V-type proton ATPase 116 kDa subunit a isoform 1	ATP6V0A1
V-type proton ATPase 116 kDa subunit a isoform 2	ATP6V0A2
V-type proton ATPase subunit d 1	ATP6V0D1
V-type proton ATPase subunit d 1	ATP6V0D1
V-type proton ATPase catalytic subunit A	ATP6V1A
Probable phospholipid-transporting ATPase IIA	ATP9A
Ancient ubiquitous protein 1	AUP1
BAG family molecular chaperone regulator 5	BAG5
Brain acid soluble protein 1	BASP1
BET1 homolog	BET1
BET1-like protein	BET1L
Biglycan	BGN
Biglycan	BGN
Golgin-45	BLZF1
Vesicle transport protein SEC20	BNIP1
Cell division cycle 42	C42
Calcitonin gene-related peptide	CALCA
Caldesmon	CALD1
Calreticulin	CALR
Calreticulin	CALR
Coiled-coil domain-containing protein 186	CCDC186
Monocyte chemoattractant protein-1	CCL2
Eotaxin-3	CCL26
T-complex protein 1 subunit gamma	CCT3
T-complex protein 1 subunit epsilon	CCT5
T-complex protein 1 subunit theta	CCT6A
CD63 antigen	CD63
CD63	CD63
Hsp90 co-chaperone Cdc37	CDC37
Clathrin heavy chain 1	CLTC
Clusterin	CLU
Clusterin	CLU
Cytosolic non-specific dipeptidase	CNDP2
Conserved oligomeric Golgi complex subunit 3	COG3

Conserved oligomeric Golgi complex subunit 5	COG5
Conserved oligomeric Golgi complex subunit 6	COG6
Conserved oligomeric Golgi complex subunit 7	COG7
Collagen alpha-1((I) chain	COL1A1
Collagen alpha-1(I) chain	COL1A1
Collagen alpha-1(III) chain	COL3A1
Collagen alpha-1(III) chain	COL3A1
Coatomer subunit epsilon	COPE
Carboxypeptidase D	CPD
Plasma glutamate carboxypeptidase	CPQ
Plasma glutamate carboxypeptidase	CPQ
Cleavage and polyadenylation specificity factor subunit 1	CPSF1
EF-hand calcium-binding domain-containing protein 4B/Rab46	CRACR2A
Exportin-2	CSE1L
Cathepsin Z	CTSZ
C-X-C motif chemokine ligand 1	CXCL1
Interleukin-8	CXCL8
NADH-cytochrome b5 reductase 3;NADH-cytochrome b5 reductase 3 membrane-bound form;NADH-cytochrome b5 reductase 3 soluble form	CYB5R3
Derlin-2	DERL2
7-dehydrocholesterol reductase	DHCR7
DnaJ homolog subfamily C member 5	DNAJC5
Protein dopey-2	DOPEY2
Dipeptidyl peptidase 4	DPP4
Dipeptidyl peptidase 2	DPP7
Desmoglein-1	DSG1
Dymeclin	DYM
Endothelin-converting enzyme 1	ECE1
Endothelin converting enzyme 1	ECE1
Endothelin-1	EDN1
Elongation factor 1-alpha 1	EEF1A1
Elongation factor 1-gamma	EEF1G
Elongation factor 2	EEF2
EGF-containing fibulin-like extracellular matrix protein 1	EFEMP1
EGF-containing fibulin-like extracellular matrix protein 1	EFEMP1
Erythrocyte initiation factor 4A-I	EIF4A1
Emerin	EMD
Alpha-enolase	ENO1
Extended synaptotagmin-1	ESYT1
Exocyst complex component 6	EXOC6
Protein NOXP20	FAM114A1
Protein FAM114A2	FAM114A2
Protein FAM134C	FAM134C
Protein FAM219A	FAM219A
Fumarate hydratase, mitochondrial	FH
Filaggrin-2	FLG2

Filamin-A	FLNA
Filamin-B	FLNB
Flotillin-1	FLOT1
Flotillin-2	FLOT2
Fibronectin	FN1
Forkhead box protein O1	FOXO1
Fascin	FSCN1
Tissue alpha-L-fucosidase	FUCA1
Plasma alpha-L-fucosidase	FUCA2
Plasma alpha-L-fucosidase	FUCA2
Fucosyltransferase 6	FUT6
Lysosomal alpha-glucosidase	GAA
N-acetylgalactosamine-6-sulfatase	GALNS
Glyceraldehyde-3-phosphate dehydrogenase	GAPDH
Glucosylceramidase	GBA
Golgi-specific brefeldin A-resistance guanine nucleotide exchange factor 1	GBF1
GRIP and coiled-coil domain-containing protein 2	GCC2
Rab GDP dissociation inhibitor beta	GDI2
Glycerophosphodiester phosphodiesterase domain-containing protein 5	GDPD5
GDP-L-fucose synthase	GFUS
Gamma-glutamylcyclotransferase	GGCT
Gamma-glutamyl hydrolase	GGH
GTPase IMAP family member 1	GIMAP1
GTPase IMAP family member 7	GIMAP7
Gap junction alpha-1 protein	GJA1
Alpha-galactosidase A	GLA
Beta-galactosidase	GLB1
Guanine nucleotide-binding protein G(I) subunit alpha-2	GNAI2
Guanine nucleotide-binding protein G(k) subunit alpha	GNAI3
Guanine nucleotide-binding protein G(s) subunit alpha isoforms XLas	GNAS
Guanine nucleotide-binding protein G(I)/G(S)/G(T) subunit beta-1	GNB1
N-acetylglucosamine-6-sulfatase	GNS
Golgin subfamily A member 2	GOLGA2
Golgin subfamily A member 3	GOLGA3
Golgin subfamily A member 4	GOLGA4
Golgin subfamily A member 5	GOLGA5
Golgin subfamily B member 1	GOLGB1
Golgi phosphoprotein 3	GOLPH3
Golgi-associated PDZ and coiled-coil motif-containing protein	GOPC
Golgi SNAP receptor complex member 1	GOSR1
Golgi SNAP receptor complex member 2	GOSR2
Glucose-6-phosphate isomerase	GPI
Gelsolin	GSN
Glutathione synthetase	GSS
Glutathione S-transferase P	GSTP1
Histone H2B type 1-K	H2BC12

Histone H4	H4C1
Probable histidyl-tRNA synthetase, mitochondrial	HARS2
Beta-hexosaminidase subunit alpha	HEXA
Beta-hexosaminidase subunit beta	HEXB
Protein Hook homolog 3	HOOK3
Heat shock protein HSP 90-alpha	HSP90AA1
Heat shock protein HSP 90-beta	HSP90AB1
Endoplasmin	HSP90B1
Endoplasim	HSP90B1
Heat shock 70 kDa protein 4	HSPA4
78 kDa glucose-regulating protein	HSPA5
78 kDa-regulated protein	HSPA5
Heat shock cognate 71 kDa protein	HSPA8
Heat shock protein beta-1	HSPB1
60 kDa heat shock protein, mitochondrial	HSPD1
Intercellular adhesion molecule 2	ICAM2
Uncharacterised protein KIAA0947	ICE1
Isocitrate dehydrogenase [NADP] cytoplasmic	IDH1
Insulin-like growth factor-binding protein 7	IGFBP7
Insulin-like growth factor-binding protein 7	IGFBP7
Ig kappa chain C region	IGKC
Interleukin 6	IL6
Acetolactate synthase-like protein	ILVBL
Inosine-5'-monophosphate dehydrogenase 2	IMPDH2
Insulin receptor related protein	INSRR
Insulin receptor-related protein	INSRR
Ras GTPase-activating-like protein IQGAP1	IQGAP1
Integrin alpha-5	ITGA5
Integrin alpha-5	ITGA5
Integrin beta-1	ITGB1
Integrin beta-5	ITGB5
Jun proto-oncogene, Activator Protein-1	JUN
Junction plakoglobin	JUP
Kinesin-like protein KIF1A	KIF1A
Kruppel-like factor 2	KLF2
Kruppel-like factor 4	KLF4
Importin subunit beta-1	KPNB1
Lysosome-associated membrane glycoprotein 1	LAMP1
Cytosol aminopeptidase	LAP3
Lamin-B receptor	LBR
L-lactate dehydrogenase A chain	LDHA
L-lactate dehydrogenase B chain	LDHB
Low-density lipoprotein receptor	LDLR
Vesicular integral-membrane protein VIP36	LMAN2
Leucyl-cystinyl aminopeptidase;Leucyl-cystinyl aminopeptidase, pregnancy serum form	LNPEP

Lipopolysaccharide-responsive and beige-like anchor protein	LRBA
Lysozyme g-like protein 2	LYG2
Lysozyme g-like protein 2	LYG2
Endoplasmic reticulum mannosyl-oligosaccharide 1,2- alpha-mannosidase	MAN1B1
Lysosomal alpha-mannosidase	MAN2B1
Epididymis-specific alpha mannosidase	MAN2B2
Epididymis-specific alpha-mannosidase	MAN2B2
Mitogen-activated protein kinase kinase kinase 11	MAP3K11
Myristoylated alanine-rich C-kinase substrate	MARCKS
S-adenosylmethionine synthase isoform type-2	MAT2A
Cell surface glycoprotein MUC18	MCAM
Cell Surface glycoprotein MUC18	MCAM
Mediator of RNA polymerase II transcription subunit 8	MED8
Matrix Gla protein	MGP
Matrix Gla protein	MGP
Multimerin-1	MMRN1
Multimerin-1	MMRN1
Protein MON2 homolog	MON2
Moesin	MSN
Major vault protein	MVP
Myosin-9	MYH9
Myosin VA	MYO5A
Unconventional myosin-Vc	MYO5C
Myoferlin	MYOF
Rab effector MyRIP	MYRIP
Nascent polypeptide associated complex subunit alpha	NACA
Alpha-N-acetylgalactosaminidase	NAGA
Alpha-N-acetylglucosaminidase	NAGLU
Alpha-soluble NSF attachment protein	NAPA
Gamma-soluble NSF attachment protein	NAPG
Neurobeachin-like protein 2	NBEAL2
Adaptin ear-binding coat-associated protein 2	NECAP2
Neurofilament heavy polypeptide	NEFH
Sialidase-1	NEU1
Epididymal secretory protein E1	NPC2
Neural proliferation differentiation and control protein 1	NPDC1
Puromycin-sensitive aminopeptidase-like protein	NPEPPSL1
Puromycin-sensitive aminopeptidase-like protein	NPEPPSL1
Sterol-4-alpha-carboxylate 3-dehydrogenase, decarboxylating	NSDHL
Nucleobindin-1	NUCB1
Nucleobindin-1	NUCB1
OCIA domain-containing protein 1	OCIAD1

Inositol polyphosphate 5-phosphatase OCRL-1	OCRL
Oxysterol-binding protein 1	OSBP
Oxysterol-binding protein-related protein 11	OSBPL11
Ubiquitin thioesterase OTUB1	OTUB1
Oxidation resistance protein 1	OXR1
Protein disulfide-isomerase	P4HB
Protein disulfide-isomerase	P4HB
Phosphofurin acidic cluster sorting protein 1	PACS1
Poly(rC)-binding protein 1	PCBP1
Protein disulfide-isomerase A3	PDIA3
Protein disulfide-isomerase A3	PDIA3
Protein disulfide-isomerase A4	PDIA4
Protein disulfide-isomerase A4	PDIA4
Pyridoxal-dependent decarboxylase domain-containing protein 1	PDXDC1
Platelet endothelial cell adhesion molecule	PECAM1
Platelet endothelial cell adhesion molecule	PECAM1
Xaa-Pro-dipeptidase	PEPD
6-phosphofructokinase type C	PFKP
6-phosphogluconate dehydrogenase, decarboxylating	PGD
Phosphoglycerate kinase 1	PGK1
Phosphatidylinositol 4-kinase type 2-alpha	PI4K2A
Phosphatidylinositol 4-kinase beta	PI4KB
Phosphatidylinositol glycan anchor biosynthesis class U protein	PIGU
Phosphatidylinositol-4,5-bisphosphate 3-kinase catalytic subunit alpha isoform	PIK3CA
Pyruvate kinase isozymes M1/M2	PKM
Membrane-associated tyrosine- and threonine-specific cdc2-inhibitory kinase	PKMYT1
Plakophilin-1	PKP1
Group XV phospholipase A2	PLA2G15
Tissue Plasminogen Activator	PLAT
Phospholipase D1	PLD1
Phospholipase D3	PLD3
Proteolipid protein 2	PLP2
Plasmalemma vesicle-associated protein	PLVAP
Plexin-D1	PLXND1
Plexin-D1	PLXND1
Podocalyxin	PODXL
DNA-directed RNA polymerases I, II, and III subunit RPABC3	POLR2H
Peptidyl-prolyl cis-trans isomerase A	PPIA
Protein phosphatase 1 regulatory subunit 7	PPP1R7
Protein phosphatase 2B	PPP3CB
Palmitoyl-protein thioesterase 1	PPT1
Lysosomal Pro-X carboxypeptidase	PRCP

Phosphatidylinositol-3,4,5-trisphosphate dependent Rac exchange factor 1	PREX1
Endothelial protein C receptor	PROCR
Endothelial protein C receptor	PROCR
Protein PRRC1	PRRC1
26S protease regulatory subunit 6B	PSMC4
26S proteasome non-ATPase regulatory subunit 11	PSMD11
Tyrosine-protein phosphatase non-receptor type 9	PTPN9
Peptidyl-tRNA hydrolase 2, mitochondrial	PTRH2
Pentraxin-related protein PTX3	PTX3
Pentraxin-related protein PTX3	PTX3
Ras-related protein Rab-11B	RAB11B
Rab11 family-interacting protein 5	RAB11FIP5
Ras-related protein Rab-13	RAB13
Ras-related protein Rab-14	RAB14
Ras-related protein Rab-15	RAB15
Ras-related protein Rab-1B;Putative Ras-related protein Rab-1C	RAB1B;RAB1C
Ras-related protein Rab-27A	RAB27A
Ras-related protein Rab-32	RAB32
Ras-related protein Rab-33B	RAB33B
Ras-related protein Rab-34	RAB34
Ras-related protein Rab-35	RAB35
Ras-related protein Rab-37	RAB37
Ras-related protein Rab-3A	RAB3A
Ras-related protein Rab-3B	RAB3B
Ras-related protein Rab-3D	RAB3D
Ras-related protein Rab-6A	RAB6A
Ras-related protein Rab-7a	RAB7A
Rac family small GTPase 1	RAC1
Guanine nucleotide-binding protein subunit beta-2-like 1	RACK1
Ras-related protein Ral-A	RALA
RAS like proto-oncogene A	RALA
Ral guanine nucleotide dissociation stimulator	RALGDS
Ras-related protein 1	RAP1B
EPAC/Rap guanine nucleotide exchange factor 3	RAPGEF3
Protein RER1	RER1
Rhomboid domain-containing protein 2	RHBDD2
Transforming protein RhoA	RHOA
Rho-related GTP-binding protein RhoC	RHOC
RAB6A-GEF complex partner protein 1	RIC1
Regulator of microtubule dynamics protein 3	RMDN3
Ribonuclease inhibitor	RNH1
Roundabout homolog 4	ROBO4
60S ribosomal protein L7	RPL7
40S ribosomal protein S20	RPS20
40S ribosomal protein SA	RPSA

S100 Calcium-Binding Protein A10/Calpactin I light chain	S100A10
Phosphatidylinositide phosphatase SAC1	SACM1L
Secretory carrier-associated membrane protein 1	SCAMP1
Lysosome membrane protein 2	SCARB2
Sec1 family domain-containing protein 1	SCFD1
Secernin-1	SCRN1
Vesicle-trafficking protein SEC22b	SEC22B
Protein transport protein Sec23A	SEC23A
Protein transport protein Sec23B	SEC23B
SEC23-interacting protein	SEC23IP
Protein transport protein Sec24B	SEC24B
Protein transport protein Sec24C	SEC24C
P-selectin	SELP
P-selectin	SELP
Serpin B12	SERPINB12
Serpin B6	SERPINB6
Serpin B9	SERPINB9
Plasminogen activator inhibitor 1	SERPINE1
Plasminogen activator inhibitor 1	SERPINE1
Serpin H1	SERPINH1
Serpin H1	SERPINH1
Protein SET	SET
14-3-3 protein sigma	SFN
Vesicle transport protein SFT2C	SFT2D3
N-sulphoglucosamine sulphohydrolase	SGSH
Zinc transporter 5	SLC30A5
Zinc transporter 6	SLC30A6
Zinc transporter 7	SLC30A7
CMP-sialic acid transporter	SLC35A1
Solute carrier family 35 member E1	SLC35E1
Mothers against decapentaplegic homolog 1	SMAD1
Stromal membrane-associated protein 1	SMAP1
Synaptosome associated protein 23	SNAP23
Synaptosomal-associated protein 29	SNAP29
SPARC	SPARC
SPARC	SPARC
Protein spire homolog 1	SPIRE1
Lupus La protein	SSB
Erythrocyte band 7 integral membrane protein	STOM
Syntaxin-12	STX12
Syntaxin-16	STX16-NPEPL1;STX16
Syntaxin-3	STX3
Syntaxin-4	STX4
Syntaxin-5	STX5
Syntaxin-7	STX7
Syntaxin-binding protein 1	STXBP1
Munc18-c	STXBP3
Syntaxin-binding protein 5	STXBP5

Sin3 histone deacetylase corepressor complex component SDS3	SUDS3
SUN domain-containing protein 2	SUN2
Synaptotagmin-like protein 4	SYTL4
Synaptotagmin-like protein 4-a	SYTL4
Transgelin-2	TAGLN2
Transaldolase	TALDO1
TBC1 domain family member 22A	TBC1D22A
Transferrin receptor protein 1;Transferrin receptor protein 1, serum form	TFRC
Protein-glutamine gamma-glutamyltransferase 2	TGM2
Protein-glutamine gamma-glutamyltransferase E	TGM3
Trans-Golgi network integral membrane protein 2	TGOLN2
Thrombospondin-1	THBS1
Thrombospondin-1	THBS1
Tight junction-associated protein 1	TJAP1
Transketolase	TKT
Transmembrane 9 superfamily member 3	TM9SF3
Transmembrane emp24 domain-containing protein 5	TMED5
Transmembrane protein 2	TMEM2
Transmembrane protein 43	TMEM43
TATA element modulatory factor	TMF1
Thioredoxin-related transmembrane protein 1	TMX1
Osteoprotegerin	TNFRSF11B
Toll-interacting protein	TOLLIP
Mitochondrial import receptor subunit TOM70	TOMM70A
Torsin-1A-interacting protein 1	TOR1AIP1
Triosephosphate isomerase	TPI1
Tropomyosin alpha-4 chain	TPM4
Tripeptidyl-peptidase 1	TPP1
Thyroid receptor-interacting protein 11	TRIP11
Tubulin alpha-1B chain	TUBA1B
Tubulin alpha-1C chain	TUBA1C
Tubulin beta chain	TUBB
Tubulin beta-2A chain	TUBB2A
Tubulin beta-3 chain	TUBB3
Tubulin beta-2C chain	TUBB4B
Tubulin beta-6 chain	TUBB6
Thioredoxin domain-containing protein 5	TXNDC5
Thioredoxin reductase 1, cytoplasmic	TXNRD1
UDP-N-acetylhexosamine pyrophosphorylase-like protein 1	UAP1L1
Ubiquitin -like modifier-activating enzyme 1	UBA1
Polyubiquitin-C	UBC
Ubiquitin-conjugating enzyme E2 J1	UBE2J1
Ceramide glucosyltransferase	UGCG

UDP-glucose 6-dehydrogenase	UGDH
Protein unc-13 homolog B/Munc13-2	UNC13B
Munc13-4	UNC13D
General vesicular transport factor p115	USO1
Vesicle associated membrane protein 3	VAMP3
Vesicle-associated membrane protein 3;Vesicle associated membrane protein 2	VAMP3;VAMP2
Vesicle associated membrane protein 8	VAMP8
Synaptic vesicle membrane protein VAT-1 homolog	VAT1
Vinculin	VCL
Transitional endoplasmic reticulum ATPase	VCP
Vimentin	VIM
Spermatogenesis-defective protein 39 homolog	VIPAS39
Vacuolar protein sorting-associated protein 13B	VPS13B
Vacuolar protein sorting-associated protein 45	VPS45
Vacuolar protein sorting-associated protein 51 homolog	VPS51
V-set and immunoglobulin domain-containing protein 8	VSIG8
V-set and immunoglobulin domain-containing protein 8	VSIG8
Vesicle transport through interaction with t-SNAREs homolog 1A	VTI1A
von Willebrand factor A domain-containing protein 5B1	VWA5B1
von Willebrand factor A domain-containing protein 5B1	VWA5B1
von Willebrand factor	VWF
Tryptophanyl-tRNA synthesase, cytoplasmic	WARS1
WD repeat-containing protein 1	WDR1
WD repeat-containing protein 11	WDR11
Nuclease-sensitive element binding protein 1	YBX1
Protein YIF1A	YIF1A
Protein YIF1B	YIF1B
Protein YIPF4	YIPF4
Protein YIPF5	YIPF5
14-3-3 protein beta/alpha	YWHAB
14-3-3 protein epsilon	YWHAE
14-3-3 protein zelta/delta	YWHAZ
Palmitoyltransferase ZDHHC13	ZDHHC13
Palmitoyltransferase ZDHHC17	ZDHHC17
Zinc finger protein-like 1	ZFPL1
Zinc finger protein 598	ZNF598

Full western blots

Phosphorylated AKT

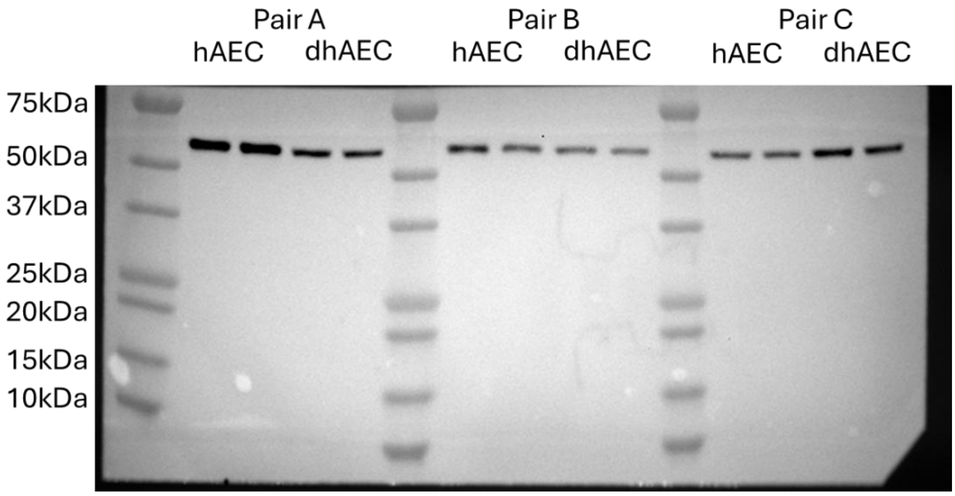

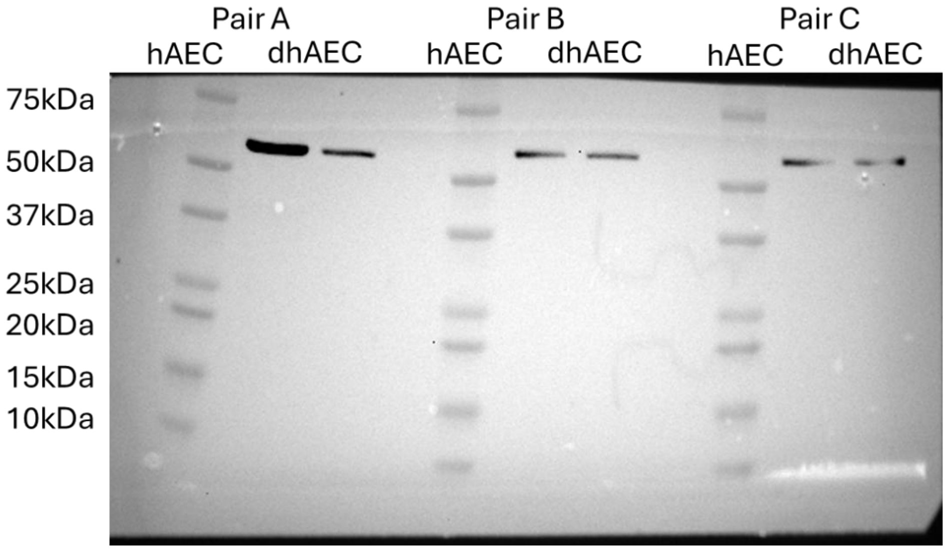

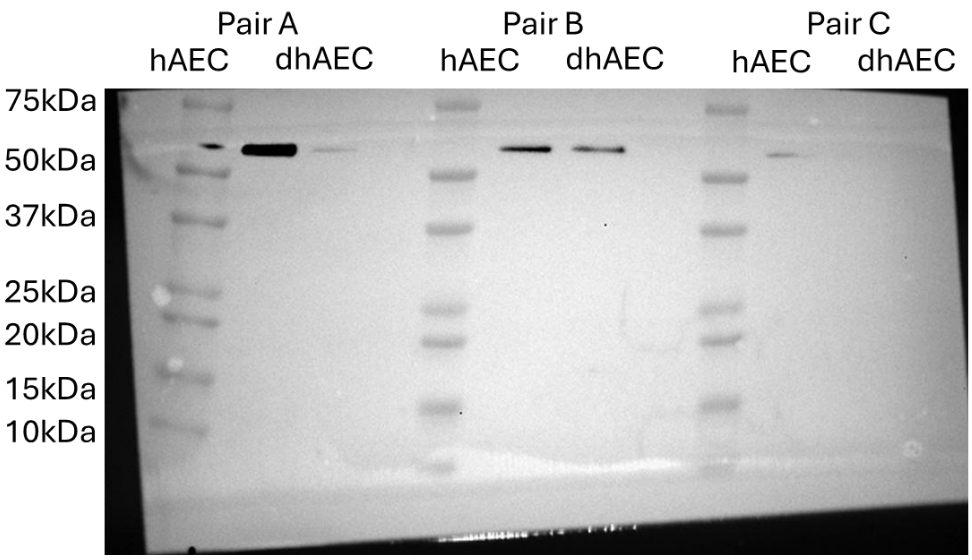

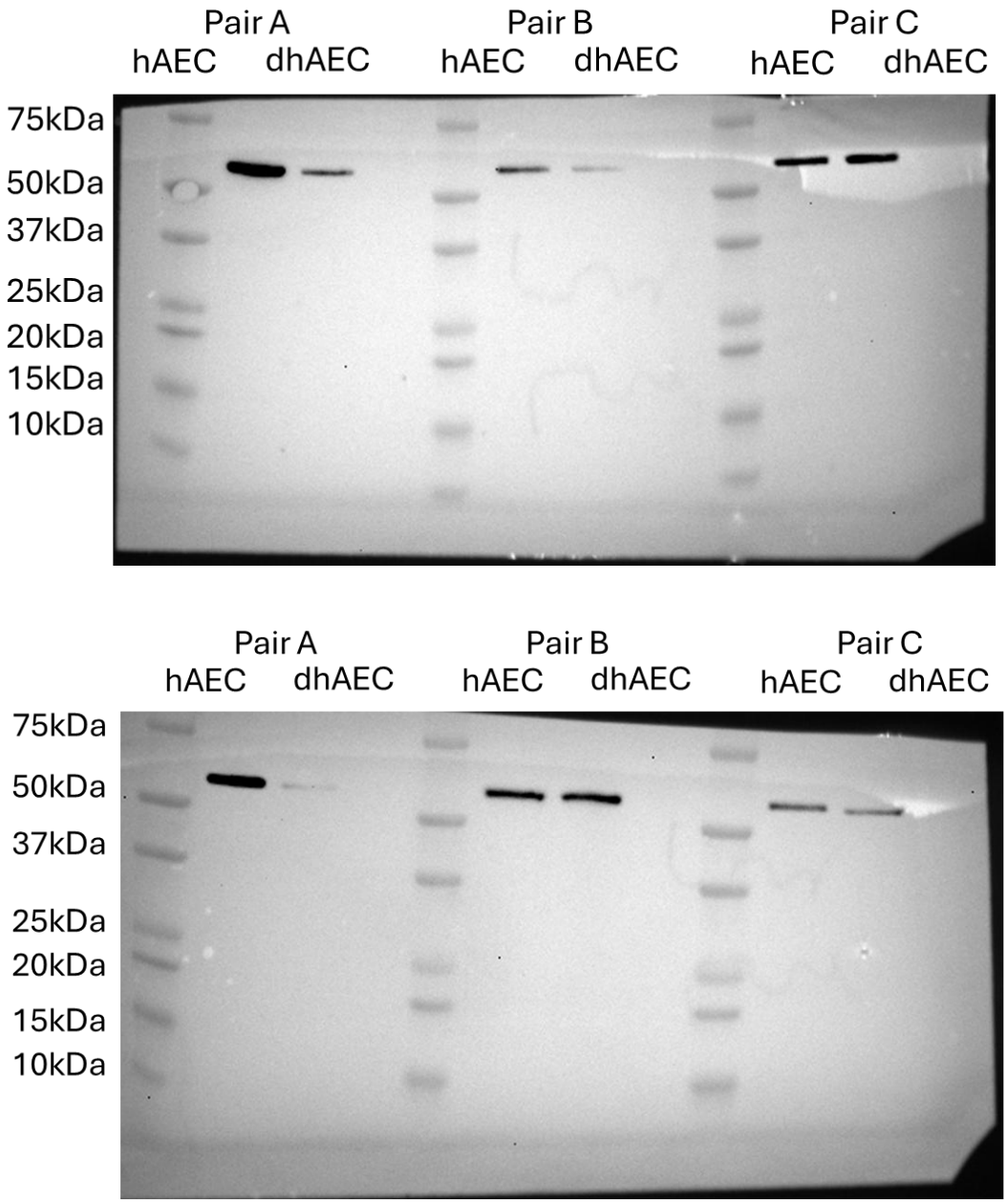

Full western blot membranes showing phosphorylated AKT (pAKT) expression at 60kDafor each repeat. Each membrane shows one repeat of control (hAECs) and diabetic (dhAEC) aortic endothelial cell lysates, for each of the three repeats.

Total AKT

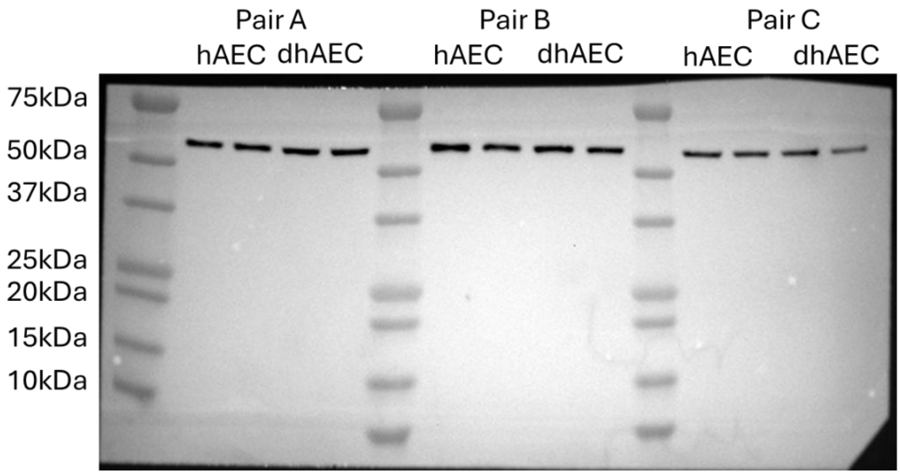
Pair A
hAEC dhAEC
Pair B
hAEC dhAEC
Pair C
hAEC dhAEC
75kDa
50kDa
37kDa
25kDa
20kDa
15kDa
10kDa

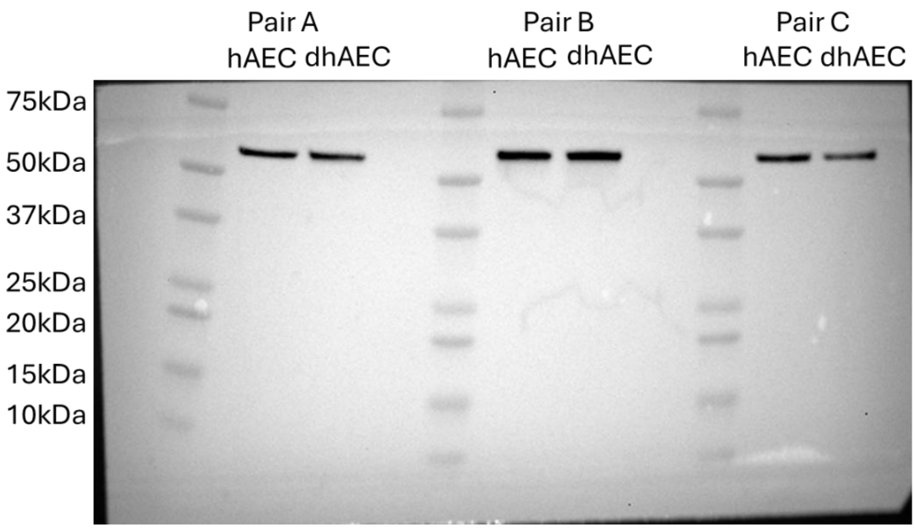
Pair A
hAEC dhAEC
Pair B
hAEC dhAEC
Pair C
hAEC dhAEC
75kDa
50kDa
37kDa
25kDa
20kDa
15kDa
10kDa

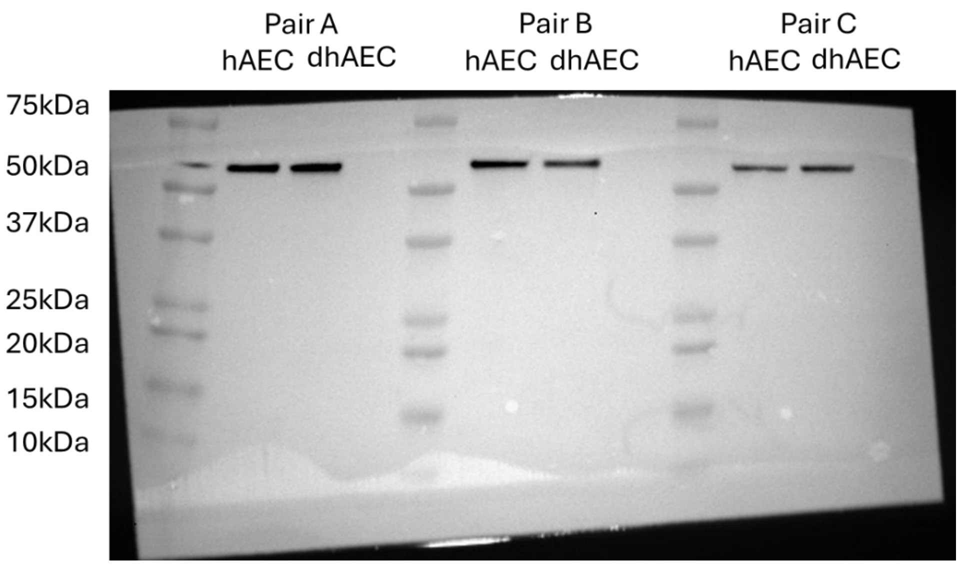
Pair A
hAEC dhAEC
Pair B
hAEC dhAEC
Pair C
hAEC dhAEC
75kDa
50kDa
37kDa
25kDa
20kDa
15kDa
10kDa

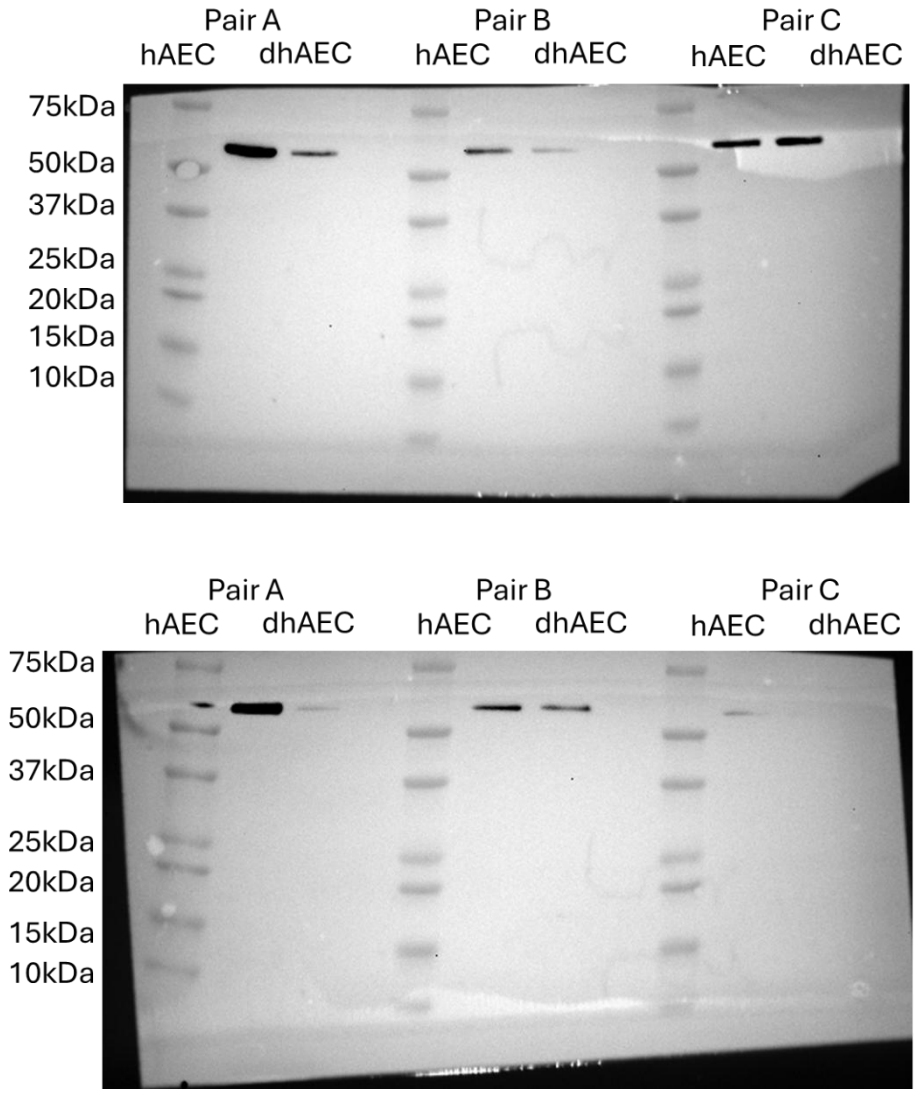

Full western blot membranes showing total AKT (tAKT) expression at 60kDa for each repeat. Each membrane shows one repeat of control (hAECs) and diabetic (dhAEC) aortic endothelial cell lysates, for each of the three repeats.

Phosphorylated eNOS

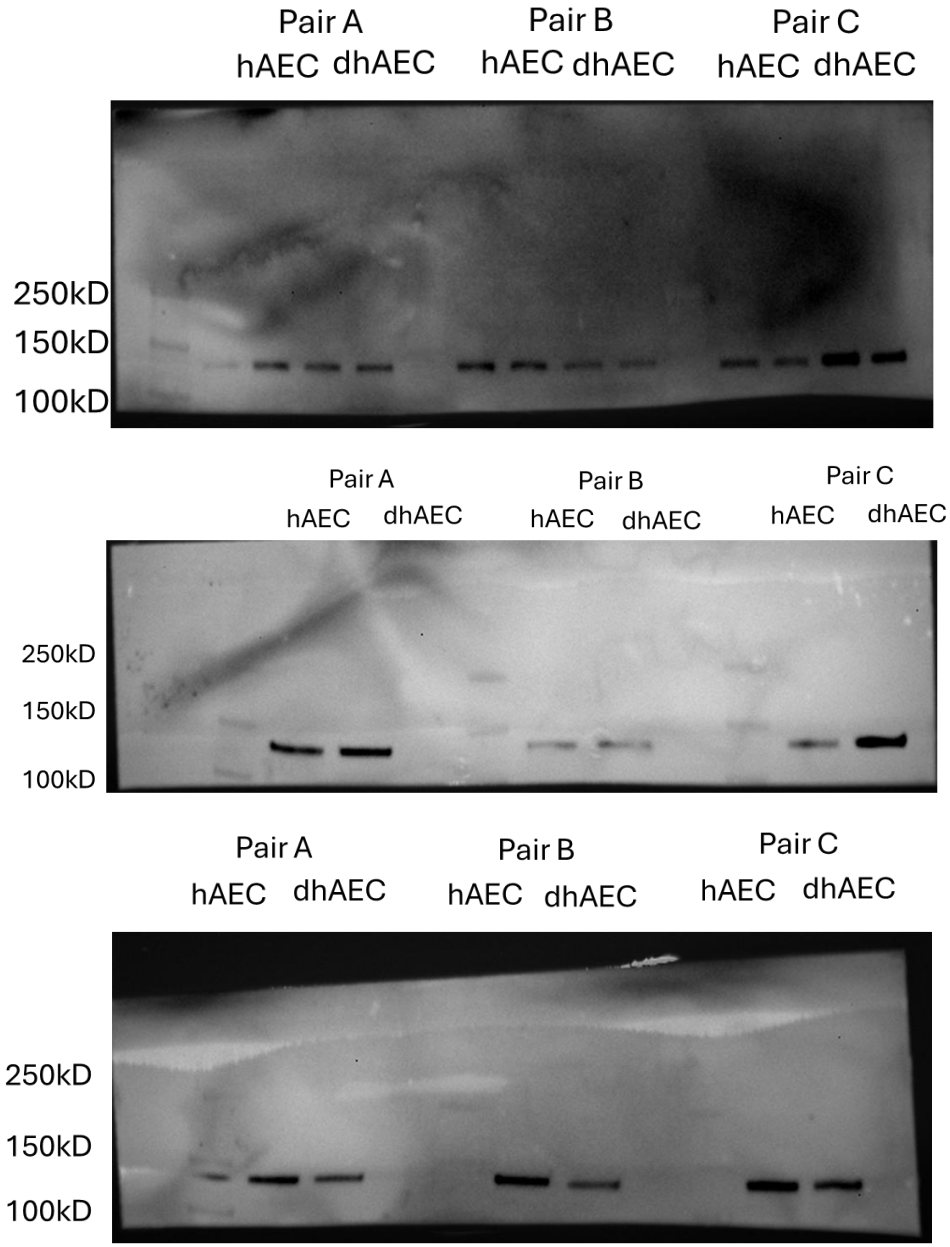

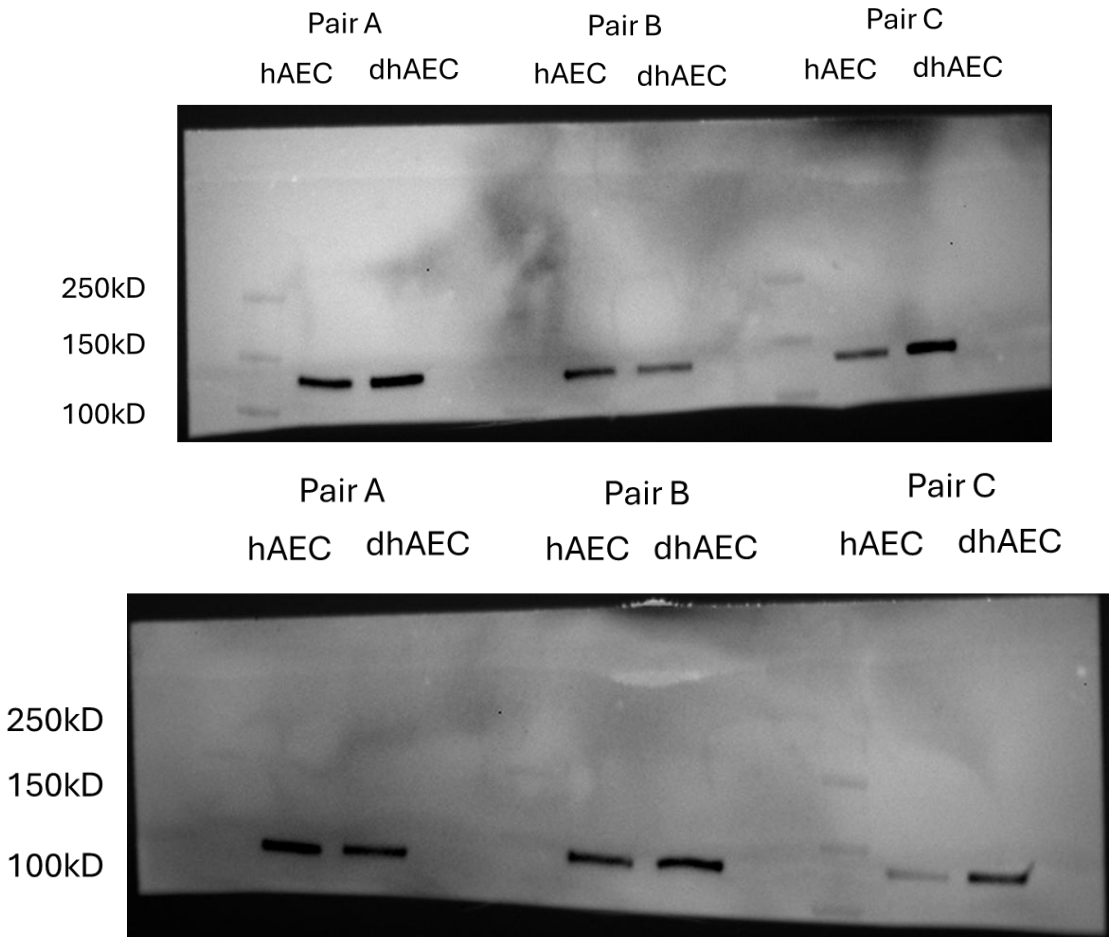

Full western blot membranes showing phosphorylated eNOS (peNOS) expression at 133kDa for each repeat. Each membrane shows one repeat of control (hAECs) and diabetic (dhAEC) aortic endothelial cell lysates, for each of the three repeats.

Total eNOS

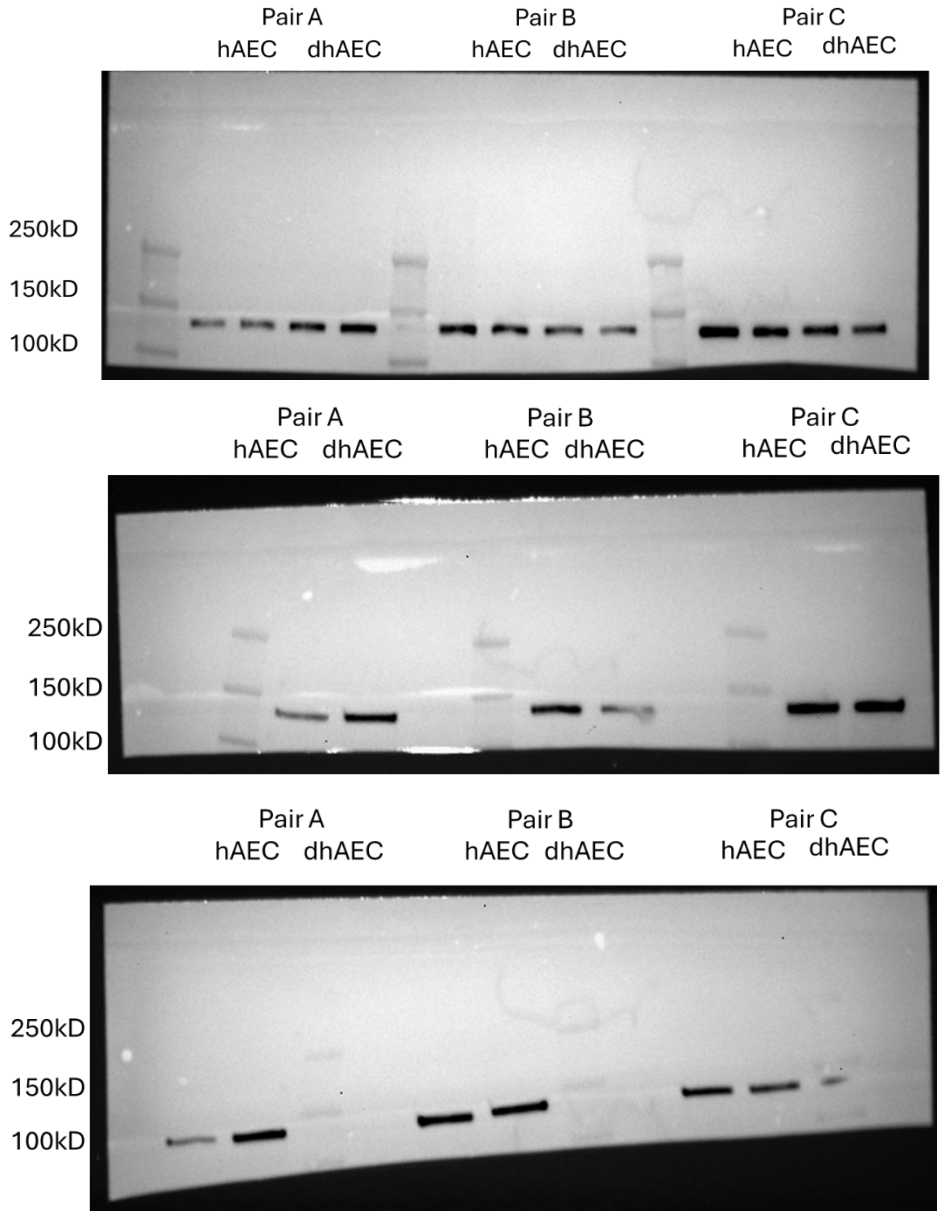
Pair A
hAEC dhAEC
Pair B
hAEC dhAEC
Pair C
hAEC dhAEC
250kD
150kD
100kD
Pair A
hAEC dhAEC
Pair B
hAEC dhAEC
Pair C
hAEC dhAEC
250kD
150kD
100kD
Pair A
hAEC dhAEC
Pair B
hAEC dhAEC
Pair C
hAEC dhAEC
250kD
150kD
100kD

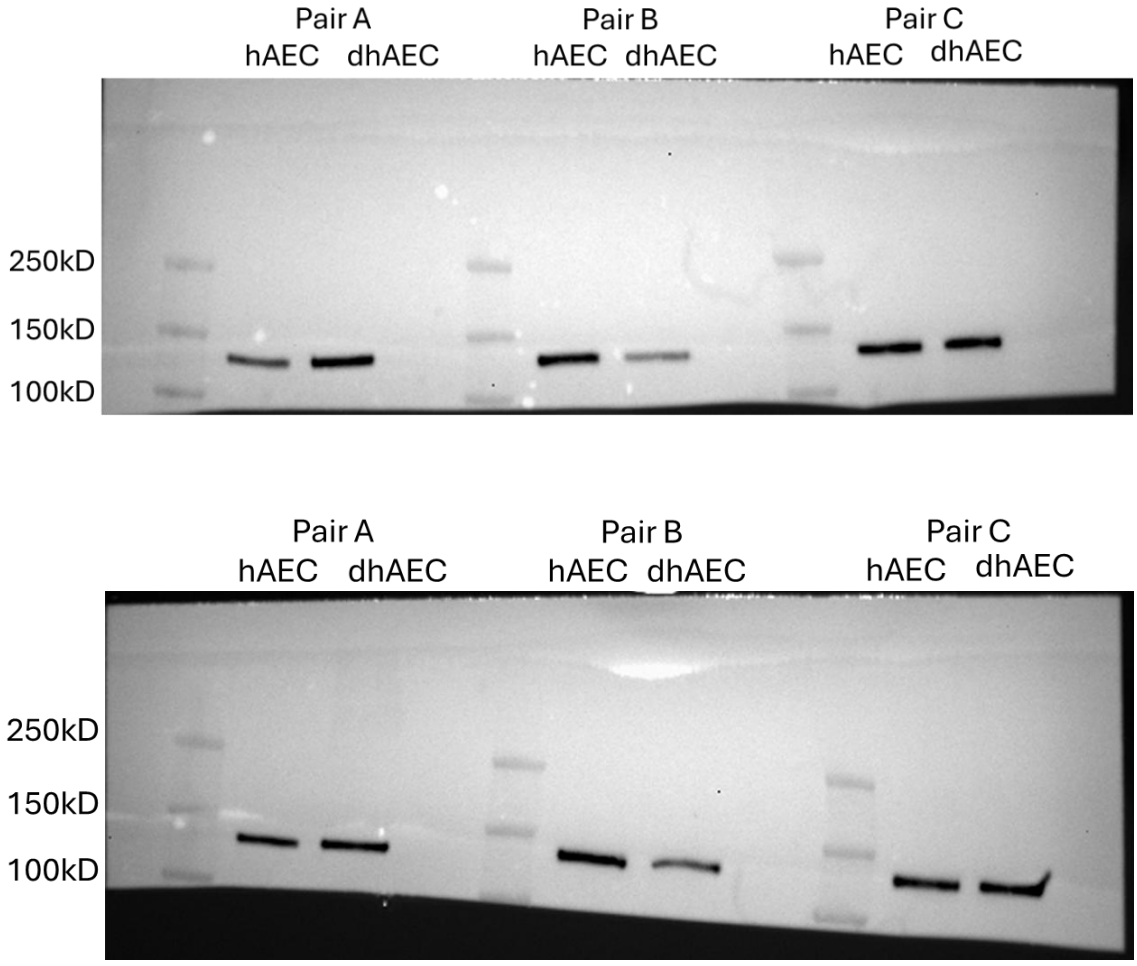

Full western blot membranes showing total eNOS (teNOS) expression at 133kDa for each repeat. Each membrane shows one repeat of control (hAECs) and diabetic (dhAEC) aortic endothelial cell lysates, for each of the three repeats.

B-Actin

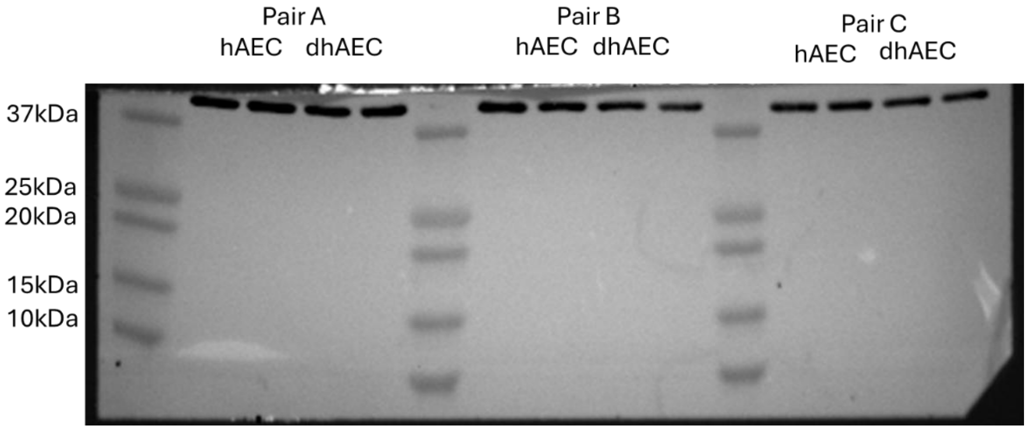
Pair A
hAEC dhAEC
Pair B
hAEC dhAEC
Pair C
hAEC dhAEC
37kDa
25kDa
20kDa
15kDa
10kDa

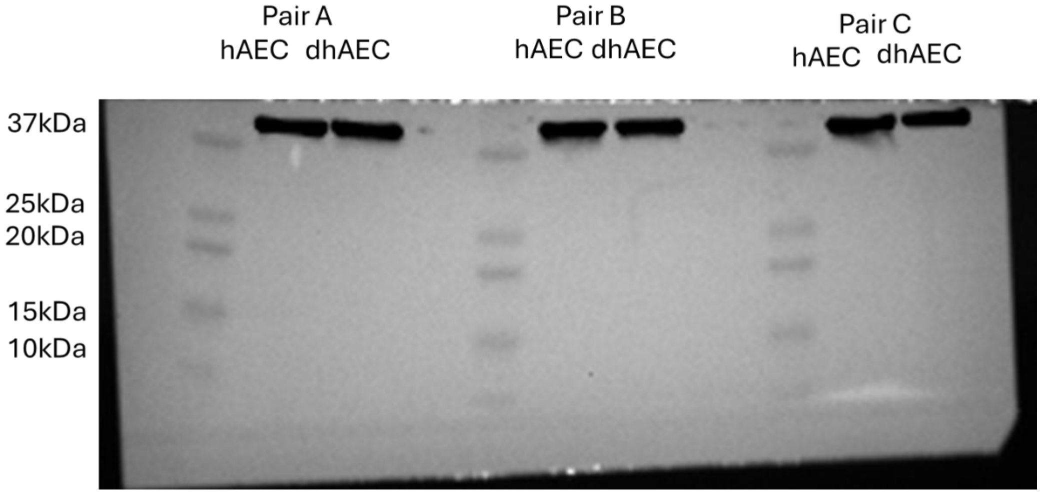
Pair A
hAEC dhAEC
Pair B
hAEC dhAEC
Pair C
hAEC dhAEC
37kDa
25kDa
20kDa
15kDa
10kDa

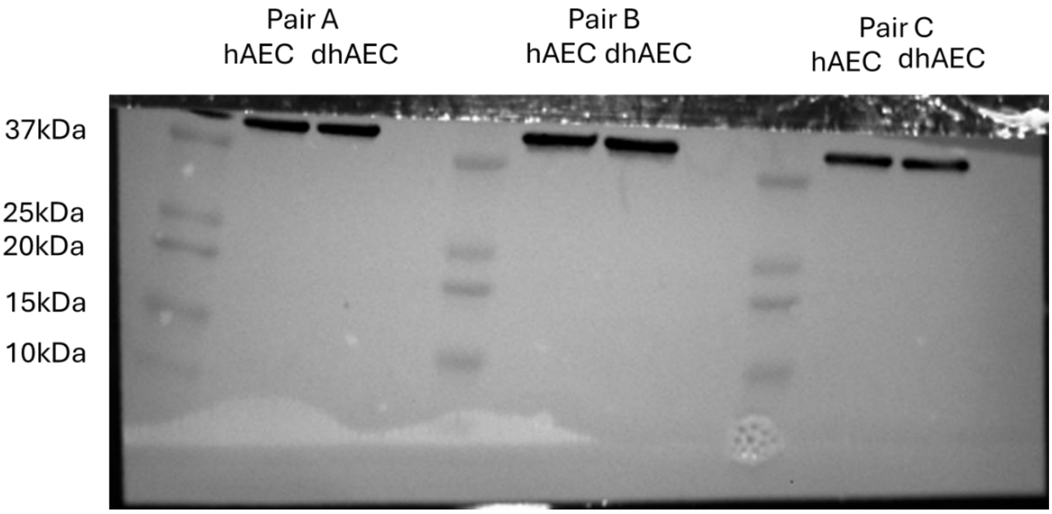
Pair A
hAEC dhAEC
Pair B
hAEC dhAEC
Pair C
hAEC dhAEC
37kDa
25kDa
20kDa
15kDa
10kDa

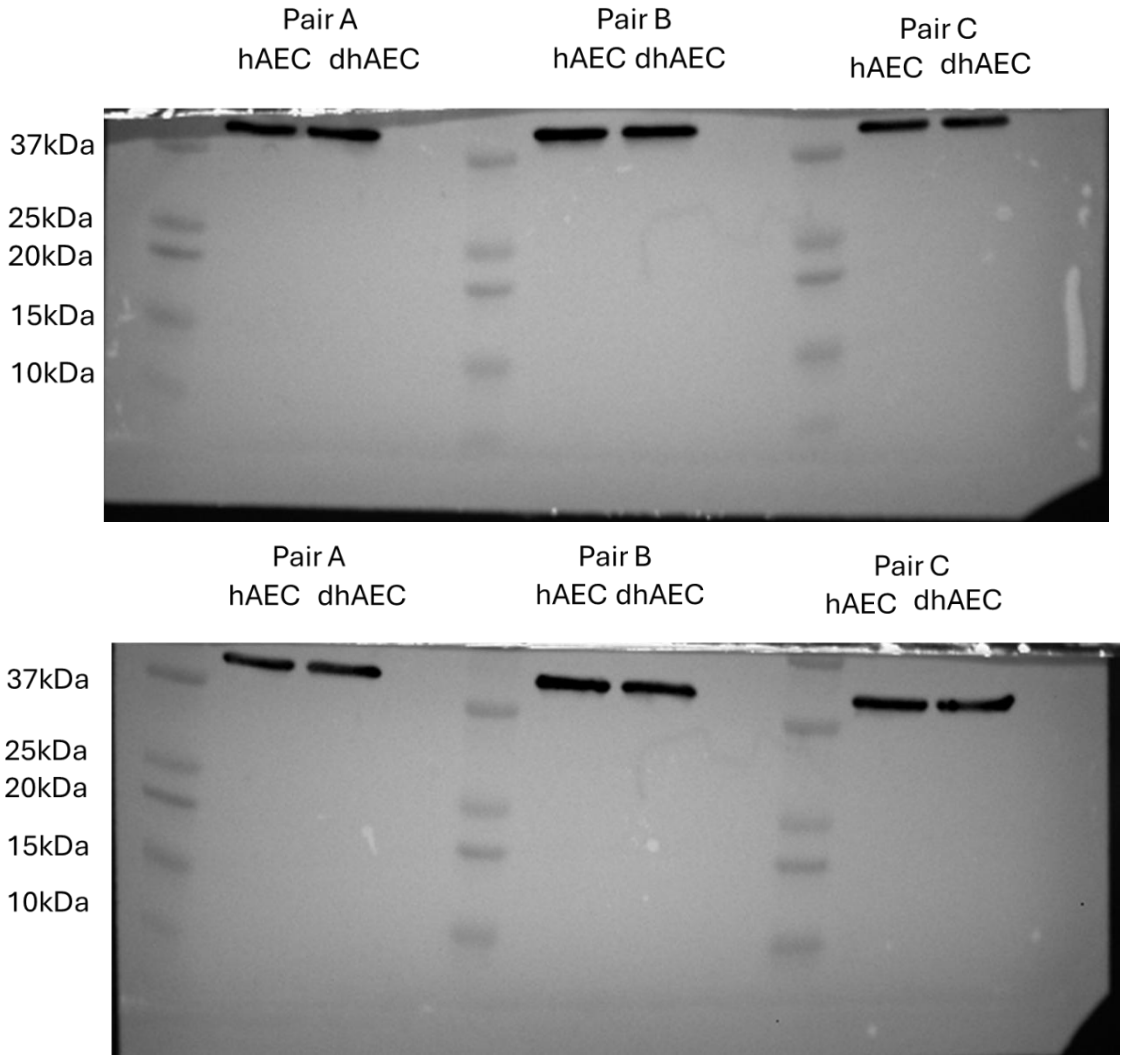

Full western blot membranes showing beta-actin expression at 42kDa for each repeat. This is the running control for this experiment. Each membrane shows one repeat of control (hAECs) and diabetic (dhAEC) aortic endothelial cell lysates, for each of the three repeats.

Full Multimer gels

Cell lysates

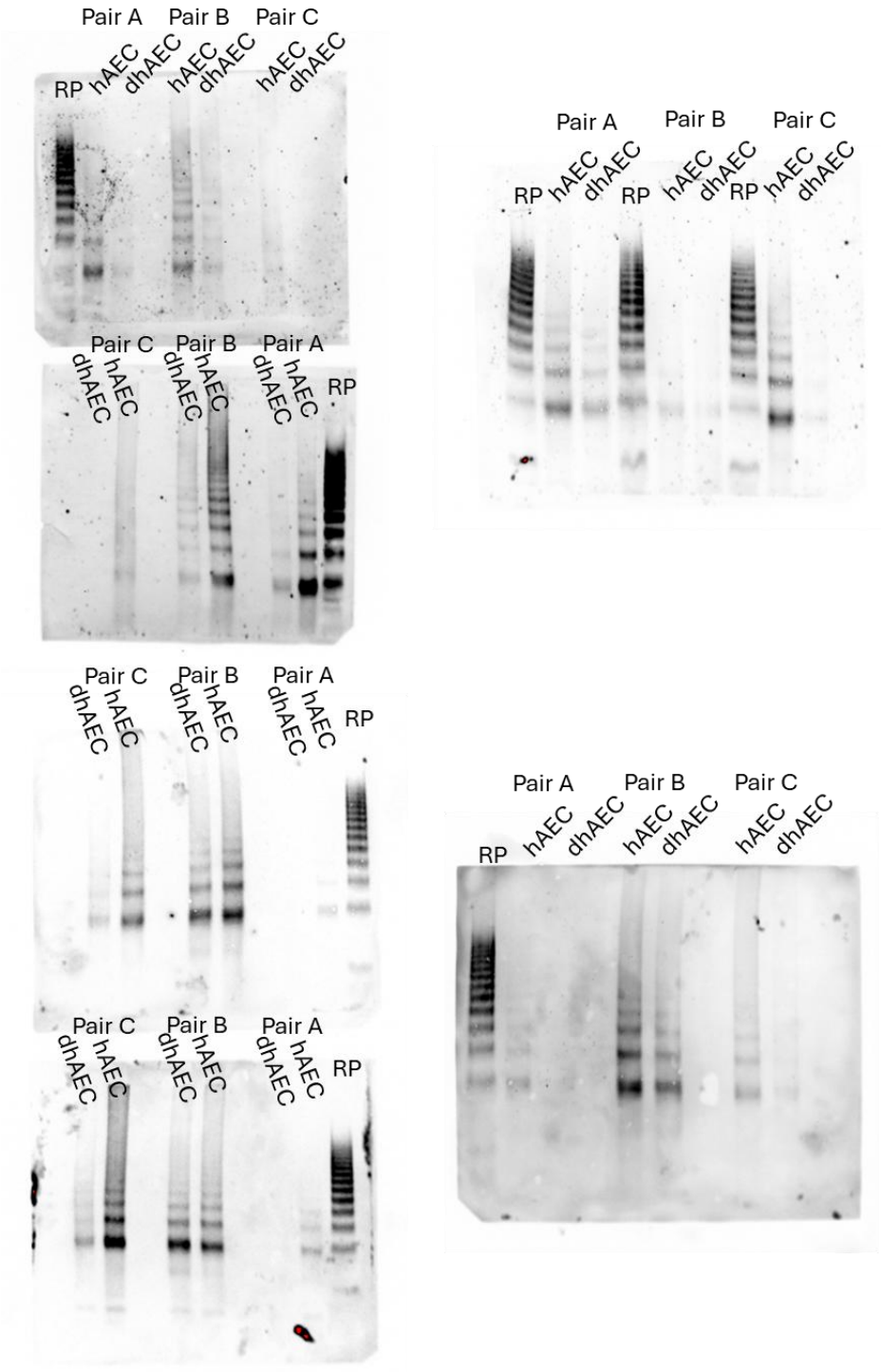

Full multimer gel membranes showing VWF profile for each one repeat of control (hAECs) and diabetic (dhAEC) aortic endothelial cell lysates. Reference plasma (RP) is the running control for each repeat.

Plasma

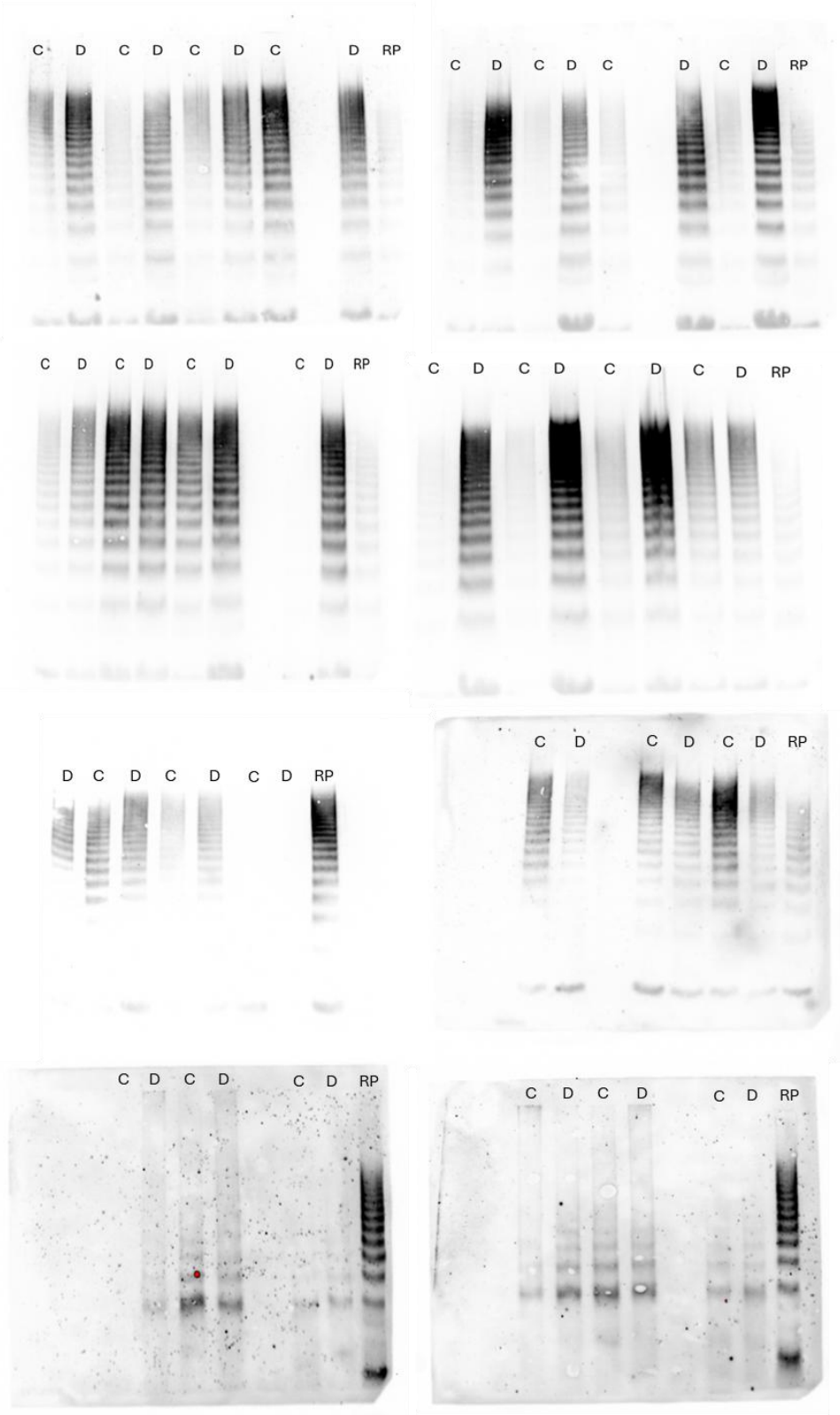

Full multimer gel membranes showing VWF profile for all diabetic (d) and control (c) patient plasma samples. Reference plasma (RP) is the running control for each repeat.

Ethics

Oct 2021 - Mar 2024: The Philippou (HSLTLM12045) and KMN (MREC-19-006) ethics were used interchangeably.

Mar 2024 - Oct 2024: The KMN ethics were used exclusively.

Oct 2024 - Present: The new, unified ethics (MREC-23-001) exclusively.